Green Mobile Networks: from self-sustainability to enhanced interaction with the Smart Grid

Doctoral Dissertation
Doctoral Program in Electrical, Electronics and Communications Engineering
(XXX cycle)

Green Mobile Networks: from self-sustainability to enhanced interaction with the Smart Grid

Daniela Renga
* * * * * *

Supervisor
Professor Michela Meo

Doctoral Examination Committee:
Paolo Dini - Centre Tecnològic de Telecomunicacions de Catalunya, Barcelona, Spain
Bart Lannoo, Referee - Universiteit Antwerpen, Belgium
Josip Lorincz - University of Split, Croatia
Vincenzo Mancuso - IMDEA Networks Institute, Leganes (Madrid), Spain
Gianluca Rizzo, Referee - University of Applied Sciences Western Switzerland

Politecnico di Torino
May 28, 2018

I hereby declare that, the contents and organization of this dissertation constitute my own original work and does not compromise in any way the rights of third parties, including those relating to the security of personal data.

.....

Daniela Renga

Turin, May 28, 2018

Acknowledgements

I would like to express my gratitude to my supervisor, professor Michela Meo, for her constant guidance during my PhD years, during which she has been very supportive and encouraging, offering me valuable opportunities to grow in my work as a researcher and allowing me to widen the scope of my studies. I really appreciated her extreme availability to have fruitful and motivating discussions about the progress of the research activities, always providing insightful comments and advice, and sharing inspiring ideas about possible new directions.

Furthermore, I am grateful for the remarkable opportunity I have been given to carry out part of my PhD research activity working with professor Marco Ajmone Marsan, who has always been keen to share his deep and distinguished expertise in the field of Telecommunication Networks.

In addition, my PhD experience has been enriched by various collaborations with researchers from other universities. In particular, I would like to thank in a special way professor Loutfi Nuaymi and PhD Hussein Al Haj Hassan from Telecom Bretagne, France, professor Ana Paula Couto da Silva from the Federal University of Minas Gerais, Brazil, and PhD Margot Deruyck from Ghent University, Belgium.

Finally, I thank my husband Paolo, for always being by my side. I thank my parents Gianni and Marisa, for their presence all the way through, and my brother Flavio with his family, for their support.

Summary

Nowadays, the staggering increase of the mobile traffic is leading to the deployment of denser and denser cellular access networks, hence Mobile Operators are facing huge operational cost due to power supply. Therefore, several research efforts are devoted to make mobile networks more energy efficient, with the twofold objective of reducing costs and improving sustainability. To this aim, Resource on Demand (RoD) strategies are often implemented in Mobile Networks to reduce the energy consumption, by dynamically adapting the available radio resources to the varying user demand. In addition, renewable energy sources are widely adopted to power base stations (BSs), making the mobile network more independent from the electric grid. At the same time, the Smart Grid (SG) paradigm is deeply changing the energy market, envisioning an active interaction between the grid and its customers. Demand Response (DR) policies are extensively deployed by the utility operator, with the purpose of coping with the mismatches between electricity demand and supply. The SG operator may enforce its users to shift their demand from high peak to low peak periods, by providing monetary incentives, in order to leverage the energy demand profiles. In this scenario, Mobile Operators can play a central role, since they can significantly contribute to DR objectives by dynamically modulating their demand in accordance with the SG requests, thus obtaining important electricity cost reductions.
The contribution of this thesis consists in investigating various critical issues raised by the introduction of photovoltaic (PV) panels to power the BSs and to enhance the interaction with the Smart Grid, with the main objectives of making the mobile access network more independent from the grid and reducing the energy bill.
When PV panels are employed to power mobile networks, simple and reliable Renewable Energy (RE) production models are needed to facilitate the system design and dimensioning, also in view of the intermittent nature of solar energy production. A simple stochastic model is hence proposed, where RE production is represented by a shape function multiplied by a random variable, characterized by a location dependent mean value and a variance. Our model results representative of RE production in locations with low intra-day weather variability. Simulations reveal also the relevance of RE production variability: for fixed mean production, higher values of the variance imply a reduced BS self-sufficiency, and larger PV panels

are hence required. Moreover, properly designed models are required to accurately represent the complex operation of a mobile access network powered by renewable energy sources and equipped with some storage to harvest energy for future usage, where electric loads vary with the traffic demand, and some interaction with the Smart Grid can be envisioned. In this work various stochastic models based on discrete time Markov chains are designed, each featuring different characteristics, which depend on the various aspects of the system operation they aim to examine. We also analyze the effects of quantization of the parameters defined in these models, i.e. time, weather, and energy storage, when they are applied for power system dimensioning. Proper settings allowing to build an accurate model are derived for time granularity, discretization of the weather conditions, and energy storage quantization.

Clearly, the introduction of RE to power mobile networks entails a proper system dimensioning, in order to balance the solar energy intermittent production, the traffic demand variability and the need for service continuity. This study investigates via simulation the RE system dimensioning in a mobile access network, trading off energy self-sufficiency targets and cost and feasibility constraints. In addition, to overcome the computational complexity and long computational time of simulation or optimization methods typically used to dimension the system, a simple analytical formula is derived, based on a Markovian model, for properly sizing a renewable system in a green mobile network, based on the local RE production average profile and variability, in order to guarantee the satisfaction of a target maximum value of the storage depletion probability.

Furthermore, in a green mobile network scenario, Mobile Operators are encouraged to deploy strategies allowing to further increase the energy efficiency and reduce costs. This study aims at analyzing the impact of RoD strategies on energy saving and cost reduction in green mobile networks. Up to almost 40% of energy can be saved when RoD is applied under proper configuration settings, with a higher impact observed in traffic scenarios in which there is a better match between communication service demand and RE production. While a feasible PV panel and storage dimensioning can be achieved only with high costs and large powering systems, by slightly relaxing the constraint on self-sustainability it is possible to significantly reduce the size of the required PV panels, up to more than 40%, along with a reduction in the corresponding capital and operational expenditures.

Finally, the introduction of RE in mobile networks contributes to give mobile operators the opportunity of becoming prominent stakeholders in the Smart Grid environment. In relation to the integration of the green network in a DR framework, this study proposes different energy management policies aiming at enhancing the interaction of the mobile network with the SG, both in terms of energy bill reduction and increased capability of providing ancillary services. Besides combining the possible presence of a local RE system with the application of RoD strategies, the proposed energy management strategies envision the implementation of WiFi

offloading (WO) techniques in order to better react to the SG requests. Indeed, some of the mobile traffic can be migrated to neighbor Access Points (APs), in order to accomplish the requests of decreasing the consumption from the grid. The scenario is investigated either through a Markovian model or via simulation. Our results show that these energy management policies are highly effective in reducing the operational cost by up to more than 100% under proper setting of operational parameters, even providing positive revenues. In addition, WO alone results more effective than RoD in enhancing the capability to provide ancillary services even in absence of RE, raising the probability of accomplishing requests of increasing the grid consumption up to almost 75% in our scenario, twice the value obtained under RoD. Our results confirm that a good (in terms of energy bill reduction) energy management strategy does not operate by reducing the total grid consumption, but by timely increasing or decreasing the grid consumption when required by the SG. This work shows that the introduction of RE sources is an effective and feasible solution to power mobile networks, and it opens the way to new interesting scenarios, where Mobile Network Operators can profitably interact with the Smart Grid to obtain mutual benefits, although this definitely requires the integration of suitable energy management strategies into the communication infrastructure management.

Contents

List of Tables

List of Figures

Chapter 1

Introduction

Nowadays, Mobile Network Operators are enforced to deploy denser and denser mobile access networks, due to the staggering increase of the mobile traffic observed in the recent years, and that is bound to further grow at remarkable pace in the next future. According to 2017 Cisco forecast [31], by 2021 there will be nearly 4.6 billion Internet users worldwide, accounting for almost 60% of the global population. 27 billion of networked devices and connections are expected by the same year, with up to 13 connected devices per capita in North America and Western Europe. Furthermore, the global IP traffic will raise to 3.3 zettabytes, of which 73% will be wireless traffic, with mobile traffic accounting for the 20% [31]. In particular, smartphone traffic will exceed PC traffic by 2021, showing a sevenfold increase in the period 2016-2021, with mobile data traffic growing twice as fast as fixed IP traffic and becoming 17% (almost 2.5 fold higher with respect to 2016) of the total Internet traffic [31]. This substantial raise in the cellular traffic entails the need of deploying properly dimensioned cellular networks, allowing to make Internet access available everywhere and providing the high bandwidth capacity required for the increasing number of mobile users and for the introduction of applications that result more and more demanding in terms of bandwidth requirements. More than 4 billion base station installations could be counted worldwide back in 2012, and this number is bound to remarkably increase due to the aforementioned reasons [92]. Considering that the access segment is responsible of up to 80% of the total network consumption, it appears evident how the energy demand to operate cellular networks is rapidly growing and Mobile Operators are facing huge operational costs due to power supply [12]. Furthermore, mobile networks are usually dimensioned for satisfying peak traffic load, hence deployed according to an over-provisioning principle, in order to always accomplish the user demand. Nevertheless, the energy consumption for Long-Term Evolution (LTE) Base stations (BSs) is very little traffic proportional. Indeed, at least 80% of the maximum BS energy demand is anyways consumed even during off peak periods. Considering that over-provisioned mobile networks actually result underutilized for most of the time, due to the high

traffic variability, this means that huge amounts of energy are wasted during periods of low traffic load. Hence, several research efforts are devoted to the deployment of effective solutions to make mobile networks more energy efficient, with the twofold objective of reducing costs and improving sustainability.
To this extent, Resource on Demand (RoD) strategies are often applied to wireless networks to make them more energy efficient, by dynamically adapting the available radio resources to the varying user demand [15]. During off peak periods, unneeded radio resources can be switched off in order to save energy, trading off energy efficiency and Quality of Service constraints, providing both acceptable levels of available bandwidth and reasonable frequencies of switching on/off operations.
In addition, the integration of renewable energy (RE) sources in mobile networks to power BSs results to be a promising approach for making the mobile network more independent from the electric grid. The installation of a local generator to produce solar energy for the cellular network operation is a solution widely deployed in real implementations. Indeed, according to estimates from [110], almost 43,000 solar powered BSs could be counted worldwide in 2014, and more than 390,000 renewable powered BSs are expected to be newly installed in the period 2012-2020, at a rate that will grow up to 84,000 per year in 2020, 6 fold higher with respect to 2012 [92]. This approach is typically adopted in some remote regions or emerging countries, in order to provide energy supply where the traditional power grid is either unreliable, due for instance to frequent power outages, or it is not available at all. This solution may result economically effective also in rural areas, where the installation of a local renewable energy generator may be less costly than bringing a power cable to the BS. Even in urban environments, bringing a power connection to a BS may require digging across a street or a park, with the associated bureaucracy burden. One of the main issues to be tackled in case of solar energy powering is represented by the intermittent nature of renewable energy generation, leading to erratic and rather unpredictable production patterns. Hence, some kind of storage must be envisioned in order to harvest any extra amount of renewable energy that is not immediately used, and to make it available for future usage when no renewable energy is currently produced. This solution looks promising also in terms of cost reduction, both capital expenditure (CAPEX) and operational expenditure (OPEX), since the initial investment for providing the required infrastructure -photovoltaic (PV) panels and a storage system to harvest extra amounts of produced renewable energy- is compensated on the medium term by the decrease in the amount of energy bought from the grid [33]. The increasing relevance of renewable energy sources in powering mobile communication networks motivated several research groups to investigate the topic. Currently, several papers are available in the literature focusing on the potentiality of powering BSs with solar energy, considering a setup where the BS is paired with a photovoltaic panel [27, 81, 24, 26, 83, 25, 6, 72, 8, 113].
In this context, the Smart Grid (SG) paradigm is deeply changing the energy market, envisioning several distributed energy sources rather than a single centralized

supplier and integrating renewable energy sources. In a similar system, the end user is not merely a consumer, but may become a *prosumer*, i.e. a consumer and a producer at the same time, possibly injecting part of its generated energy into the electric grid. Hence, the power grid has become not merely a provider supplying energy to passive end users, but an active and dynamic interaction between the grid and customers is entailed, leading to bidirectional flows both in terms of energy and information exchanges. In particular, the SG framework enables the grid operator to effectively perform critical tasks, such as load leverage and voltage control. One of the challenges of new electricity generation and distribution networks is coping with the mismatches between electricity demand and supply, mismatches that are more difficult to predict due to the presence of renewable sources. Indeed, the increasing penetration of distributed renewable energy generators in the SG, integrated alongside traditional synchronous centralized generators, has been responsible of the huge diffusion of the Demand Response (DR) paradigm in recent years. On the one hand, the presence of several additional distributed power generators may more frequently lead to overrun the absorptive capacity of the traditional power grid, causing system instability or failure [79]. On the other hand, the erratic nature of renewable energy production increases the risk of requiring the activation of additional high inertia generators, in case of peak power demand and low renewable energy production, and this is neither desirable nor effective in providing the needed energy supply in a short time. The DR approach represents a typical paradigm adopted with the purpose of adapting the energy demand to the energy supply availability rather than vice-versa. In particular, *Price Based Programs* are often adopted as effective methods to flatten the pattern of energy demand, by adjusting the energy prices over time, depending on the varying energy load. Users are incentivized to shift their demand from high peak to low peak periods, by receiving a monetary reward or penalty, depending on whether they are able or not to accomplish the request from the SG of increasing or decreasing their consumption [79]. To balance the demand and supply, the smart grid operator (SGO) may ask its users to decrease their energy consumption during periods of peak demand and raising the grid consumption when the demand is low and excess grid energy is available. In return, the SG provides monetary incentives. By satisfying the requests from the grid, the end user contributes to provide *ancillary services* [54] to the SG, for which it receives some rewards, resulting in a reduction of the energy bill. Clearly, the Demand Response policies applied by the SG operator may highly affect the energy costs, by introducing huge variability in the energy prices over time. In this scenario, big consumers can have a central role. While they can significantly contribute to DR objectives by adapting their (huge) demand, their convenience consists in the possibility to obtain important electricity cost reductions. Telecommunication mobile operators are an example of such big consumers. Today, operators are experiencing huge costs to power their devices and this is expected to get even worse in the future. At the same time, they

have some possibility to act on their network by dynamically modulating its energy consumption in accordance with SGO requests. In this context, the cooperation between a renewable powered mobile network and the SG in a Demand Response framework gives raise to great potential for achieving mutual benefits, in terms of enhanced ancillary service provisioning for the SGO and cost reduction for the Mobile Network Operator (MNO). To this aim, properly designed energy management strategies can be useful to improve the interaction of the mobile network with the smart grid and to decrease the MNO operational expenditures. In particular, the reaction to the requests of decreasing the consumption from the grid can be accomplished by exploiting the local production of renewable energy to power the BSs, or by drawing previously harvested energy from the battery. In addition, the application of Resource on Demand strategies allows to switch off unneeded BSs to reduce the energy taken from the grid. A further option that will be specifically investigated in this work is the implementation of WiFi offloading (WO) techniques, allowing to move some of the mobile traffic to neighbor Access Points (APs), in order to satisfy the requests of decreasing the consumption from the grid, even by possibly increasing the number of BSs that can be switched off under Resource on Demand policy. Finally, requests of increasing the grid consumption cannot be accomplished by raising the traffic load on demand. Nevertheless, in case of a green mobile network, the presence of a local storage may allow to draw some extra energy from the grid when required, that can be harvested in the battery and used in the future.

In this work a scenario consisting of a mobile access network is considered in order to investigate various critical issues raised by the introduction of renewable energy to power the BSs and by the possible interaction with the Smart Grid, with the main objectives of making the mobile network more independent from the grid and reducing the energy bill. In particular, focusing first on the PV powering system of a BS that is part of a mobile network, this work proposes a simple stochastic model of the energy produced by PV panels and investigates the impact of the energy generation variability on the power supply system performance and its dimensioning (Chapter 4). In relation to various stochastic models that are proposed to characterize the green mobile network operation (Chapter 5), we investigate the impact of parameter quantization on the design of RE power systems for cellular BSs (Chapter 6). Furthermore, the problem of renewable energy system dimensioning is studied, both by means of simulation tools and by deriving analytical formulas for system dimensioning (Chapter 7). To this extent, techniques aiming at increasing the energy efficiency are deployed and their impact on the dimensioning of the renewable energy system is analyzed. In addition, part of this work is

devoted to investigate the impact of energy saving techniques on RE system dimensioning and costs (Chapter 8). Finally, a consistent part of the study focuses on the design of energy management strategies allowing to enhance the interaction between the MNO and the SG, with the twofold objective of cost saving and ancillary service provisioning (Chapter 9). These energy management strategies envision the introduction of local RE generators equipped with some storage units, besides the possible application of RoD policies and WiFi offloading techniques to further improve the interaction with the SG. The potentiality of a local RE generator and of each energy saving technique, either applied alone or variously combined with each other, to improve the capability of providing ancillary services and saving operational costs, is analyzed via simulation and by means of Markovian models.
Further details about the objectives of our work and the various topics addressed in our study, along with related work information, are provided in the next chapter (Chapter 2). In Chapter 3 a general description of the investigated scenario is proposed and a methodology overview is presented. Moreover, this chapter provides the description of the energy saving techniques introduced in this study end of the energy management policies proposed to operate in a Demand Response context. Finally, Chapter 10 presents the conclusions.

Chapter 2

Contribution and related work

The specific contributions provided by this study in relation to different topics connected to renewable powered mobile networks are now detailed, and the related work is discussed in each corresponding section.

2.1 Coping with the intermittent nature of renewable energy production

Mobile system implementations where RE derived from the conversion of solar radiation by means of PV panels is used to power BSs, are currently deployed to address the unreliability or unavailability of the traditional electric grid in remote regions, islands or in some emerging countries. Indeed, the frequent and unpredictable power outages that the grid may undergo in some countries, like in India [90], affect the continuity of the mobile service. This aspect has represented the main driver pushing the research towards feasible solutions to provide a continuous energy supply, alternative to those usually available, like diesel generators. The latter are typically adopted as additional power supply, but they may show some drawbacks besides not being a green energy source (high fuel transport cost, possible fuel stealing in unattended areas) [90]. Several examples of actual implementations of mobile access networks can be found in the literature, where the solar energy produced by locally installed PV panels is exploited to supply the BSs demand, especially in developing countries[23]. The interest about the use of RE to make communication networks more energy efficient and to reduce the electricity bill is further confirmed by the increasing number and variety of works available in the literature related to this topic [2, 59, 53].
Nevertheless, the intermittent nature of RE production is one of the main issues to be addressed when powering mobile network with green energy sources. On the one hand, the erratic production of RE makes it difficult to predict the solar energy generation profiles well in advance (i.e. more than one day in advance). On

the other hand, the mobile network operation requires a continuous power supply. Indeed, mobile traffic is very little delay tolerant, since mobile users are typically not willing to postpone their traffic demand due to mobile service unavailability for BSs running out of power supply. Hence, the presence of some storage component must be envisioned in order to save some extra amount of RE, that is not immediately used, into a battery bank, from which it can be drawn during periods in which the RE is not produced, for instance by night. Furthermore, this entails considerable criticalities in terms of system dimensioning: due to the intermittent provisioning of RE, the PV panel should be over-sized with respect to the average network power need, in order to feature sufficient capacity to guarantee high RE production level, hence satisfying the current operation need, and producing extra amounts of RE large enough to accomplish future power demand during period of null production. In addition, also the storage capacity should be properly sized to harvest extra amounts of energy required for operating the network. Of course, the dimensioning must trade off the need for continuous network operation, the requirements in terms of energy self-sufficiency of the network, along with cost and feasibility constraints. The resiliency of similar systems to power outages and their capacity to reduce or nullify the energy demand from the grid can be evaluated only in relation to the RE production, which is location dependent. Indeed, the analysis leading to a proper system dimensioning, both in terms of PV panel and battery storage size, strictly depends on a reliable characterization of the RE production profile.

Various studies are available in the literature specifically addressing the dimensioning of PV panels and storage capacity, in relation to the mobile system energy need, the possibility of taking energy from the traditional grid and the constraints imposed by costs. Real profiles of sun irradiance are often used to estimate the solar energy that can be harvested depending on the PV size and either simulate [84, 80, 18] or model [21] the behavior of the storage system [57]. It is known that RE production and PV system performance are highly affected by weather variability; for this reason, predicting and modeling this variability is a quite critical task. Many studies in the literature provide stochastic models of solar irradiance, rather than energy production, over different time scales. In [50] both the short-term and long-term variations of daily solar power are characterized. In [98], the authors start from data collected during twenty years in a region in Algeria and model the monthly production using several distributions: the Weibull, Gamma, Normal, logistic, lognormal and loglogistic distributions. Some of these distributions are used in [28] for predicting daily solar irradiance, for six different locations in Taiwan that have limited seasonal variability. While modeling a hybrid wind/solar system, in [78] a Beta distribution is used to model solar irradiance observed on a shorter time scale of the order of a few hours. Beta distribution for solar irradiance is used also in [9] and in [39]. For [9], the focus is on a stochastic model for dimensioning hybrid wind/solar systems; the model takes into account also demand variability

and the solar irradiance is considered at peak demand. In [39], the Beta distribution is used to model the hourly global solar irradiance. Stochastic models of hourly solar irradiance are proposed also in [10], that uses several distributions, including Exponential, Weibull, Geometric, lognormal, Gamma. A shorter time scale of 5 minutes is employed in [69], in this case the Normal distribution is used; one-minute irradiance is considered in [117].

Our work, considering the PV powering system of a BS that is part of a mobile network, aims first at proposing a simple stochastic model for the energy produced by PV panels of relative small size. The model is deployed from the study of real patterns of the solar irradiance in the city of Turin, and a shape function is identified, corresponding to the typical production profile of a day. The function is then scaled through a random variable, that represents the daily variations of the RE production. The model can be used at different time scales, in order to model the RE production either adopting a hourly or daily time granularity. Second, this study investigates the impact of the energy generation variability on the power supply system performance. Finally, the same model is exploited to analyze the effect of RE production variability on the system dimensioning. The related results, presented in Chapter 4, show that the mean and variance of the random variable representing the daily generation are the key parameters needed to predict, with high accuracy, the system performance. Performance is evaluated, mainly, in terms of probability of depleting the energy storage and energy demand from the grid. Finally, as it will be better described later on Chapter 7, the proposed model will be used to derive an analytical formula that can be employed as a useful tool for system dimensioning.

2.2 Designing models to characterize the green mobile network operation

Several studies are available in the literature that investigate the operation and performance of green mobile networks [46, 7, 95, 33, 36, 41, 96, 105, 47, 88]. Some authors analyze the behavior of the RE powered mobile system by means of simulation processes, like in [80] and [85], whereas many papers are based on stochastic models to characterize the green mobile network operation. In particular, Markovian models are frequently adopted to represent the dynamics of the battery charge level in scenarios where BSs are powered by hybrid energy sources. These models based on Markov chains represent an effective tool for studying systems at the steady state, allowing to investigate the average behavior of the system, which is useful for system dimensioning and cost prediction. [19] adopts a multistate Markov model representing the hourly harvested solar energy, whereas [21] proposes an analytic model to evaluate the outage probability of a renewable powered BS, and a discrete time Markov process is adopted to represent the battery charge level. Even

in [116] a discrete time Markov chain is used to model the green network operation and to evaluate the battery depletion probability. Authors in [25, 112, 77] relied on Markovian models for computing the BS outage probability for solar powered BS. [25] proposes a discrete-time Markov chain of the battery charge at the BS, also taking into account weather conditions to classify the day type in terms of solar energy production level. In [112], a Markovian model of the energy storage model is employed to deploy a power availability framework for solar energy generation. Authors in [77] consider two Markov chain models based on solar irradiation data in two or three consecutive days, to investigate the impact of correlations in weather conditions.

In accordance with studies available from the literature, the analysis of the solar powered mobile system performance is performed in our work either via simulation tools or by means of stochastic models. In particular, various types of Markov chain models are designed, featuring different connotative characteristics depending on the different aspects they are focused on and on the main investigation objectives they aim to achieve. These Markovian models are presented in Chapter 5.

First, a Markovian model embedding weather condition information is deployed in Sec. 5.1. A discrete time Markov chain is employed to represent the operation of a RE powered BS, with states characterized by state variables corresponding to the battery charge level, the daytime and the type of daily weather condition. The purpose of this model is to investigate the impact of the quantization adopted for various parameters, included in the configuration settings of the model, on the design of RE power systems for cellular BSs. The results related to the quantization issue are presented in Chapter 6.

Second, a very simple model, based on a 3-state only discrete time Markov chain, is designed in Sec. 5.2 to model the state of the battery charge of a single RE powered BS. In this case, the 3-state Markov chain is built as a simplified easy-to-use model to derive an analytical formula for system dimensioning purposes, as it will be detailed in Chapter 7.

Finally, a more complex Markov model, described in Sec. 5.3, is deployed to represent the operation of a mobile network in a scenario where multiple BSs are present, powered by RE and grid energy. This N-state model is deployed with the aim of specifically studying the interaction of the cellular network with the Smart Grid in a Demand-Response framework. Hence, in this model, each states is defined not only by the battery charge level and by the day time, but also by the type of requests issued by the SG over time. Results derived from the application of this model will be presented in Chapter 9.

2.3 Quantization issues in modeling green mobile networks

As already mentioned in the previous section, several studies about solar powered mobile networks rely on Markovian models for computing the BS outage probability for solar powered BS. Depending on the considered work, different granularities are adopted for the discretization of the various parameters adopted in the model configuration, like the battery charge and RE production levels, the mobile network energy demand, the time of the day, the type of day based on the weather conditions. For example, [25] proposes a discrete-time Markov chain of the battery charge at the BS. As stated by the authors, the model can be used to quantify the relationship between system parameters, such as PV panel size, battery size, harvested solar energy and load profiles, on the BS outage probability. In this model, time is discretized with time slots of 1 hour. As regards weather conditions, each day is classified according to 3 categories, resulting in 3 different possible levels of daily renewable energy production, and of harvested energy profiles. The battery charge level is quantized into rather large blocks of 1 kWh. In [112], a Markov-chain-based energy storage model is defined, to develop a power availability framework for PV panel generation. The model may assist in planning both large and small-scale grid-integrated PV generation, and also quantify power availability. This work investigates the application of the model in a scenario where the load is represented by 300 households, with an average daily energy usage of about 17.6 kWh per household. The time granularity adopted in this study is 1 hour, whereas the energy storage is quantized into steps of 20 kWh (note that the average hourly energy consumption is about 220 kWh, so that the battery charge quantization is about 1/10 of the energy consumption in a time slot). No classification of the daily level of renewable energy production based on historical data is considered. Leonardi *et al* [77] consider two Markov chain models in their analysis: the first one based on solar irradiation data in two consecutive days, and the second based on solar irradiation data in triples of consecutive days, with the objective of exposing the influence of correlations in weather conditions. Different numbers of quantization levels (5, 8 and 10) are considered for the daily irradiance. A fixed number of quantization levels is assumed for the energy storage, equal to 100, hence the discretization step sizes vary depending on the considered battery capacity (10 kWh, 25 kWh, 50 kWh). Both solar energy generation and energy consumption are accounted on a daily basis. Moreover, only the impact of different battery size on the system performance is analyzed. The main result is that both models produce almost equivalent results, so that the impact of weather correlation is small.
The selection of variable discretization settings of the various parameters defined in similar models may have the potential of highly affect the evaluation of the system

performance when the model is applied to investigate the operation of a green mobile network. Indeed, different choices made in terms of parameter discretization may potentially lead to different results that actually depend on the parameter quantization that is adopted rather than on the specific scenario that is investigated. However, none of the studies available in the literature takes into account the effects derived from configuring the setting of the various model parameters. Hence, in order to perform this analysis, we deploy a Markovian model, that is described in Sec. 5.1. Although our model is similar to the one based on solar irradiation data in two consecutive days proposed in [77], to the best of our knowledge this is the first work that carefully investigates the impact of quantization of i) weather characteristics, ii) time slot duration, and iii) battery capacity, on the key performance measures of power systems based on renewable energy for cellular network BSs. Our results, presented in Chapter 6, show that the discretization steps play a significant role in understanding the behavior of such power systems, hence in correctly dimensioning them.

2.4 Dimensioning renewable energy generation systems in mobile networks: trading off energy self-sufficiency and feasibility

As already mentioned, the erratic nature of RE generation raises significant criticalities in terms of RE system dimensioning, strictly linked to the location depending variability of solar energy generation cited in Sec. 2.1. The process of system dimensioning should carefully balance opposing interests, like the guarantee of service continuity, the requirements in terms of energy self-sufficiency of the network, along with cost and feasibility constraints.
Various studies in the literature investigate algorithms to efficiently manage the locally produced renewable energy and to properly exploit the energy storage, or Resource on Demand techniques, in order to make the green mobile network more independent from the electric grid and to improve the capability of facing possible power outages, sometimes providing cost analysis [46, 7, 95, 33, 36, 41, 96, 105, 47, 88]. In some paper studying the application of energy management strategies in green mobile networks connected to the Smart Grid, performance evaluations are conducted under variable combinations of PV panels and battery sizing [105]. Authors in [87] propose a stochastic model to represent the photovoltaic energy produced to power BSs. The model is applied considering different locations and solar panel sizes. Other works, aim at modeling the behavior of BS power systems based on renewables, with the objective of understanding the characteristics of these systems, so as to provide generic guidelines for correct dimensioning [81, 24, 26, 83, 25, 112, 77]. Nevertheless, only few studies explicitly focus on the system dimensioning

issue and thoroughly evaluate the impact of variable system sizing on the renewable powered network performance, in order to derive a proper system dimensioning [33, 118, 80, 85, 18, 19, 21, 52, 5]. Authors in [118] aim at achieving a feasible system dimensioning by proposing an algorithm to dynamically adapt the mobile service of a renewable powered base station, based on the current energy available at the storage, the weather forecast and the historical pattern of base station consumption. [80] and [85] analyze, via simulation, the problem of properly sizing a PV generator and the energy storage in order to provide adequate power supply for a single BS, providing cost analysis and battery lifetime evaluation. Authors in [18] deploy a model to derive the optimal combination of PV panel and storage size for powering a BS, subject to the predefined constraint on the worst month outage probability. [19] adopts a multistate Markov model representing the hourly harvested solar energy to find the optimal system dimension allowing to minimize cost, given the limit on the maximum allowed battery depletion probability at a solar powered BS. The analytic model proposed in [21] is applied to evaluate the outage probability of a renewable powered BS, and a discrete time Markov process is adopted to represent the battery charge level. In [52] a green energy provisioning method is proposed, in order to address the system sizing issue when deploying a green energy system to power base stations. The presented solution applies a traffic load balancing algorithm with the aim of minimizing the CAPEX, still satisfying the constraints on the Quality of Service. [20] proposes a methodology for sizing the capacity of a RE generator system to power stand-alone base stations. Unlike most studies that usually base the prediction of RE production on the irradiation data observed during the Typical Meteorological Year (TMY), [20] employs series-of-worst-months (SWM) meteorological data, making the technique more accurate in obtaining a proper dimensioning.

To this extent, in our work a renewable powered mobile network is first studied via simulation under different combinations of PV panel and system sizes, with possible application of Resource on Demand strategies, and trading off the battery depletion probability, the feasibility constraints and the capital expenditures. Then, we investigate the introduction of RoD and WiFi offloading techniques to improve the interaction of a green mobile network with the Smart Grid, in a Demand Response context. The impact of the system dimensioning on the capability of accomplish the Smart Grid requests of dynamically increasing or decreasing the energy consumption is evaluated via simulation under various configurations of the renewable powered network scenario. Our results, presented in Chapter 7, show that while a feasible PV panel and storage dimensioning can be achieved only with high costs and large powering systems, by slightly relaxing the constraint on self-sustainability it is possible to significantly reduce the size of the required PV panels, by up to 41.3%, along with a reduction in the corresponding capital and operational expenditures. Results related to the impact on system dimensioning of energy saving techniques (i.e. RoD and WiFi offloading), possibly applied in a Demand Response

framework, are presented in Chapters 8-9. Considering a green mobile network in a Demand Response framework, our results prove that even with relatively small PV panel and storage dimension, the energy bill can be completely nullified, whereas under larger RE system size positive revenues can be achieved.
Finally, the papers available in the literature typically address the dimensioning issue proposing simulation or optimization methods. However, the process of dimensioning a renewable generation system to power BSs by means of simulations or optimization models may be computationally complex and require long computational time. A further contribution presented in this study in Sec. 7.2.2 aims at providing a simple analytical method for properly sizing a renewable system in a green mobile network, based on the local RE production profile. To the best of our knowledge, this is the first work proposing an analytical formula allowing to determine the capacity of PV panels and batteries required to power BSs in a given location, in order to guarantee the satisfaction of a defined constraint on the maximum allowed storage depletion probability.

2.5 Looking for energy efficiency and cost reduction in green mobile access networks

Given the intermittent and unpredictable nature of RE production, the design of the BS power supply requires a careful dimensioning of the generators and energy storage capacity. Moreover, the possibility to introduce energy efficient techniques to adapt the electric load of the BS (i.e. its consumption) to renewable energy availability is very interesting to this extent. Indeed, the introduction of RE alone may help to reduce the energy cost but it may not be sufficient to make the mobile network completely self-sufficient in terms of energy consumption. Typically, the traffic load in a mobile access network dynamically varies over time and peak loads are achieved only for limited periods. Hence, the deployed radio resources result to be redundant for a considerable fraction of time. RoD strategies allow to target this issue by dynamically adapting the available radio resources to the current actual energy need of the network, making the network energy consumption more proportional to the actual user demand [15]. Based on user demand, unnecessary BSs can be turned off when the load is low and energy can be saved. RoD approaches implying BS sleep modes are commonly adopted to make mobile networks more energy efficient, often combined with the use of RE to power the BSs and make mobile networks more independent from the grid [120, 59, 17]. Various studies are currently available related to the application of BS sleep mode based RoD strategies to RE powered BSs, and, depending on the objectives, various sleep mode based algorithms can be applied for managing the radio resources [47, 88, 36, 125]. [125] proposes an optimal sleep policy obtained through dynamic programming, along with a computationally simpler heuristic algorithm allowing to avoid power outages

for BSs exclusively relying on renewable energy production. In [88] an ON/OFF switching algorithm, based on reinforcement learning, is deployed to optimize the self-sustainability of RE powered small cells in mobile networks. [36] considers a real mobile network in a urban area to deploy different switching ON/OFF strategies, that aim at reducing the energy bought from the grid and whose algorithms take into account the probability of facing power outages in the next future. Authors in [47] propose a framework to efficiently allocate spectrum resources to users and, at the same time, switch off unneeded BSs, in order to minimize the power consumption. Whereas the available studies are usually focused on the objective of making the RE powered BSs more (or fully) self-sustainable, by reducing the risk of power outages, the relationship between the application of RoD strategies and the dimensioning of the RE system and its effects on the probability of facing some outage due to storage depletion are not well investigated. Moreover, cost analysis does not usually include the evaluation of capital expenditures due to the installation of PV panels and battery, and the operational cost related to the system maintenance and battery replacement.
In this work, we study how the application of an energy saving strategy based on a RoD approach affects the operation of a mobile access network in which BSs are powered by PV panels and equipped with energy storage units. We investigate the effectiveness of the RoD strategy in reducing the energy need of the green mobile system, making the network more self-sustainable. Furthermore, we evaluate the impact of the strategy on the energy storage and PV panel dimensioning. A specific contribution of our work consists of a cost analysis that is conducted including not only operational expenditures (OPEX), but also the initial investment (CAPEX) for the PV panels and the storage. The cost estimation is performed keeping into account the expected lifetime of solar panels and battery units, depending, in the case of batteries, on the deterioration processes occurring during the system operation due to several different factors. Our results, derived by means of simulation tools and reported in Chapter 8, show that up to almost 40% of energy can be saved when RoD is applied under proper configuration settings, with a higher impact observed in traffic scenarios in which there is a better match between communication service demand and RE production. Furthermore, a slight relaxation of the network energy self-sufficiency constraint allow to obtain a remarkable raise in the cost saving, with up to more than 40% reduction in CAPEX+OPEX costs.
As it will be better described in Sec. 2.6, an additional contribution provided by this study is investigating the role of RoD in a Demand Response framework, in order to better react to the requests from the Smart Grid. Highlights about the related results, extensively presented in Chapter 9, are given in the following Section.

2.6 Mobile network operators as new significant stakeholders in the Smart Grid

In the recent years, an increasing diffusion of the Smart Grid concept has been observed. The power grid has become not merely a provider supplying energy to passive end users, but it can dynamically interact with its clients by means of a bidirectional communication channel, almost in real-time. In particular, the SG framework enables the grid operator to effectively perform critical tasks, such as load leverage and voltage control. One of the challenges of new electricity generation and distribution networks is coping with the mismatches between electricity demand and supply, mismatches that are more difficult to predict due to the presence of renewable sources. However, by making the grid "smart" and capable of interacting with the customers, it is possible to introduce new paradigms of electricity supply and consumption in which the customers take actively part in the process.

A typical paradigm adopted to this extent is represented by the Demand Response approach, aiming at adapting the energy demand to the energy supply availability rather than vice-versa. With DR approaches the SG Operator aims at maintaining the demand-supply balance, by providing monetary incentives to adapt the energy consumption to the production curve. To cope with production excesses, the SGO enforces its users to decrease their energy consumption during periods of peak demand, by letting energy prices rise. Conversely, users are induced to increase the grid consumption when the demand is low and excess grid energy is available, by setting low energy prices or by providing some kind of reward. By satisfying the requests from the grid, the end user contributes in providing *ancillary services* [54] to the SG. Furthermore, in the Smart Grid context, the use of harvested RE can be directed into several objectives such as reducing the grid energy, decreasing the carbon emissions and minimizing the energy cost [54]. The latter is of high importance considering the huge and continuous increase of mobile networks electric cost, which is caused by the tremendous increase in traffic. Thus, many studies focus on managing the usage of harvested RE (consuming, procuring, storing or sharing) and using energy efficiency techniques (radio resource management, switching-off base station, etc.) to reduce the grid energy cost. It should be noted that using renewable energy to satisfy other objectives are extensively studied and interested readers can see more studies in [54, 2]. The problem of minimizing the electricity bill for a cellular BS powered by the Smart Grid and locally harvested RE considering hourly-varying electricity prices known a day ahead is considered in [75]. Several online energy management strategies that require only causal knowledge of RE generation and the power consumption profiles are proposed and compared with the optimal energy management policy. Simulation results show that the performance of the proposed online strategy deviates from

the optimal by 2% at most. Similarly, authors of [91] study adaptive power management for wireless BS powered by local RE sources and the Smart Grid under several uncertainties such as generated power from renewable sources, power price from the electrical grid, and power consumption of the wireless BS due to varied traffic. The aim is to minimize the cost of energy consumption as well as meet the users demand. A multi-period stochastic programming model is formulated and then translated into linear programming for finding the solution of adaptive power management. Results have shown that the optimal decision of adaptive power management can successfully minimize the power cost. In [94], the authors studied the grid energy cost minimization under dynamic pricing by joint power allocation and battery management for one BS. In addition to RE allocation, the energy demand of the BS is reduced by delaying some data when the price of electricity is high. The problem is modeled as a stochastic program. Without the knowledge of future information, an online algorithm is proposed and solved using Lyapunov optimization technique. In [48], the authors proposed a heuristic algorithm to achieve a trade-off between the network operator profit and its CO_2 gas emissions while satisfying a certain Quality of Service (QoS) requirement. An energy procurement scheme for active BSs is provided from different retailers, and further energy savings and CO_2 emissions reduction is achieved using BS ON/OFF switching. In [55], the authors proposes an iterative approach that manage the use of renewable energy, adapt the transmitting power and switch-off base stations to reduce the energy operational cost of the network considering real-time price of grid energy. A dynamic programming approach to minimize the on-grid energy consumption in a large-scale green cellular network supported by the SG is employed in [29]. BSs are aggregated as a microgrid equipped with RE and central energy storage. The authors jointly designed an optimal BS ON/OFF operation and on-grid energy purchase policies in a time-varying traffic load and real-time price of grid energy. Authors in [40] employ stochastic geometry to determine the amount of energy provided by multiple energy suppliers to various mobile operators, in order to maximize their profitability while satisfying the Quality of Service requirements in terms of mobile coverage. In [45], the authors combine a RoD approach based on BS switching on/off with an energy management policy in a Demand Response context. The interactions between multiple mobile operators and energy retailers with a number of renewable sources are investigated by formulating an optimization problem, aiming at maximizing profits of collaborative mobile operators, achieving environmental goals and introducing more fairness among mobile operators in the procurement decision. The performance analysis in terms of impact of the RE production uncertainty is conducted by simulation, whereas no stochastic models are proposed. In [108], the authors use energy sharing and load shifting to minimize the grid energy expenditure of cellular networks powered by both grid and renewable energy. The problem is formulated as a mixed-integer non-linear programming (MINLP) and proposes a cost-efficient centralized algorithm leveraging the univariate search

technique. Moreover, the authors proposed a three-phase distributed control policy, where base stations and mobile users adjust their strategies independently only with their local information. In [41], the authors proposed a hybrid energy sharing framework for cellular network where physical power lines and energy trading with other BSs using smart grid is used. The energy management framework determines the quantities of electricity and RE to be procured and exchanged among BSs, respectively, while considering battery capacities and real-time energy pricing. Both the proposed paper and our work aim at reducing the energy cost of the cellular network. For more studies of cellular networks powered by renewable energy and the Smart grid see [60]. In the mentioned studies, cellular networks apply energy management algorithms and use energy efficient techniques to reduce the energy cost by enrolling in *demand response methods* based on real-time price of energy. To the best of our knowledge, we were the first to consider the case of renewable-powered mobile network to provide the Smart Grid with ancillary services [58]. In contrast to previous studies, where network decisions are made based on the real-time price of grid energy, the Smart Grid explicitly asks the cellular network, enrolled in demand response based on provide ancillary services, to increase or decrease its consumption in return for monetary incentives. This approach aims not only at minimizing the energy operational cost, but also participates in providing ancillary services to help the SG balance its energy load in a Demand Response framework [58]. Techniques to provide ancillary services in a Demand Response context have been widely investigated in the case of industrial, household, Heating, Ventilation and Air Conditioning (HVAC) loads and with electric vehicles in Vehicular-to-Grid (V2G) scenarios [68]. On the contrary, in the telecommunications field, the provisioning of ancillary services has only been studied mainly in Data Centers [62, 119], whereas very few papers have considered its application in mobile access networks.

In [58], ancillary services are provided in a RE-powered mobile network scenario by exploiting delay tolerant users. Delay tolerant users are flexible users that agree on accepting a possible additional (limited) delay before accessing the network. Their availability to postpone their access to the network services allows to reduce the energy consumption, for example by deactivating some sectors of a BS, either for obtaining longer periods of energy saving or for adapting the load to better accomplish the Smart Grid requests. The study is limited to a single base station managed by a heuristic algorithm, whereas results are solely based on simulations. Our study aims at investigating the performance of a renewable energy-powered heterogeneous cellular network that is providing ancillary services to the Smart Grid. An energy management strategy is designed to better react to the SG requests, hence increasing the received rewards, possibly applying a Resource on Demand strategy. The network is modeled as a Markov chain, and the performance is evaluated in terms of probability of low storage, probability of wasting harvested renewable energy and the total cost of network operation, under different configuration of the system

sizing, thus supporting the process of properly dimensioning the RE system. Unlike most of the studies that solely focus on the benefits of cellular network (decrease in operation cost usually) while engaging in the demand response, this work evaluates the effect of the cellular network on the Smart Grid by calculating the probability of satisfying the requests of the Smart Grid. Moreover, an optimization algorithm is used to derive proper configuration settings of the proposed energy management strategy, which allows minimizing the energy operational cost. To the best of our knowledge, our work is the first study that considers a stochastic model for studying the interaction of a renewable powered mobile network (where Resource on Demand can also be applied) with the Smart Grid in a Demand Response framework, with one of the main objectives specifically being improving the capability of providing ancillary services.

The mobile network operator may hence play a relevant role in the DR framework, by making the mobile access network actively interact with the SG and dynamically modulate its energy consumption in accordance with SGO requests. In this study, we investigate a scenario in which a green mobile network, powered by the grid and by its own RE generator, interacts with the SG to provide it with ancillary services. Among the possible DR programs, the one considered in our work envisions that every day each user, hence also the MNO, forecasts its energy consumption for the following day depending on the expected traffic, which is estimated based on historical data. The information from end users is hence collected by means of aggregators and provided to the SGO with a granularity of a timeslot with constant duration. Aggregators are entities in the electric market acting as mediators between several aggregated users and the utility operator. Since each aggregator represents a significant amount of total demand in the DR market, it can negotiate on behalf of the end users with the operator more efficiently [51].

During the next day, at every timeslot the SG announces to the end users its current request, that may be of *increasing* or *decreasing* the energy consumption from the grid with respect to the energy level forecast the day ahead. In some cases, no specific action is required. Whenever the MNO is able to accomplish the SG request of raising or decreasing the consumption, it receives a reward, proportional to the increase or reduction in the consumption, respectively; in case it does not satisfy and even opposes the request, a penalty is due, proportional to the gap with respect to the expected demand. In this way, end users are incentivized to dynamically shift their loads in order to accommodate the SGO requests, hence leveraging the consumption from the grid and balancing the energy demand with the energy supply. To properly respond to the SG requests, the green mobile network implements an energy management policy that takes into account a number of aspects: the energy that the mobile network can locally harvest through its own RE production, the availability of energy in local storage units, the possibility to

use RoD policies consisting in switching on and off micro-BSs that provide additional capacity in the considered area. The scenario is studied through a stochastic model based on Markov chains. The stochastic characterization of input variables, such as RE production, traffic load, SG requests, is based on real traffic traces. The system performance is evaluated by deriving various performance parameters, like the average storage level, the probability of a low storage level, the probability of satisfying the requests of the SG, the RE wastage and the operational cost. Finally, this work analyses the impact of a RoD approach in increasing the gain in terms of cost, thanks to a better response to the grid demands. The results, reported in Chapter 9, show that the introduction of RE to power the mobile access network, combined with Resource on Demand strategies, has the potential for improving the interaction with the SG within a DR dynamics, resulting in a more autonomous network capable of better answering the requests from the grid. This results, on one hand, in a remarkable contribution of the mobile network in providing ancillary services. On the other hand, this leads to a significant additional cost reduction for the MNO, thanks to the improved interaction with the SG.
A further contribution provided in this study is the introduction of WiFi offloading technique to evaluate its impact on improving the interaction with the Smart Grid of a green mobile network in a Demand Response context. WiFi offloading consists in transferring a portion of the mobile traffic from the BSs to some nearby WiFi Access Points (APs). This technique is commonly adopted to relieve mobile access networks from a part of their traffic load during peak hours in heterogeneous networks. Indeed, WO represents a widely adopted technique allowing to migrate traffic from cellular networks to WiFi networks to tackle the recent explosion of mobile data traffic [61, 99]. Authors in [47] analyzed the effects of cooperation between a renewable powered mobile network where RoD is applied, on the one hand, and, on the other hand, private femto cell access points that accept to serve external users. However, the application of WiFi offloading to a green mobile network in a Demand Response context to evaluate the impact on the interaction with the Smart Grid has not yet been investigated in the literature.

In our study, WiFi offloading is introduced as a way to decrease the traffic load whenever the SG requests a reduction of the consumption. WiFi offloading alone may not lead to remarkable reduction in the consumption, due to the limited load proportionality of energy consumption. However, when applied in a scenario where the base stations can also be switched on and off, WiFi offloading allows to further decrease the number of active BSs, hence to further reduce the system consumption. The impact of WO on improving the energy efficiency and reducing operational costs in a renewable powered mobile access network interacting with the SG, with possible application of BS sleep mode RoD strategies, is an aspect that still remains to be investigated.
Our work aims at investigating a portion of a RE powered mobile access network interacting with the Smart Grid in a Demand Response framework, where WiFi

offloading techniques are introduced to enhance the response of the cellular network to the SG requests. The assumptions and conditions under which WiFi offloading is applied in the considered scenario will be detailed and discussed at the beginning of Sec. 9.2 and in Sec. 9.2.3. The role of WiFi offloading in reducing the energy bill is analyzed via simulation and its impact on improving the capability of providing ancillary services is examined as well. Moreover, we evaluate whether the WiFi offloading approach may further benefit from the introduction of Resource on Demand strategies. Our results, presented in Chapter 9, show that the introduction of WiFi offloading provides mutual benefits for the MNO and the SG. Indeed, the application of WiFi offloading techniques combined with a properly designed energy management strategy allows to save up to 100% of the energy bill in our scenario, when WiFi offloading is applied jointly with RE powering. Furthermore, the introduction of WiFi offloading is effective in increasing the capability of providing ancillary services, in particular by raising the probability of satisfying the SG requests of decreasing the grid consumption by up to almost 75% in the scenario investigated in our study. Finally, under the application of WiFi offloading, an increase of the RE generation system size contributes to significantly increase the network performance in terms of both raising the probability of providing ancillary services and reducing operational costs, even achieving positive revenues.

Chapter 3

Scenario and methodology

A general description of the renewable powered mobile access network scenario considered in this work is provided hereafter in Sec. 3.1. Specificities of single subtypes of the main scenario are detailed in the corresponding section of chapters related to the Results (Chapters 4-9). Details about how the green mobile network is modeled in this work are presented in Sec. 3.2. Furthermore, Sec. 3.3 describes the energy saving techniques adopted in our study to make the network more energy efficient and to better react to requests from the Smart Grid, aiming at leveraging the user energy consumption. Sec. 3.4 presents the Demand Response policy implemented by the Smart Grid Operator to balance the demand-supply mismatch. Finally, Sec. 3.5 illustrates various possible energy management strategy adopted by the Mobile Operator in a RE powered network, either integrated in a traditional power grid or assuming the interaction with the Smart Grid in a Demand Response framework. In Sec. 3.6, some remarks are exposed about methodology and an overview about the topics addressed in each result Chapter is presented.

3.1 Scenario overview

The scenario considered in this work, shown in Fig. 3.1, consists of a relatively small geographical area where the Internet mobile access is provided by a macro Long Term Evolution (LTE) BS, capable of guaranteeing a baseline coverage over the whole area. In order to face the increased demand that can be experienced during peak times, m additional micro BSs are distributed in different points of the same area to locally increase the overall capacity in case of huge traffic demand. The cluster of BSs is connected to the electric grid for power supply; in addition, it can also be powered by locally produced RE, by means of a set of PV panels. To face the RE production intermittence, the system is equipped with some storage units, where the extra amounts of produced RE can be harvested and used when RE is not produced, so that the irregular pattern of RE availability can be leveraged.

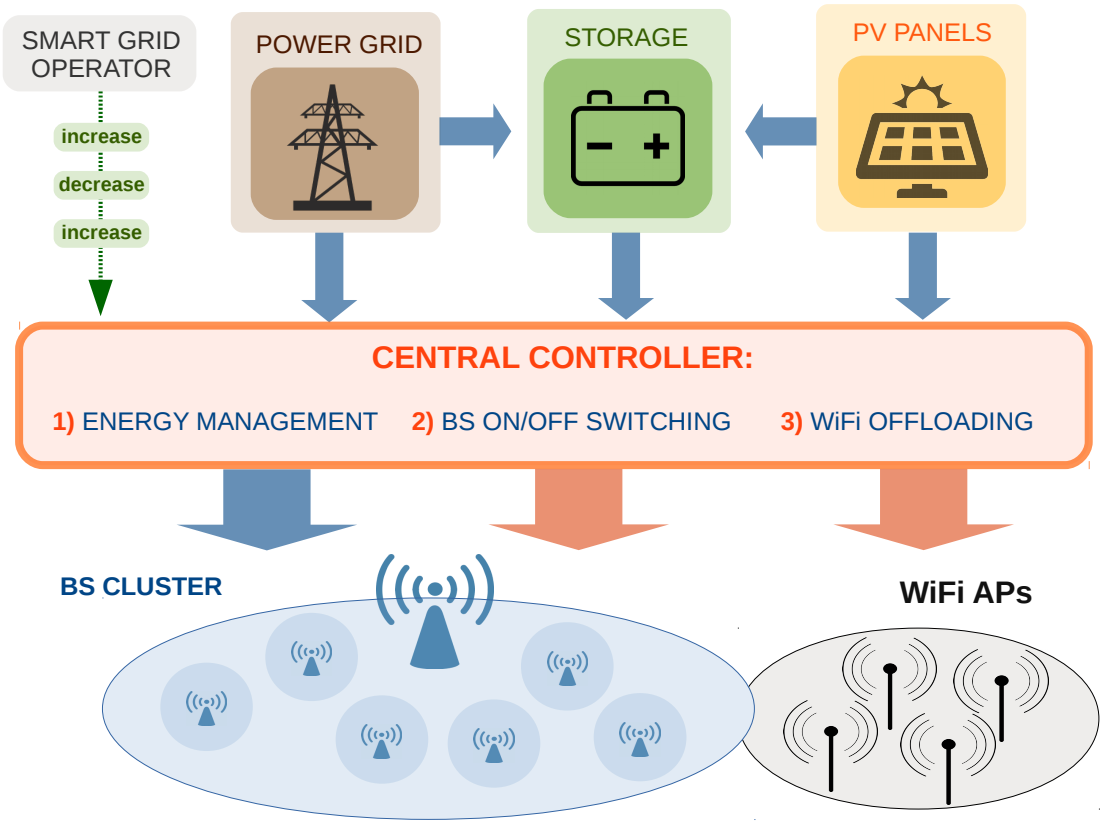

Figure 3.1: The green mobile access network structure. The blue arrows represent the energy flows, the orange arrows represents the management of the Resource on Demand and WiFi offloading strategies by the central controller, whereas the green arrow represents the requests from the Smart Grid Operator.

Typically, storage is only connected to the solar system for energy harvesting. In our case, an additional connection between the storage and the smart grid is envisioned. Hence, in some cases, storage may be used to harvest energy drawn from the grid. An active interaction with the Smart Grid in a Demand Response framework may be envisioned. Hence, the mobile access network can exploit various techniques to adapt its energy demand from the grid to the Smart Grid request, in order to reduce its cost, thanks to the rewards provided by the SGO for satisfying its requests, and to contribute in providing ancillary services. For energy saving purposes, or in order to enhance the capability of responding to the Smart Grid requests, a Resource on Demand strategy can be applied, by dynamically switching off unneeded micro BSs when the traffic demand is low. This approach allows to adapt the overall energy consumption to the actual traffic load, making it more load proportional. Furthermore, neighbor WiFi Access Points (APs) may be exploited to transfer and handle some of the traffic from the micro BSs, in order to reduce

the load of the mobile access network and better answering the requests from the SG.
All the components of this scenario are reported in Fig. 3.1. The blue arrows show the possible energy flow directions. A central controller is in charge of handling the communication and power exchanges between all the system components and managing the RoD strategy and the WiFi offloading techniques (orange arrows), when applied. When a Demand Response framework is envisioned, the energy management decisions are taken also based on the requests sent by the Smart Grid Operator (green arrow), that may ask its customers to dynamically increase or decrease their consumption from the grid. The messages coming from the Smart Grid Operator as inputs for the central controller are represented by the green arrow in the figure. Furthermore, besides taking care of the energy management policy, the central controller is also in charge of managing the Resource on Demand strategy, taking decisions about which BSs should be periodically switched off. Finally, the central controller takes care of the application of the WiFi offloading policy, when it is required. The presence of storage units contributes as well in enhancing the capability of satisfying the SG requests, by guaranteeing the availability of an energy source alternative to the grid even when RE is not currently produced. Indeed, when the smart grid asks to decrease the consumption, the mobile network can satisfy this request not only by powering the BSs using the currently produced RE, but also by drawing some energy from the storage.

3.2 The green mobile access network

This study focuses on the investigation of a portion of a mobile access network where BSs are powered not only by the traditional power grid, but also by locally produced solar energy. The mobile network is hence equipped with a set of photovoltaic panels for the renewable energy generation and with a battery bank, in order to harvest energy which is not immediately employed to power BSs for future usage. The power model adopted for evaluating the BS consumption, the characterization of the traffic demand, the components of the renewable energy generation system and the characterization of the renewable energy production are described hereafter.

3.2.1 BS consumption model

Power models for both macro and micro BSs include a constant component that is load independent and a variable component, which is proportional to the traffic load. The proportionality with traffic load is mainly due to the Power Amplifier (PA) component of the transceiver, whose consumption scales down in case of lower traffic load. The load proportionality is more evident for the macro BS, where more

Table 3.1: Values of the parameters of the consumption model for macro and micro LTE BSs [65].

BS type	N_{TRX}	P_{MAX} [W]	P_0 [W]	δ_p
Macro (without RRU)	6	20	130	4.7
Macro (with RRU)	6	20	84	2.8
Micro	2	6.3	56	2.6

than 55% of the overall power consumption at full load is accounted for by the PA [65]. On the contrary, the PA component is responsible for less than 40% of the whole power consumption in a micro BS, making it less load dependent [65]. The BaseBand (BB) processor component of power consumption, which is load independent, amounts up to 38% in the latter case, almost 3 fold the value observed in macro BSs [65].
The European project EARTH developed a model [38] to estimate the power consumption of a macro BS, which has become the standard in the field. The linear model from [65], denoted as EARTH model, is adopted in our study to estimate power consumption required by the BS during the operation, denoted as P_{in}:

$$P_{in} = N_{TX} \cdot (P_0 + \Delta_p \cdot P_{out}), \quad 0 \leq P_{out} \leq P_{max} \tag{3.1}$$

where N_{TX} is the number of transceivers, P_{max} represents the maximum radio frequency output power at full load, P_0 corresponds to the fixed power consumption when the radio frequency output power is null and Δ_p is the slope of the load dependent power consumption; P_{out} is the radio frequency output power due to the actual BS load, denoted as ρ, and it is expressed as:

$$P_{out} = \rho \cdot P_{max}, \quad 0 \leq \rho \leq 1 \tag{3.2}$$

The value of the BS load ρ actually corresponds to the BS traffic load normalized with respect to the maximum traffic amount that can be handled by the BS. The consumption of the BS in sleep mode is considered negligible.
Different values of the parameters are used to characterize the consumption of macro and micro BSs. In the case of a macro BS, the values of these parameters also depend on the presence of the Remote Radio Unit (RRU) technology, which allows to reduce losses, hence decreasing the consumption by 40% with respect to the case without RRU, thus making the BS more energy efficient [123]. Typical values of the parameters are listed in Table 3.1 for a LTE macro BS, either with or without RRU, and for a micro BS. In this study, macro BS with RRU technology are usually assumed, unless differently specified.
Part of the results have been derived by assuming a constant consumption for a BS, based on the fact that the energy demand is very little traffic proportional. In other cases, a different model has been adopted for the BS consumption, i.e.

the model proposed in [14], in order to compare results obtained under the typical model against those obtained assuming a more recent and energy efficient LTE technology. In case the adopted consumption model is different from the model presented above, it will be specified in the corresponding section. [33]

3.2.2 Traffic profiles

In order to characterize the parameter ρ, and its variability during the day, real traffic profiles have been considered, derived from real traces provided by one of the main Italian mobile operators [124]. The daily traffic profiles for a cell in a business area (BA) and a cell in a residential area (RA), during week-day (wd) and week-end (we), measured in a network in operation are provided in Figure 3.2. Traffic values are obtained by averaging and normalizing the measurements collected at 15-minute intervals during a week. Normalization is such that, for both BA and

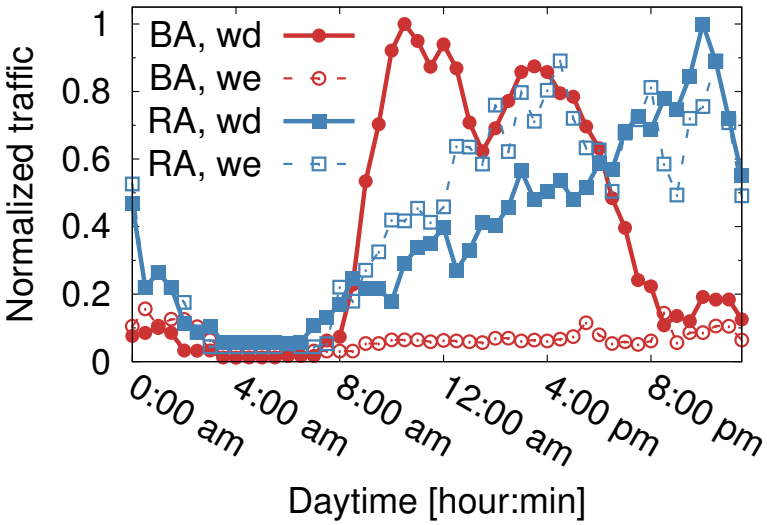

Figure 3.2: Week-day (wd) and week-end (we) traffic loads in a business (BA) and residential (RA) area.

RA, the maximum 15-minute average load is set equal to the maximum load that can be carried by the BS (i.e., $\rho = 1$). This is quite a pessimistic assumption in terms of power consumption, since significant levels of over-provisioning exist in the network, especially when a new high-capacity technology is introduced (as is now happening with 4G), but guarantees that the performance targets are met for any BS load.
For both the business and residential profiles, traffic fluctuates significantly during a day, and long periods of low activity can be observed. Fig. 3.2 reports the average daily traffic patterns observed in a sample week during the weekdays and

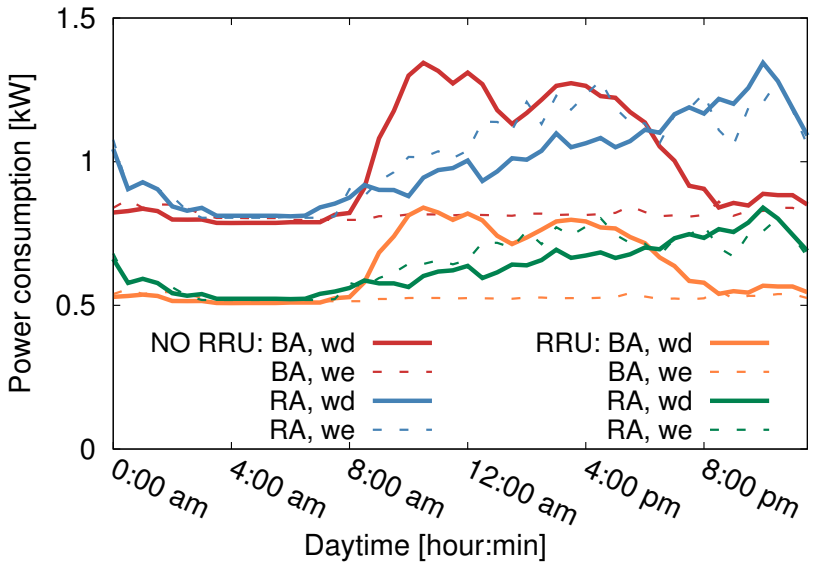

Figure 3.3: Week-day (wd) and week-end (we) energy consumption for an LTE macro BS without RRU in a business (BA) and residential (RA) area, based on the EARTH model [38].

the weekend. In a typical weekday, in the BA (continuous red curve, with circles) the traffic remains very low during the night hours, and sharply increases from 8 a.m. until lunchtime, when a temporary decrease is observed, then raising again before a new decrease starts at mid afternoon. The traffic pattern in the RA (continuous blue curve, with squares) shows a different behavior. A slow traffic increase is observed in the morning, lasting for the whole day, with peak in evening hours and some traffic persisting during night. During the weekend, in case of RA (dashed blue curve, with squares), the traffic pattern results rather similar to weekdays, except for a steeper ascent during daytime hours, with an earlier peak; by converse, the BA traffic (dashed red curve, with circles) results always very low in the weekend. These traffic patterns clearly show that outside the peak hours there are some periods of time during the day in which the radio resources are redundant with respect to the actual demand. Due to the low traffic proportionality of BS consumption, a lot of energy is wasted during off-peak periods. This can be clearly observed in Figure 3.3, showing the corresponding energy consumption (computed with the EARTH model) for a macro cell without RRU and with RRU, in BA and RA, both in the weekdays and in the weekend. Even during periods of low traffic load, around 800 W are consumed by the macro BS (without RRU) due to cooling, signaling, baseband processing, etc [11]. Similarly, even the power consumption of a macro BS with RRU never goes below half a kW, even during the weekend in the BA, when the traffic is almost null for most of the time.
As it will be discussed later on, if the unnecessary resources can be turned off in

case of low traffic, potentially high amounts of energy can be saved. This can be done by applying Resource on Demand strategies, allowing to dynamically adapt the network consumption to the actual traffic demand, by switching off unneeded BSs when the traffic is low in order to reduce the power consumption. The margin for saving energy may vary depending on the different day types and traffic areas. Furthermore, the potential amount of saving may be influenced by the traffic load varying for each BS, by the adopted RoD strategy and the configuration settings of its parameters.

3.2.3 Renewable energy generation system

The system used for locally produce solar energy is here presented and detailed in its main components, i.e. the photovoltaic panels and the energy storage. Furthermore, the characterization of the renewable energy production profiles is described, based on data derived from real renewable energy production traces.

Photovoltaic panels

The cluster of BSs is equipped with a set of PV panels, made up by multiple modules enabling the conversion of solar radiation into electricity with an efficiency that depends on the adopted PV technology. The nominal capacity of a PV module corresponds to the maximum DC output power obtained by the PV device under standardized environmental conditions (including a light intensity of 1000 W/m^2 and a temperature of 25°C) from the conversion of solar radiation into electricity, and it is commonly measured in peak Watt [W_p]. Regardless the adopted PV technology, the size of a PV panel can be expressed in terms of nominal capacity of the set of PV modules composing it. The efficiency of currently available commercial modules, built with traditional technologies (crystalline silicon), wafer-based crystalline silicon and thin-films), may achieve 20%, while emerging technologies (like CPV - Concentrating Photovoltaics) allow to almost double these values (up to 38.9% in laboratory tests, 33% for commercial solutions) [89, 43, 64]. Considering some among the most efficient PV modules built with traditional technologies, i.e. crystalline silicon, and currently available on the market, a nominal capacity of 0.333 kWp is observed for modules with an area of 1.63 m^2, hence a PV panel surface of about 4.9 m^2 can be assumed per each kWp of PV panel capacity [80]. In a real scenario, the actual energy output of the whole PV system is influenced by multiple factors [37]. Configuration settings such as the tilt angle of the modules and the azimuth angle of the PV panel may affect the RE production variability over seasons and within the day. Furthermore, besides temperature and sun radiation, several other environmental factors may induce losses in the RE production process and should be kept into account. For instance, soiling on the surface of PV modules and shadows from buildings or trees may reduce the incident solar

radiation. A performance impairment over time can be observed in PV modules, due to light-induced cell degradation and aging caused by weathering. In addition, the DC-to-AC inverter efficiency may affect the level of solar energy production and electrical and resistive losses may occur, due for example to manufacturing imperfections, wiring and electrical connectors [37]. Finally, the PV system performance may be temporarily reduced in case of system unavailability, due to scheduled shutdowns for maintenance reasons or unpredictable power outages [37].

Storage

The mobile network is equipped with a variable number of lead-acid batteries for harvesting purposes, this being one of the most common storage technology adopted in PV systems [63]. The storage capacity is provided by lead-acid batteries, a storage technology widely adopted for PV systems [63]; storage elements with capacity 200 Ah and voltage 12 V are considered, corresponding to 2.4 kWh of nominal storage capability. Battery represents a rather critical component of the PV system, especially in relation to its charging efficiency and life-cycle duration. Indeed, the charging efficiency depends on the state of charge (SOC), showing an optimal operation point at a rather high SOC level ($\sim$80% [114]). Furthermore, maintaining a high SOC operation allows to prevent sulfation processes, some of the main responsible of battery aging [107] and capacity loss [63]. However, due to the naturally intermittent production of RE and the need to continuously power the BS, lead-acid batteries undergo frequent deep charging and discharging cycles, thus operating under partial SOC and inducing a variable charging efficiency over time. This behavior also affects the battery service time, since the lifetime duration decreases inversely with the Depth of Discharge (DOD), dramatically shortening by one order of magnitude for DOD>80%. A tight constraint of maximum DOD$\leq$50-70 is recommended in RE systems, due to the possibly very slow and irregular recharge [73]. With a maximum DOD set to 50%, up to 1000 battery cycles of lifetime duration can be achieved, whereas a maximum allowed DOD of 80% just guarantees a halved battery lifetime of 500 cycles [44, 66, 86]. The charging/discharging efficiency may vary depending on the SOC and the maximum allowed DOD. An average charge efficiency of 85% is commonly assumed for lead-acid batteries [114]; when considering also the discharging process, the total energy efficiency is estimated to be 75% [44], meaning that for each energy unit (1 kWh) drawn from the storage, around 1.33 kWh of RE must have been produced and harvested in the battery bank. Typically, a maximum DOD of 70% can be assumed in RE generation systems, in order to prevent charging efficiency impairment [114], battery aging [107] and capacity loss [63]. Under this value of DOD, a lifetime duration of 500-600 cycles can be assumed [66]. Finally, high charging and discharging rates may reduce battery lifetime and impair its efficiency, especially in case of frequent charging and discharging events occurring in RE systems. Constraints on

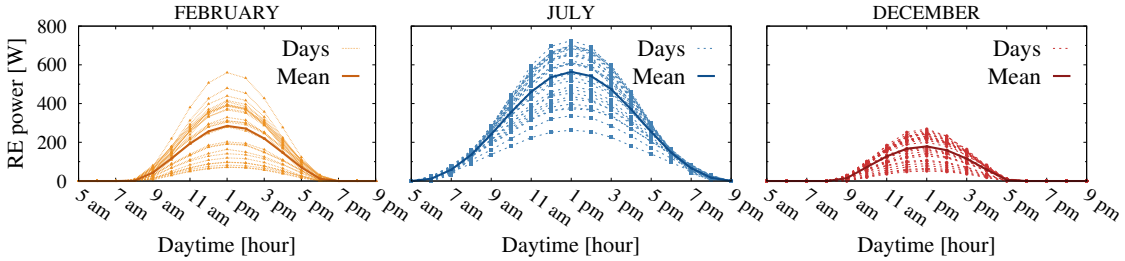

Figure 3.4: Daily profiles of RE power production [W] per 1 kWp in different sample months in Torino (PVWatts).

the maximum charging and discharging rate must therefore be taken into account, by assuming a conservative value for the maximum charge and discharge current of C/10 A, where C is the numerical value of the battery capacity in Ah [67]. This means that, for example, the energy drawn in an hour from a battery of 200 Ah will be at most 240 Wh, from which efficiency losses must then be curtailed. The same holds in case of battery charging.
In the considered scenario, the RE which is not immediately used by the cluster is stored into a set of lead-acid batteries, whose overall capacity is denoted as C_B $[kWh]$. C_B represents the available capacity that can actually be used, based on the maximum DOD.

Renewable energy generation

In this study, the characterization of the RE production has been performed by using real RE generation profiles obtained from PVWatts [37]. The tool provides, on an hourly basis and for a given location, the average levels of RE power production obtained from a standard PV panel with capacity of 1 kWp during the typical meteorological year (TMY). As mentioned above, a crystalline silicon technology is assumed for the PV modules. A DC-to-AC inverter efficiency of 96% is considered. Given an optimal setting of tilting and azimuth angles for the considered location (20° and 180°, respectively), an average daily solar radiation of 4 kWh/m^2 is observed over the whole year. Typical performance losses found in real systems, about 14%, are taken into account. The RE production patterns may vary a lot within the same day, from day to day and over seasons, depending on the location and on the weather conditions. Fig. 3.4 shows sample curves of the RE production during different days, curves are grouped by some months representative of different seasons, namely February, July and December. The solid line in each graph reports the average curve for the selected month. A typical bell shape can be identified, with the RE production gradually rising in the morning hours, achieving a peak in the middle of the day, then decreasing in the afternoon until the beginning of the night time, when no RE can be produced. Each month has its own variability, but, clearly, seasonal variations are even more significant, with much higher production

in summertime with respect to winter months.
For deriving part of the results reported in Chapter 4, the RE generation has been characterized by considering also irradiation data obtained from traces available in the Solar Radiation Data (SoDa) web service [111], based on which the actual RE production level can be obtained.
The real data about RE generation have been used either as input data for simulations or for deriving different types of stochastic models representing the production of solar energy. Within each of the various chapters reporting the results of our work, further details are provided about how these data have been used in the specific part of the study.

3.3 Energy saving techniques

This section presents the techniques applied to reduce the energy consumption of the mobile access network, either based on BS on/off switching or on the implementation of WiFi offloading.

3.3.1 Resource on Demand strategy

As already mentioned, due to the fact that the BS power consumption is very little proportional to the traffic demand, a lot of energy is wasted during periods of low demand. This is even more evident for micro BSs: indeed, whereas in case of a macro BS (with RRU) around 58% of the consumption at full load is consumed when there is no traffic, more than 77% of the energy consumption at full load is consumed by a micro BS when no traffic is present. Hence, the unneeded resources can be switched off in case of low demand, by applying a Resource on Demand strategy, in order to provide a dynamic adaptation of the energy consumption to the actual users' need and to save energy.
The basic idea of the main proposed policy is quite simple. A time window is defined, over which the cluster can be reconfigured and some micro BSs can be switched off (we assume a time window of half an hour to avoid frequent system reconfigurations). At the beginning of each window, in case of low traffic, one or more micro BSs are put to sleep mode, i.e., they are turned off, and their traffic is moved to the macro BS, as long as the macro BS has enough capacity to handle the traffic. The same maximum capacity, denoted as C, is assumed for all the BSs. We, thus, define a threshold, ρ_{min}, over the traffic load of micro BSs. At every system check granularity, a set S of BSs is switched off if the two following conditions hold:

$$\begin{cases} \lambda_i < \rho_{min} & \forall i \in S \\ C_r = C - \lambda_M \geq \sum_S \lambda_i \end{cases} \tag{3.3}$$

where λ_M is the current traffic load of the macro BS and C_r represents the *residual* capacity in the macro BS. For simplicity, we assume that micro BSs can be switched

on and off in negligible time. Indeed, switching can take up to a few minutes and this time can be considered negligible with respect to the time window of half an hour that we use to decide possible system reconfigurations.

3.3.2 WiFi offloading

WiFi offloading consists in transferring a portion of the mobile traffic from the BSs to some nearby WiFi Access Points (APs). Currently, WiFi APs are increasingly deployed by more and more operators and private users, making the WiFi technology become available almost everywhere. This technique is hence commonly adopted to relieve cellular networks from a part of their traffic load during peak hours in heterogeneous networks, hence increasing the available bandwidth [61]. However, WiFi offloading can be also exploited as a way to decrease the traffic load in order to save the energy consumed by BSs, although this technique alone may not lead to remarkable reduction in the consumption, due to the limited load proportionality of energy consumption. Nevertheless, when applied in a scenario where the base stations can also be switched on and off, WiFi offloading allows to further decrease the number of active BSs, hence to further reduce the system consumption.
We assume that the neighbor APs available for carrying a fraction of the mobile traffic in case of DOWN requests are owned by some local business holders and/or by private individuals residing in the area. Further assumptions and conditions under which WiFi offloading is applied in our scenario are detailed and discussed at the beginning of Sec. 9.2 and in Sec. 9.2.3.

3.4 Demand-Response

The green mobile access network presented above is connected to a SG, from which energy can be taken. The SG operates according to a specific DR program, deployed in order to leverage the energy demand from its users to better match the power supply. This is done for example by asking users to reduce their consumption in case of high peak demands or to increase the amount of energy drawn from the grid, in order to mitigate voltage unbalance. Those users willing to participate to the DR program perform an agreement with the SG operator and they will receive monetary rewards or penalties for positively react or opposing, respectively, to the SG requests. Every day each user forecasts its energy demand that will be likely needed from the grid during the following day, providing an estimation of the predicted consumption level during the next day for every timeslot in which the day is divided. The duration of each timeslot may typically be of the order of 15 minutes to one hour. Thanks to aggregators, the SGO in turns knows the overall expected energy demand from all the end users for the following day, on a timeslot basis.

Table 3.2: Energy prices, rewards and penalties in [€/MWh] [106].

Price, reward or penalty	p_G	r_U	r_D	p_U	p_D
Value [€/MWh]	37	24	60	12	30

During the following day, at every timeslot, based on the day-ahead forecasts about energy demand and on the current energy availability, the SGO sends a request to its end users. The request is UP (or DOWN) in case the SG is asking the users to increase (or decrease) their energy consumption, in the following timeslot, with respect to the energy need foreseen the day ahead. If the SGO does not ask for any adjustment of the end user consumption from the grid, the request is $NULL$. Rewards are envisioned for the amounts of energy used to increase or decrease the energy taken from the grid with respect to the level predicted the day ahead, in response to the SG. The requests of type UP and DOWN do not imply the demand for a specific amount of energy increase or decrease, respectively, with respect to the forecast consumption. Nevertheless, the provided rewards result proportional to the energy raise (or reduction) with respect to the predicted levels, hence higher levels of energy increase or decrease are fostered. The average price per unit of energy drawn from the grid is denoted as p_E. If the user is able to answer the grid request of UP or DOWN, by increasing or decreasing its grid consumption respectively, it receives a reward from the grid, since it is contributing to provide ancillary services. The grid pays a reward, denoted as r_U, for each unitary increase of energy with respect to the day-ahead forecast, in case of request of type UP. Similarly, r_D denotes the reward for a unitary energy decrease with respect to what announced the day before, in case of request of type DOWN. Tab. 3.2 reports the values of energy prices, rewards and penalties adopted in this study, obtained from real pricing adopted by the Réseau de Transport d'Electricité (RTE)-France, the French electricity transmission system operator [106]. p_G is the cost for unit of energy bought from the grid. r_U and r_D are the rewards per unit of energy traded to provide ancillary services in case of U and D, respectively. p_U and p_D are the penalties paid for each unit of energy opposing the SG request with respect to the predicted consumption, in case of U and D, respectively. Let us denote as E_G the energy bought from the grid during a timeslot, whereas E_{G^*} denotes the predicted amount of energy bought from the grid during the same timeslot. In case of request of type DOWN and UP, respectively:

$$\begin{aligned} Case\ DOWN: &\quad if\ \ (E_G - E_{G^*} < 0)\ \ then: \quad Reward = \ (|E_G - E_{G^*}|) \cdot r_D \\ Case\ UP: &\quad if\ \ (E_G - E_{G^*} \geq 0)\ \ then: \quad Reward = (E_G - E_{G^*}) \cdot r_U \end{aligned}$$

These rewards lead to an overall cost reduction, whose value depends on the frequency at which the user can satisfy the grid requests and on the amount of grid

energy increase/reduction.

3.5 Energy management policies

In a green mobile access network, BSs can be powered by the grid or by the solar energy produced by the photovoltaic panels or by the energy previously harvested in the storage. Furthermore, extra amounts of renewable energy, that cannot be immediately used for the network supply, must be harvested in the storage for future usage, for example during the night period when renewable energy is not produced. In a Demand-Response framework, it may be convenient to take advantage of the incentives provided by the SGO when its users accomplish its requests of decreasing or increasing the consumption. However, whereas the mobile network can reduce its consumption from the grid by using the renewable energy currently being produced, or by exploiting the energy storage, or by applying some Resource on Demand strategy, the mobile network cannot increase its energy consumption on purpose, since it depends on the current traffic demand, which, in turns, cannot be scaled up on demand. Hence, in this case, it is possible to buy some additional amount of energy from the grid to be stored in the battery, in order to satisfy the request of the SGO to raise the energy demand.
The decisions about the handling of the energy flows are taken according to properly designed energy management policies, based on several possible factors, like the current energy demand, the renewable energy production, the battery charge level, the likelihood of future power outages, the requests from the SGO in case of Demand-Response. In this study, two different types of energy management policies are considered, i.e. a *baseline energy management policy*, implemented when the mobile operator is not enrolled in any Demand-Response program, and a *Demand-Response energy management policy*, envisioning an active interaction with the Smart Grid, based on an agreement to negotiate the participation in a Demand Response program. These policies are briefly presented hereafter, whereas specific variants and possible implementations are detailed in the corresponding chapters where they are adopted.

3.5.1 Baseline energy management policy

The energy generated by the panels is first used to power the BSs and, in case of extra production, is fed into the batteries, according to a *first use-then harvest* principle. Any extra amount of renewable energy that is not needed for current network operation and cannot be immediately stored in the battery is wasted. Whenever no renewable energy is currently available, the base stations drain energy from the batteries for their supply. In case batteries are discharged, the base stations can be supplied by the power grid. This kind of operation allows to minimize energy

losses. It corresponds to the application of a Harvest-Use-Store (HUS) policy [97, 122, 71], meaning that as RE is produced during daytime, it is directly used by the BS, if needed; only the amount of produced RE exceeding the BS energy demand is stored in the battery for future usage, as long as there is still free available space. Thanks to the recent deployment of more advanced storage devices improving technical feasibility of the HUS mode [70], this configuration featuring two harvested energy flows in parallel (directly to the BS or through the traditional storage) is preferred to the traditional and less energy efficient Harvest-Store-Use (HSU) architecture, where the harvested energy follow a single/unique flow, since it is first saved to the storage device before being used to power the BS, thus implying higher losses [115]. An hybrid energy storage system (HESS) is hence envisioned, where a power efficient storage device, i.e. a supercapacitor, is introduced beside the lead-acid battery [49, 71, 70], in order to provide immediate use of produced RE. In fact, supercapacitors feature high power density, fast charging efficiency and longer lifetime with respect to lead-acid batteries, hence resulting fitted to this purpose. Furthermore, they allow to smooth RE production on a short time scale to obtain a constant power output. By converse, they show low energy capacity and high self-discharge rate with respect to lead-acid batteries, which are more energy dense devices, hence better suitable to store extra amounts of energy for future usage [49].
We assume that the renewable energy generator system is shared among the base stations of the group and energy management decisions are taken in a centralized way for the whole group of base stations. This means that decisions are based on the total available energy and the total power demand regardless the actual implementation of the power system that, in its turn, can either be distributed, with small solar panels and storage units co-located with the base stations, or composed of a few larger generators.

3.5.2 Energy management policy in a Demand-Response framework

When the mobile access network actively interacts with the Smart Grid in a Demand-Response program, the energy management policy must also take into account, and possibly accommodate, the requests issued by the SGO, in order to increase the MNO revenues for satisfying the SG requests and, at the same time, contribute in providing ancillary services.
At every timeslot, different actions can be taken, based on the type of grid request and the amount of produced RE. The BSs need may be derived from the produced RE, from the storage (always respecting the maximum discharging rate) or from the grid. RE may be used to power BSs, harvested into battery or wasted in some cases. As already mentioned, the RE management is based on a *first use - then harvest* principle, meaning that the produced RE can be directly used to power

the BSs and only the extra amounts are possibly harvested afterwards. In order to better answer requests of increasing the consumption, an additional amount of energy can be drawn from the grid and harvested into battery for future usage, as long as there is still enough space in the storage.
Please note that variants of this policy are possible. For instance, this energy management policy can be applied even when no RE generation system is present, by simply assuming photovoltaic panels and battery with null capacity. Furthermore, specific behaviors are envisioned in the case Resource on Demand and WiFi offloading techniques are applied, since these strategies can be exploited to better respond to the requests of reducing the energy taken from the grid. Actual implementations of this energy management policy are better detailed in the corresponding chapters.

In case of U request, a reward is obtained if the total energy taken from the grid, E_g, is larger than the predicted consumption C_f. The reward is proportional to the extra amount of energy taken from the grid. By converse, in case it is lower, a penalty is paid proportional to the energy gap with respect to the reference level C_f predicted the day ahead. Similarly, in case of D, a reward is obtained if $E_g < C_f$, and vice versa for the penalty.

3.6 Methodology remarks

Depending on the focus of single parts of the study, different and sometimes simplified variants of the main presented scenario have been adopted in the various sections of the work, based on the aspects which had to be investigated. For instance, when the focus is mainly centered on modeling the renewable energy production, the scenario is simplified by considering a portion of the mobile access network where only a macro BS is present. Hence, the parameter m, corresponding to the number of micro BSs, is set equal to 0. Conversely, when the focus is mainly set on operational costs or on RE system dimensioning, a complete scenario with multiple micro BSs ($m>0$) is more likely considered, in order to more accurately investigate the actual system operation and performance. Furthermore, although the mobile network is always assumed to be powered by the traditional power grid, besides the possible use of renewable energy, only in some scenarios an active interaction with the Smart Grid in a Demand Response framework is envisioned, whereas in other cases no Demand Response policies from the Smart Grid side are assumed. Finally, the application of Resource on Demand strategies and WiFi offloading techniques is only adopted in specific scenarios. The details of the specific variants adopted for the scenario in the different parts are specified within the corresponding section in each chapter related to the results (Chapter 4-9).

In this work, the green mobile network operation is investigated not only via simulation, but also using stochastic models, either to represent the storage or the

renewable energy generation. Specific models adopted in the various parts of this study are detailed in the corresponding Chapters. The outline of the rest of this manuscript is highlighted below:

- In Chapter 4, a simple stochastic model of the amount of energy that is produced by PV panels is proposed, based on just a pair of input parameters that allow to characterize the renewable energy production: the mean value and the variance of the level of solar energy daily generation.

- In Chapter 5, various stochastic models designed to model the green mobile network operation are presented.

- In Chapter 6, the impact of the granularity of the parameter settings on the performance of the green network operation model is discussed.

- In Chapter 7, useful simulation and analytical tools are presented, deployed for proper dimensioning of a renewable energy generation system in green mobile networks. In particular, the stochastic model proposed for characterizing the renewable energy production is exploited to derive a simple analytical formula to derive the proper capacity of photovoltaic panels and storage, based on the mobile network demand and on the local renewable energy generation profile.

- In Chapter 8, different energy saving techniques, either based on the application of BS on/off switching or WiFi offloading, are investigated via simulation, in order to evaluate their impact on the system dimensioning, on the energy consumption from the grid and on MNO cost.

- In Chapter 9, the interaction between the mobile network and the Smart Grid in a Demand-Response framework is deeply analyzed, via simulation and by deploying stochastic models, in order to deploy energy management policies that allow to enhance this interaction, with the twofold objective of reducing energy cost for the mobile operator and contributing in providing ancillary services, that represent a remarkable benefit from the SGO side.

Chapter 4

Modeling renewable energy production

Part of the work presented in this Chapter has already been published in:

- D. Renga and M. Meo. "Modeling renewable energy production for base stations power supply". In: *2016 IEEE International Conference on Smart Grid Communications (SmartGridComm)*. Nov. 2016, pp. 716–722

The intermittent nature of RE production is one of the main criticalities to be addressed when powering mobile network with solar energy. The variability of the RE generation over time, which is location dependent, highly affects the system performance in terms of energy self-sufficiency of the network and resiliency to power outages. Furthermore, a proper system dimensioning should be based on a reliable characterization of the RE production profile.
In this study, the renewable energy production has been modeled in different ways, depending on the aspects of the green mobile network system that had to be investigated. As it will be shown later on in this manuscript, in some cases real traces about renewable energy production have been simply employed as input data for simulations, for instance to analyze the system performance for dimensioning purposes or to study the interaction of the green network with the smart grid in a realistic setup. In other cases, real data about renewable energy production in a given location have been exploited to build probability distribution functions, to provide an empiric stochastic model for the solar energy generation to be applied in the study of the system performance. Nevertheless this Chapter, focusing on the PV powering system of a BS that is part of a mobile network, aims at proposing a simple stochastic model of the energy produced by photovoltaic panels of relatively small size and investigating the impact of the energy generation variability on the power supply system performance. The peculiarity of this model is represented by

the fact that only two parameters are sufficient to characterize the renewable energy generation in any location, by means of a random variable with a mean value and a variance.
The stochastic model is described in Sec. 4.1, whereas in Sec. 4.2 the model is applied to simulate the system, carry out a performance analysis and validate its effectiveness in representing the RE generation in a real scenario.

4.1 Stochastic model of the renewable energy production

Based on the analysis of data about the solar irradiance in the city of Turin, a simple stochastic model is proposed to characterize the RE production by PV panels, with its variability. The model is based on the identification of a shape function that represents the typical production profile of a day; the function is then scaled through a random variable that represents the production daily variations. The model can be applied at different time scales, e.g., for representing the daily or the hourly production. Our results, derived for various dimensioning of PV panels and storage, show that the mean and variance of the random variable representing the daily generation are the key parameters needed to predict, with high accuracy, the system performance; performance is evaluated, mainly, in terms of battery depletion probability and energy demand from the grid.
The considered scenario is simplified with respect to the general one presented in Chapter 3 and it is reported in Fig. 5.3. It consists of a single macro LTE BS (the number of micro BSs, m, is set to 0), that is equipped with a PV panel and an energy storage. In order to allow normal operation, the BS is first powered by the RE, when it is currently available. Any amount of solar energy exceeding the BS need is stored in the battery, as long as there is residual capacity available. When no RE is produced, the BS can draw the required energy from the battery as a second option. Finally, in case this is not sufficient for satisfying its demand, the energy is taken from the grid. No active interaction is envisioned with the Smart Grid, hence the baseline energy management policy is applied. The model is derived from the analysis and understanding of data obtained from PVWatts [37] about RE production during the typical meteorological year (TMY) in Turin. While fitted and tested for Turin, the model can in general be used to represent the production in locations in which, similar to Turin, the intra-day weather variability is limited. As is shown below, the model consists of two elements: a shape function that represents the profile of production in a day, and a random variable that represents the daily variability and it is a scale factor to be applied to the shape function.

As mentioned above, the model is derived from data obtained by PVWatts, a tool that provides, on an hourly basis, the average levels of RE power production obtained from a standard PV panel with capacity of 1 kWp over the typical year.

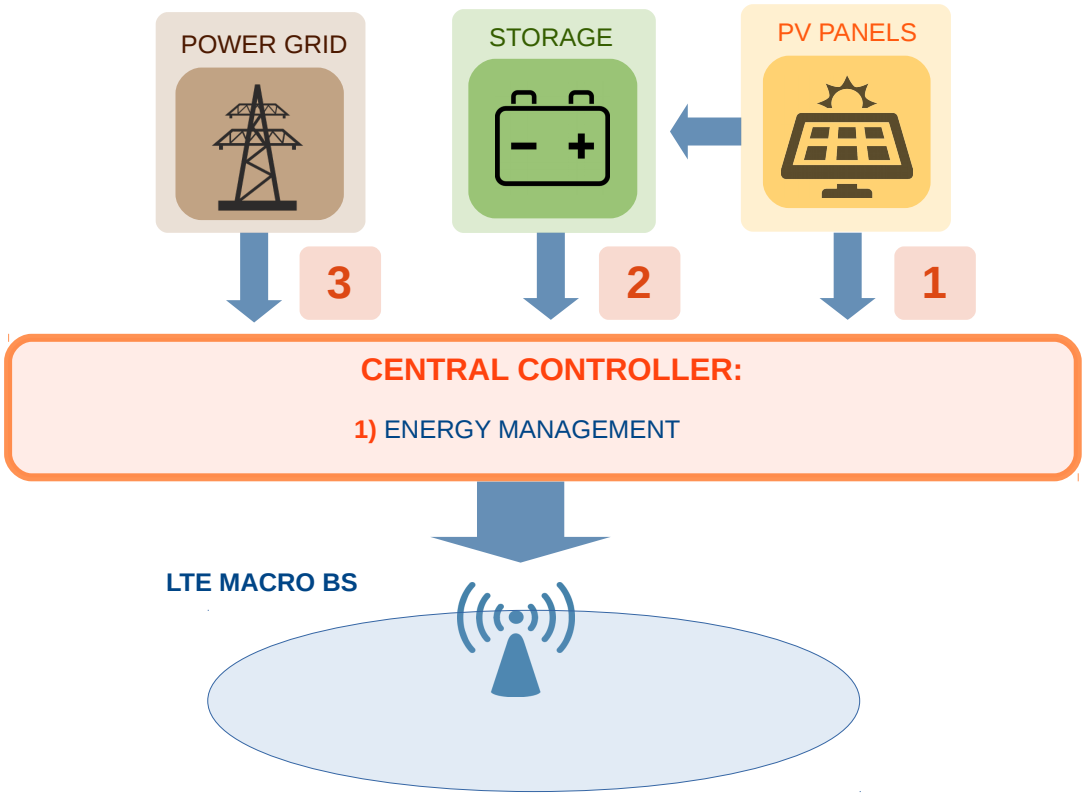

Figure 4.1: The single on-grid green LTE BS.

Fig. 3.4 shows sample curves of the RE production during different days, curves are grouped by some months representative of different seasons, namely February, July and December. The solid line in each graph reports the average curve for the selected month. Each month has its own variability, but, clearly, seasonal variations are even more significant, with much higher production in summertime with respect to winter months. To deploy a model suitable also for a proper dimensioning of PV panels and batteries, a worst-case approach is taken and the season in the year with the lowest RE production is considered. For the selected location, such period is represented by the months of November, December and January (92 days), when an average solar radiation of 1.18 kWh/m^2 per day is achieved. Let us denote as RE_p the RE power production [W] at peak time, for a unitary PV panel (1 kWp) and denote with RE_d the daily total amount of RE production [kWh]. An average RE_p of about 193 W per 1 kWp is observed (range [42,349] W); as a reference consider that the mean value for the whole year is 390 W (range [41,760] W).

To investigate the similarity of the daily patterns of the RE production during the 3-month period, Fig. 4.2a reports the daily curves of RE production, with sample granularity of 1 hour, normalized with respect to the RE_p value of each

day; the curve of the mean normalized RE production for the whole period is reported along with the range corresponding to *mean value* $\pm SD$. Given the RE_p, the *shape* of RE production is very similar in each day. The production in a given day can then be represented by the red dashed line (obtained by averaging the production hour by hour) multiplied by a factor that corresponds to the RE_p of that day. Hence, RE_p is the only parameter needed to represent the daily production and to distinguish the production in different days. Fig. 4.2b reports also the

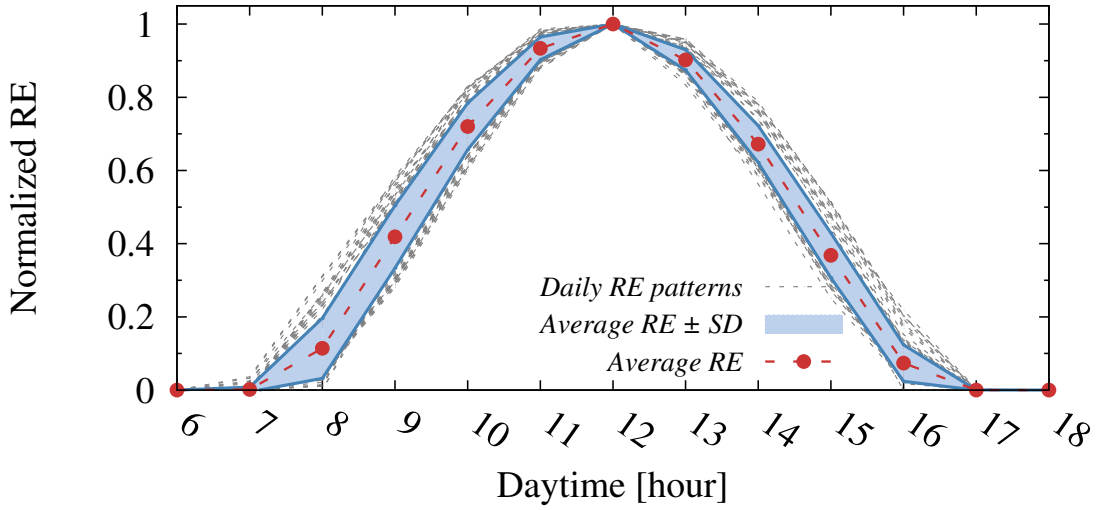

(a) Daily patterns of normalized RE production

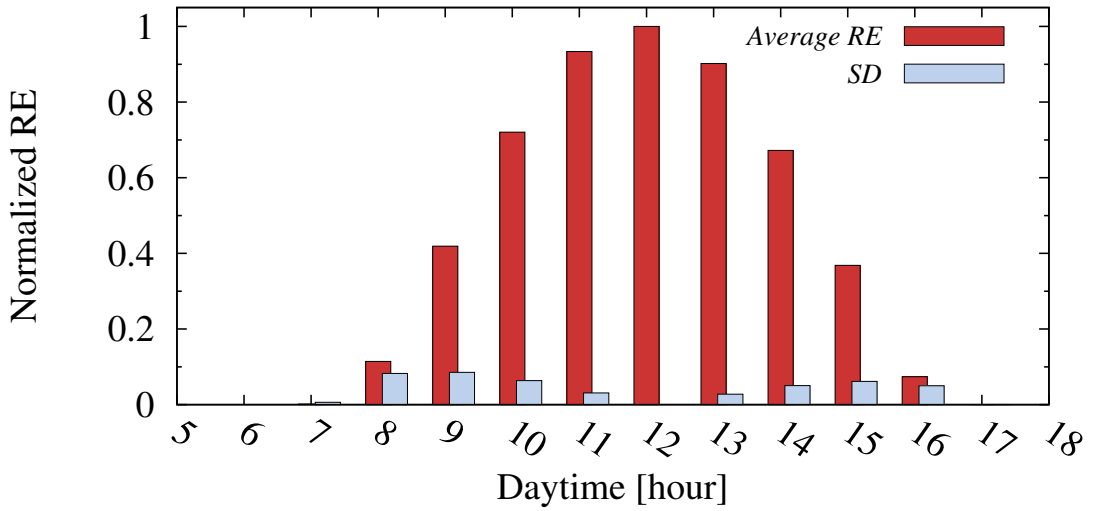

(b) Hourly normalized RE production

Figure 4.2: Daily normalized RE production patterns (average and standard deviation) in the cold season.

standard deviation of the normalized RE production, for each hour of the day. SD is always $< 10\%$ of RE_p, and it is larger as we get closer to the curve tails, with a maximum of 8.6% of the normalized RE_p. These variations are negligible with respect to the central peak hours, in terms of total daily RE production. The curve representing the average normalized RE production during the 3-month period, denoted by $f_N(t)$ (red dashed curve in Fig. 4.2a), can be derived by averaging the normalized production for each time in a day and interpolating the new obtained points. The actual RE production curve, denoted as $f(t)$, represents the real RE pattern production in a specific day:

$$f(t) = RE_p \cdot f_N(t). \tag{4.1}$$

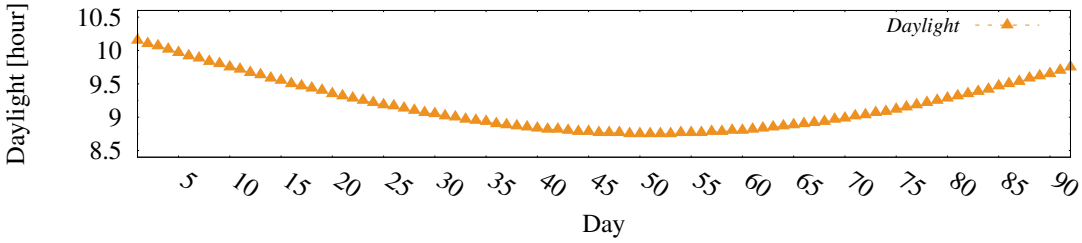

(a) Daylight duration.

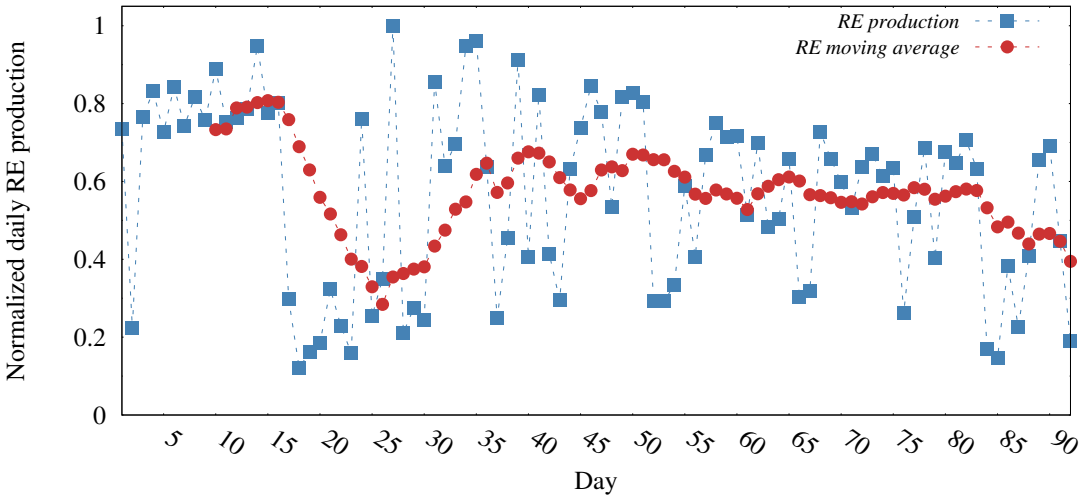

(b) Normalized daily RE production.

Figure 4.3: Daylight time duration across the three months and normalized daily RE production with its moving average.

The *support* of the RE production curves is related to the duration of the daylight time; in our case, its average is about 9 hours. The selected 3-month period

is characterized by a period of daylight ranging from 8 h and 45 min to 10 h and 9 min. A maximum variation of just ±10% with respect to the mean value (9 h and 12 min) is observed. Such a relatively low variability range does not seem to have a direct and significant impact on the RE production variability, as it can be seen from Fig. 4.3. The blue curve in Fig. 4.3b represents the value of the daily production, RE_d, normalized with respect to the maximum RE_d in this period (that is 1.76 kWh), while the red curve is the corresponding moving average over the previous 10 days; the orange curve in Fig. 4.3a corresponds to the duration of daylight for each day. The moving average varies within a pretty limited range, hence resulting rather unrelated to the daylight time variation, which, by converse, is first decreasing and then increasing in the same period. The lowest values of the moving average are actually seen around November 27^{th} and January 31^{st}, in two moments in which the daylight time is longer than in those days showing higher RE production. Therefore, the small differences in the daylight duration among days in this period do not affect significantly the level of daily production in the corresponding days. These observations allow us to assume a profile with a constant support over the considered period. Given the fixed common shape for the normalized daily RE production (holding for the whole period), $f_N(t)$, the actual daily RE production pattern can be represented as in (4.1) by multiplying $f_N(t)$ by a random variable that represents RE_p. Denoting the r.v. by A, a sample a_i of A defines the amplitude of RE_p in day i and the production curve in day i is given by $a_i f_N(t)$. The r.v. A is simply defined by the probability distribution function. We will show in what follows that if we simply fit the mean and the variance of the r.v. A to those of the peak production RE_p, we obtain a simple model that well captures the system behavior.

Summarizing, the proposed model for the RE production consists in obtaining a daily profile of production by multiplying the shape function $f_N(t)$ by a r.v. A whose mean and variance are set equal to those typical of the peak production in the considered location. The proposed model can be applied for locations with limited intra-day weather variability, like in the case of Turin and several other locations, according to PVWatts traces.

4.2 Simulating the system

To prove the utility of the model, we now apply it to a case of practical interest, a BS equipped with PV panels and battery storage. We analyze the system behavior to understand how the RE production profile affects its performance. In this section, we describe the simulation environment used for deriving the results.

To define the system we use the following parameters: C_{BS}, the BS power consumption (in kW), assumed to be constant (1 kW on average); S_{PV}, the PV panel size (in kWp); B, the storage size (in kWh), intended as the portion of the

whole capacity provided by the batteries that can actually be exploited. Indeed, the storage amount defined by this parameter is limited by the maximum Depth of Discharge (DOD) allowed for each battery element and it may range from 50% to 70% of nominal capacity, depending on the minimum battery life duration that we are willing to accept. The RE production is characterized by using the model described in the previous section, keeping into account that variable amounts of RE are produced each day, depending on the panel size, S_{PV}, and on the peak production distribution in the considered location, RE_p. Furthermore, the proposed model assumes that each day the RE is produced only during a limited period of time (*daytime*), whereas during the rest of the day (*nighttime*) no RE can be produced. The amount of RE that is produced during daytime, denoted as RE_D, is derived as $RE_D = RE_d \cdot S_{PV}$. According to the proposed model, RE_d can be related to RE_p by means of a constant coefficient, R_N:

$$RE_d = R_N \cdot RE_p = \int_D f_N(t) \cdot RE_p$$

where D is the support of $f_N(t)$, i.e. the daytime period, varying with latitude. $f_N(t)$ represents the curve of the normalized RE production per kWp in a given location. In this work, R_N is derived in the worst-case period for the city of Turin, where latitude is 45.2°N and *daytime* is about 9 h. The locally produced RE can be used to directly power the BS; the extra amount is stored in the battery to be used later on, if there is still space available. In case of battery depletion, the BS demand can be satisfied by taking energy from the grid. Storage charging and discharging losses are taken into account, considering a battery efficiency of 85%. In our simulation, the storage level, along with other performance parameters, is sampled daily, both at the beginning of daytime (the most critical point for RE availability), denoted by $Sd_{(i)}$ for day i, and at the beginning of nighttime, $Sn_{(i)}$. The battery levels are related by:

$$Sd_{(i)} = min(B, max(0, Sn_{(i-1)} - Cn_{(i-1)}))$$

where $Cn_{(i-1)} = C_{BS} \cdot nighttime$ is the BS energy consumption during nighttime. The storage level at the beginning of nighttime, is computed for day i as:

$$Sn_{(i)} = min(B, max(0, Sd_{(i)} + R_{(i)} - Cd_{(i)}))$$

where $Sd_{(i)}$ is the storage level at the beginning of daytime in the same day, $R_{(i)}$ is the RE produced during daytime and $Cd_{(i)} = C_{BS} \cdot daytime$ is the daytime BS energy consumption.
For BS service continuity and reasonably low values of the depletion probability, the storage size B must be large enough to store at least the amount of energy needed to cover the nighttime demand, when no RE is produced.

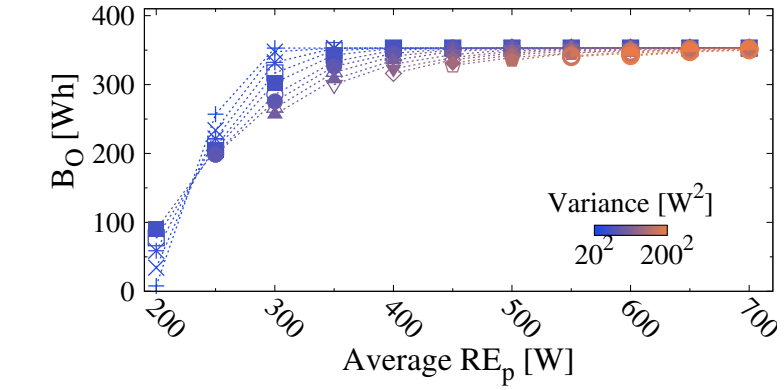

(a) ND of RE_p.

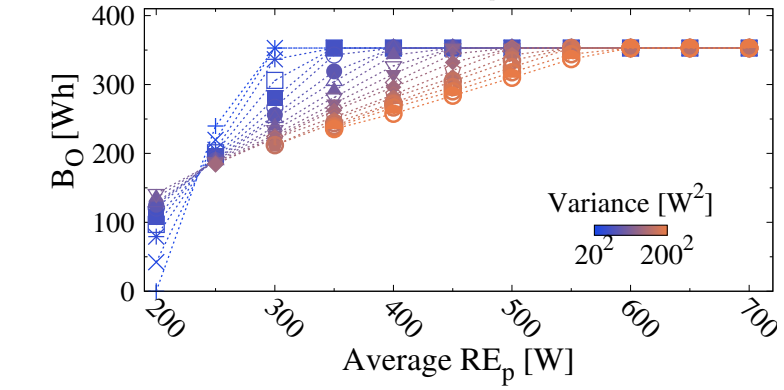

(b) UD of RE_p.

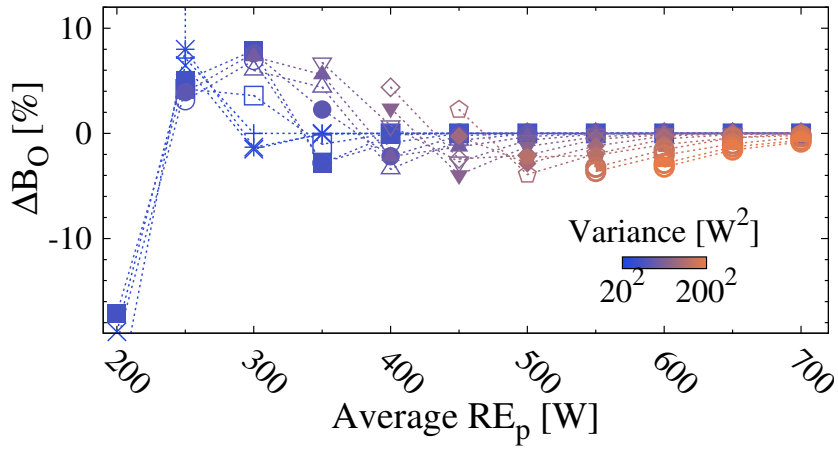

(c) Δ_{B_O} between ND and UD case.

Figure 4.4: Battery occupancy, B_O, under normal (ND) and uniform distribution (UD) of RE_p and Δ_{B_O} versus average RE_p in scenario 1.

4.3 Performance analysis

In this section, we analyze the performance of the system, focusing on the impact of the main stochastic characteristics (mean and variance) of the daily energy production.

Several simulations were run under many different configuration settings of input parameters, and considering different types of distribution for the random variable A that represents the daily production RE_p. In particular, to test the impact of the distribution of energy production, normal (ND) and uniform distributions (UD) have been tested, under multiple combinations of the values of mean and variance. The BS consumption is assumed to be $C_{BS} = 1$ kW. Results from these two distributions have been compared with those derived from the simulation under the empirical distribution (ED) obtained from real traces of sun radiation in Turin. 10,000 samples were collected on a daily basis for each simulation, both at the beginning of daytime and of nighttime, but only the first kind of results are reported, since they correspond to the worst-case. The system performance has been evaluated by means of the following performance indicators: B_O, average daily battery occupancy; Q_{90}, 90^{th} percentile of battery occupancy; P_D, storage depletion probability; G, average daily grid demand. Two scenarios, 1 and 2, have been selected to represent the general trend of the results. In scenario 1, the storage capacity is $B = 18$ kWh, and the panel size is $S_{PV} = 24$ kWp; in scenario 2, $B = 20$ kWh, $S_{PV} = 26$ kWp.

Transition from scarce to sufficient RE production regime Fig. 4.4 shows the average battery occupancy (B_O) versus the mean daily production in scenario 1, both in case of normal distributed production and uniformly distributed production. Each curve represents a different variance. Clearly, the average charge B_O increases with the average production, with a much faster increase for lower values of the mean and of the variance. In particular, for low mean production, a higher variance allows higher levels of charge, whereas, starting from a transition point in the RE_p (between 200 W and 250 W), there is an inversion such that, for higher variance, lower charge levels are observed. The reason is that when production is low, variance helps in giving more chance to fill the battery; conversely, when production is enough, variance causes more chances not to fill the battery.

The same considerations hold under the other distributions. However, although the general trend is similar, for low values of the variance of the production, v_R, the ascent is slightly steeper under UD rather than ND. Similar trends are observed in scenario 2 (data not reported for lack of space), featuring larger PV panel and storage size. To better evaluate the differences between the two types of RE_p distribution, Fig. 4.4c reports the relative difference observed in the values of B_O under ND versus UD, denoted as Δ_{B_O}, computed for each configuration of $[RE_p, v_R]$ in scenario 1. Except for the lowest value of production (200 W), Δ_{B_O} is never larger

than ±10%, a quite small value. This shows that the main impact of the variability of the production can be quite well represented simply by the mean and the variance of the daily production.

Results about depletion probability, P_D, are reported versus the average RE_p in Fig. 4.5, in scenario 2 and under UD of RE_p. The trend is the opposite with respect to the behavior of the battery occupancy B_O, since depletion probability decreases for increasing values of the mean production, RE_p, with a huge decrease and steep descent for low values of average RE_p. Again, the transition point in RE_p

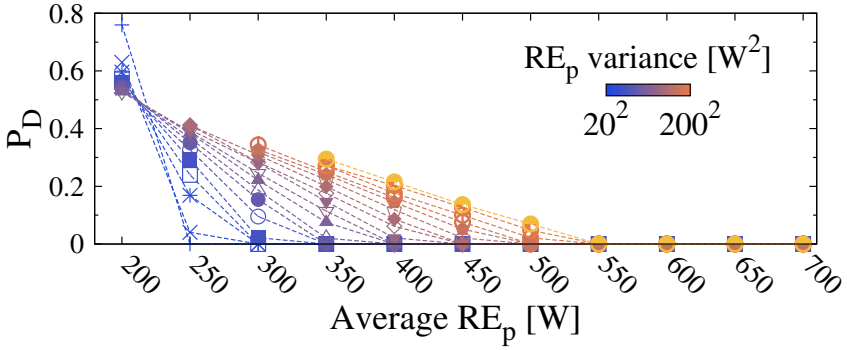

Figure 4.5: Depletion probability, P_D, under UD of RE_p in scenario 2.

can be identified between 200 W and 250 W, below which the depletion probability remains smaller than 50% for any value of the variance, v_R. In relation to the patterns of P_D, three regime zones in RE_p can be identified for system operation:

- *low regime*: range of RE_p values for which depletion probability is $> 20\%$ for any value of variance; daily RE production is not sufficient to satisfy a significant portion of BS energy demand;
- *intermediate regime*: range of RE_p values for which depletion probability may be $< 20\%$, depending on RE production variance; daily RE production is sufficient to provide a consistent amount of energy for BS operation;
- *high regime*: range of RE_p values for which depletion probability is constantly $< 20\%$ for any RE production variance; daily RE production is sufficient to make the BS much more independent from the grid and, for variance values low enough, it may potentially make the BS completely off-grid. In a location where the variance of RE_p is rather large, the objective of an off-grid BS can be achieved only for higher values of daily RE production, hence larger PV panels may be required.

The identified transition range, i.e. intermediate regime, corresponds to the switching between two regimes: a RE production not sufficient to significantly satisfy the BS need and a regime providing a sufficient amount of energy for BS operation.

Results show that larger values of the battery and PV panel (scenario 2) allow to more rapidly reduce depletion probability. As observed before, the general trend is similar under ND and UD, but in the UD case for low values of the variance of production, the descent is steeper than for ND, while it becomes more gradual, with respect to the ND case, for higher values of the variance v_R. The relative difference of P_D between ND and UD case, Δ_{P_D} results to be higher than for B_O, but still within $\pm 30\%$; higher values of Δ_{P_D} are found only when P_D is low (less than 6%).

Effects of RE_p variance The system is now investigated in terms of how its performance is affected by the variance of production v_R, for fixed average RE_p. Fig. 4.6a shows the trend of B_O versus the variance for scenario 2 in case of uniform distribution of RE_p. Each curve represents a different value of average RE_p. It can be observed that for high average values, B_O tends to gradually decrease as v_R grows larger. For intermediate values of RE_p, the descent becomes faster, especially for small v_R. For the lowest v_R values, B_O tends to rapidly increase, instead of decreasing, as v_R becomes higher. The opposite trend is seen for P_D (data not shown). P_D rapidly decreases as v_R increases. In general, relatively low values of depletion probability (smaller than 15%) can be achieved only for average RE_p higher than a minimum threshold ($\sim$250 W in the presented results, but it would be higher in case of smaller S_{PV}). However, v_R may deeply affect the P_D that can be observed. This means that, for a given value of average production, as v_R increases it becomes more and more difficult to have the BS off-grid, unless high values of mean RE_p are made available, for example by increasing the PV panel size. A very similar behavior can be observed for B_O and P_D in case of normally distributed average production.
The average daily grid demand, denoted as G, is shown in Fig. 4.6b in case of UD. G increases as v_R becomes larger, with sharper ascent for low RE_p values. The curve corresponding to RE_p=200 W clearly shows that, for low RE_p, in no case the produced RE is enough to make the BS completely off-grid, unless by increasing the PV size: in fact, even with the lowest v_R, at least $\sim$2kWh must be required from the grid. Notably, despite the difference in the P_D curve slopes between ND and UD case, the G curves result to be much more overlapped even under the two different distributions (ND data not reported), meaning that although the frequency of energy requests from the grid may slightly differ in the two cases, the actual average amount of energy taken from the grid is approximately the same. Wider differences in B_O between ND and UD are seen for higher v_R. This results more evident from Fig. 4.7, showing Q_{90} versus v_R for various RE_p mean values and comparing ND (curves with circle points) versus UD (curves with star points) case. The transition between a constant not null $Q_{90}\sim$2.3kWh (which is the maximum possible level of residual storage remaining after the nighttime BS consumption) and Q_{90}=$0kWh$ is very sharp, especially when v_R is low with respect

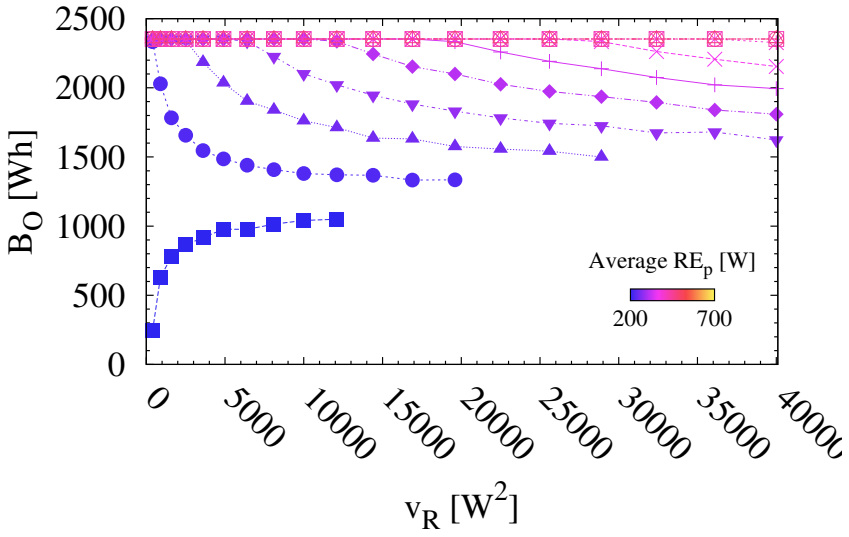

(a) B_O, UD

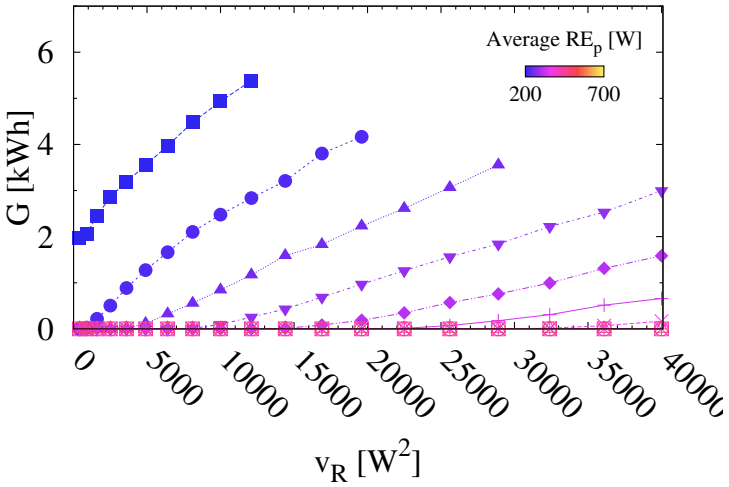

(b) G, UD

Figure 4.6: Battery occupancy, B_O, and grid demand, G, under uniform distribution (UD) of RE_p.

to the mean RE_p. The v_R corresponding to this transition point tends to become higher for larger mean RE_p, until the average RE_p reaches values such that Q_{90} never becomes null. Furthermore, for the same mean RE_p, the switching point becomes higher and higher under ND with respect to UD case, as v_R grows larger. This behavior is consistent with results presented in Fig. 4.6, where P_D appears to

increase faster with raising v_R under UD rather than ND case, that seems slightly outperforming UD to this extent. However, considering the similar trends shown for G under ND and UN, the difference in Q_{90} between ND and UD case may not be relevant, especially for small RE_p, unless an off-grid target is pursued.

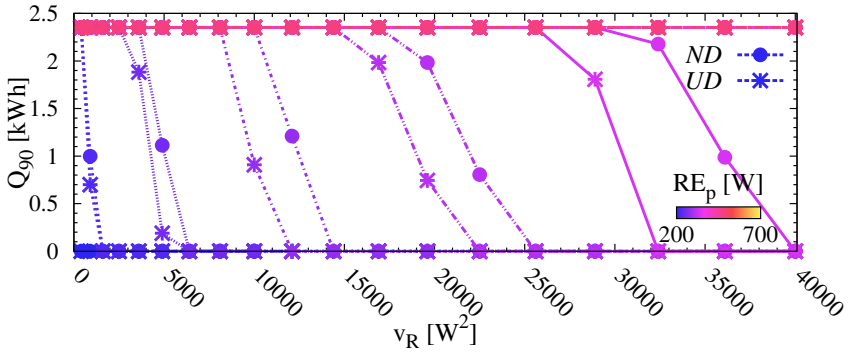

Figure 4.7: 90^{th} percentile of battery occupancy, Q_{90}, under normal (ND) and uniform distribution (UD) of RE_p in the scenario 2 (B=20 kWh, PV=26 kWp).

4.3.1 Further model validation

Further results for model validation are here presented, showing that the uniform distribution can accurately represent the system behavior and outperforms to this extent other types of distributions commonly adopted in the literature to represent the RE production.

Testing the system under empirical distribution of RE_p

Finally, to further validate the model and confirm the previous findings, we test the system behavior under the empirical distribution (ED) of RE_p, as it is derived from real data of RE production in Turin in the worst-case 3-month period. Fig. 4.8 shows the probability density function (*pdf*) and cumulative distribution function (*cdf*) of RE_p computed from the empirical data. Two peaks can be identified in the *pdf*, likely corresponding to the prevalent types of daily weather conditions during the whole period. We now compare the results obtained with the ED of energy production against the other two considered distributions, ND and UD, under the same values of mean and variance of the daily production. In Fig. 4.10, P_D and G versus S_{PV} are reported for the three types of distribution and two battery sizes (B=18 kWh and B=26 kWh). The patterns are very similar and curves almost overlap.

These results show that the proposed model, despite being simple, is accurate and representative of the RE production in a location, like Turin, in which the daily weather is quite stable. As indicated in (4.1), the model is simply given by

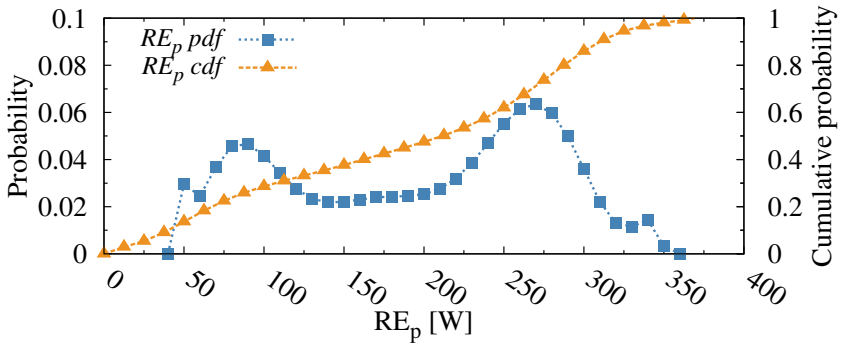

Figure 4.8: Peak production RE_p: *pdf* and *cdf* of the empirical distribution

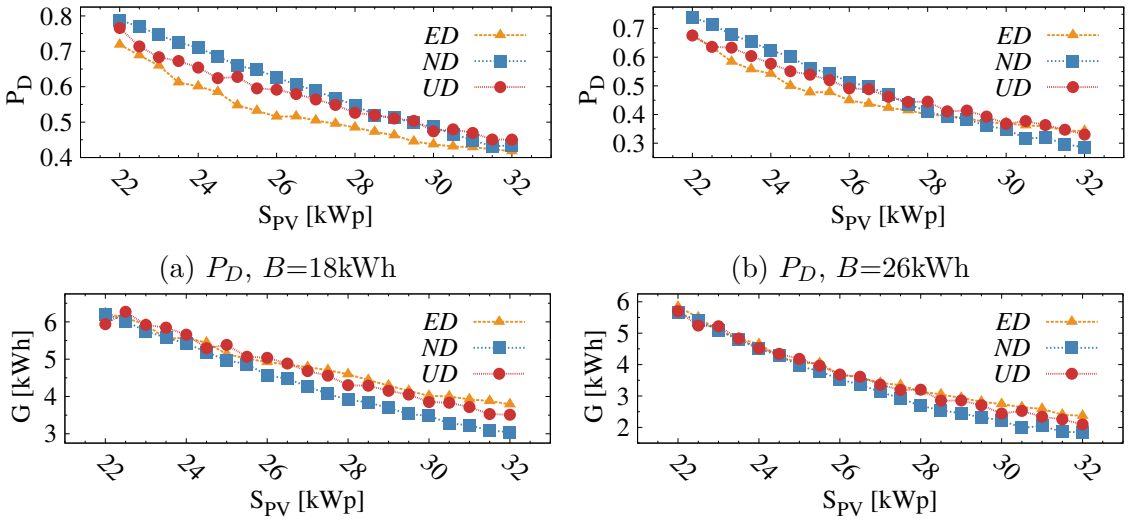

(a) P_D, B=18kWh

(b) P_D, B=26kWh

(c) G, B=18kWh

(d) G, B=26kWh

Figure 4.9: Depletion probability, P_D, and grid demand, G, under ED, ND and UD of RE_p, for B=18 kWh and B=26 kWh.

two components: a function that gives the shape of the production in a day, and a random variable that, multiplied by this function, gives the actual value of the production. In addition, most of the system behavior can be caught by simply focusing on the mean and variance of this random variable.

Validating the model against additional types of distributions used in the literature

As already highlighted, the proposed model is generically representative of the RE production profiles from locations showing a limited intra-day weather variability, like in the case of the city of Turin. Based on the results presented above, the use of the uniform distribution to represent the RE_d can model the real system

operation better than the normal distribution. Furthermore, the values of some performance parameters, like the probability of battery depletion or the amount of energy that must be bought from the power grid, are close to those obtained under the empirical distribution derived from the real data about RE generation. In order to further validate the application of a uniform probability distribution to represent the random variable RE_d, additional types of probability distributions have been tested and the obtained results compared against those derived under the empirical (ED), normal (ND) and uniform (UD) distributions. The ED of RE_d allows to test the system behavior in a realistic setting, since it is derived from real data of RE production in Turin in the worst-case 3-month period. Various distributions that are typically adopted in the literature to model the RE generation, i.e. the Gamma (GD), Beta (BD) and Weibull (WD) distribution, have been evaluated by simulating the operation of the green radio access network (RAN) under each of them. For all the distribution types, the same mean value (E[RE_d]) and variance (v_R) of RE_d obtained from the empirical data have been applied: E[RE_d]=1.005 kWh, $v_R = 439.15^2$ Wh^2, with coefficient of variation $CV = 43.7\%$. The average probability of storage depletion, denoted as P_D, and the average amount of daily on-grid energy demand, denoted as G, have been analyzed. Fig. 4.10 reports the values of P_D and G under the various types of RE_d distribution, for increasing PV panel sizes, S_{PV}, and two different battery capacity (18 kWh and 26 kWh), denoted as B. The results derived using a real location-based distribution of RE_d are consistent with results derived from the model using a more general RE_d distribution. In general, P_D and G tend to decrease as S_{PV} becomes larger. For PV panel capacity higher than 26 kW_p, ND, GD and WD tend to slightly underestimate the daily energy demand from the grid G with respect to ED, whereas the depletion probability P_D is overestimated under these distributions for any PV panel size. Under UD and BD, the estimation of P_D is very close to the real values for any PV panel size and the values of G obtained are mostly completely overlapping with those derived under ED. These results confirm that other types of distributions typically used to model the RE generation, like GD and WD, do not outperform the UD in modeling the RE powered RAN operation. Furthermore, the Beta distribution shows a behavior similar to the uniform distribution in predicting the real system performance. Hence, the selection of the UD distribution to model the daily RE production is further confirmed by these results. Moreover, although the system behavior under UD and BD is rather similar, the first distribution is preferred to the latter due to the lower computational complexity required during the analysis process.

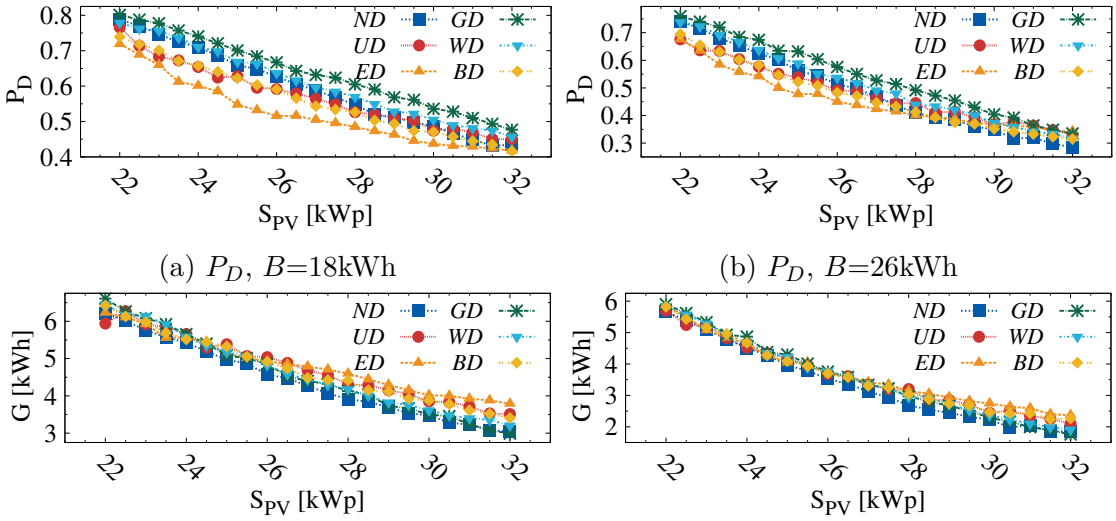

(a) P_D, B=18kWh

(b) P_D, B=26kWh

(c) G, B=18kWh

(d) G, B=26kWh

Figure 4.10: Depletion probability (P_D) and grid demand (G) under empirical (ED), normal (ND), uniform (UD), Gamma (GD), Weibull (WD), Beta (BD) distribution of RE_d, with B=18kWh and B=26kWh.

Chapter 5

Modeling the green mobile network operation

Part of the work presented in this Chapter has already been published in:

- A. P. Couto da Silva et al. "The Impact of Quantization on the Design of Solar Power Systems for Cellular Base Stations". In: *IEEE Transactions on Green Communications and Networking* 2.1 (Mar. 2018), pp. 260–274

- D. Renga et al. "Improving the interaction of a green mobile network with the smart grid". In: *2017 IEEE International Conference on Communications (ICC)*. May 2017, pp. 1–7

The operation of a mobile access network powered by RE can be modeled by means of stochastic models that basically represent the state of the battery charge over time. This state changes according to the RE availability, based on the dynamic variations of the mobile network energy demand and depending on the application of energy management strategies. Part of the results presented in the following Chapters have been obtained by using simulation tools, whereas some of the results have been derived by applying stochastic models to represent the renewable powered mobile network operation. Three different stochastic models, based on Markov chains, have been deployed and are now presented. Each of them feature different connotative characteristics depending on the different aspects they are focused on and on the main investigation objectives they aim to achieve. They can be summarized as follows:

1. First, a stochastic model is proposed in Sec. 5.1 to describe the operation of a system consisting of a single BS powered by RE energy. The model takes into

account the variability of weather conditions from day to day. It is deployed to study the impact of the quantization adopted for various parameters, included in the configuration settings of the model, on the design of RE power systems for cellular BSs. The results related to the quantization issue are presented in Chapter 6.

2. Second, a very simple Markov chain model, presented in Sec. 5.2, is designed to model the state of the battery charge in the same scenario with a single RE powered BS. This model is exploited to derive an analytical formula allowing to easily dimension the PV panel and battery size to proper values, allowing to achieve a battery depletion probability lower than a target value, based on the average RE production and its variability in a given location as input parameters. The model is described within the current Chapter, whereas the results related to system dimensioning will be presented in Chapter 7.

3. Finally, a more complex Markov model, described in Sec. 5.3, is deployed to represent the operation of a mobile network in a scenario where multiple BSs are present, powered by RE and grid energy. This model allows to investigate a more complex scenario with multiple BSs and possible application of Resource on Demand strategy to dynamically adapt the consumption to the actual traffic load. Furthermore, this model is adopted in the studying of the interaction of the cellular network with the Smart Grid in a Demand-Response framework, as it will be shown in Chapter 9.

5.1 A Markovian model embedding weather condition information

The stochastic model that is now presented is deployed considering a simple scenario with a single off-grid LTE BS powered by renewable energy (see Fig. 5.1). A probabilistic model of the system must account for the energy production process, for the energy consumption process, and for the evolution of the battery charge with time. In particular, the model must account for the periods of the day in which energy production is significant (how high depends on the weather conditions), and for the periods of no production, for example at night. The model must also consider that the BS power consumption varies during the day according to the volume of services offered to end users.

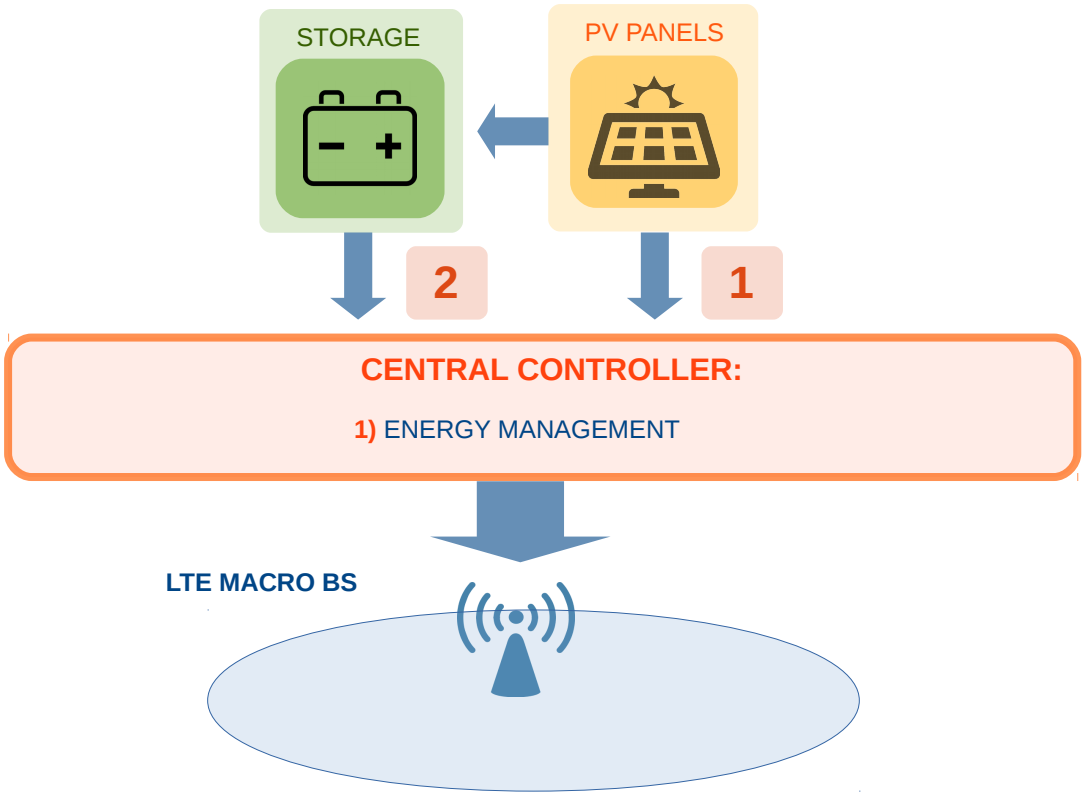

Figure 5.1: The single off-grid green LTE BS.

5.1.1 Model Formulation

We define a discrete time Markov chain (DTMC) model over time slots of duration ΔT [h]. The DTMC state is defined by three variables:

$$\overline{s} = (W, T, S)$$

where W indicates the weather state; T represents the time of the day, and S corresponds to the current charge of the battery.

The time granularity ΔT drives the dynamics of the DTMC model. The daily evolution of the system spans a number of time slots equal to $N_T = 24/\Delta T$. Hence, the DTMC moves from a state with $T = i, i \in \{0,1,\cdots N_T - 1\}$ to a state with $T = (i + 1 \bmod N_T)$.

The value of the weather variable W, together with the PV panel size, and energy loss parameters, determines the amount of energy produced by the PV panel in a time slot. W defines if a day is sunny (high production) or cloudy (low production). Then, the production in a given time slot depends on both W and the time of the day represented by the time slot: for example, whatever the value

of W is, time slots that correspond to night hours have zero production, while time slots that correspond to midday have large production levels, whose actual value depends on W, i.e., on whether the day is sunny or cloudy. Since W defines the weather in a day, its value changes only at the beginning of a new day, that is with the transition of the variable T from the value $N_T - 1$ to the value 0.

The definition of possible values for W is based on long-term (20 years) historical data about the daily solar irradiance. The daily solar irradiance is quantized over a number of levels equal to N_W, so that we can define N_W types of daily weather, W_i, with $i \in \{0, N_W - 1\}$. From the same data we compute the probability that after a day of type W_i a day of type W_j follows, with $i, j \in \{0, N_W - 1\}$. Given a daily solar irradiance level W_i, the irradiance over time slots is derived from fine-grained short-term (2 years) solar irradiance historical data, that reflect the variability of irradiance in different moments of the day, with low irradiance occurring after dawn and before sunset, and peaks occurring around midday. From the historical data (long- and short-term), for each type of day, and for each time slot, we compute the average energy production. The data about solar irradiance are taken from the SoDa service[1].

Finally, the state variable S represents the battery charge level. Let C_B, measured in kWh, represent the battery capacity. By choosing a quantization step Q_s, the set of values for S is $\{0,1,\cdots,N_S - 1\}$, with $N_S = C_B/Q_s + 1$.

At every DTMC state transition, we compute the energy level in the battery at the beginning of the next slot as the sum of the energy already in the battery at the beginning of the current slot, plus the energy produced during the time slot (that depends on W and T), minus the energy consumed in the same time slot (that depends on T). The value of S is the energy in the battery at the beginning of the time slot, while the energies produced and consumed refer to the whole time slot (they are the integrals of the respective powers during the time slot).

5.1.2 Transition Probabilities

The DTMC model deployed to investigate the renewable powered mobile system operation is depicted in Figure 5.2, where only some of the state transitions are shown. Each state $\overline{s}_i = (W_i, T_i, S_i)$ is characterized by different values of day-type W_i, time of the day T_i and battery charge level S_i. Only a sample of all the possible transitions between different states is highlighted in the figure. In particular, the transitions starting from states $(W_i,0, S_i)$ and (W_i, N_{T-1}, S_i) are represented. These states correspond to the first and last timeslots of a day of

[1] http://www.soda-pro.com/. Two different data sets are used: the first one provides solar irradiance data at 15 minutes intervals for a period of 2 years, with a spatial resolution of about 5 km; the second one provides daily solar irradiance data for a period of 20 years, with a spatial resolution of about 20 km

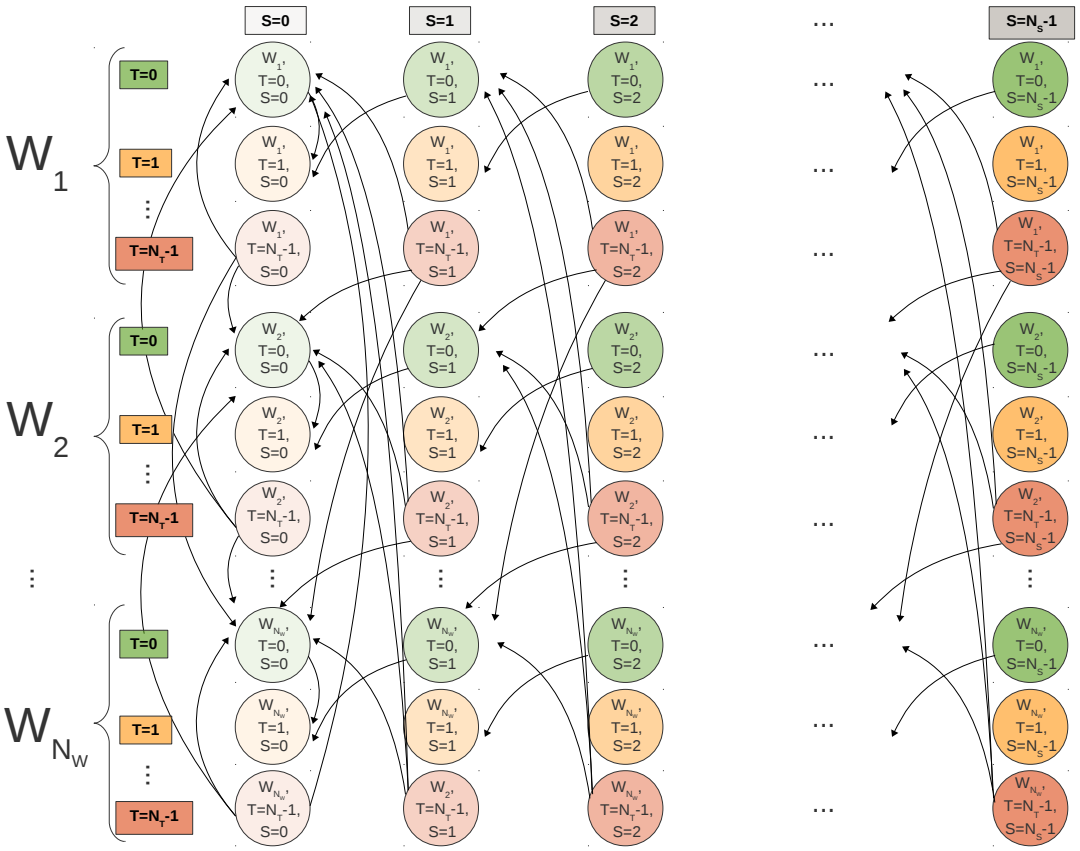

Figure 5.2: Markovian model representing the renewable powered mobile system operation.

each type W_i, respectively, with any possible value of battery charge level. The cardinality of the state space of the DTMC model is the product of the number of time slots during a day N_T, times the number of solar irradiance levels N_W, times the number of levels considered for the battery charge N_S.

However, since the type of day can change only when a new day starts, given the type of day and the daily traffic profile, the transition from a state $\overline{s}_i$ to a state $\overline{s}_j$, with $\overline{s}_i = (W_i, T_i, S_i)$, and $\overline{s}_j = (W_j, T_j, S_j)$, with $T_i \in \{0,1,\cdots N_T - 2\}$, is possible only with $W_j = W_i$ (the type of day cannot change during the same day), $T_j = T_i + 1$ (the time slot increases along the same day), and $S_j - S_i$ equal to the (fixed) difference between the energy produced and consumed during the time slot.

On the contrary, the transition from a state $\overline{s}_i$ to a state $\overline{s}_j$, with $T_i = N_T - 1$ is possible with any value of W_j (the type of day can change at the beginning of a new day), $T_j = 0$ (the first time slot of the new day), and $S_j - S_i$ equal to the energy consumed during the time slot (no solar irradiation is present around midnight at the considered latitudes).

As it can be observed from Figure 5.2, this means that for all states $\overline{s}_i$ with

$T_i = N_T - 1$ the number of possible outgoing transitions is equal to the number of day-types N_W, while for all other states only one outgoing transition is possible. As a result, the DTMC transition probability matrix is quite sparse.
The model here presented has been adopted to evaluate the impact of quantization of various parameters on the design of RE power systems for cellular BSs and to evaluate the model performance under different configuration settings. Related results are reported in Chapter 6.

5.2 A 3-state Markov chain model for the battery charge

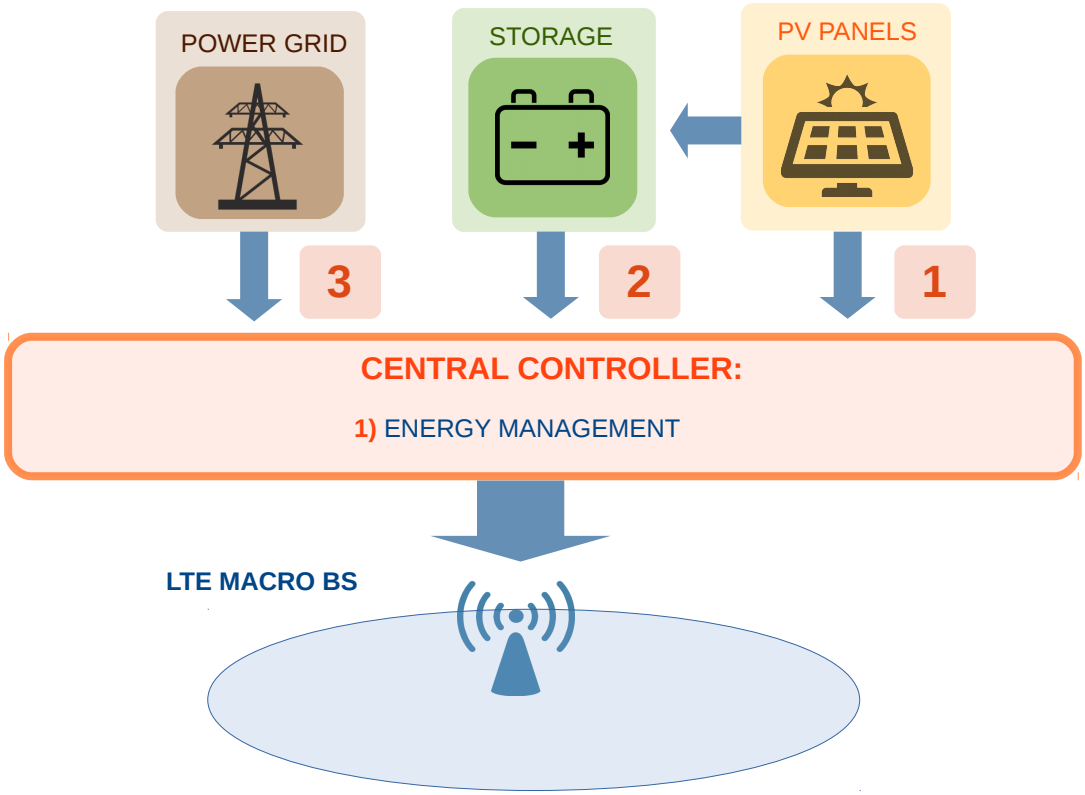

Figure 5.3: The single green LTE BS.

The stochastic model here described is again designed to represent the operation of a simple system consisting of a single LTE BS supplied by the electric grid and by locally produced solar energy, as depicted in Fig. 5.3. The baseline energy management policy is applied, i.e., as the RE is produced, it is utilized to power the BS, according to the *first-power-then-harvest* paradigm. This means that the

solar energy is first used to power the BS, whereas only the extra amounts of RE that are not immediately used for powering the BS are harvested into the storage afterwards, as long as there is still enough space. Following this principle, charging/discharging losses can be minimized with respect to the principle *first-harvest-then-power*, in which the battery is first charged and then the energy is drawn from the storage to satisfy the BS demand. When no RE is currently being generated or if its production is not sufficient to satisfy the BS demand, energy can be drawn from the storage. Only in case the battery results empty, the energy required is taken from the power grid.

5.2.1 Model formulation

A simple Markovian model is proposed to represent the charging state of the storage in the same scenario shown in Fig. 5.3, i.e. a single macro BS with constant power consumption. Based on the stochastic model presented in Chapter 4, the daily renewable energy production for a PV panel with capacity 1 kWp, denoted as RE_d, is proportional to the daily peak production and it can be modeled by means of a random variable, characterized by a mean value and a variance, which depend on the location, and featuring a uniform probability distribution. Of course, the actual total amount of energy that is produced per day during the daylight period, denoted as RE_D, depends on the actual PV panel capacity, denoted as S_{PV}. It can hence be derived as:

$$RE_D = RE_d \cdot S_{PV} \tag{5.1}$$

In our scenario the storage consists of S_B battery units, each with capacity 2.4 kWh. The total nominal capacity of the storage, denoted as B, is defined as:

$$B = S_B \cdot 2.4 \ [kWh] \tag{5.2}$$

The actual available capacity, denoted as C_B, is derived as:

$$C_B = B \cdot DOD^* \tag{5.3}$$

where DOD^* is the maximum allowed DOD.
We assume that, for a battery of capacity B, the maximum total available storage charge is C_B, due to the constraint on the maximum DOD. Hence, we consider C_B as the actual capacity of the storage to be modeled. A 3-state Markov chain is defined, with each state, denoted as S, corresponding to a possible battery charge level that is observed at the beginning of the day, i.e. at the beginning of the daytime period, when RE starts being produced. The Markov chain model is represented in Fig. 5.2 and the 3 states are here defined:

- *state E (Empty)*: no energy is available in the battery and the storage charge is null:
$$E = 0 \quad [kWh]$$
- *state L (maximum Level at the beginning of the day)*: this state represents the maximum charge level that might be observed at the beginning of the day after a night of normal BS operation, assuming that, at the beginning of the previous night period (i.e. after the last hour of RE generation on the day before), the battery was at full charge (i.e. the battery charge was equal to C_B). Let us denote as D_n the BS energy demand during the night hours. Considering that during the nighttime no RE is produced, L is defined as follows:
$$L = C_B - D_n \quad [kWh]$$
- *state M (Intermediate)*: the battery charge is at an intermediate level, defined as:
$$M = \frac{L}{2} \quad [kWh]$$

The transition from current state S_i to state S_{i+1} occur with a timestep of 24 hour. In order to define how transition probabilities have been computed, let us denote as D_d the BS energy demand during the daytime, whereas D_n represents the nightly demand. Since traffic is very little load proportional, with rather high power consumption also in those periods during which the traffic is very low, BS consumption is assumed to be constant. The variable H denotes the amount of energy that can be harvested daily in the battery, in case the BS daily consumption is lower than the total RE produced:

$$H = RE_d - D_d - D_n \tag{5.4}$$

Finally, assuming that the current state S_i may be either E, I or L, the transition probability from state S_i to state S_{i+1}, denoted as $p_{i,i+1}$, can be computed as follows:

Case $S_{i+1} = E$

$$p_{i,i+1} = p(S_i + H \leq 0) \tag{5.5}$$

Case $S_{i+1} = M$

$$p_{i,i+1} = p(0 < S_i + H \leq L) \tag{5.6}$$

Case $S_{i+1} = L$

$$p_{i,i+1} = p(S_i + H \geq L) \tag{5.7}$$

In the computation of transition probabilities, charging and discharging losses are kept into account.

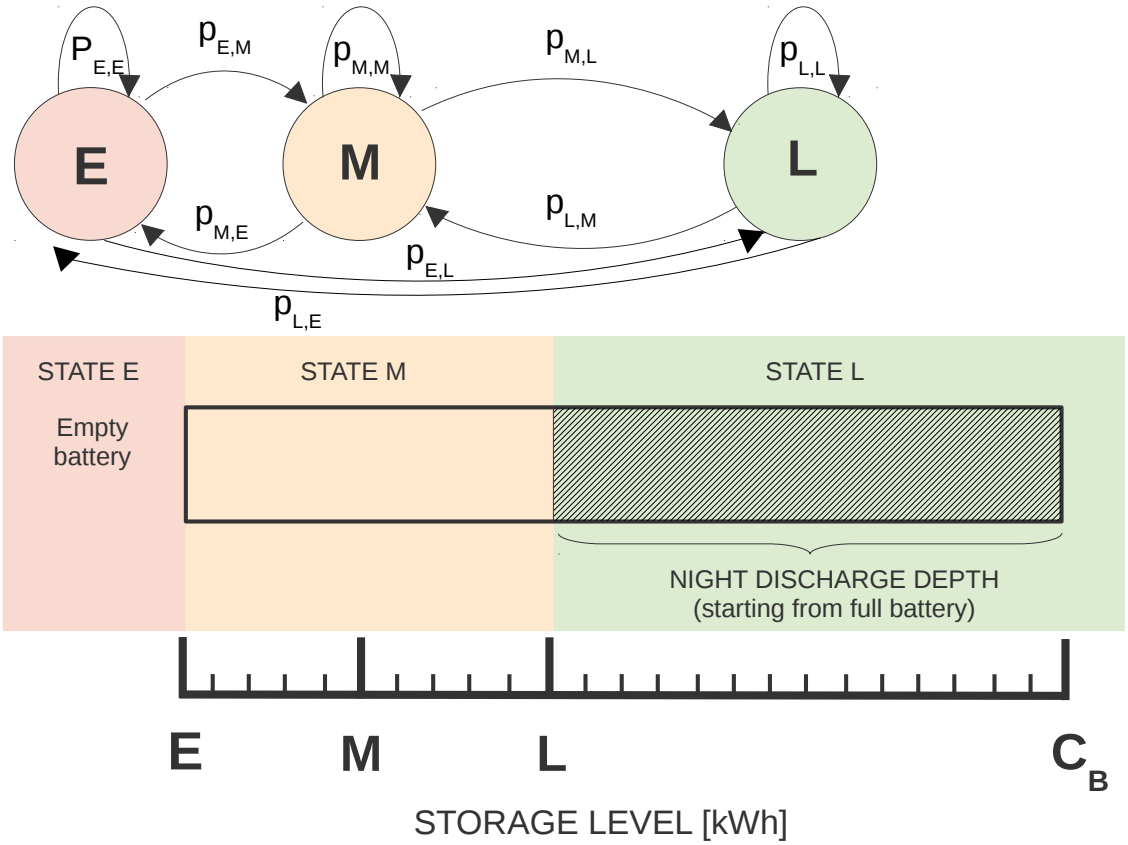

Figure 5.4: Markovian 3-state model for the storage.

5.2.2 Storage model validation

The Markovian model proposed to analyze the RE generation for powering a mobile system has been validated by comparing the performance results obtained under the model against results derived by investigating the same scenario via simulation. The scenario consists of an on-grid LTE BS powered by photovoltaic panels and equipped with a set of lead-acid batteries as energy storage. The system is located in the city of Turin. The BS power consumption is assumed to be constant, with an hourly energy demand, denoted as D_h, of 1 kWh. The daily RE generation per kW_p, RE_d, has a uniform distribution, with mean value E[RE_d]=1.005 kWh,

variance $v_R = 439.15^2\ Wh^2$, and coefficient of variation $CV = 43.7\%$, as derived from the empirical distribution of RE production in the city of Turin. Since the system is analyzed during the coldest months, the average light-time duration is 9 hours, hence the daytime energy demand, D_d, corresponds to $9 \cdot D_h$. RE_D represents the average daily peak of total renewable power that can be obtained in a given location where a PV system of size S_{PV} is present. The local solar radiation determines the mean value of RE_d, i.e. the daily energy production per unitary PV panel capacity, whereas the PV system size S_{PV} is a factor that scales up the renewable power generation to its actual value RE_D. RE_D is hence defined as:

$$RE_D = RE_d \cdot S_{PV} \tag{5.8}$$

The model has been validated under several combinations of system sizing (S_{PV},C_B). At the initial conditions, the battery is assumed to be fully charged. Losses due to PV panel efficiency and environmental conditions are considered. Charging and discharging losses are kept into account as well.
Let us denote as p_D the battery depletion probability at the beginning of the daytime: $p_{D_{Sim}}$ represents the value of p_D obtained by simulation, whereas $p_{D_{Mod}}$ is the estimated value of $p_{D_{Sim}}$, predicted by the Markovian model. $p_{D_{Mod}}$ actually corresponds to the steady state probability π_0 for the three-state Markov chain.

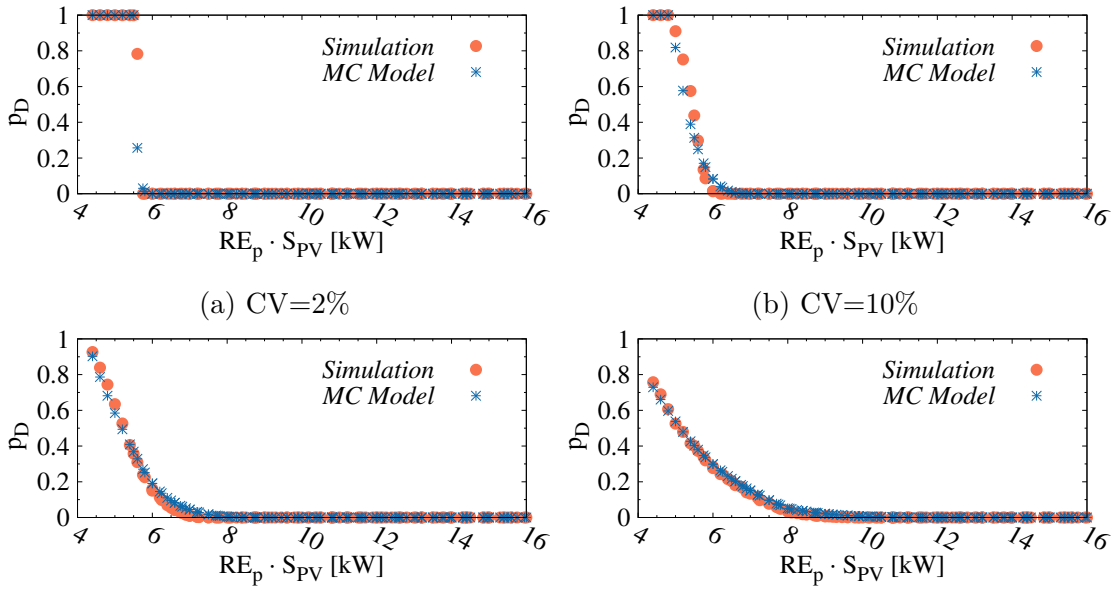

(a) CV=2% (b) CV=10%

(c) CV=20% (d) CV=30%

Figure 5.5: Battery depletion probability, p_D, obtained through simulation and from the Markovian model.

Fig. 5.5 reports the values of $p_{D_{Sim}}$ and $p_{D_{Mod}}$ for increasing levels of peak solar

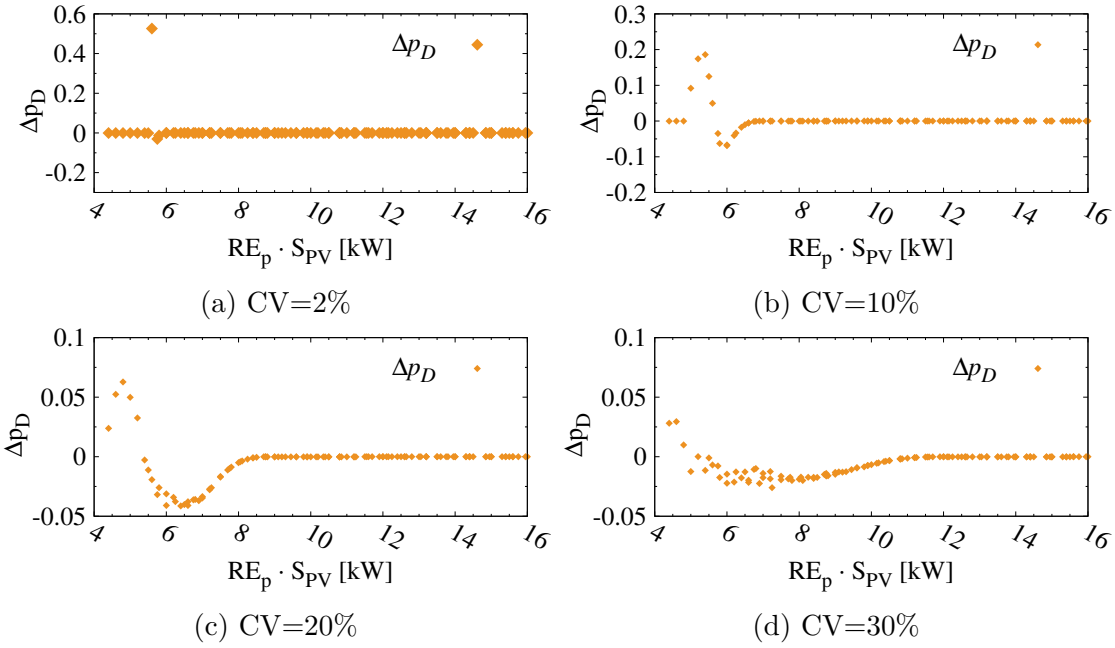

(a) CV=2% (b) CV=10%

(c) CV=20% (d) CV=30%

Figure 5.6: Difference between $p_{D_{Sim}}$ and $p_{D_{Mod}}$ (Δp_D) versus RE production level.

power generation (i.e. $RE_p \cdot S_{PV}$) -corresponding to increasing levels of average daily RE production- and under different values of CV. A fixed C_B is assumed (26 kWh). Several values of CV have been tested, although here only some sample values are shown, in order to highlight the general changes in the p_D behaviour under increasing variance. In particular, the range of CV [0,35]% appears to be more interesting for observing the impact of CV on the battery depletion probability. Values of CV as high as those empirically observed for RE_p in the city of Turin (43.7%) are hence not shown in this case.

The values of p_D obtained by simulation or under the model tends to decrease sharply for RE_d around 5-6 kWh in case of lower values of CV (2-10%). Conversely, when the variance is higher, p_D is below 1 even for very low RE_d and it decreases gradually as the RE generation increases. The curve representing $p_{D_{Mod}}$ is almost overlapping to the pattern of the depletion probability derived from the simulation for any S_{PV}, given a fixed location or, alternatively, for any value of RE_d, given a fixed S_{PV}. Indeed, the difference between the depletion probability obtained from the simulation and its model predicted value, denoted as $\Delta p_D = |p_{D_{Sim}} - p_{D_{Mod}}|$, is always negligible and it is almost null under most set of values of mean RE production and variance CV (hence variance), as shown in Fig. 5.6. Higher differences between the simulated and predicted values of p_D can be found in the range of RE_d values that correspond to the window during which the switch between two operating regimes occurs: the regime of insufficient production (low regime) and the regime of production sufficient for BS operation (high regime). The width of this

window is larger as the CV becomes higher, but the maximum difference between simulated and predicted value is much lower than in case of smaller CV. In almost all cases, Δ_{p_D} is $\leq$0.05, whereas in most cases it results to be negligible. Fig. 5.7 shows the values of $p_{D_{Sim}}$ and $p_{D_{Mod}}$ for increasing values of RE_D, considering a location with RE_d CV=20%. For small RE generation, there is a larger Δp_D in case of larger battery size, whereas a small battery allows to limit this difference. Nevertheless, Δp_D is always below 0.05 and, for $RE_D > 9\ kWh$, it is negligible. When RE_D is lower, the model results to be very accurate in predicting the simulated value of p_D, since the battery is so small with respect to the average RE generation level that it will result empty most of the time at the beginning of the day both in the simulation and under the model, with no effect due to RE generation variability. When the size of the battery is larger, the model results just slightly less accurate within the RE_D window of transition between the two regimes of operation, due to edge effects occurring when the battery size is small, hence the impact of RE production variability on the average battery charge level is rather limited.

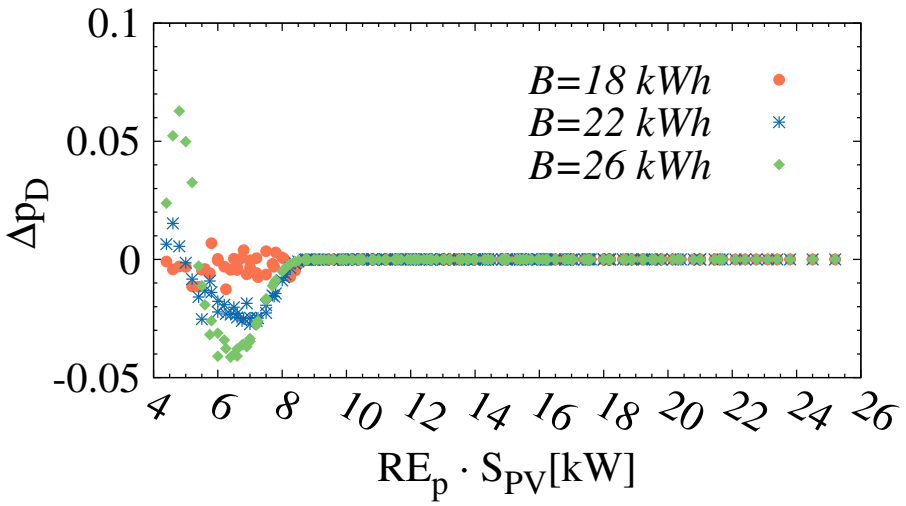

Figure 5.7: Difference between $p_{D_{Sim}}$ and $p_{D_{Mod}}$ (Δp_D) under different values of battery capacity.

The model can be easily extended and applied to other locations featuring different RE generation profiles, by simply considering the corresponding mean value of RE_d and its variability. The value of CV is adopted instead of the variance, since it allows to immediately compare the variability degree of RE_d between different locations, regardless the actual mean value.
Chapter 7 will describe how this Markovian model can be applied to derive an analytical formula, allowing to properly dimension the total required RE system capacity, in terms of S_{PV} and C_B, based on the location and on the target level of energy self-sufficiency (with respect to the electric grid).

5.3 An N-state Markov chain model for a complex scenario

In this section a stochastic model is proposed to investigate the operation of a portion of a mobile access network powered by the grid energy and by locally produced RE, along with its interaction with the SG. The modeled mobile network consists of a macro BS and m micro BS. Furthermore, this model takes into account the dynamic variations of consumption of the cluster of BSs that may occur over time, due for example to the varying traffic demand. Hence, this model is suitable to study the mobile scenario even when BS switching on/off strategies are applied. In addition, the RE production variability is considered as well. Finally, this model is meant to be employed for a mobile network operating in a Demand-Response framework, in order to investigate the capability of the cellular network of enhancing its interaction with the Smart Grid and reducing cost, by accomplishing its requests. Therefore, the model is designed so as to include the dynamic requests coming from the SG, that aim at shifting electric loads for better balancing the energy supply and demand. Fig. 5.8 shows the scenario for which this Markovian model can be applied.

A discrete time Markov chain is considered, where each state is defined by 3 state

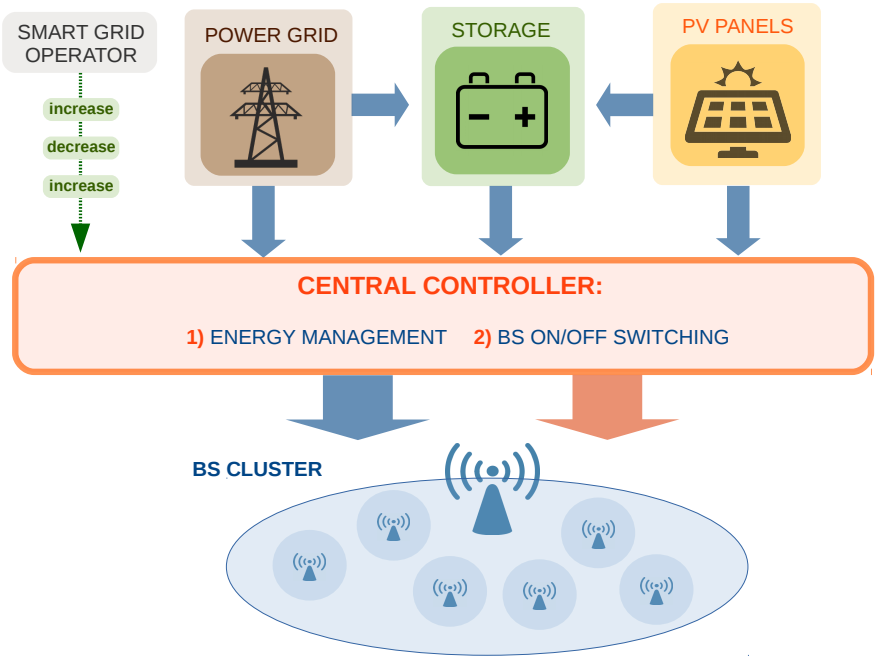

Figure 5.8: Cluster of RE powered BSs interacting with the Smart Grid in a Demand Response framework.

variables: P, indicating the period of the day; S, representing the current energy

level of the storage; G, corresponding to the type of the request sent by the smart grid (UP, DOWN or NULL). Each state in the Markov chain, denoted as x, is hence defined as $x = (P, S, G)$. The day is divided in five periods, corresponding to the periods that typically succeed each other over 24 hours: the *night* period, during which no RE is produced; the *morning* period, with intermediate levels of RE production; the *peak* period, with the highest RE generation levels; the *evening* period, with intermediate RE production; the *evening* period, without significant RE generation. The total number of battery energy levels, N, is given by $\frac{C_B}{Q_s} + 1$, where Q_s is the quantization step used to quantize the energy harvested in the storage, as well as the produced renewable energy and the energy consumed by the mobile network.
Transition probabilities, i.e. the probabilities of moving from current state at time step i, x_i=(P_i,S_i,G_i), to state x_{i+1}=(P_{i+1},S_{i+1},G_{i+1}), are derived combining a number of factors. Changes of P, period of the day, occur in such a way that the average time spent in a period is equal to the period duration, that may differ from period to period and is proportional to the number of timeslots included in the specific period.Let G_i be the grid request at timeslot i in our model. The transition probability from G_i to G_{i+1} is given by the statistical frequency with which requests of type G_{i+1} follow request G_i. The transition probabilities are also derived keeping into account the predicted average energy consumption of the BS cluster during a timeslot, namely E_c, that is forecast the day ahead. The traffic profiles tends to be repetitive and they are rather predictable from day to day, given the type of residential rather than business area [103]. The application of a RoD strategy may add some variability in the consumption, but, again, the consumption is rather predictable, since the number of active BSs is decided based on the current traffic demand and it can be easily forecast the day ahead, based on the predicted traffic profiles. The fact that the traffic load variation is rather limited within the same period, together with the little load proportionality in the BS consumption, allows to assume a constant value for the cluster power demand within each period [65, 35]. Hence, the value of E_c is fixed within each period of the day and it is obtained by averaging the cluster consumption within the period, considering the traffic fluctuations and the possible application of the RoD strategy. On the top of this, any further variability in the actual consumption of the radio access network, with respect to the level forecast, is only represented by that generated in response to requests from the smart grid. For example, if the SG requires to increase the consumption, an extra amount of energy, besides the energy needed for the network operation E_c, is drawn from the grid, in order to satisfy the SG request. Finally, for the RE production, within each period of the day, P, the amount of RE produced during a timeslot is represented by a random variable, denoted as R_p, whose probability density function depends on the location and on the period of the day. The possible occurrence of fast and short term (of the order of minutes) variations

in the renewable power may lead to slightly overestimate the actual energy production per each timeslot, but the error would be limited, with slightly optimistic, still acceptable, results. The quantization step Q_s is adopted also to quantize the cluster consumption E_c and the amount of RE, R_p, produced during each timeslot. Clearly, the transition probabilities also depend on the management of the interaction with the SG, performed according to adopted energy management strategy.
The application of this model is helpful to investigate the interaction of the green mobile network with the Smart Grid and to study to what extent a properly designed energy management strategy allows to improve the capability of the mobile network of contributing in providing ancillary services to the SG operator and at the same time to reduce its energy bill. The related results will be presented in Chapter 9.

Chapter 6

Impact of parameter quantization on the design of RE power systems for cellular BSs

Part of the work presented in this Chapter has already been published in:

- A. P. Couto da Silva et al. "The Impact of Quantization on the Design of Solar Power Systems for Cellular Base Stations". In: *IEEE Transactions on Green Communications and Networking* 2.1 (Mar. 2018), pp. 260–274

In Chapter 5 various stochastic models have been proposed to represent the operation of a green mobile access network, possibly actively interacting with the Smart Grid. Each model features different discretization step values for the quantization of the different parameters considered in the model, i.e. battery charge level, amount of RE generation, timestep, day-type in terms of weather conditions. Different configurations of the discretization settings for the parameters defined in these models may affect the outcome of the system performance investigation. Nevertheless, the impact of the quantization granularity has not been investigated in the literature. This Chapter provides useful insights regarding the impact of quantization on the design of RE power systems for cellular BS. In particular, the presented results will show how the discretization step for each parameter in a model should be properly set in order to obtain a model that is representative of the studied system, still trading off accuracy and model complexity.
A probabilistic model of the system must account for the energy production process, for the energy consumption process, and for the evolution of the battery charge with time. In particular, the model must account for the periods of the day in which energy production is significant (how high depends on the weather conditions), and

for the periods of no production, for example at night. The model must also consider that the BS power consumption varies during the day according to the volume of services offered to end users.

Here we consider a macro BS that is equipped with PV panels and a set of batteries in order to satisfy the energy demand for the mobile system operation in a scenario where the grid is absent, according to the scenario depicted in Figure 5.1. The discrete time Markov chain model introduced in Chapter 5.1 is adopted to model the renewable powered mobile system operation and to perform the investigation about the impact of quantization granularity. Transitions probabilities are defined according to what discussed in Section 5.1.2. Next, we introduce the energy consumption model used in our analysis in Section 6.0.1. The key performance indicators for the BS solar power system are described in Section 6.1. Section 6.2 discusses the main model design choices, as regards the effect of the discretization of the various parameters. Finally, in Section 6.3 the system performance is evaluated focusing on the impact on the self-sustainability of different traffic profiles, of new generations of BSs and of considering locations featuring different irradiance patterns.

6.0.1 Energy Consumption Model

The model adopted to estimate the power needed to operate a macro BS is the EARTH model, described in Chapter 3.2.1 [65]. Typical values of the parameters are listed in Table 3.1 for a LTE macro BS, either with or without RRU, and for a micro BS. In our study, the data of the case of a LTE macro BS without RRU are used, since it is both more frequent and more critical.

In order to characterize the parameter ρ, i.e. the instantaneous normalized BS load, and its variability during the day, we consider the traffic profiles corresponding to real traces provided by one of the Italian mobile network operators, that have been presented in Chapter 3.2.2, both for a business (BA) and a residential (RA) area, during the weekdays and in the weekend [124].

6.1 Performance Measures

From the steady-state solution of our DTMC model, we evaluate a few key performance indicators for the BS power system. Let $\pi(\overline{s}) = \pi(W, T, S)$ be the steady-state probability of state $\overline{s} = (W, T, S)$, with $W \in \{0, \cdots, N_W - 1\}$, $T \in \{0, \cdots, N_T - 1\}$, $S \in \{0, \cdots, N_S - 1\}$.

We define:

1. $E[S]$, the average battery level:

$$E[S] = \sum_{\forall W} \sum_{\forall T} \sum_{\forall S} S \; \pi(W, T, S);$$

2. P_D, the empty battery probability:

$$P_D = \sum_{\forall W} \sum_{\forall T} \pi(W, T, 0);$$

3. P_f, the full battery probability:

$$P_f = \sum_{\forall W} \sum_{\forall T} \pi(W, T, N_S - 1).$$

6.2 Model Parametrization

We now discuss the main model design choices, as regards the effect of the discretization of the energy production and consumption models (Section 6.2.1), discretization of time (Section 6.2.2), and of energy storage (Section 6.2.3). Then, we present some lessons learned from our analysis (Section 6.2.4).

6.2.1 Renewable Energy Production Model

As previously mentioned, the parameters of the energy production stochastic model are derived from traces available in the Solar Radiation Data (SoDa) website. In particular, we used the SoDa 20-year trace collected from January 1st 1985 to December 31st 2004 in the cities of Turin, Italy, Paris, France, and Maiduguri, Nigeria. This data is provided by NASA (USA) and MINES Paris Tech/Armines (France), considering global radiation in the horizontal plane. In the cases of Turin and Paris, for each year we only looked at the 3 winter months (December, January, February, i.e., 90 or 91 days per year). These are the periods which result most critical for the solar power system design, because of shorter daylight periods and lower irradiance levels at the latitudes of Turin and Paris, in the winter season of the northern hemisphere. As shown in [77], if the solar power system in Turin is dimensioned based on the summer period, its performance in winter becomes unacceptable. We will instead consider the 3 most rainy months (July, August and September) when looking at the Maiduguri location in Section 6.3.

Starting from the individual values of the daily energy production of a 1 kW peak solar panel (i.e., a solar panel large enough to produce an output power of 1 kW in standard conditions, including a solar irradiance of 1 kW/m^2 - about 5 m^2 with the current normal solar cells), we first created a histogram by applying an equal-range discretization. That is, we first divided the total production range (i.e., the difference between the maximum and minimum productions observed over the 20-year period) into N_W ranges of equal size. Then, we computed the frequency (probability) of each interval, and defined N_W energy production levels as the middle values of each interval. Figure 6.1 reports the histograms, and the daily energy production ranges, in the two cases $N_W = 5$ and $N_W = 10$. The blue bars

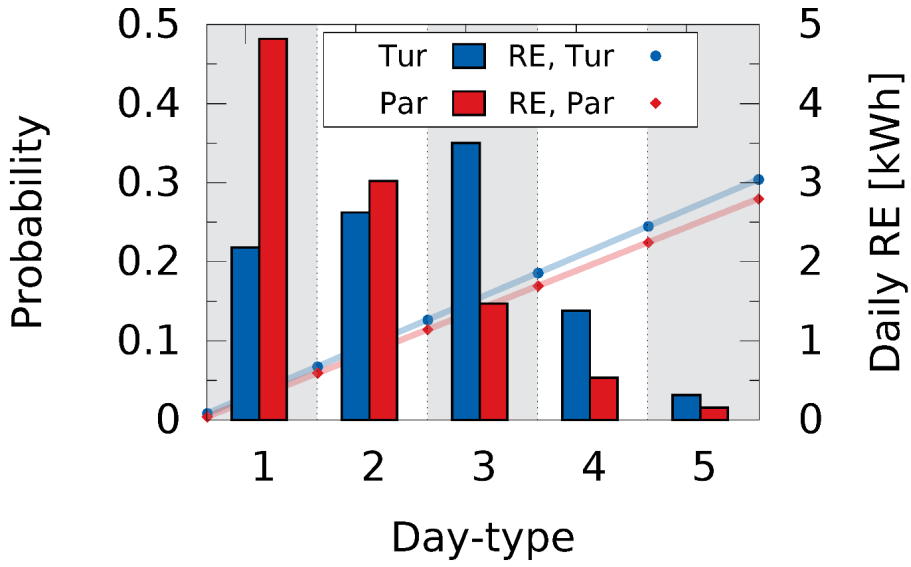

(a) N_W=5

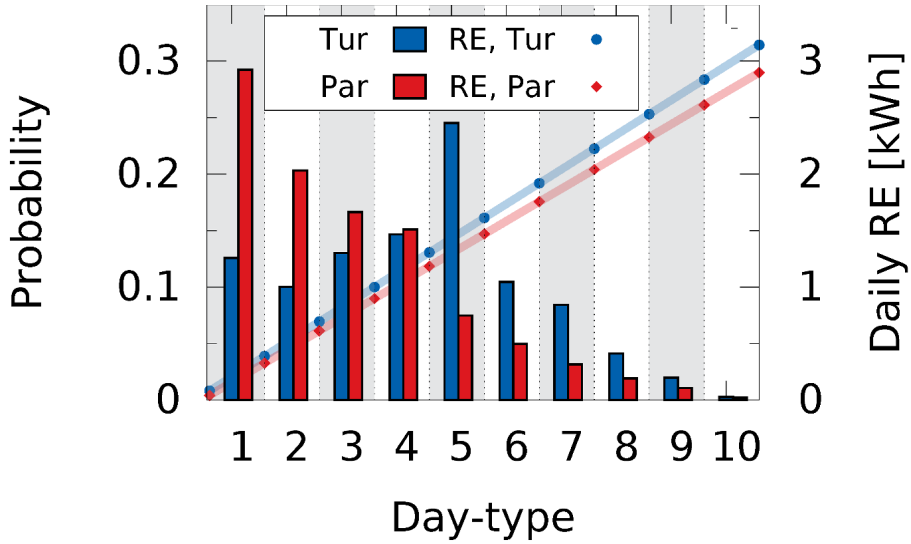

(b) N_W=10

Figure 6.1: Day-type probability distribution for 5 and 10 day-types (N_W=5 and N_W=10) with equal-range discretization, in Turin and Paris, with corresponding daily produced renewable energy (RE) discretization levels, assuming a 1 kW peak PV panel.

in the histograms refer to Turin, while the red ones refer to Paris. Probabilities are reported on the left vertical scale. The blue markers are associated with the right vertical scale, and report the extremes of the daily energy production ranges for Turin. The red markers refer instead to Paris. We see, for example, that in the case $N_W = 10$, the production range number 5, in the case of Turin has extremes

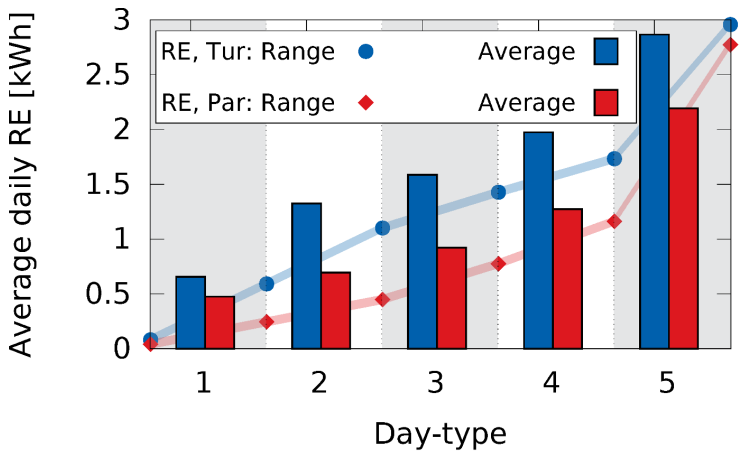

Figure 6.2: Day-type average values of daily renewable energy (RE) production of a 1 kW peak PV panel, for 5 day-types (N_W=5) with equal-probability discretization, in Turin and Paris, along with the corresponding discretization levels of daily RE.

1.3 kWh and 1.6 kWh, and probability 0.25. The same production range 5 in the case of Paris has extremes 1.2 kWh and 1.4 kWh, and probability 0.075.

It is also possible to create a histogram by applying an equal-probability discretization. That is, to divide the total production range into N_W ranges of different sizes, so that the frequency of each interval is the same, and to define N_W energy production levels as the middle values of each interval. Figure 6.2 reports the energy production levels obtained with this procedure, for $N_W = 5$, in the cases of Turin and Paris. With this discretization procedure, the resulting average hourly production for each day-type, with N_W=5, for Turin is reported in Figure 6.3a, and for Paris in 6.3b. These curves are generated by using both the long- and short-term solar irradiance datasets, as explained before. We also evaluate the statistical frequency of consecutive day-types. For each daily production level W_i (i.e., for each day-type W_i), we count the number of dataset instances where the following day is of type W_j, and dividing this number by the total number of day pairs we compute the statistical frequency with which day-type W_j follows day-type W_i. The statistical frequency is then mapped into the transition probabilities of the Markov chain. For what concerns the DTMC model design, the most critical decision with respect to energy production is the discretization of the meteorological data, i.e., the selection of the number N_W of energy production levels (also called day-types).

Figure 6.4 depicts the three main performance indicators of the macro BS power system for Turin, namely the average battery charge, and the empty and full battery probabilities, versus values of N_W, chosen in the set $\{3, 5, 7, 10\}$. The quantization of the energy production in this case uses equal-ranges over the Turin data, the battery capacity is 25 kWh, and three different PV panel sizes are used: 20, 30

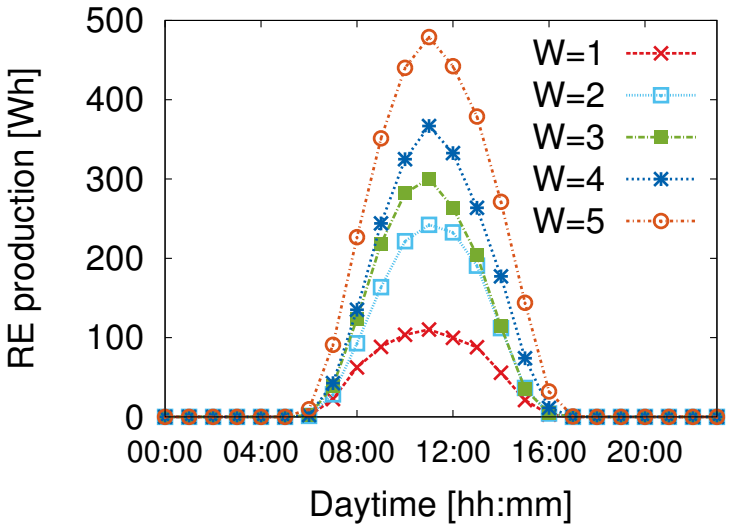

(a) Hourly RE production, Turin

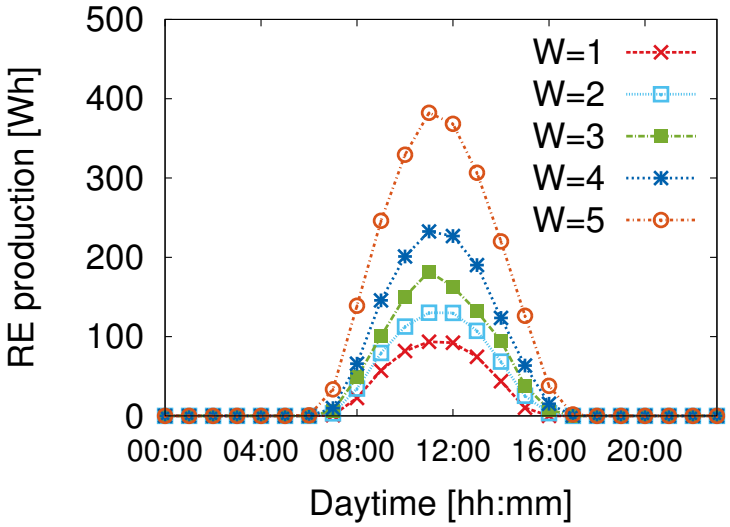

(b) Hourly RE production, Paris

Figure 6.3: Hourly energy production of a 1 kW peak PV panel, per each day-type in Turin and Paris, for N_W=5 with equal-probability discretization.

and 40 kW peak. The time slot is 1 h, and the battery charge quantum is 100 Wh. The results show that the number of day-types has a marginal impact on the performance indicators: the average battery charge varies within less than ±5 %, while empty and full probabilities, whose absolute values are quite small, exhibit acceptable variations. Hence, while a higher number of possible day-types could be considered preferable, because it provides a more accurate distinction among

production levels, the impact on results is limited.

Moreover, it must be considered that the choice of N_W should also take into account the fact that with N_W energy production levels, we need to estimate $N_W \cdot N_W$ probabilities that after a day of type W_i a day of type W_j follows. A small value of N_W is thus desirable to guarantee not only a smaller size of the DTMC state space, but also a more reliable estimation of the transition probabilities from the available data. Considering the 3 winter months in 20 years, we have 1,805 days; from which we need to estimate N_W^2 probabilities. With $N_W = 10$ this means about 18 samples to estimate one probability, in case of uniformly distributed probabilities, but actually much less for infrequent cases (such as the sequence formed by a very cloudy day followed by a most sunny day). From the results in Figure 6.4 we can thus conclude that good choices for N_W could be 5 or 7.

Results for the city of Paris in the same conditions as above are shown in Figure. 6.5. Paris weather is quite different from the one in Turin, with much quicker variations that are reflected in a somewhat higher variability in the results for different values of N_W. An explanation for this behavior can be found by looking at the histograms of the daily energy productions in Turin and Paris, shown in Figure 6.1, for N_W=5 and N_W=10. The daily energy production histogram in Paris has a triangular shape, so that some energy levels are much more likely to occur than others, meaning that the estimation of transition probabilities for these less likely levels is not accurate. In cases like this one, it can be convenient to adopt an equal-probability (rather than equal-range) discretization. Note that this is not the case for Turin, whose histogram exhibits rather a bell shape.

The results with this kind of discretization are reported in Figure 6.6 for the case of Paris, and, as expected, are more stable. The results for the case of Turin are reported in Figure 6.7, and they show similar stability.

In conclusion, the results of our analysis suggest that, depending on the shape of the day-type histogram, we can choose an equal-range or an equal-probability discretization. When the histogram is bell-shaped either discretization is acceptable. Instead, when the histogram shows a triangular shape, an equal-probability discretization should be preferred. As for the choice of the number of levels N_W, a trade-off between accuracy in representing the production levels and reliability in the transition probability estimation should be decided.

6.2.2 Time Granularity

Here, we investigate the impact of the choice of the time granularity, i.e., of the value of the parameter ΔT, which represents the time slot in the DTMC model. We consider 5 options: (i) Daily model, M_D in short, in which ΔT =24 h and $N_T = 1$; (ii) Periods of day model, M_P in short, in which ΔT =6 h and $N_T = 4$; (iii) Hourly model, M_H, with ΔT =1 h and $N_T = 24$; (iv) 30-minute model, M_{30}, with ΔT =0.5 h and $N_T = 48$; and (v) 15-minute model, M_{15}, with ΔT =0.25 h

and $N_T = 96$. We discuss the effect of time granularity on the data for Turin. Same conclusions hold for the case of Paris.

Figure 6.8 presents results for a macro BS located in Turin, loaded with the residential traffic profile, and powered by a PV panel of variable size, with energy storage capacity $C_B = 25$ kWh, modeled with granularity 100 Wh. We can highlight several interesting observations from this first set of results:

1. The daily model, M_D, tends to overestimate the average battery charge and the probability of full battery, when compared against the other considered time granularity models. This is due to the fact that, with this time granularity, the DTMC model globally accounts for all energy produced and consumed in one day, overlooking the short term phenomena, such as, for example, the fact that the battery may become full in some periods during the day, so that the produced energy is lost, even if in other periods of the same day the battery is not full. This phenomenon can be understood by looking at the curves in Figure 6.9, which show the average battery charge for the case of a macro BS in Turin, with $N_W = 5$, PV panel sizes equal to 20, 30, and 40 kW peak, battery capacity equal to 25 kWh, and stored energy granularity equal to 100 Wh, for both the residential and business traffic profiles. The time granularity of the curves is 1 h, and this allows us to see that the daily dynamic of the battery charge is significant. For example, in the top middle plot we see that, in a day of type 5, the battery is full from 11 am to 6 pm. In this period, no energy produced by the PV panel which is not immediately consumed by the macro BS can be stored. For the rest of the day the battery is not full, and the excess energy production can be stored. However, if we look at the whole day, we see that most of the excess energy production can be stored. This causes the overestimation of the average battery charge, because the highest energy production occurs in the periods when the battery is full.

2. The periods of day model, M_P, with respect to the daily model, tends to better capture the fluctuations between periods of battery charge and discharge during the day, but exhibits a behavior similar to the daily model when the PV panel size grows large, because of the same phenomena mentioned above. Under this model, the empty battery probability results to be significantly overestimated with respect to the other models. This is due to the fact that, besides two 6-hour periods in which the renewable energy production is either null (during night) or very high (in the middle of the day), the other two periods exhibit energy generation profiles that include hours of low production along with hours of higher generation. In these periods, a model with a finer time granularity (e.g. 1 hour) is such that hours with higher production reduce the probability of empty battery (which is measured at the end of the time interval), whereas under the M_P model the total production over these

6-hour time slots is not enough to balance energy consumption, resulting in a null battery charge at the end of the period.

3. The hourly, 30-minute, and 15-minute models generate similar values for the analyzed performance measures in the considered cases. This is an indication of the fact that going below the time granularity of 1 h does not lead to significant variations in results.

6.2.3 Stored Energy Granularity

The last parameter that must be considered from the point of view of granularity is the energy storage. This means that we must define what is the quantum of energy to be considered within the battery. Since the quantization impacts the accounting of the amounts of consumed (and produced) energy during one time slot, and these amounts depend on the slot duration, we look at pairs of values (Δ_T, Q_s). Considering that the macro BS consumes between about 1300 W (at peak traffic) and about 800 W (when no traffic is present), and that the PV panel production must be of the same order of magnitude (with somewhat higher peak, to compensate for periods of low or no production), with a time granularity of 1 h we look at stored energy granularity values equal to 100 Wh, 50 Wh, as well as 25 Wh. Assuming a peak hourly production from the PV panel around 2 kWh, this mean that the stored energy quantum is about 1/20, 1/40, 1/80 of the peak hourly energy production, about 1/13, 1/26, 1/52 of the maximum hourly energy consumption, and about 1/8, 1/16, 1/32 of the minimum hourly energy consumption. Results in Figure 6.10 show that for the hourly model the three quantization values produce very similar results of the average battery charge. When we go to a 30 minute time granularity, keeping the same stored energy quantum values means using 1/4, 1/8, 1/16 of the hourly energy consumption. With a 15 minute time granularity, keeping the same stored energy quantum values means using values that are 1/2, 1/4, 1/8 of the hourly energy consumption. Then, Figure 6.10 shows that values of the stored energy quantum of the order of 1/10 of the maximum hourly energy consumption can be a reasonable choice.

Figure 6.11 confirms this indication, since the values of average battery charge, of full and empty battery probability computed for $\Delta_T = 1$ h, 30 and 15 minutes, $Q_s = 100$, 50 and 25 Wh do not show significant differences, except for the case of very large PV panel, where the finer granularities allow a more accurate evaluation of the amount of energy that can be accepted in the battery.

6.2.4 Takeaways

From our analysis we can draw the following conclusions. First of all, quantization has important effects on the model outputs. Developing models with a daily

time granularity is not sufficient. A careful assessment of the system performance requires a time granularity that allows capturing the energy production and consumption variations during the day. If the model cannot carefully account for the fact that the energy that is produced when the battery is fully charged is lost and cannot be used, the predictions turn out to be optimistic. Our experiments indicate that a time granularity of 1 h can be a reasonable choice.

The impact of the day-type quantization is also relevant, specially if the histogram of the weather conditions produced with the equal-range approach turns out to have a triangular shape. In this case, an equal-probability quantization seems advisable. When an equal-probability quantization is used, 5 or 7 levels should be sufficient to capture the system performance with acceptable accuracy.

Finally, our results indicate that a quantization in the energy storage of the order of 1/10 of the maximum energy consumption per time slot is acceptable.

6.3 Evaluation of the BS Power System Performance

In this section we evaluate, through numerical results derived from the model presented in Section 5.1, the system performance, and we provide insight into its behavior. Our main goal in performing these experiments is three-fold: i) measure how different traffic profiles impact the amount of consumed/stored energy, so as to understand what can be the potential for the use of RES in different portions of the Radio Access Network (RAN), ii) discuss the impact, on the use of RES, of new generations of BSs, that are more parsimonious and more load proportional in energy consumption [14] with respect to current BSs [38], and iii) present the results that can be obtained in regions with irradiance patterns very different from what we considered so far (Turin and Paris); for this we look at the city of Maiduguri in Nigeria.

6.3.1 Impact of traffic profiles

First, we analyze how the user traffic pattern impacts the dimensioning of the solar power system of the BS, in order to understand what can be the potential for the use of RES in different portions of the RAN.

Turin

Figure 6.9 shows the hourly average energy storage level for Turin. In night hours, the BS activity drains the energy stored in the battery during the peak production hours. At the end of the day, the balance can be positive (for good weather days, e.g., type 5), or negative (for bad weather days, e.g, type 1). We

see that the differences between the curves for the residential and business traffic profiles are marginal. In addition, as expected, increasing PV panel sizes lead to larger amounts of stored energy in the battery. However, doubling the PV panel size (from 20 to 40 kW peak) has a large effect only for bad weather days, whose curve shows much higher energy values in the battery. For good weather days, the impact is minimal.

The main effect of the traffic profile is in the rate at which energy is drained from the battery during the evening (9:00 pm to midnight) and night (midnight to 5:00 am): the load from residential users is heavier on these time periods than that from business users, so that the battery level goes down faster for the residential traffic load.

To better visualize the differences between the two types of traffic profiles, Figure 6.12 shows the *maximum* values for the empty and full battery probabilities, respectively, versus the PV panel size. Each of these probabilities corresponds to the maximum value observed over all day hours, and over all day-types. We can see that the business area traffic is easier to handle, since it yields lower empty battery probability, and higher full battery probability for the same size of the PV panel. This is largely due to the higher correlation between the energy consumption induced by the business traffic profile and the energy generation of the PV panel. The fact that in a business area most of the traffic is generated during working hours allows the PV panel power to be immediately used to run the BS.

Paris

Figure 6.13 shows the hourly average energy storage level for Paris. The behavior of the curves is qualitatively similar to Turin, but the quantitative differences between different PV panel sizes are now much more pronounced.

To further visually compare the effect of different traffic profiles, in Figure 6.14 we plot the hourly average storage level for PV panel size equal to 30 kW peak, in residential and business areas, in Turin and Paris. Here we just show curves for days of types 1 and 5, and the average over all days. Once more, we see that differences are small, and this means that the solar option to power BSs is equally viable in business and residential areas.

6.3.2 Impact of new generation base stations

The next aspect that we investigate is related to the technological evolution of BS technology, in particular as regards energy consumption. We evaluate the reduction of PV panel size that can be achieved with the BS technology transitioning from the one that led to the power model that we used so far and that we call EARTH model [38], to the one presented in [14], that we call the 2020 model. The latter type of BS exhibits an energy consumption pattern which is much lower, and

also more proportional to the traffic load.

We derived results for the 2 x 2 macro BS model described in [14], which leads to a power saving of 47.7% at full load, when compared against [38][1].

Figure 6.15 presents results for residential and business traffic profiles in Turin, while Figure 6.16 refers to Paris. By looking at the curves we see that the 2020 model yields better performance than the EARTH model, with half the panel size (20 kW peak instead of 40). For instance, the empty probability for a 20 kWp panel size and 2020 model is 1/4 of the value of the EARTH model in Turin (6.15.b) and almost zero in Paris (6.16.b). Moreover, the battery remains full almost twice the time with the 2020 model, for all panel sizes. This means that the new generations of BSs are making the use of solar power less expensive, so that we can expect an increased diffusion of solar BSs in the coming years. The parallel technological improvements in solar panels will further reinforce this trend.

6.3.3 Impact of solar irradiance patterns

Finally, we look at the influence of geographic characteristics, which can have a big impact on solar irradiance patterns. Considering that, as we stated earlier in this work, renewable energy sources can be particularly useful in areas where the power grid does not exist or is extremely unreliable, we look at the city of Maiduguri in Nigeria. Maiduguri is the capital of the Borno State in north-east Nigeria, and its population is around 1 million people. The city had severe energy problems over the last years, and is thus a very interesting candidate for the use of solar panels to power cellular communication equipment. The sub-Saharan location of Maiduguri, at a latitude of about 12° north, guarantees a very high solar irradiance, somewhat diminished in the most rainy months, i.e., July, August and September. Considering, as usual, the least favorable period of the year for the analysis of the BS power system performance, we look at the solar irradiance in those three months. Even so, comparing the daily solar irradiance in Maiduguri to those of Turin and Paris, after a classification into 5 day-types, we see that in the least favorable day-type the maximum solar irradiance in Maiduguri is about four times higher than in both Turin and Paris, while the advantage of Maiduguri reduces to a factor 2 for the most favorable day-type.

Figure 6.17 shows the hourly battery charge for the case of residential area traffic, with battery capacity 25 kWh, and with PV sizes of 10, 20, 30, and 40 kW peak, respectively, in plots a), b), c) and d). We can note that the PV panel size significantly impacts only the curves for day-type 1 (the one with least irradiance). Otherwise, the curves are much more packed than in the cases of Turin and Paris,

[1]From [14], a BS with full load needs 702.6 W at full load and 114.5 W at zero load. From [38], instead, a BS with full load needs 1.344 kW at full load and 130 W at zero load.

Table 6.1: Full and empty battery probability, Maiduguri, residential profile, C_B = 25 kWh.

PV Size [kWp]	P_f	P_D
10	0.23	5.9e-02
20	0.36	5.6e-02
30	0.40	5.2e-02
40	0.40	5.0e-02

the only difference being in the speed at which the battery charge rises at the beginning of the day. The full and empty battery probabilities are reported in Table 6.1 for different PV panel sizes. In this case we see that outage probability differences are very small, in spite of large PV panel size variations. This result tells us that the system bottleneck is more in the battery capacity rather than in the energy production capacity.

For this reason, Figure 6.18 shows the hourly average battery charge with PV size 10 kW peak, and with battery capacity equal to 25, 35, and 50 kWh, respectively, in plots a), b), and c). We can note that the average battery charge grows significantly for all day-types for increasing battery capacity, thanks to the excess energy production in days of high solar irradiance which is not wasted with batteries of adequate size. The empty battery probability remains close to 5% for all battery capacities, mainly due to longer sequences of rainy days.

The observation of the Maiduguri results, and their comparison against those of Paris and Turin, tell us that optimal BS power solutions based on PV panels and batteries can be extremely different from one geographical location to another. In Maiduguri a small PV panel is sufficient, but a larger battery is necessary to obtain very small outage probabilities. Turin and Paris require much larger PV panels, but can live with smaller batteries, since the outage probability is more driven by the PV panel size than by the battery capacity. In order to be able to observe these effects, carefully engineered stochastic models are necessary, and this is the issue we address in this study.

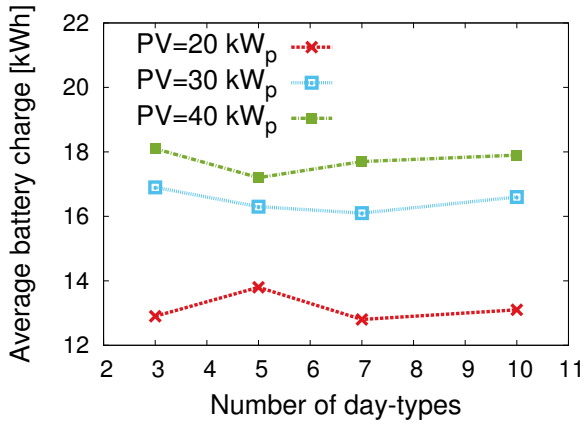

(a) Average battery charge

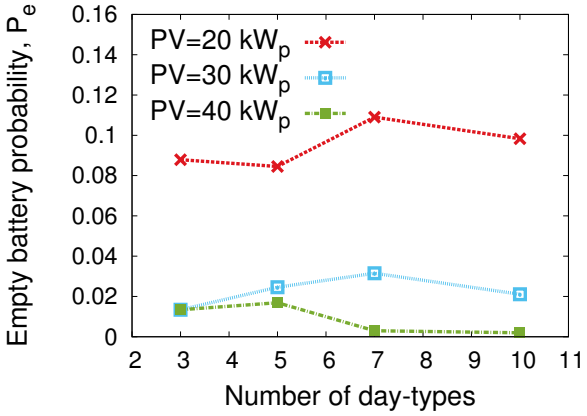

(b) P_D

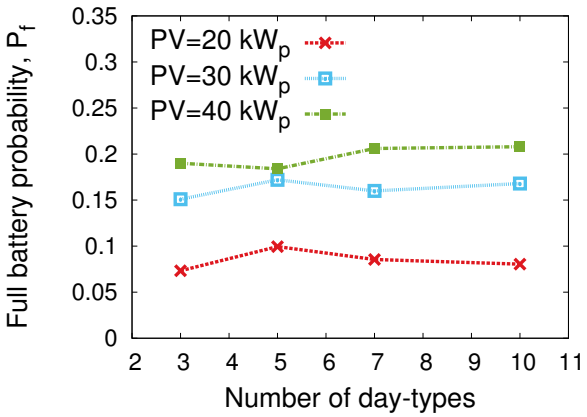

(c) P_f

Figure 6.4: Average battery charge, empty (P_D) and full (P_f) battery probabilities versus number of day-types N_W, for different PV panel sizes, for Turin, with *equal-range discretization* and time slot $\Delta T = 1$h, for $C_B = 25$ kWh, $Q_S = 100$ Wh, with residential weekday traffic profile, adopting the Earth model.

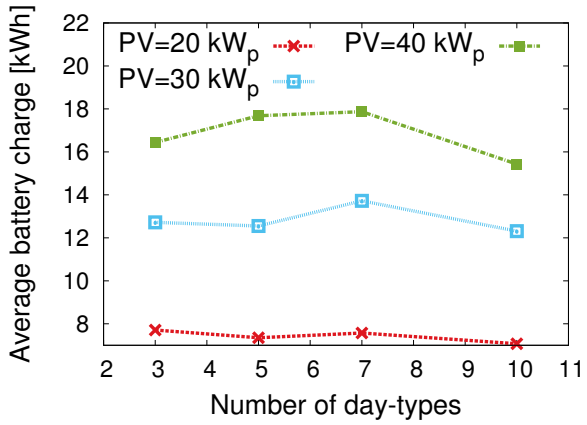

(a) Average battery charge

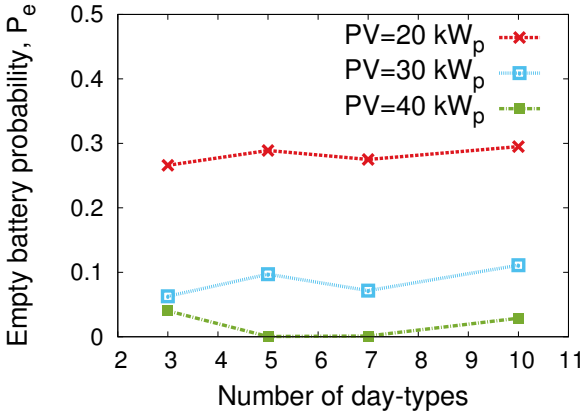

(b) P_D

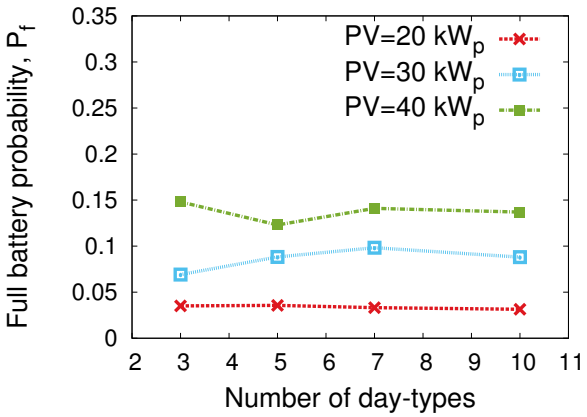

(c) P_f

Figure 6.5: Average battery charge, empty (P_D) and full (P_f) battery probabilities versus number of day-types, for different PV panel sizes, for Paris, with *equal-range discretization* and time slot $\Delta T = 1$h, for $C_B = 25$ kWh, $Q_S = 100$ Wh, with residential weekday traffic profile, adopting the Earth model.

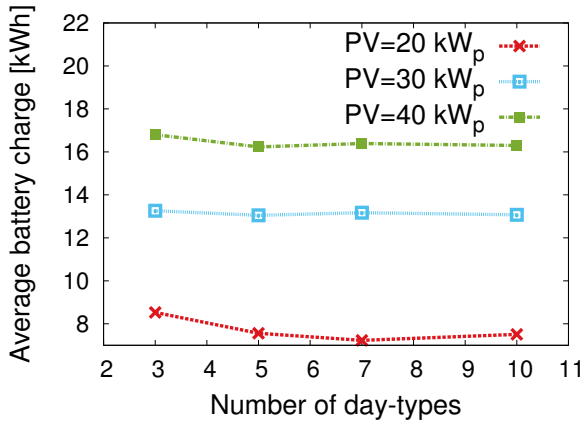

(a) Average battery charge

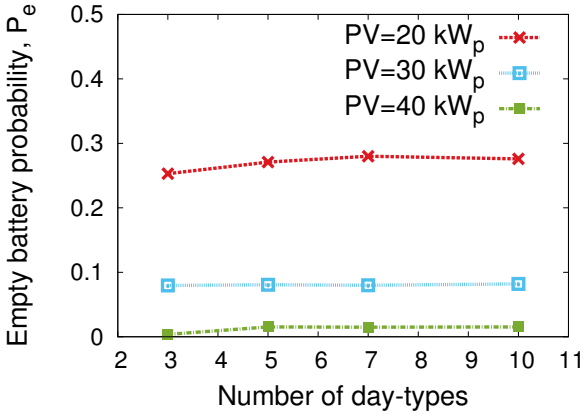

(b) P_D

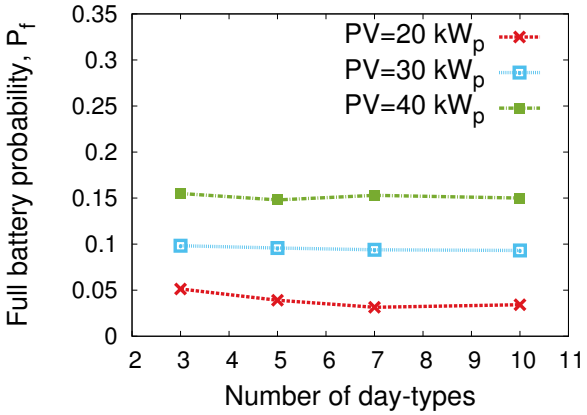

(c) P_f

Figure 6.6: Average battery charge, empty (P_D) and full (P_f) battery probabilities versus number of day-types, for different PV panel sizes, for Paris, with equal-probability discretization and time slot $\Delta T = 1$h, for $C_B = 25$ kWh, $Q_S = 100$ Wh, with residential weekday traffic profile, adopting the Earth model.

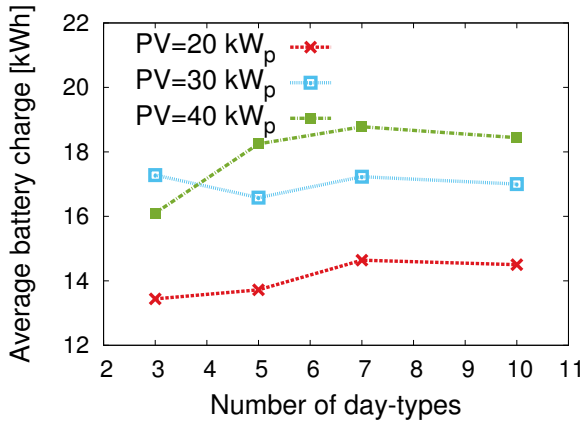

(a) Average battery charge

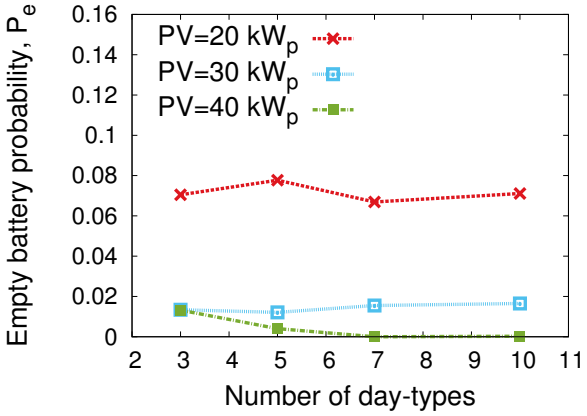

(b) P_D

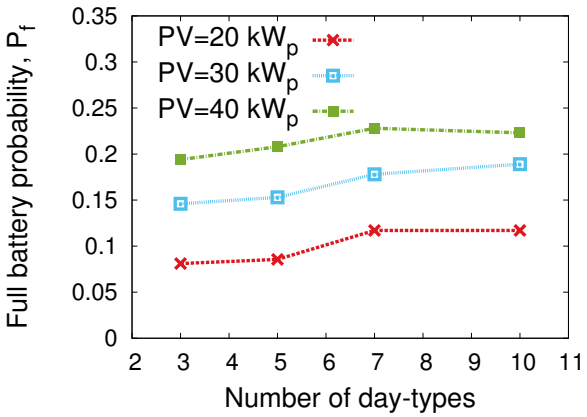

(c) P_f

Figure 6.7: Average battery charge, empty (P_D) and full (P_f) battery probabilities versus number of day-types, for different PV panel sizes, for Turin, with equal-probability discretization and time slot $\Delta T = 1$h, for $C_B = 25$ kWh, $Q_S = 100$ Wh, with residential weekday traffic profile, adopting the Earth model.

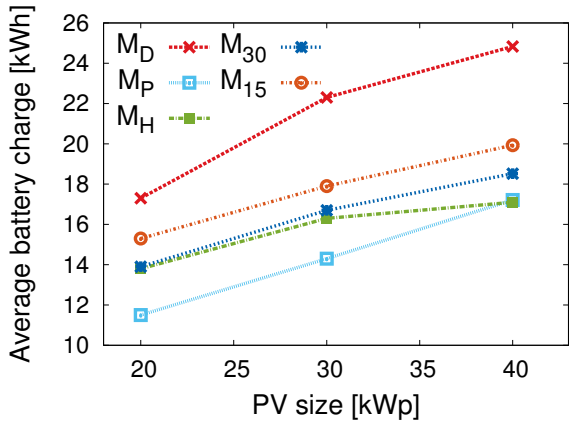

(a) Average battery charge

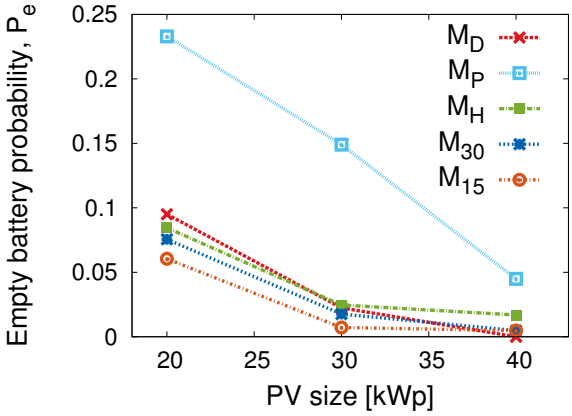

(b) P_D

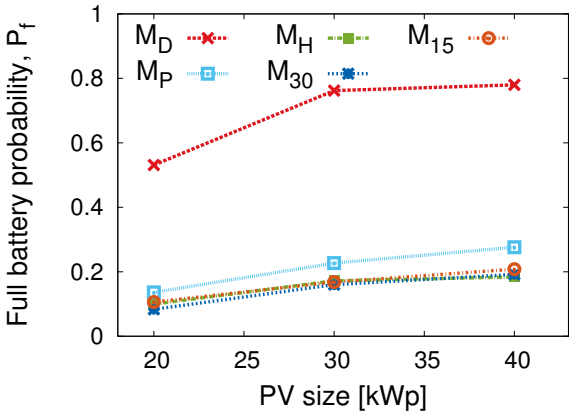

(c) P_f

Figure 6.8: Average battery charge, empty (P_D) and full (P_f) battery probabilities versus PV panel size, for different time slots, for Turin, with 5 day-types, with equal-range discretization, for $C_B = 25$ kWh, $Q_S = 100$ Wh, with residential weekday traffic profile, adopting the Earth model.

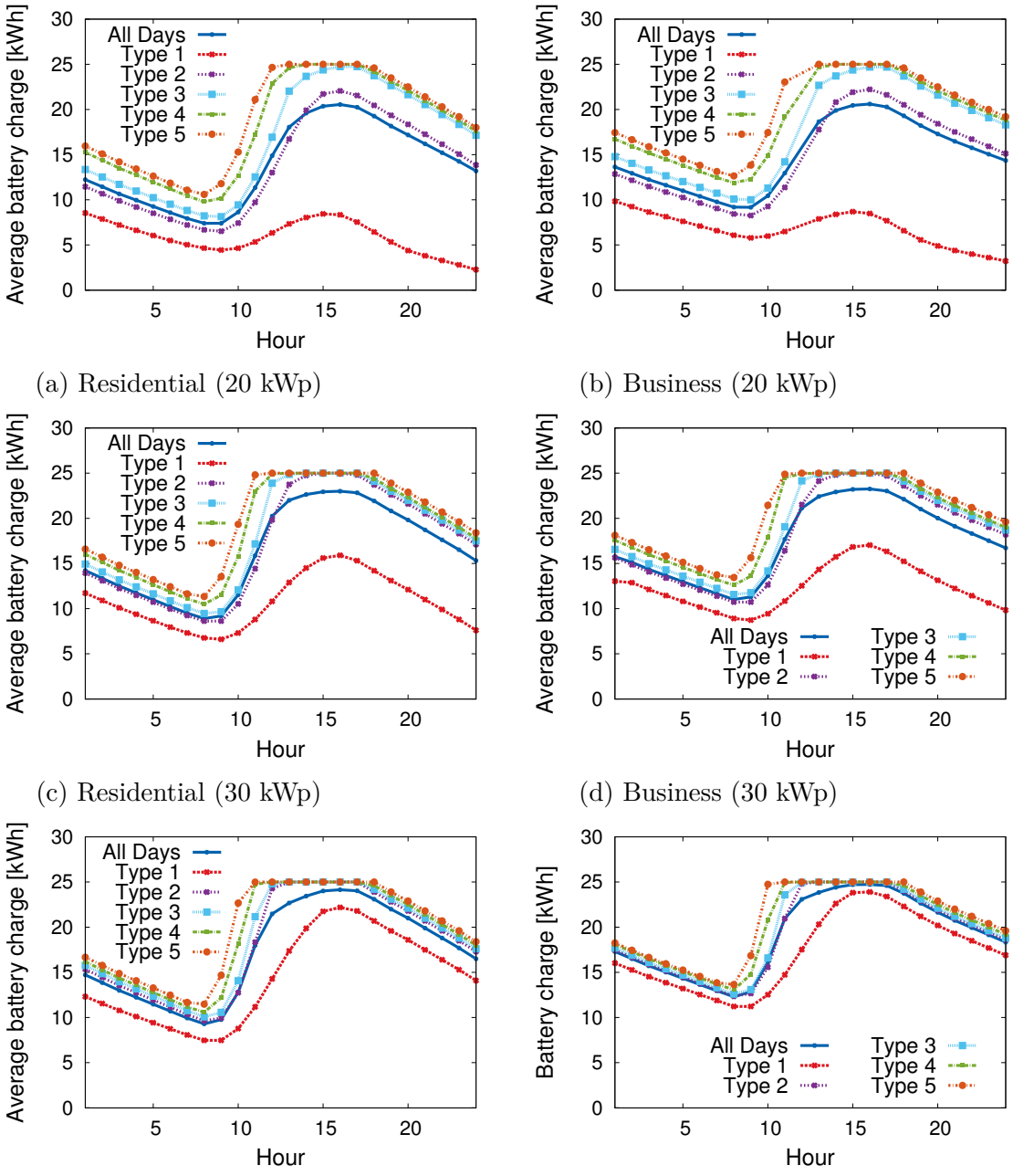

(a) Residential (20 kWp)

(b) Business (20 kWp)

(c) Residential (30 kWp)

(d) Business (30 kWp)

(e) Residential (40 kWp)

(f) Business (40 kWp)

Figure 6.9: Average hourly battery charge for a macro BS in Turin versus time, with $N_W = 5$ and equal-range discretization, time slot $\Delta T = 1$h, PV panel sizes 20, 30, and 40 kW peak, $C_B = 25$ kWh, and $Q_S = 100$ Wh, for both the residential and business weekday traffic profiles, adopting the Earth model.

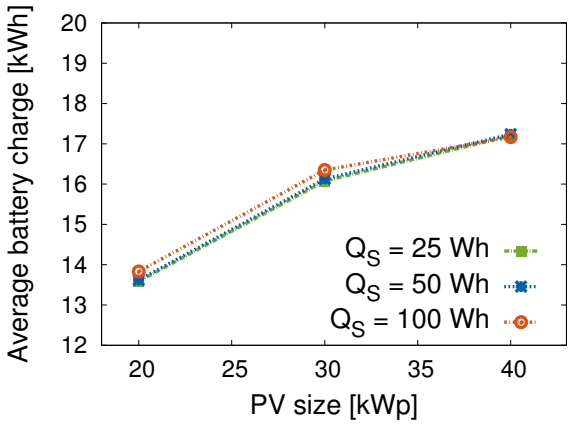

(a) M_H

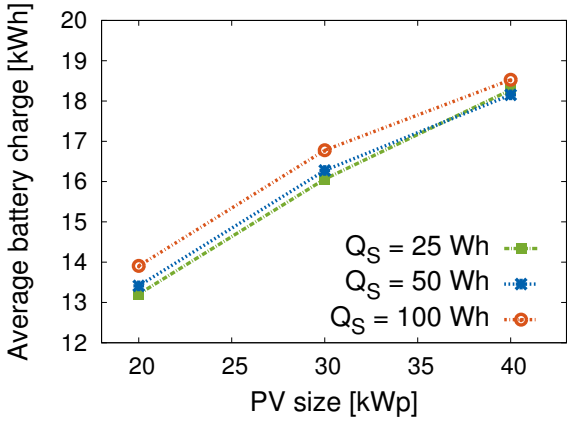

(b) M_{30}

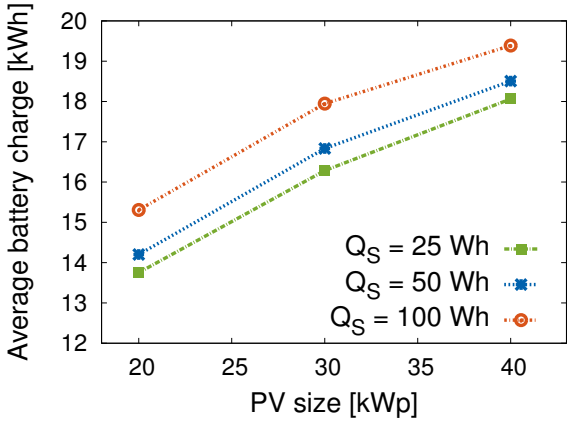

(c) M_{15}

Figure 6.10: Average battery charge versus PV panel size, under different discretization values of the energy storage (with capacity $C_B = 25$ kWh) and for increasing time granularity (M_{15}, M_{30}, M_H), for Turin with $N_W = 5$ and equal-range discretization, for residential weekday traffic profile, and adopting the Earth model.

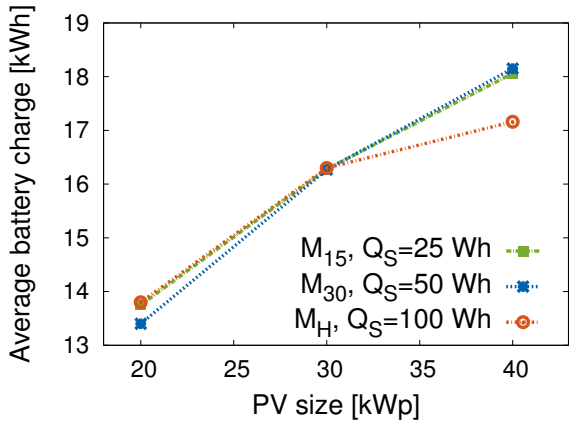

(a) Average battery charge

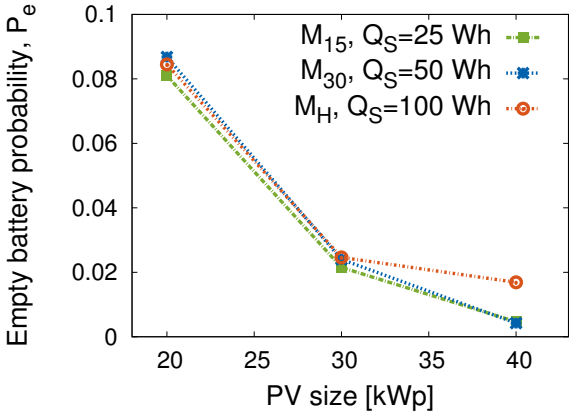

(b) P_D

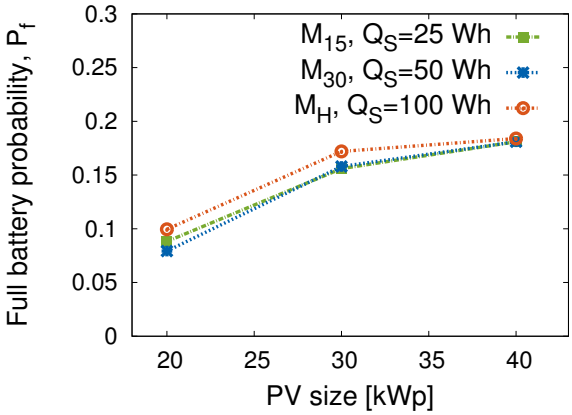

(c) P_f

Figure 6.11: Average battery charge, empty (P_D) and full (P_f) battery probabilities versus PV panel sizes, for different time slots, for Turin with $N_W = 5$ and equal-range discretization, for $C_B = 25$ kWh, with residential weekday traffic profile, adopting the Earth model.

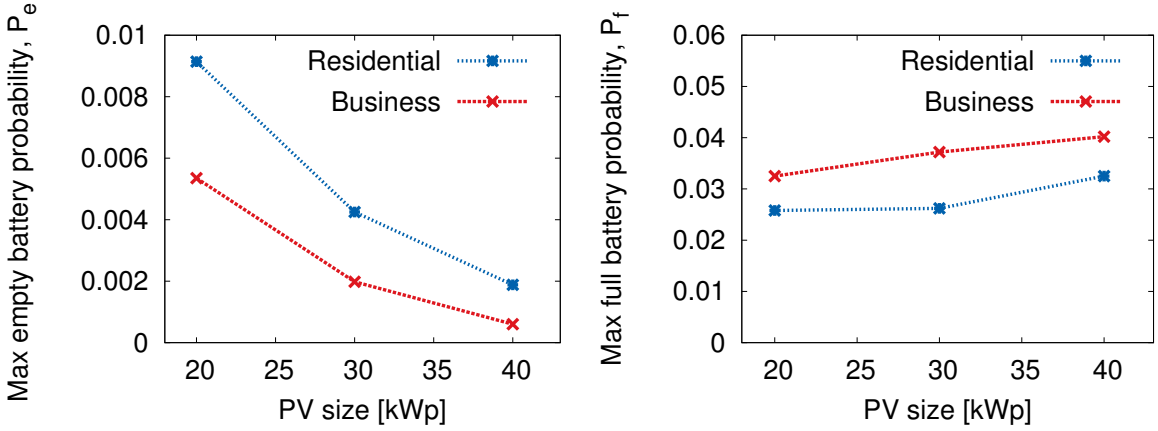

(a) P_D (b) P_f

Figure 6.12: Maximum hourly empty (P_D) and full (P_f) battery probabilities versus PV panel size, for Turin, with 5 day-types and equal-range discretization, time slot $\Delta T = 1$h, for $C_B = 25$ kWh, $Q_S = 100$ Wh, with residential and business weekday traffic profiles, adopting the Earth model.

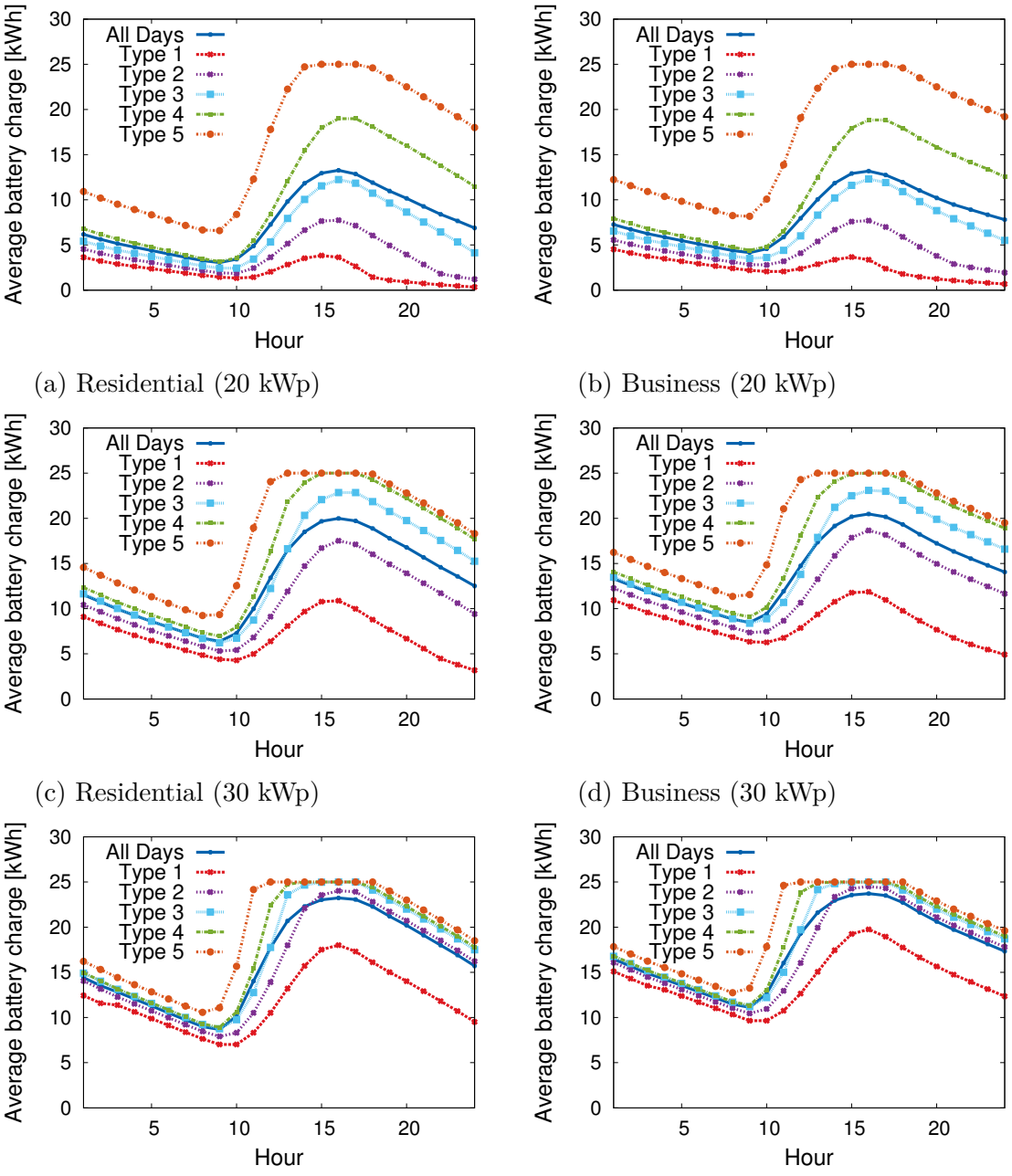

(a) Residential (20 kWp)

(b) Business (20 kWp)

(c) Residential (30 kWp)

(d) Business (30 kWp)

(e) Residential (40 kWp)

(f) Business (40 kWp)

Figure 6.13: Average hourly battery charge for a macro BS in Paris versus time, with $N_W = 5$ and equal-probability discretization, time slot $\Delta T = 1$h, PV panel sizes 20, 30, and 40 kW peak, $C_B = 25$ kWh, and $Q_S = 100$ Wh, for both the residential and business weekday traffic profiles, adopting the Earth model.

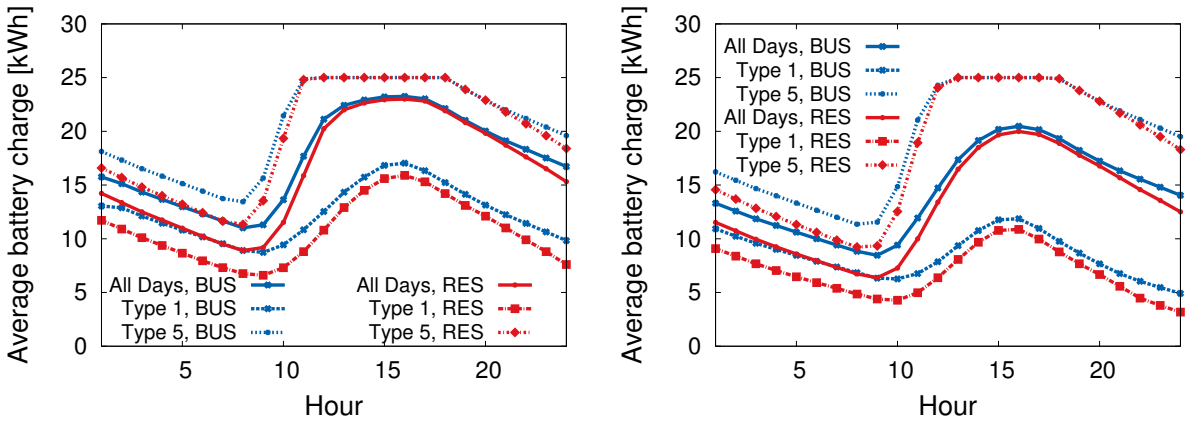

(a) Turin (b) Paris

Figure 6.14: Average hourly battery charge for a macro BS in Turin (equal-range discretization) and Paris (equal-probability discretization) versus time, with $N_W = 5$ and time slot $\Delta T = 1$h, PV panel size 30 kW peak, $C_B = 25$ kWh, and $Q_S = 100$ Wh, for both the residential and business weekday traffic profiles, adopting the Earth model.

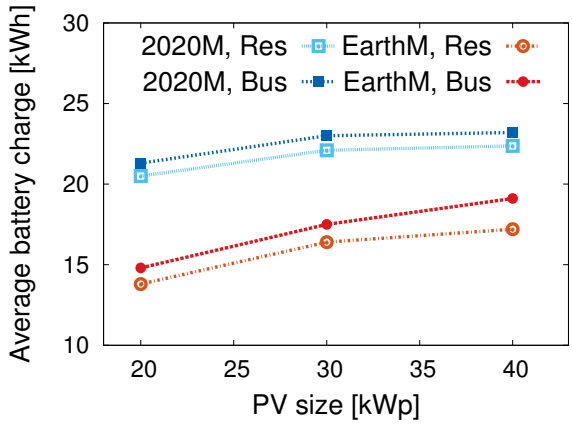

(a) Storage level

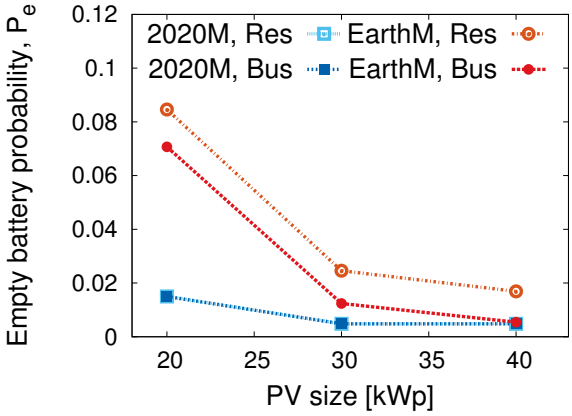

(b) P_D

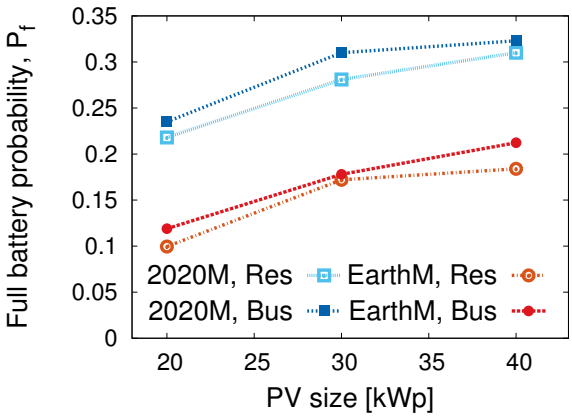

(c) P_f

Figure 6.15: Average battery charge level, empty (P_D) and full (P_f) battery probabilities versus PV panel size, for 2020 and Earth models (2020M and EarthM, respectively), in residential and business areas in the city of Turin. $N_W = 5$ and equal-range discretization, $\Delta T = 1$h, $C_B = 25$ kWh, and $Q_S = 100$ Wh.

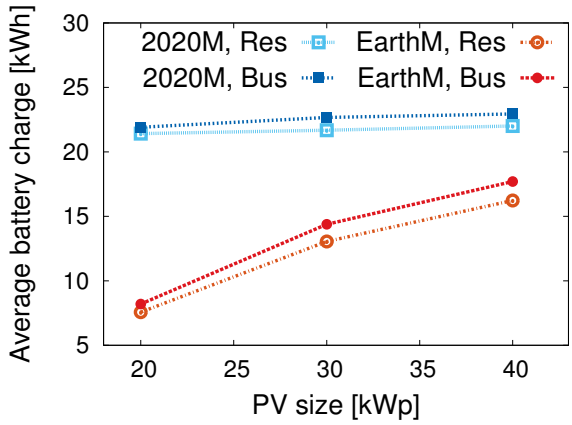

(a) Storage level

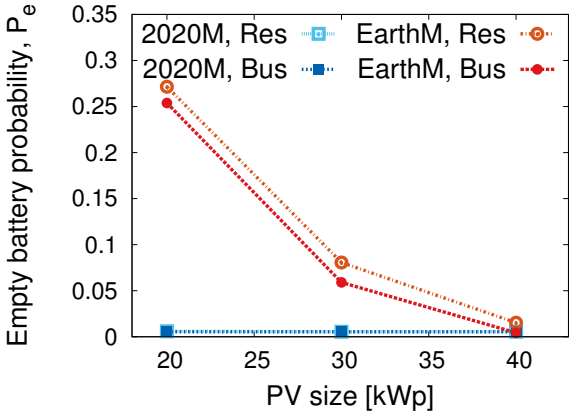

(b) P_D

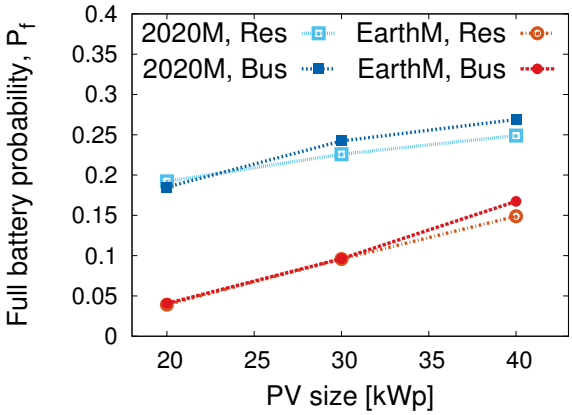

(c) P_f

Figure 6.16: Average battery charge level, empty (P_D) and full (P_f) battery probabilities versus PV panel size, for 2020 and Earth models (2020M and EarthM, respectively), in residential and business areas in the city of Paris. $N_W = 5$ and equal-probability discretization, $\Delta T = 1$h, $C_B = 25$ kWh, and $Q_S = 100$ Wh.

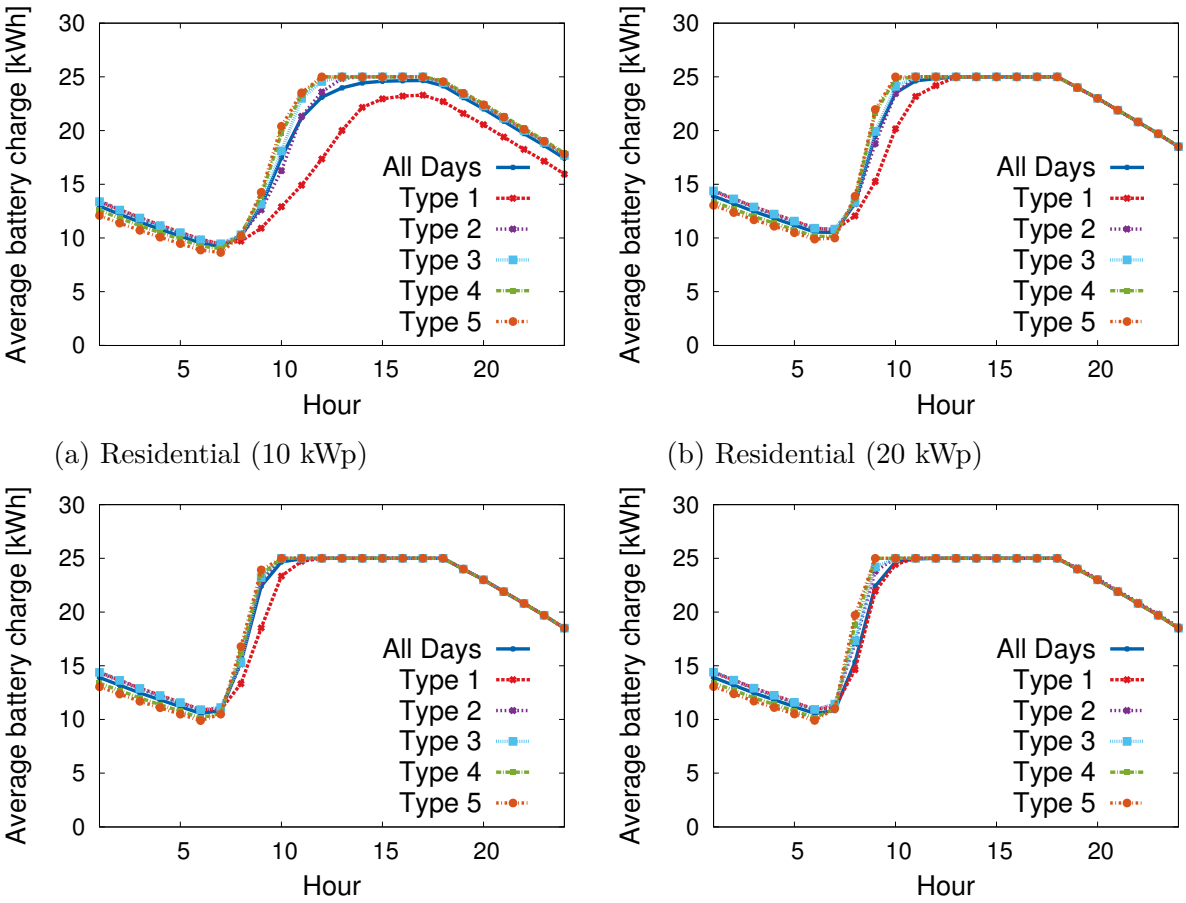

(a) Residential (10 kWp)

(b) Residential (20 kWp)

(c) Residential (30 kWp)

(d) Residential (40 kWp)

Figure 6.17: Average hourly battery charge for a macro BS in Maiduguri versus time, with $N_W = 5$ and equal-probability discretization, time slot $\Delta T = 1$h, PV panel sizes 10, 20, 30, and 40 kW peak, C_B= 25 kWh, and Q_S= 100 Wh (50 Wh in case of PV panel size 10 kW peak), for the residential weekday traffic profiles, adopting the EARTH model.

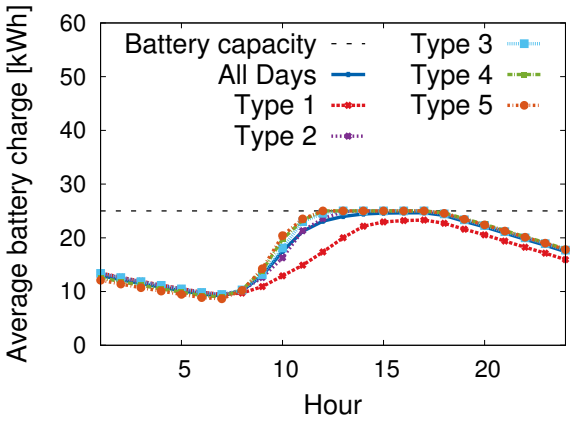

(a) Residential (25kWh)

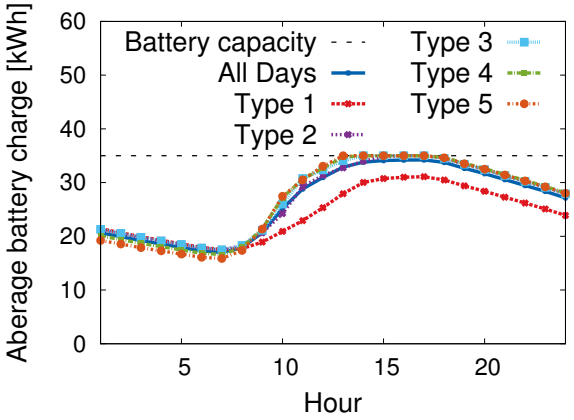

(b) Residential (35kWh)

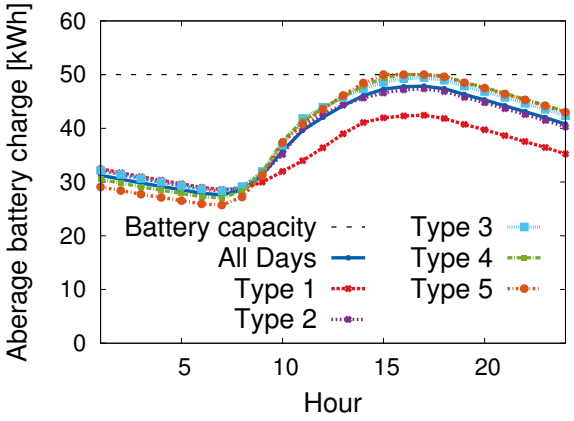

(c) Residential (50 kWh)

Figure 6.18: Average hourly battery charge for a macro BS in Maiduguri versus time, with $N_W = 5$ and equal-probability discretization, time slot $\Delta T = 1$h, PV panel size 10 kW peak, battery capacities 25, 35, 50 kWh, and $Q_S = 100$ Wh, for the residential traffic profiles.

Chapter 7

System dimensioning

Part of the work presented in this Chapter has already been published in:

- M. Dalmasso, M. Meo, and D. Renga. "Radio resource management for improving energy self-sufficiency of green mobile networks". In: *Performance Evaluation Review*. Vol. 44. 2. Sept. 2016, pp. 82–87
- D. Renga and M. Meo. "Modeling renewable energy production for base stations power supply". In: *2016 IEEE International Conference on Smart Grid Communications (SmartGridComm)*. Nov. 2016, pp. 716–722

In this Chapter, the RE generation system dimensioning issue is addressed. In particular, in Sec. 7.1, the impact of photovoltaic panel and battery size on the mobile system performance is evaluated in a baseline scenario, envisioning a single on-grid macro BS powered by locally produced RE, assuming constant power demand. The model proposed in Chapter 4 is used to represent the daily production of the PV system providing power supply to the BS, in order to investigate the impact of the energy generation variability on the system performance and its dimensioning. The daily RE generation is represented by a random variable with location dependent mean value and variance. The system performance is evaluated in terms of probability of storage depletion and energy demand from the grid.
Afterwards, under the same RE model, an analytical formula is deployed in Sec. 7.2 to provide a simple tool for system dimensioning in the same scenario. This formula is derived by exploiting the Markovian model for the storage proposed in Sec. 5.2. Cost and feasibility considerations are provided as well, raised by the need of trading off performance and expenditure constraints.
Finally, a more complex scenario, consisting of a single macro BS and multiple micro BSs, is considered in Sec. 7.3, in order to investigate the system dimensioning problem taking into account the dynamic load variations over time in a portion of the mobile access network.

7.1 Impact of photovoltaic panel and battery size in a baseline scenario

First, a simple scenario is considered, assuming a single LTE BS with constant power consumption of 1 kW (see Fig. 5.3). The RE system dimensioning is investigated by characterizing the RE production based on the stochastic model proposed in Chapter 4, in the city of Turin. The PV panel size, S_{PV}, and the battery size, B, are the only parameters that, given a location, can be properly tuned in order to optimize the system performance. In order to better understand their impact on system performance, the related results are presented considering the coefficient of variation (CV) of the RE peak production, RE_p, instead of its variance:

$$CV = \frac{\sigma}{\mu} \tag{7.1}$$

where σ is the standard deviation of RE_p and μ is the average value of RE_p. Considering a fixed CV, the average amount of RE that can be produced in a day (RE_D) can be easily defined as:

$$RE_D = M \cdot R_N = M \cdot \int_D f_N(t) \tag{7.2}$$

where $f_N(t)$ is the function representing the curve c_N and D its support, R_N represents the area under the curve c_N and $M = RE_p \cdot S_{PV}$. In this way, RE_D is simply expressed as the product of a constant coefficient, R_N, by a multiplicative factor, M, which includes and depends on the location specific mean RE_p and the adopted PV panel size, S_{PV}. To obtain the same level of RE_D in locations showing the same CV but a different mean value of RE_p, S_{PV} must be properly selected. Fig. 7.1 presents various plots showing how P_D vary with respect to the value of M, under a normal distribution of RE_p and considering all the possible combinations of average RE_p and S_{PV}. Three sets of results are reported in the figure, each corresponding to a fixed value of CV. In order to highligh the differences in the impact on P_D of rather low, intermediate and higher values of CV, the values 4%, 16%, and 32% have been selected for CV, respectively. Multiple curves are reported in each graph, one per each value of battery size. For all the three values of CV, there are two values of B ($B = 16kWh$ and $B = 17kWh$) for which depletion probability results to be constantly equal to 1 for any value of M. In these cases the battery size is clearly under-dimensioned with respect to the BS need; this is further confirmed by the fact that the average grid demand always remains well above 1 kWh even for large values of M, corresponding to very high RE production and very large panel sizes. Considering $B \geq 18kWh$, P_D tends to be very high for low values of M, with P_D ranging from higher values (P_D=1) in case of low CV to lower values (P_D=0.5-0.6) in case of larger CV. As M increases, P_D decreases in a sharp way in case of lower CV, more gradually in case of higher CV. At some point, for

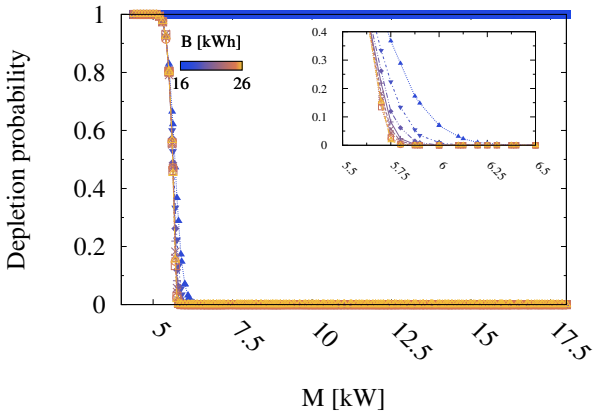

(a) CV=4%

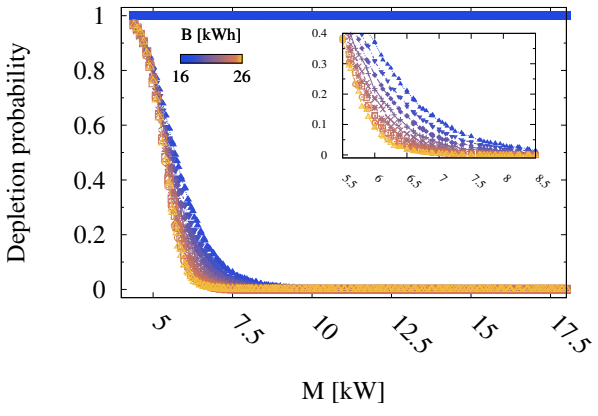

(b) CV=16%

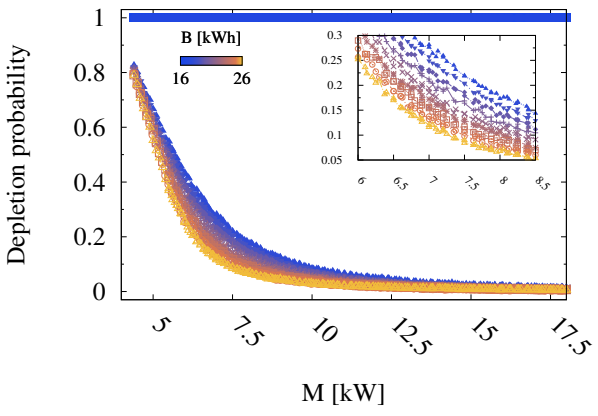

(c) CV=32%

Figure 7.1: Battery depletion probability versus RE production level for different battery capacity values.

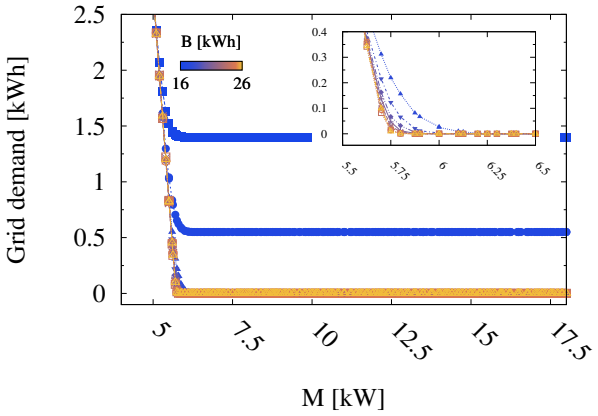

(a) CV=4%

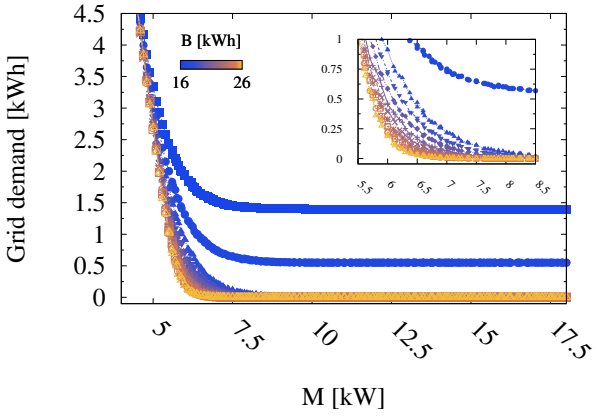

(b) CV=16%

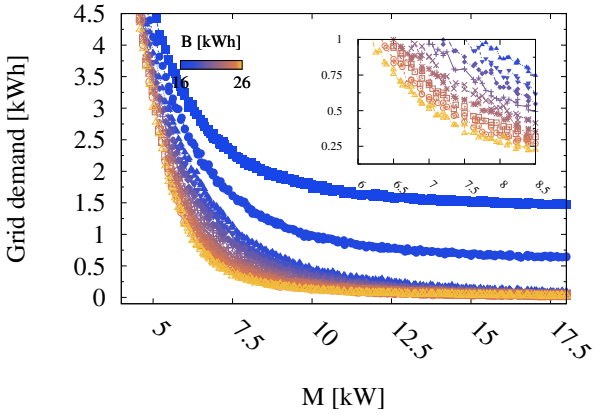

(c) CV=32%

Figure 7.2: Average daily grid demand versus RE production level for different battery capacity values.

sufficiently high values of M (very low M for CV=4%, very high M for CV=32%), P_D reduces to values very close to 0. Furthermore, the descent becomes steeper as B increases.
A similar trend is observed for average grid demand, G, reported in Fig.7.2. In case of $B \geq 18kWh$, G decreases as M grows larger, with a sharp descent for low values of M, until it reaches almost null values; in case of CV=32%, G values close to 0 are achieved only for very high M and only for sufficiently high values of B ($\geq 18kWh$). Just as for P_D, the descent results steeper for higher values of B. However, considering very small values of M, whereas P_D is lower in case of higher CV than in case of low CV, G results to be higher when CV is high rather than when it is lower. This means that when the PV panel is under-dimensioned, although a higher variability in the RE production allows to decrease the probability of battery outage, the aggregated amount of energy that must be drawn on average from the grid not only is not reduced, but it is even increased.
Higher values of CV determines a higher variability in the amounts of energy requested from the grid when different battery sizes are considered, whereas in case of very low CV the battery size does not have a deep impact in contributing to make the BS independent from the grid (a minimal battery may be sufficient, no need to further increase its size). Similarly, when the CV is very low, the BS can be independent from the grid for very low values of M, hence there is not significant gain in extremely increasing the PV beyond the minimal acceptable value. For very high CV it might happen that the off-grid target -or a slightly relaxed 95% off-grid target, meaning being independent from the grid for 95% of the time (i.e. $P_D < 5\%$)- cannot be achieved, since this would occur for very high values of M and the required S_{PV} might be too huge to be a feasible solution in practice.

7.2 Analytical system dimensioning in a simple scenario

The simple scenario of Fig. 5.3 is again considered, assuming a single renewable powered LTE BS with constant power consumption of 1 kW. The daily RE production is characterized based on the stochastic model proposed in Chapter 4, considering the city of Turin as location. The energy storage is modeled according to the 3-state Markovian model introduced in Sec. 5.2.

7.2.1 Estimating depletion probability p_D

Given a location with specific average and variance of daily RE production RE_d, different combinations of system dimensioning pairs (S_{PV}, C_B) lead to different values of battery depletion probability, p_D. For a fixed combination of (S_{PV}, C_B), the expected value of storage depletion probability can be estimated by applying the

Markovian model proposed, a fast method that provides reliable results, showing sufficient accuracy with respect to those derived via simulation. Fig. 7.3 reports

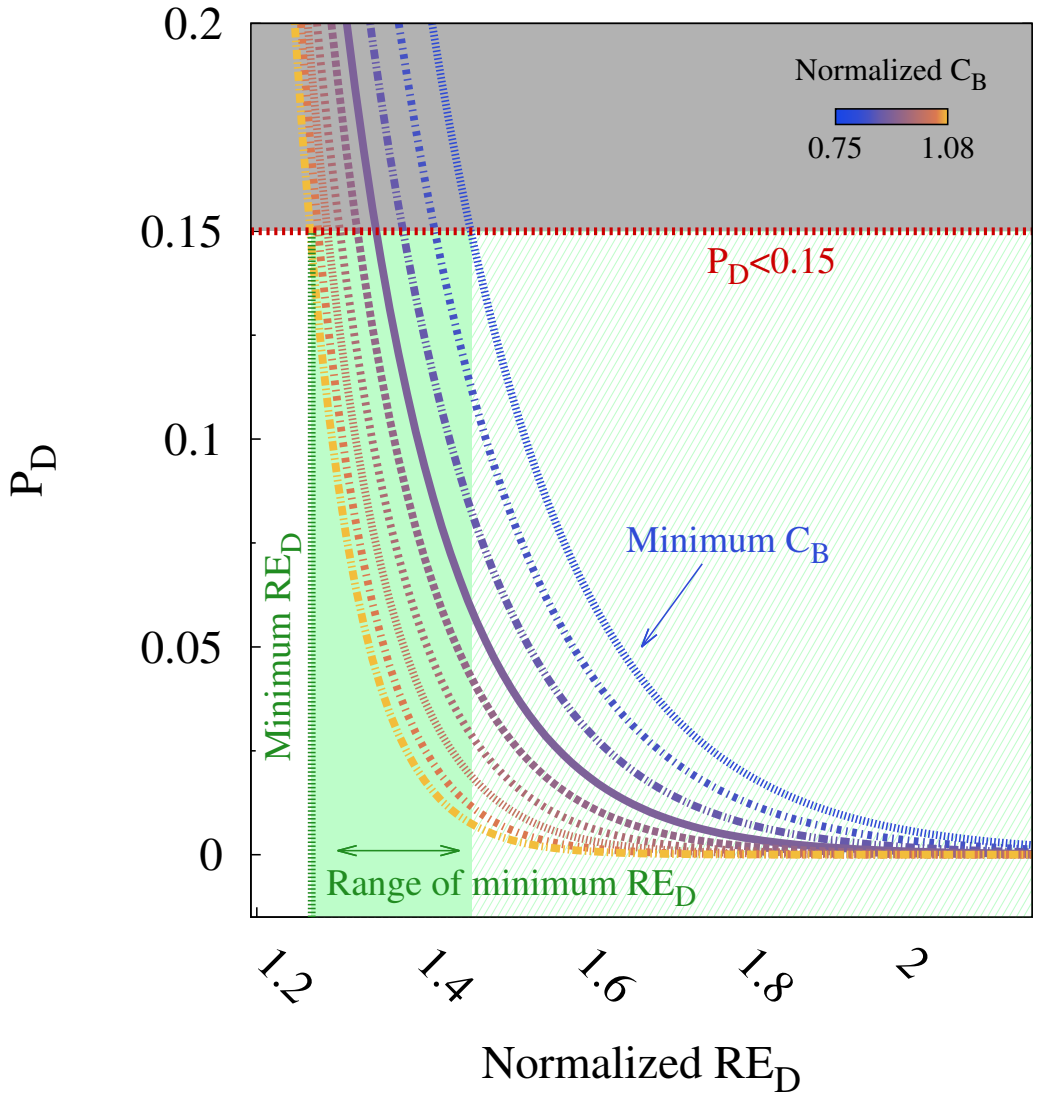

Figure 7.3: Example of system dimensioning based on the Markovian model, for $CV = 16\%$.

the values of p_D obtained from the Markovian model, $p_{D_{Mod}}$, for increasing values of daily RE production RE_D, in a location with CV of RE_d 16%. The average level of RE_D is normalized on the x axis with respect to the daily BS demand, $C_{BS} \cdot 24$, i.e. 24 kWh. Each curve in the plot represents a different size of the storage. Similarly to the RE production levels, the values of the battery capacity

C_B are normalized with respect to the daily BS demand. The results can hence be easily extended to BSs showing a different power consumption, scaling them up by a factor corresponding to the daily BS consumption. The curves plotted in the graph are exponential functions obtained by interpolation of the points obtained from the model, with a coefficient of determination $R^2 \geq 0.95$ in all cases. The storage depletion probability sharply decreases as the RE_D grows larger, becoming null for high RE production. As the storage capacity becomes larger, the curves tends to shift left, meaning that smaller PV panels are sufficient to provide the same value of storage depletion probability.
Let us assume a location with mean R_p=400 W and CV=16%. In order to proper dimension the RE system for the considered location, we set the constraint on the maximum value of P_D as 0.15, that defines an upper bound limit on p_D (red horizontal line in Fig. 7.3). According to this constraint, we can move on any battery curve showing at least a portion below the upper limit of p_D and corresponding to a normalized battery size $\geq C_{B_{min}}/(24 \cdot C_{BS})$, where $C_{B_{min}}$ is the minimum battery size required to guarantee the energy supply from the storage during the night. Keeping into account the duration of the nighttime (15 hours) and the charging losses, $C_{B_{min}} = 0.75 \cdot 24 \cdot C_{BS}\ kWh$. Hence, a battery with capacity $C_{B_N} \geq 18$ must be selected. In order to respect the constraint on the maximum p_D, the minimum admitted value of RE_D depends on the selected storage size (range in the green vertical rectangle). Considering C_B=18 kWh, the normalized RE_D must be at least equal to 1.27 (green vertical line). This means that the PV panel size must be at least:

$$S_{PV} \geq \frac{1.27 \cdot C_{BS} \cdot 24}{E[RE_d]}$$

Assuming an average RE_d =2 kWh, for example, we need at least S_{PV}=15.24 kWp, corresponding to an area of about 76 m^2, which may result to be feasible. Given fixed battery, we can further reduce p_D by using larger PV panels. If a smaller PV panel size is required due to feasibility and cost constraints, a larger C_B can be considered, in order to achieve a better trade-off between the storage size and the PV panel capacity. When feasibility issues force the use of rather small PV panels, slightly larger batteries allow to highly reduce the storage depletion probability. However, when larger PV panel capacities are adopted, increasing the battery size does not have a relevant impact on decreasing the p_D.
This method allows not only to derive the storage depletion probability for specific combinations of PV panel and storage sizes in a given location, but, most importantly, it theoretically allows to dimension the RE generation system in a specific location providing the average value of RE_d and its CV, in order to provide a target maximum depletion probability. Nevertheless, the method is time consuming due to the high number of combinations of pair (S_{PV},C_B) that must be tested in order to increase the accuracy and several interpolation operations that must be performed afterwards. Furthermore, this process must be repeated for any location

showing a different variability of RE generation.
Hence, as it will be better described in the next subsection, this study aims at deploying an analytical formula allowing to provide a proper system dimensioning to reduce the probability of storage depletion p_D below a target threshold, based on the RE production level (mean value and variance) in a given location.

7.2.2 Deriving an analytical formula for system sizing

An analytical formula is here proposed, based on the Markovian model, to dimension the RE generation system in order to obtain a value of the probability of storage depletion p_D lower than a target threshold. Given a location with mean value and CV of the RE generation and the constraint on the maximum p_D, this formula allows to easily identify a set of feasible combinations of values for the PV panel size and the storage capacity. Within this feasibility region of possible solutions, the decision of adopting a specific combination of values can then be taken based on additional parameters, like costs, for example, considering either the capital expenditures and the system operation.
Let us consider a generic location with mean value of renewable energy generation $E[RE_D]$ and coefficient of variation CV, denoting as p_D* the constraint set on the maximum storage depletion probability allowed. The PV panel size S_{PV} and the storage capacity C_B represents the unknown parameters whose (sets of) feasible values must be found to properly dimension the system. Based on the Markovian model, the relations between the transition probabilities and the steady state probabilities can be expressed in a closed form by the following system of equations:

$$\pi_0 = \pi_0 \cdot p_{0,0} + \pi_M \cdot p_{M,0} + \pi_L \cdot p_{L,0} \tag{7.3}$$

$$\pi_L = \pi_0 \cdot p_{0,L} + \pi_M \cdot p_{M,L} + \pi_L \cdot p_{L,L} \tag{7.4}$$

$$\begin{aligned} \pi_M &= \pi_0 \cdot p_{0,M} + \pi_M \cdot p_{M,M} + \pi_L \cdot p_{L,M} = \\ &= \pi_0 \cdot (1 - p_{0,0} - p_{0,L}) + \pi_M \cdot (1 - p_{M,0} - p_{M,L}) \\ &\qquad + \pi_L \cdot (1 - p_{L,0} - p_{L,L}) \end{aligned} \tag{7.5}$$

where π_i is the steady state probability for state i and $p_{i,j}$ represents the transition probability from state i to state j.
For any i, the probability $p_{i,j}$ of moving to state j, given that the current state is i, depends on the daily energy demand, i.e. $D_d + D_n$, which is fixed, and on the daily RE production, which is a random variable. By knowing the probability density function of RE_D, the values of $p_{i,j}$ can easily be computed. For example, the value $p_{0,0}$, that is derived as the probability $p(RE_D < D_d + D_n)$, can be obtained by integrating the probability density function of RE_D between the minimum possible value of daily RE production and the value of the daily BS demand. Similarly, the probability $p_{L,0}$ is equal to $p(L + RE_D - D_d - D_n \leq 0) = p(RE_D \leq D_d + D_n - L)$.

Hence, it can be computed by integrating the probability density function of RE_D between the minimum possible value of daily RE production and the difference between the daily BS demand and the current level of battery charge. Similar computations can be performed for obtaining the probability of any transition from state i to state j.
The relations between the parameters provided as inputs (i.e. mean value and CV of the RE generation, the constraint on the maximum depletion probability allowed p_D*) and the system size parameters, searched as output, can hence be derived as reported hereafter. For higher accuracy, charging and discharging losses are taken into account. Let us denote as $U_{RE_D}(x)$ the probability density function of the random variable RE_D having a uniform distribution, such that $U_{RE_D}(x) = U_{RE_d}(x) \cdot S_{PV}$. Remember that:

$$U_{RE_d}(x) = \frac{1}{2\sigma\sqrt{3}} \; for \; RE_{min} \leq x \leq RE_{max} \tag{7.6}$$

where σ is the standard deviation of RE_d, whereas RE_{min} and RE_{max} are the extremes of the support of $U_{RE_d}(x)$.
From Equation 7.3:

$$\pi_0 = \pi_0 \cdot \int_{a_1}^{a_2} U_{RE_D}(x) + \pi_M \cdot \int_{b_1}^{b_2} U_{RE_D}(x) + \pi_L \cdot \int_{c_1}^{c_2} U_{RE_D}(x) \tag{7.7}$$

where:

$$\begin{aligned}
&U_{RE_D}(x) = U_{RE_d}(x) \cdot S_{PV} \\
&a_1 = b_1 = c_1 = RE_{min} \cdot S_{PV} \\
&a_2 = D_d + D_n \\
&b_2 = -\frac{M}{1 - l_f} + D_d + D_n = -\frac{L}{2 \cdot (1 - l_f)} + D_d + D_n \\
&c_2 = -\frac{L}{1 - l_f} + D_d + D_n \\
&RE_{min} = E[RE_d] - 2\sigma\sqrt{3} = E[RE_d] \cdot (1 - 2\sqrt{3} \cdot CV) \\
&L = C_B - D_n
\end{aligned}$$

l_f denotes the *loss factor* due to energy losses occurring during the charging or discharging process, and corresponds to 15%, whereas RE_{min} represents the minimum possible value of daily RE production per 1 kWp PV panel capacity. $E[RE_d]$ is the mean value of RE_d.
From Equation 7.4:

$$\pi_L = \pi_0 \cdot \int_{d1}^{d_2} U_{RE_D}(x) + \pi_M \cdot \int_{e_1}^{e_2} U_{RE_D}(x) + \pi_L \cdot \int_{f_1}^{f_2} U_{RE_D}(x) \tag{7.8}$$

where:

$$d_1 = D_d + D_n + \frac{L}{1 - l_f}$$
$$e_1 = D_d + D_n + \frac{M}{1 - l_f} = D_d + D_n + \frac{L}{2 \cdot (1 - l_f)}$$
$$f_1 = D_d + D_n$$
$$d_2 = e_2 = f_2 = RE_{max} \cdot S_{PV}$$
$$RE_{max} = E[RE_d] + 2\sigma\sqrt{3} = E[RE_d] \cdot (1 + 2\sqrt{3} \cdot CV)$$

RE_{max} represents the maximum possible value of daily RE production per 1 kWp PV panel capacity.
From Equation 7.5:

$$\begin{aligned} \pi_M = \pi_0 \cdot \Big[1 - \int_{a_1}^{a_2} U_{RE_D}(x) - \int_{d_1}^{d_2} U_{RE_D}(x)\Big] \\ + \pi_M \cdot \Big[1 - \int_{b_1}^{b_2} U_{RE_D}(x) - \int_{e_1}^{e_2} U_{RE_D}(x)\Big] \\ + \pi_L \cdot \Big[1 - \int_{c_1}^{c_2} U_{RE_D}(x) - \int_{f_1}^{f_2} U_{RE_D}(x)\Big] \end{aligned} \tag{7.9}$$

Based on these algebraic relations, the PV panel size S_{PV} and the battery size C_B can be expressed by means of analytical formulas as functions of the mean value of RE_d, its CV and π_0. These formulas can then be used to dimension the system, deriving the set of feasible values of the unknown variables S_{PV} and C_B allowing to provide $\pi_0 \leq p_D*$, given the mean value and CV of RE_d in the considered location. No constraints are set on the values of π_M and π_L, except:

$$\pi_0 + \pi_M + \pi_L = 1$$

Note that the variable C_B represents the portion of the storage corresponding to the maximum DOD of the whole battery, B. The real size of the battery should therefore be derived by increasing C_B by a fraction such that $B = \frac{C_B}{DOD}$.

7.2.3 Application of the analytical dimensioning tool

The analytical formulas introduced in the previous section have been applied for dimensioning the system, in order to identify the feasibility regions for the PV panel and the storage sizes, based on the local RE production and the objective storage depletion probability. Furthermore, the impact of the RE generation variance on the system dimensioning has been analyzed.

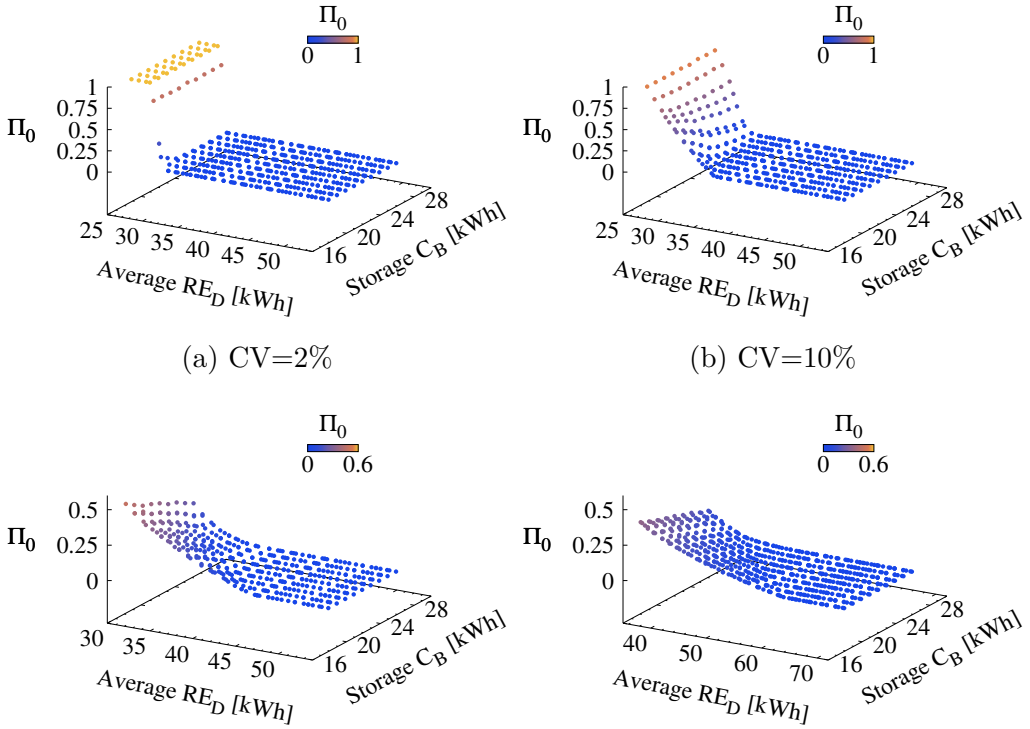

Figure 7.4: Battery depletion probability at the steady state, π_0, for multiple combinations of RE generation levels and battery size, under increasing values of CV.

Feasibility regions for system dimensioning

The proper combinations of PV panel and battery sizes allowing to reduce the storage depletion probability below a target threshold the can be identified by solving the system consisting of Equations 7.7, 7.8 and 7.9, subject to the constraints:

$$\pi_0 + \pi_M + \pi_L = 1$$
$$\pi_0 \leq p_D*$$

Fig. 7.4 reports the values of the target battery depletion probability at the steady state, π_0, in relation to the combination of battery capacity and RE generation levels that, according to the Markovian model, allow to achieve the desired value of π_0, for different values of CV. In each plot, the first horizontal axis represent the average daily amount of produced RE, denoted as $E[RE_D]$; the latter horizontal axis corresponds to the storage capacity C_B; the vertical axis reports the value of the depletion probability at the steady state, π_0. In general, for any CV, π_0 tends to be higher for combinations with low values of C_B and S_{PV}, whereas for very large values of storage and PV panel capacity π_0 becomes null. However, the shape

of the transition between these two extremes varies a lot depending on the variance of RE production. For locations where the RE production is rather constant over time (CV=2%), π_0 is equal to 1 if the PV panel and the storage are low, but it rapidly decrease by slightly increasing the size of both the PV panel and the storage. As the variance of the RE production increases, the maximum values of depletion probability becomes lower, up to less than 0.4 in case of CV=40% even with the smallest system size. Furthermore, the transition from size combinations providing high depletion probability to combinations assuring $\pi_0 = 0$ becomes more gradual as the variance in the RE production becomes larger. This means that in those locations where the variance, hence the CV, is low, small system sizes are sufficient to obtain a null depletion probability. However, even a slightly under-dimensioned system may give raise to a steep increase of the depletion probability. For larger variances, small to intermediate system sizes are sufficient to obtain depletion probability values lower than 0.25, but larger system sizes are required for improving the system performance in terms of depletion probability, up to values below 0.05. When the CV is high, increasing the PV panel size alone is not sufficient to deeply decrease π_0 if the battery is very small, but combining a larger PV panel and a battery with higher capacity may highly decrease the battery depletion probability.
Let us consider a location where the average daily RE production per kWp, $E[RE_d]$, is equal to n kWh and CV=30% (Fig. 7.4c). Setting a target threshold p_D* for the depletion probability on the z axis, the feasible combinations of PV panel and storage sizes can easily been derived from the set of pairs $(E[RE_D], C_B)$ on the x and y axes, respectively, corresponding to values of $\pi_0 \leq p_D*$. Considering that $E[RE_D] = E[RE_d] \cdot S_{PV}$, the required PV panel size for the considered location is obtained as $S_{PV} = \frac{RE_D}{n}$. Finally, the total required capacity for the battery is derived as $B = \frac{C_B}{DOD}$.

Impact of RE generation variance

Fig. 7.5 shows the feasibility regions in terms of combinations of battery size C_B and average daily RE production RE_D for various values of CV, both normalized with respect to the average daily consumption of a macro BS, assumed to be 24 kWh. Since the average daily RE generation RE_D is proportional to the PV panel size S_{PV}, for a given average daily RE generation per kWp, RE_d, observed in the considered location, the various regions correspond to different sets of combinations of PV panel size S_{PV} and storage capacity C_B allowing to achieve different target depletion probabilities, hence π_0:

- $\pi_0 < 0.005$ (blue squares);
- $0.005 \leq \pi_0 < 0.01$ (light blue asterisks);
- $0.01 \leq \pi_0 < 0.05$ (orange circles);

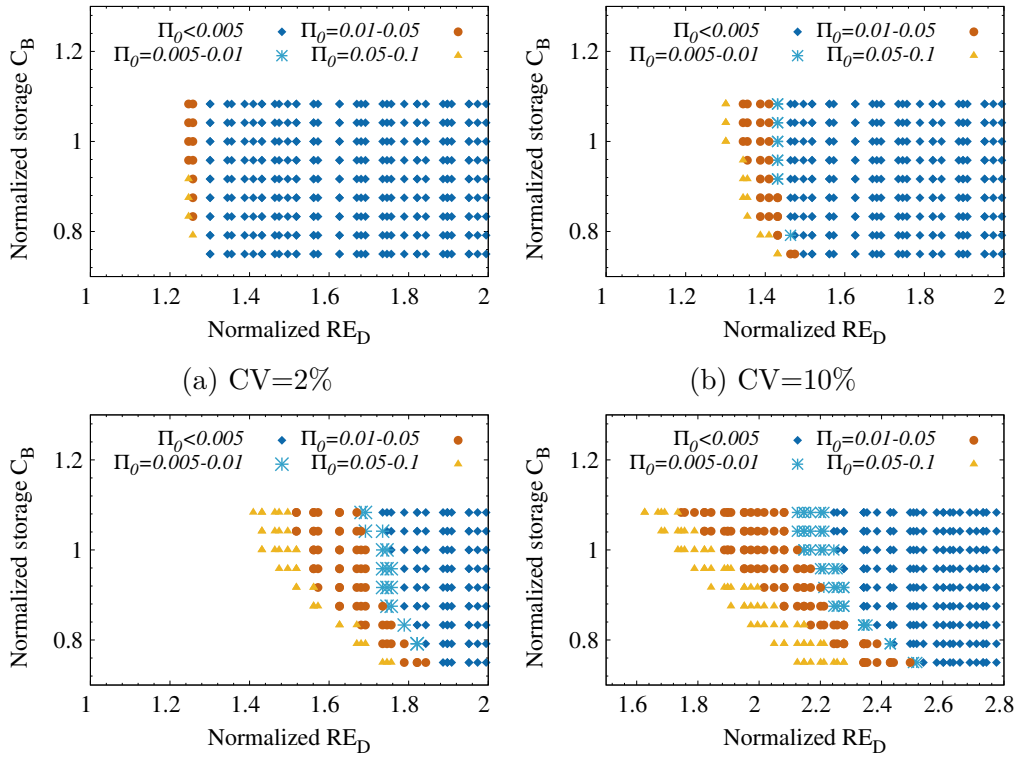

(a) CV=2% (b) CV=10%

(c) CV=20% (d) CV=30%

Figure 7.5: Feasibility regions in terms of target of battery depletion probability at the steady state, π_0, for multiple combinations of RE generation levels and battery size, under increasing values of CV.

- $0.05 \leq \pi_0 < 0.1$ (yellow triangles).

Furthermore, the graphs highlight the impact of the variance of RE generation on the distribution of the feasibility regions.
The minimum sizing required to achieve values of π_0 as low as 0.005 or less highly depend on the CV. For fix RE_d, a PV panel size capable to provide 1.3 the BS daily consumption may be sufficient if the variance of the RE production is low; moreover, the battery size shows no significant impact, hence a small storage with capacity of less than 4 fold the BS daily need is enough to guarantee very low depletion probabilities. Conversely, when the CV is higher, the minimum PV panel size assuring $\pi_0 < 0.005$ must be capable of providing a RE_D that is up to more than 2.5 the BS daily need. However, when the CV is higher, the impact of the battery size is higher. For example, in case CV=30%, increasing C_B by up to 40% allow to reduce S_{PV} by up to 11.8%, still maintaining the same target on the battery depletion probability. This aspect is relevant when feasibility issues are considered, since PV panels with lower capacity require a smaller physical area to

be installed, besides having lower capital costs.
When the variance of RE_D is high, although the system size is generally larger, a slight relaxation on the constraint on the target depletion probability -for example by moving to the feasibility region where π_0 is between 0.005% and 0.01%- allows to reduce the system dimensioning. This becomes more evident by shifting to the next feasibility region, where $\pi_0 = 0.01 - 0.05\%$. Furthermore, a small increase in the battery capacity (from 0.75 up to 1.05 the daily BS need) leads to a reduction of the PV panel size of almost 30%. Conversely, in case the variance is low, it is not convenient to relax the constraint on the target depletion probability, since the gain in terms of PV panel and battery size reduction would be negligible and there would be the risk of sharply shifting to a region with very high battery depletion probability.

7.2.4 Considerations on cost and feasibility

In the process of system dimensioning based on the definition of a target battery depletion probability in a given location, costs may play a relevant role. In particular, capital expenditures can be taken into account in order to refine the identification of the proper system size, hence selecting the best combination of PV panel size and storage capacity within the feasibility region identified by applying the proposed analytical method. A cost of 750 €/kWp can be assumed for the panels, whereas the cost per kWh of battery capacity can be as high as 58.33 € [33]. Considering the range of sizes for PV panels and storage observed within the feasibility regions in our results, the weight of the PV panel costs is definitely dominant with respect to the cost of the battery. This means that, in locations with high variability of the RE generation a small increase in the battery size will allow to decrease the battery depletion probability at the price of a small raise in the cost; furthermore, it will be possible to decrease the PV panel size, still maintaining the same target depletion probability, and significantly reduce cost. For instance, let us assume a location where the average daily RE generation RE_d is 2 kWh, its CV is 30% and the target battery depletion probability is between 0.001 and 0.05. A system with $C_B = 17\ kWh$ (hence $B = 34\ kWh$, assuming a DOD=50%) and $S_{PV} = 28.2\ kWp$ is capable to meet the target constraint on the battery depletion probability. Nevertheless, by increasing the battery size by 40%, the PV panel size S_{PV} can be reduced by 30%, leading to a cost reduction of about 26.5%. Conversely, in those locations showing low variability in the RE generation, an increase in the battery size does not have a relevant impact on the PV panel capacity reduction. Hence, once the minimum PV panel size allowing to meet the constraint on p_D is identified, it is advisable to rather select a smaller battery, although the total CAPEX will result only slightly decreased with respect to the case of a larger storage. Further investigation is required for more reliable

cost evaluations, by considering the cost required for the energy storage maintenance. Indeed, whereas a PV panel can remain in place up to 25 years, lead-acid batteries need to be replaced much more frequently, and their lifetime duration is highly influenced by the high number and the frequency of charging/discharging cycles they undergo in a RE scenario. To this extent, further insights on RE system cost evaluation and more details about OPEX will be provided in Sec. 7.3.

On the one hand, the selection of a larger battery may reduce the PV panel size in locations where the variability of RE production is higher. On the other hand, this results in an improvement of the system feasibility, since the area of the surface required to install the PV panel is reduced as well. Assuming an efficiency of the PV panel of around 19%, an area of about 5 m^2 is needed per each kWp of PV panel capacity [33]. In the aforementioned case (location with $E[RE_d] = 2\ kWh$, CV=30%, p_D between 0.001 and 0.05) the PV panel size S_{PV} is reduced by 30%, and the area needed for the installation shrinks from more than 140 m^2 to less than 99 m^2.

7.3 System dimensioning in a complex scenario

In this section, a more complex network scenario is considered for system dimensioning analysis, i.e. a cluster of a macro BS and m=6 micro BSs, powered by locally produce RE and by the electric grid (see Figure 7.6). Real RE production patterns derived from PV-Watts are used, assuming the city of Turin as location. Furthermore, real traffic traces have been adopted in order to take into account the dynamic variations of the user demand, by considering both a residential (RA) and business (BA) area for the input traffic profiles. The system dimensioning analysis is performed via simulation.

7.3.1 Trading off system size and grid demand

We now investigate the relationship between the PV panel and storage dimensioning and the energy self-sufficiency of the system.
Fig. 7.7 reports the total energy demand from the smart grid over one year, denoted as E_G, for increasing values of the PV panel capacity, here denoted as S_{PV}. Each curve corresponds to a different value of the capacity of the battery, that is expressed in terms of number of battery units, here denoted as S_B, either in RA or BA. In general, larger batteries allow to reduce E_G. E_G can be reduced below 50 kWh only with $S_{PV} > 40kW_p$.

Even though larger PV panel sizes allow to reduce E_G, hence making the system more self-sufficient, this occurs at the price of increasing the RE waste, especially in summer. We denote as E_W the wasted energy over a year, i.e. the yearly amount

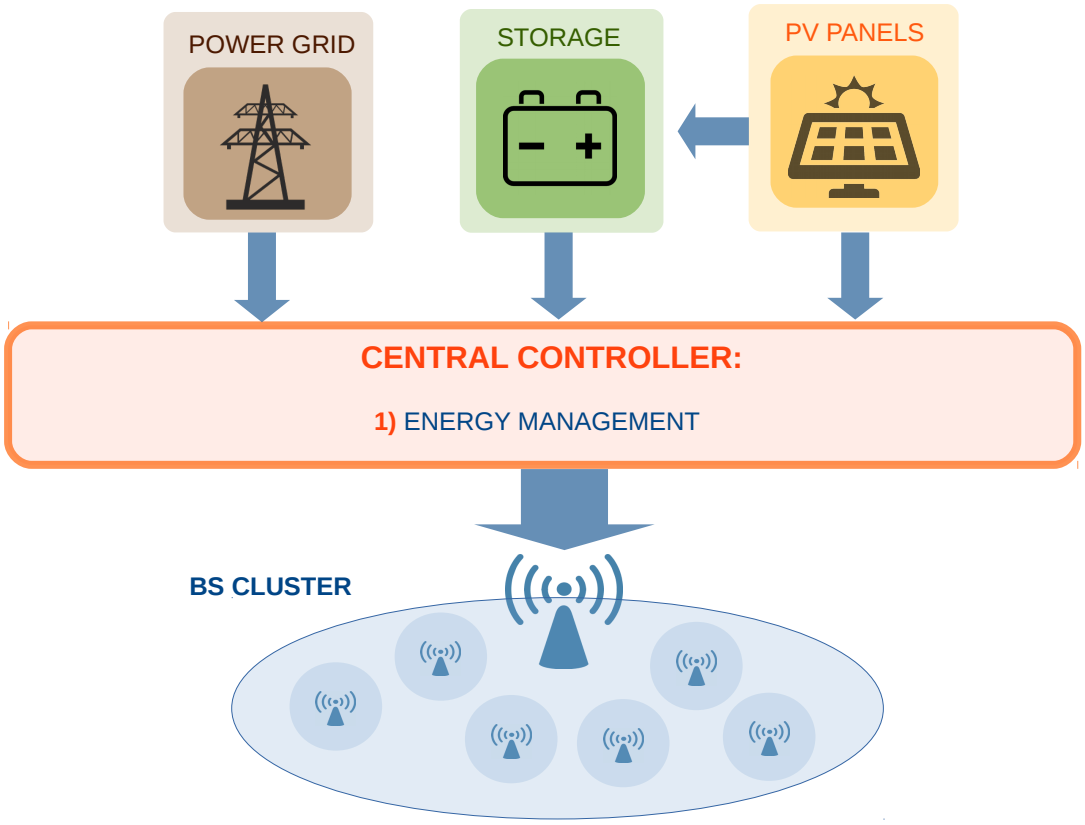

Figure 7.6: The cluster of on-grid renewable-powered BSs.

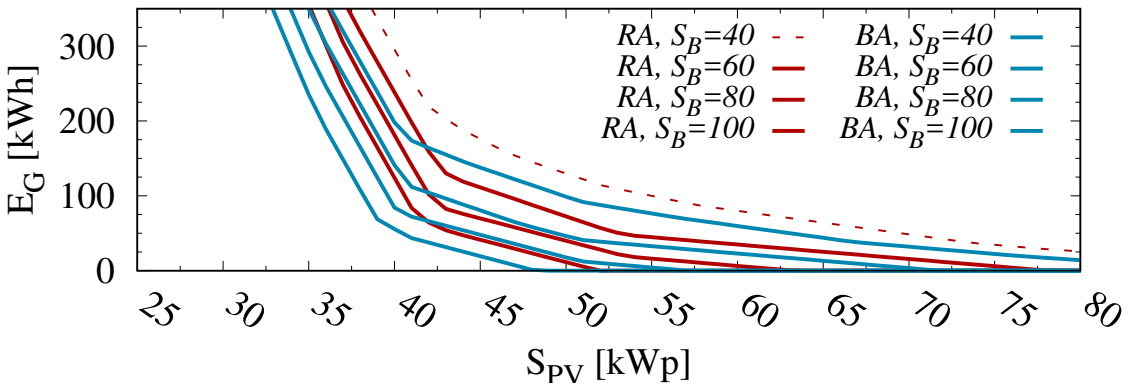

Figure 7.7: Yearly grid energy, E_G, versus S_{PV} in Residential and Business area (RA and BA), for different values of the energy storage capacity.

of RE production exceeding the BS need that the cannot be completely stored in the battery, due to capacity overflow. In Fig. 7.8, E_G is reported with respect to S_{PV} in the RA, with $S_B = 40$. As S_{PV} increases, E_W has an opposite and mirroring

trend, as shown in the same figure on the right-hand side y-axis.

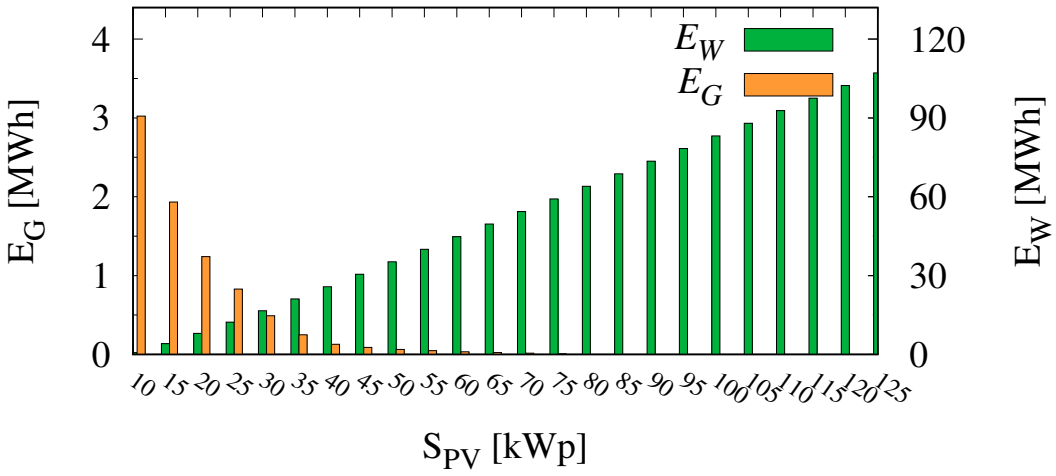

Figure 7.8: Yearly grid energy demand (E_G) and wasted energy (E_W) versus S_{PV} in the Residential area (RA).

It is to be noted that a very large S_{PV} is required, ≥ 80 kW_p, in order to achieve $E_G \sim 0$ kWh. By denoting as f_G the frequency of energy requests from the smart grid over one year (measured considering the time granularity of half an hour that is used in our simulator), this condition corresponds to $f_G \sim 0\%$. However, if the constraint on f_G is only slightly relaxed, for instance by admitting the less tight constraint $f_G < 1\%$, a consistent reduction (of 41.3%) of the minimum PV panel size can be achieved. Further relaxations of the constraint on f_G do not provide such a remarkable further reduction of S_{PV}. This is evident also when other values of S_{PV} are assumed, as it can be seen from Fig. 7.9, reporting the values of S_{PV} required to target various f_G constraints for different S_B, in case of a RA. The gain obtained by softening the constraint on f_G is even more significant when a smaller storage is used. A similar behavior is confirmed in the BA, although smaller S_B are sufficient to satisfy the same constraints on maximum f_G. By converse, the energy waste as measured by E_W tends to be rather high even with loose constraints on the maximum f_G. This means that relaxing the constraint on the maximum permitted f_G by just one percentage point allows to significantly reduce the required PV panel capacity, while the RE waste is not decreased to the same extent.
Similar considerations can be drawn for storage capacity dimensioning given PV panel capacity (data table not reported here for the sake of brevity). For instance,

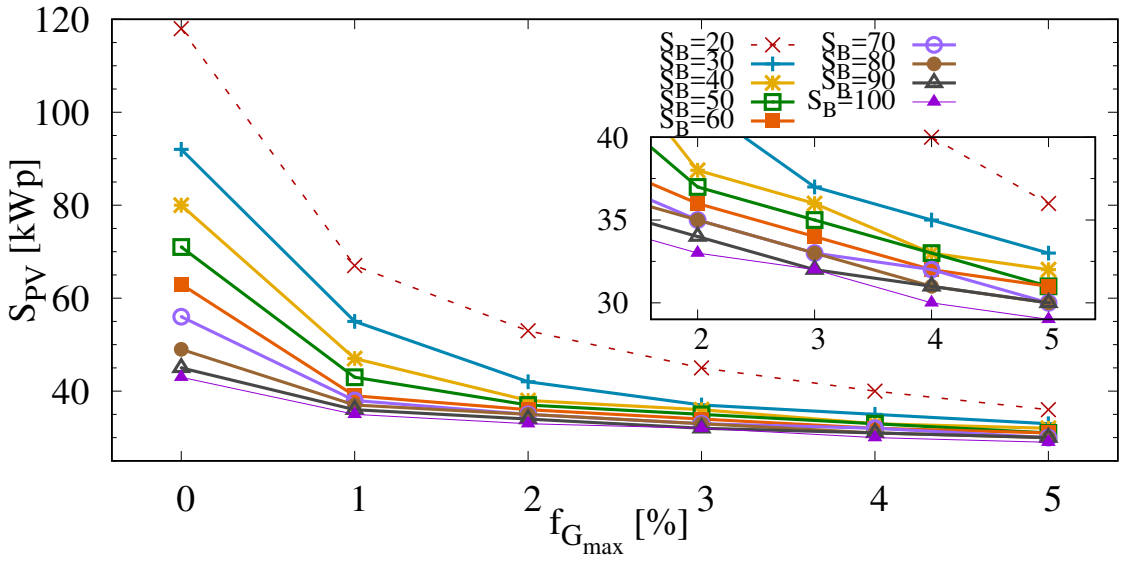

Figure 7.9: S_{PV} needed to satisfy the constraint $f_G < f_{G_{Max}}$, for increasing values of $f_{G_{Max}}$ and for different storage sizes.

lessening the constraint from $f_G \sim 0\%$ to $f_G < 1\%$, with a PV panel sized 60 kWp, allows a reduction in the storage size by 60% and 63% in a RA and a BA respectively; on the contrary, a further increase by 1% in f_G constraint allows to further reduce S_B by only 14% and 8% the original size.
Fig. 7.10 reports the frequency at which the mobile network must draw some energy from the grid for its operation, denoted as f_G, and the frequency of wasting the produced RE that is neither immediately used nor stored in the battery, denoted as f_W, for increasing PV panel size. f_G tends to sharply decrease as the PV panel size increases, whereas f_W gradually increases as the PV panel capacity grows larger. Even with very small PV panels some RE go wasted, whereas for very large PV panel F_W does not show remarkable raise when the PV panel capacity is increased. Nevertheless, despite the trend observed in the f_W pattern for increasing PV panel size, the actual amount of energy that is wasted over a year tends to increase almost linearly with the dimension of the RE system, as it will be shown. In order to reduce f_G at least below 5%, $f_W \geq 24\%$ must be admitted; this is true also in the BA. f_G shows a sharp decrease for small values of PV panel size and a more gradual decrease when PV panel size reaches larger values. On the contrary, a rather gradual increase in f_W is uniformly observed within the whole range of considered PV size values. , even for low values of PV size, given the considered PV size range which allow to achieve a reasonably low f_G ($< 5\%$) for our purposes.
Note that these results are obtained considering a worst-case period, during which the average RE production level is the lowest in the year. Hence, we can observe that if a RE generation system is dimensioned to be efficient during the cold season,

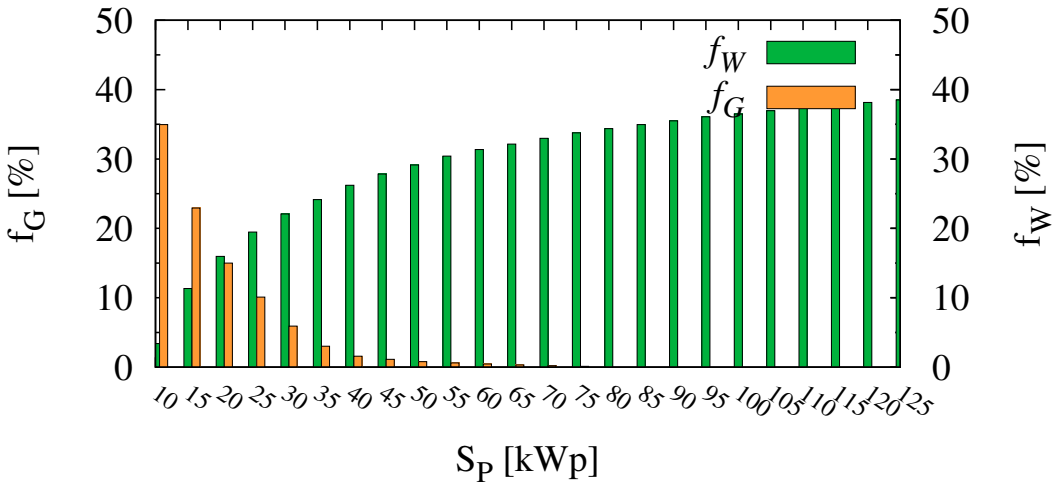

Figure 7.10: Frequency of drawing energy from the grid (f_G) and wasting renewable energy (f_W) versus S_{PV} in Residential area (RA).

it clearly results over-sized during the summer, leading to further energy wastage with respect to that observed from these results. Conversely, a system that works with few redundancies during the summer is inefficient during the cold season. In a smart grid integrated system, in order to compensate the extra amounts of energy that is produced but not immediately used and that cannot be harvested in the storage, the extra amounts of RE that cannot be stored for future usage may be sold to the grid, receiving a reward for the energy exchange.

Chapter 8

Studying the impact of energy saving techniques on system dimensioning and costs

Part of the work presented in this Chapter has already been published in:

- M. Dalmasso, M. Meo, and D. Renga. "Radio resource management for improving energy self-sufficiency of green mobile networks". In: *Performance Evaluation Review*. Vol. 44. 2. Sept. 2016, pp. 82–87

This chapter investigates the impact on system dimensioning and cost of energy saving techniques applied to green mobile networks. In particular, the effect of a Resource on Demand strategy based on BS on/off switching is analyzed. A renewable powered mobile access network consisting of a macro BS and multiple micro BSs is considered (see Figure 8.1). The number of micro BSs m is set to 6. The green network operation in this scenario is studied via simulation in order to evaluate the impact of the application of the Resource on Demand strategy proposed in Sec. 3.3.1 on the RE system dimensioning (Sec. 8.2) and on cost (Sec. 8.3). The RoD strategy is applied under the optimal configuration settings for maximizing energy savings, that are derived based on the results presented in the next Sec. 8.1. The optimization study in terms of energy saving of the configuration settings of the RoD strategy described in Sec. 3.3.1 is now presented. Afterwards, the influence on the system dimensioning and costs of the RoD strategy application in the green mobile access network is investigated. Finally, some observations on the effect of the varying traffic profiles are proposed.

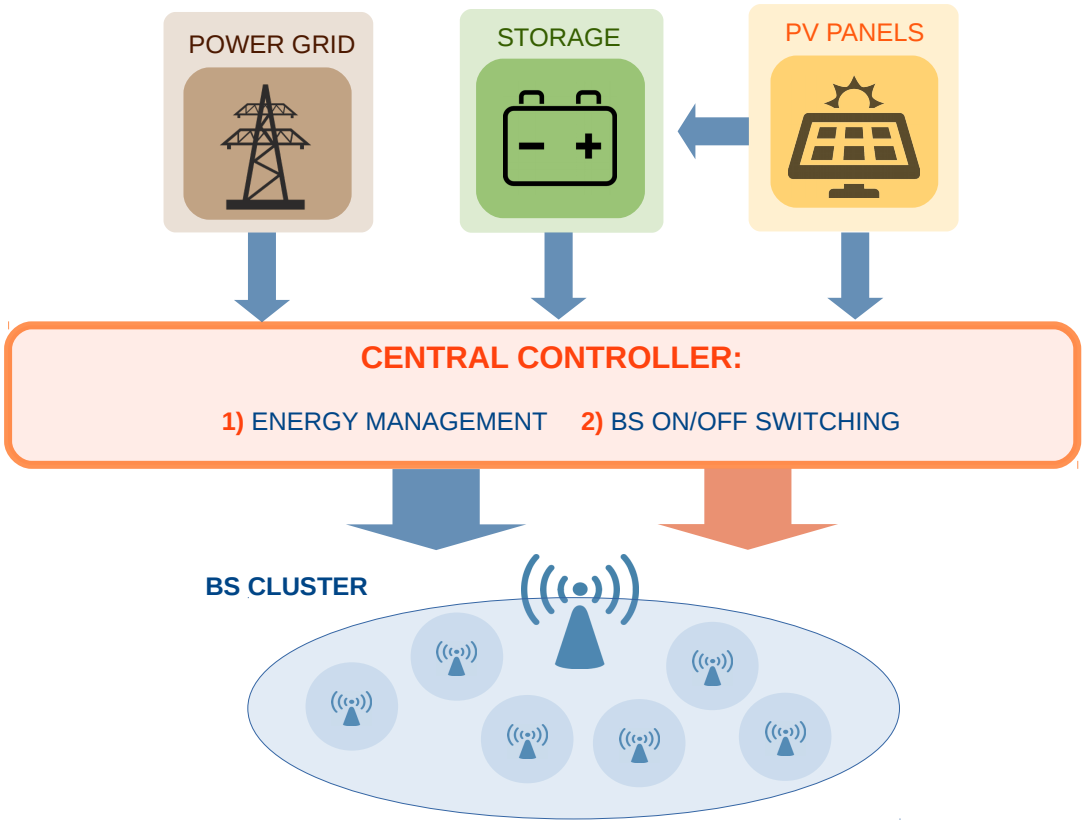

Figure 8.1: The cluster of on-grid renewable-powered BSs.

8.1 Finding optimal thresholds for Resource on Demand

This section presents how the optimization of the configuration settings for the application of the RoD strategy presented in Sec. 3.3.1 has been achieved. The parameter ρ_{min} defines the threshold on the load of the micro BSs below which a micro BS is switched off and its traffic moved to the macro BS. The simulations performed to study the impact of RoD strategy have been conducted by setting its value in order to maximize the possible savings. As already mentioned, we consider a scenario with a macro BS and m=6 micro BSs, assuming that each micro BS is in charge of handling the traffic share exchanged in its area of coverage. Although the shape of the normalized traffic pattern, as described in Sec. 3.2.2, is the same for all the m micro BSs, the amplitude of the actual traffic curve, hence the absolute value of peak traffic, may vary among the various micro BSs. The ratio between the traffic load of each micro BS and that of the macro BS is expressed by the parameter $\mu_i \in (0,1]$, with $i = 1,2,...,m$. Fig. 8.2 shows the total energy consumption with

respect to the case with all the BSs always active for increasing values of ρ_{min} in a Business and in a Residential area. Each curve corresponds to a different scenario in terms of relative traffic load; the values of μ_i are reported in the legend. When no strategy is applied, the yearly overall consumption, denoted as E, is similar in the RA (12.148 MWh) and in the BA (11.672 MWh). Nevertheless, under RoD, up to 38% of energy can be saved in the BA, almost twice the maximum saving obtained in RA. Due to the steeper transition between peak and off-peak periods and to the low traffic load during the weekend, the business traffic profile leads to lower energy consumption than the RA profile.

For low values of ρ_{min}, the energy consumption rapidly decreases as ρ_{min} increases; indeed, the RoD kicks into play often and for long periods of time. For the same reason, the steep decrease becomes more evident for those scenarios in which some BSs are less loaded. The advantage of RoD stabilizes for larger values of ρ_{min}. This is due to the different relative cost of carrying traffic through the macro and micro BSs. To investigate this, consider the total power consumption P_{in} of the macro and micro BSs carrying a traffic λ. The consumption consists in a constant component and a load proportional component and can be expressed by using two coefficients, A and B, according to the following formula:

$$P_{in} = A + B \cdot \lambda \tag{8.1}$$

where $A = N_{TRX} \cdot P_0$ and $B = N_{TRX} \cdot \Delta_p \cdot P_{max}$. Denote by G the cost, in terms of energy, derived from switching off the i^{th} micro BS and transferring its traffic load λ_i on the macro BS:

$$G = E_{off} - E_{on} \tag{8.2}$$

where E_{off} is the energy consumption when the traffic of the micro BS is moved to the macro BS, while E_{on} is the consumption when both BSs are kept active. Hence:

$$G = A_M + B_M \cdot (\lambda_M + \lambda_i) - (A_M + B_M \cdot \lambda_M + A_m + B_m \cdot \lambda_i) \tag{8.3}$$

where M and m stand for macro and micro BS respectively. A negative cost (i.e., a saving) is guaranteed for $G < 0$, hence for:

$$B_M \cdot \lambda_i - A_m - B_m \cdot \lambda_i < 0 \tag{8.4}$$

$$\lambda_i < \frac{A_m}{B_M - B_m} \tag{8.5}$$

When (8.5) is not satisfied, the additional cost to carry the traffic of the micro BS through the macro BS does not compensate the saving that can be achieved by switching off the micro BS. Hence, switching off is of no advantage. On the contrary, switching off is effective as long as (8.5) holds. The optimal choice for ρ_{min}, denoted by ρ^*_{min}, is then,

$$\rho^*_{min} = \frac{A_m}{B_M - B_m} \tag{8.6}$$

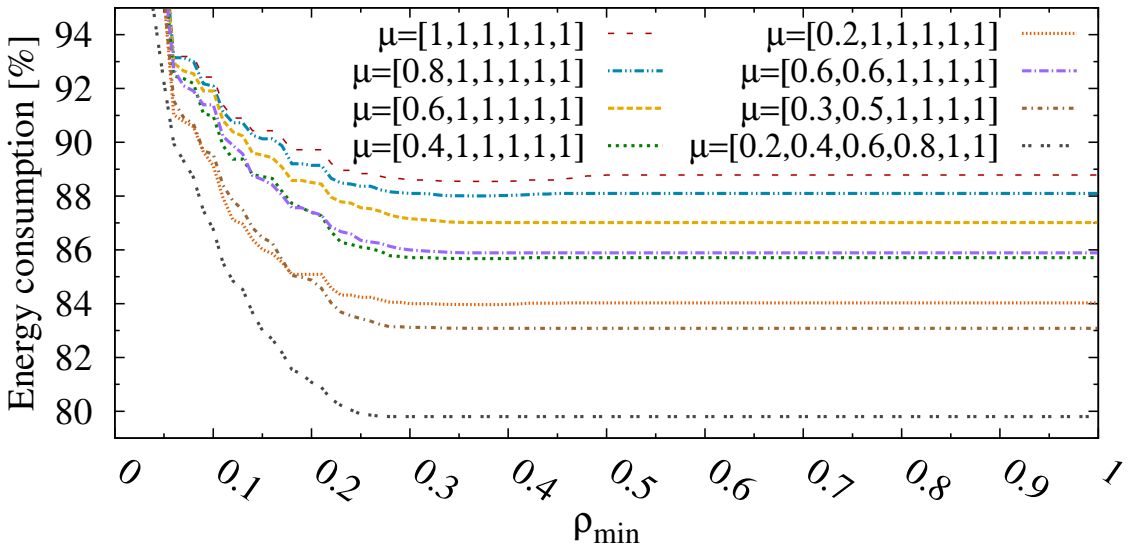

(a) Residential area

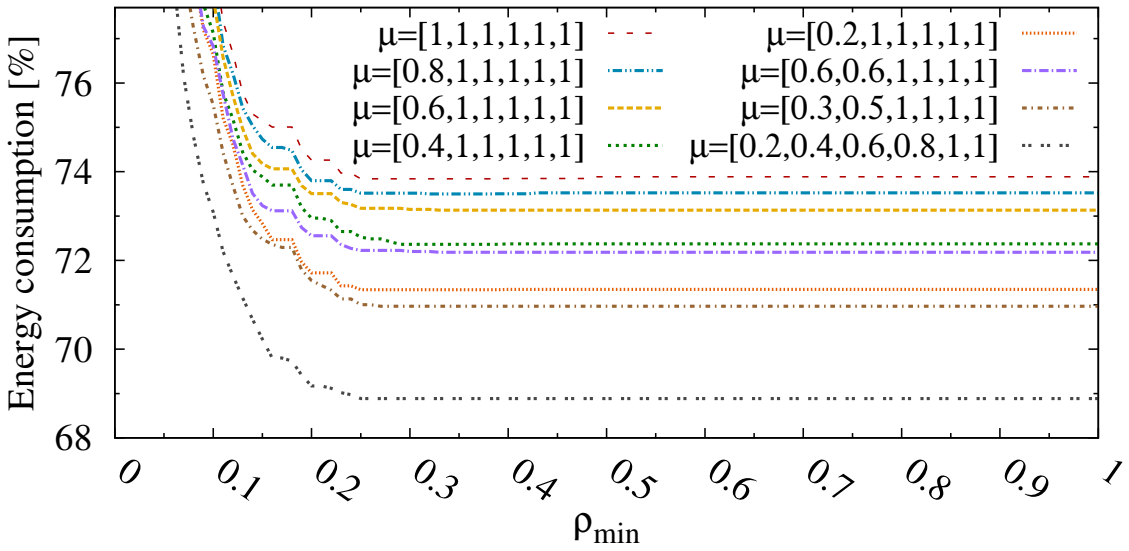

(b) Business area

Figure 8.2: Energy consumption in RA and BA, in different scenarios of traffic load distribution among micro BSs: $\mu_{array} = [\mu_1, \mu_2, ..., \mu_6]$

Adopting the parameter values reported in Tab. 3.1, $\rho^*_{min} = 0.37$. This value is adopted for all the results that will be presented below.

Finally, from the same figure observe that for values of $\rho_{min} > \rho^*_{min}$ only a slight increase in energy consumption can be observed. The tiny increase (almost invisible in the figure) can be explained by two reasons. On the one hand, even though a high value of ρ_{min} is used, the traffic load λ_i remains smaller than ρ^*_{min} for long

periods of time, especially when $\mu_i < 1$. On the other hand, most importantly, the total capacity of the macro BS imposes a limit on the maximum traffic load that can be transferred from the micro BSs.

8.2 System dimensioning under Resource on Demand

Here we investigate how the RoD strategy affects the RE generation system dimensioning and the energy self-sufficiency of the network. Let us assume $\mu_i = 1$ for all the BSs and $\rho_{min} = \rho^*_{min}$, that is the optimal configuration setting of the strategy to maximize energy saving. Fig. 8.3 shows the total yearly energy demand from the smart grid, E_G, for increasing values of the PV panels, S_{PV}, comparing the case without any RoD strategy (Fig. 8.3a) and the case where RoD is running (Fig. 8.3b). Each curve corresponds to a different value of the capacity of the battery, S_B, either in RA or BA. In general, as already observed in Sec. 7.3.1 for the case without RoD, larger batteries allow to reduce E_G. When no RoD is applied, E_G can be reduced below 50 kWh only with $S_P > 40kW_p$, whereas under RoD, E_G is remarkably decreased for any PV size. Noticeably in RA, $E_G < 50$ kWh can be provided with much lower S_{PV} than in BA and the largest S_B allows to achieve this target with a S_{PV} resulting 34% smaller than under no RoD.

8.3 Feasibility issues and CAPEX/OPEX cost under Resource on Demand

When trading off independence from the grid and PV panel and battery dimensioning, feasibility and cost issues should be considered as well. In particular, the PV module efficiency affects the PV panel area per kW_p. Considering a module efficiency of 19%, a total capacity of $120kW_p$ might not be feasible even with a distributed PV system, since it would require a total area of about 600 m^2. In this section, we make a preliminary analysis of the impact of RoD on the costs of the powering system, considering both CAPEX of the PV panels and batteries and OPEX due to energy purchase from the grid when production is not enough and the batteries are discharged.

Denote by c the cost per year of a system with a given combination of S_{PV} and S_B. The cost can be evaluated from:

$$c = \frac{S_{PV} \cdot c_P}{l_P} + \frac{S_B \cdot c_B}{l_B} + c_G \cdot E_G \tag{8.7}$$

where c_P is the cost for 1 kW_p of PV panel capacity, c_B is the cost for a 200 Ah-12 V lead-acid battery, c_G is the cost for 1 kWh of energy bought from the grid, l_P

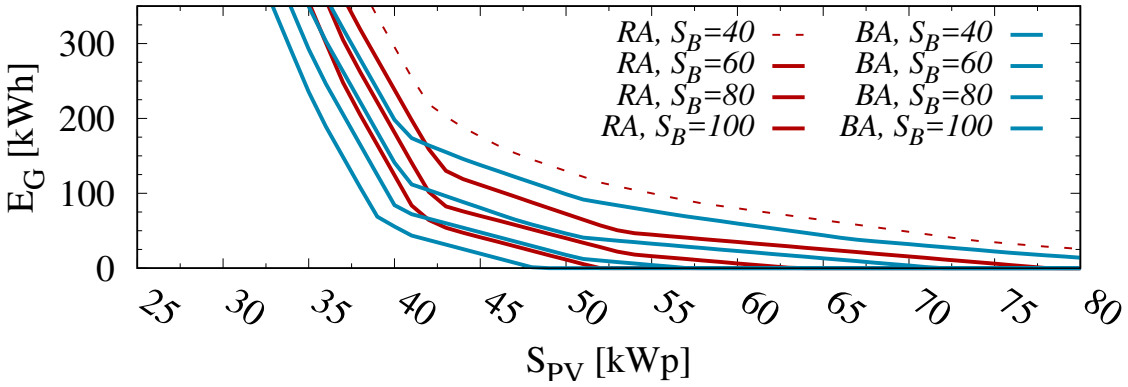

(a) No RoD

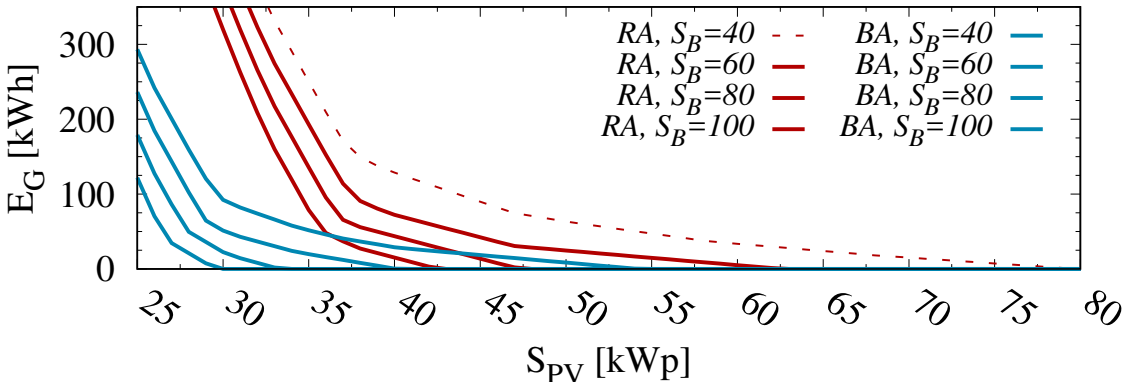

(b) Under RoD

Figure 8.3: Yearly grid energy, E_G, versus S_{PV} in Residential and Business area (RA and BA), for different values of the energy storage capacity.

is the life-cycle of a PV panel (in years), l_B is the expected lifespan of the set of batteries (in years) and E_G is the yearly amount of energy taken from the grid. The life-cycle of a PV panel, l_P, can be estimated to be around 25 years, whereas the sets of batteries need to be replaced more frequently and their lifetime duration is highly influenced by the number of charge/discharge cycles they undergo. Assume that the set of batteries is replaced after 500 cycles [66], hence $l_B = \frac{500}{n}$, where n is the number of battery cycles during one year of system operation. A lower value of n implies a lower frequency of battery replacement, hence less need for human maintenance. The introduction of the RoD strategy determines a considerable reduction in n with respect to the no RoD case. The decrease may amount up to 16.6% in RA, while it becomes even more remarkable in BA, where n can be reduced by percentages as high as 85%. In addition, n may vary depending on the number of batteries, S_B. For small to intermediate S_{PV}, n tends to sharply increase as S_{PV} grows larger. By converse, for intermediate to very large PV panel sizes, n slightly

decreases as S_{PV} increases, according to a roughly inverse proportionality. In our simulations, the maximum value of n achieved under the RoD strategy results to be higher in RA (n=180.2) rather than in BA (n=121.6). Given the same S_B, the batteries lifespan l_B tends to be higher in the BA scenario, with worst-case values over 4 years, against only 2.8 years in the RA case. For the price of panels, batteries and electricity we assume c_P=750 €/kW_p, c_B=140 €/battery and a rather high c_G=0.223 €/kWh (as for the Italian electricity market).

Fig. 8.4 shows the values of the yearly cost c together with the requested size of the PV panel, S_{PV}, for some values of the percentage of energy requests to the grid, indicated as $f_{G_{Max}}$, that corresponds to the powering system design target. For example, the case $f_{G_{Max}} = 0$ corresponds to a design target that requires that no energy should be bought from the grid; the case $f_{G_{Max}} = 1\%$ allows that up to 1% of the times energy can be purchased from the grid.

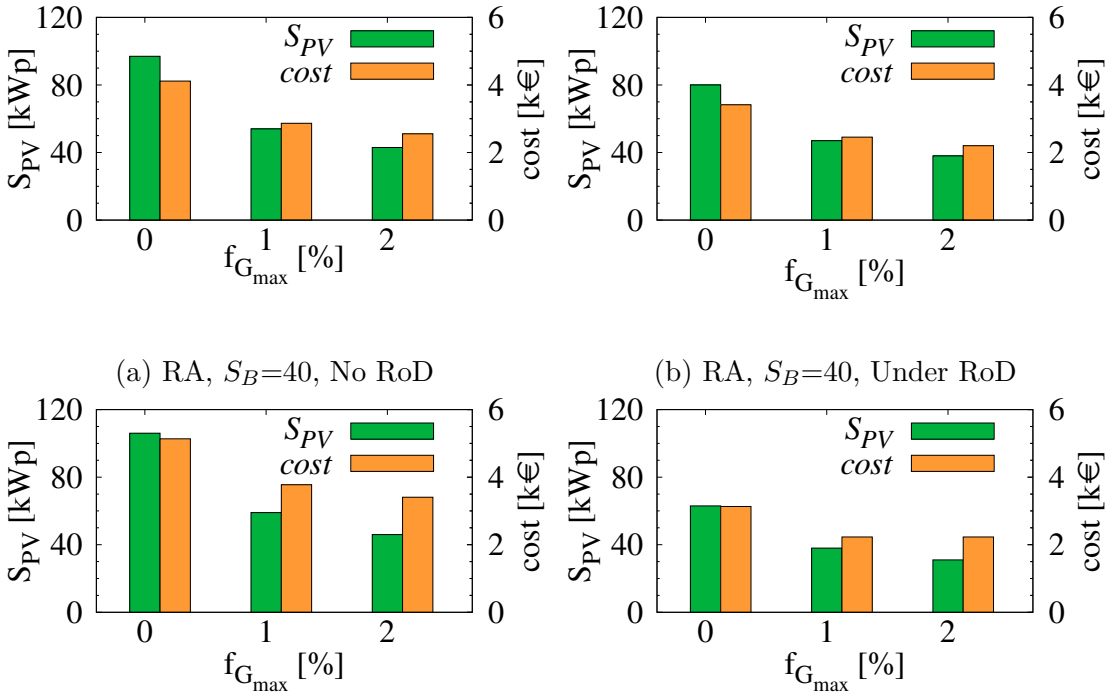

(a) RA, S_B=40, No RoD

(b) RA, S_B=40, Under RoD

(c) BA, S_B=30, No RoD

(d) BA, S_B=30, Under RoD

Figure 8.4: S_{PV} and c with no RoD strategy and under RoD strategy, in RA and BA, with different constraint on f_G.

When all the BSs are always kept active, E is comparable in the RA and in the BA, but the energy saving that can be obtained under RoD in the BA (26.2%) is more than twice the saving achieved in the RA (11.5%). When the system is kept totally independent from the grid, the RoD strategy reduces c by 17% in

RA, against a 39% decrease obtained in BA, thanks to a larger decrease in S_{PV}. When up to 1% of requests from the grid are allowed, RoD never reduces c by more than 14.3% in RA, while a 41% reduction is observed in BA, thanks to the smaller required S_{PV}. Under RoD strategy, the most significant contribution in improving the system feasibility in relation to S_{PV} and in terms of c reduction is obtained when the constraint on f_G is slightly softened from a self-sufficiency system to $f_G < 1\%$, with up to 41.3% reduction in S_{PV}. By converse, it is not very effective to further lessen the constraint on f_G. Finally, c could be further reduced by selling to the grid the amounts of produced RE exceeding the BS cluster energy demand and the storage capability, energy that would be otherwise wasted.

8.3.1 Comparing traffic patterns

From the presented results, it appears that, after introducing the traffic-based RoD strategy, higher energy savings can be achieved in BA rather than in RA. Moreover, the RoD strategy has a deeper impact on S_{PV} dimensioning and on c in case of BA with respect to RA. This behavior can be explained by the fact that the traffic pattern in the BA almost follows the trend of sun irradiation during the day, like it can be seen from Fig. 3.2. The coupling between RE production profiles and traffic patterns makes the usage of RE energy more effective and it reduces the need for energy storage support.

Finally, given the same total amount of traffic for the BS cluster, the load distribution among the different BSs highly influences the amount of energy saving that can be achieved through the RoD approach, even under the same setting of S_{PV} and S_B. This can be deduced, for instance, from Fig. 8.2, considering the case where all the micro BSs show $\mu_i = 1$ except for $\mu_1 = 0.2$ and the case where 2 micro BSs show $\mu_1 = \mu_2 = 0.6$. The total normalized traffic is the same, but the curve representing the energy consumption in the latter case is almost always above the curve representing the first case.

Chapter 9

Improving the interaction with the Smart Grid in a Demand Response framework

Part of the work presented in this Chapter has already been published in:

- D. Renga et al. "Improving the interaction of a green mobile network with the smart grid". In: *2017 IEEE International Conference on Communications (ICC)*. May 2017, pp. 1–7
- M. Ali, M. Meo, and D. Renga. "WiFi offloading for enhanced interaction with the Smart Grid in green mobile networks". In: *2017 IEEE 14th International Conference on Networking, Sensing and Control (ICNSC)*. May 2017, pp. 233–238

The interaction of a renewable powered mobile access network with the Smart Grid is now investigated. As depicted in Figure 3.1, we consider a scenario consisting of a portion of the cellular access network possibly powered by PV panels, besides the electric power grid. We assume that the Mobile Operator participates in the Demand Response program deployed by the SG, with the twofold objective of obtaining a reduction of the energy bill and contributing in providing ancillary services. In order to accomplish the requests coming from the SG to adapt the user load to the actual energy supply, the MNO may operate in different ways. In case the SG is asking its users to decrease their consumption, the MNO can exploit the presence of a local RE generator to power the BSs, either using the solar energy currently produced by PV panels or drawing from the storage the previously harvested energy. In addition, it can exploit the application of energy saving techniques, like RoD or WiFi offloading, to reduce the energy network demand.

Conversely, if an increased energy consumption is required by the SG, the MNO can positively react only if a storage is locally present, allowing to draw from the grid an extra amount of energy to be stored in the battery for future usage. In order to dynamically manage the responses of the mobile access network to the SG, a central controller is in charge of implementing the energy management strategies presented in Sec. 3.5.
In Sec. 9.1 we investigate the system performance when a local RE generator is introduced to power the BSs and a RoD can be applied to reduce the energy consumption from the grid. The performance analysis is conducted by applying the Markovian model proposed in Sec. 5.3, by evaluating the increase of the capability of providing ancillary services and the reduction in the energy bill. Results about the impact on system dimensioning are also derived.
In Sec. 9.2, we analyze the impact of the application of WiFi offloading on enhancing the interaction with the Smart Grid, again considering the probability of providing ancillary services and the reduction of the saving in terms of operational costs. Further insights on the effects of WO on system dimensioning are presented, and some remarks about criticalities raised by the application of WiFi offloading are discussed as well. In this case, the analysis is conducted via simulation.
Finally, Sec. 9.3 provides further final cosiderations about costs.

9.1 Renewable energy and Resource on Demand for providing ancillary services and reducing the energy bill

We now present the results of the performance study of a renewable energy-powered heterogeneous cellular network that is providing ancillary services to the Smart Grid. The smart grid periodically asks the cellular network to increase or decrease its energy consumption. An energy management strategy is proposed to satisfy the Smart Grid's request, and thus obtain a positive monetary reward. Indeed, according to the algorithm deployed in this work, the decisions about energy management are taken considering the requests from the smart grid of increasing or decreasing the on-grid energy consumption, with the objective of satisfying them as frequently as possible, so as to receive monetary rewards from the smart grid operator, proportionally to the contribution provided. Furthermore, a RoD strategy that switch-Off/On BSs is applied to make the network more energy efficient and further improving the interaction with the SG.

The network is modeled as a Markov chain, taking into account the randomness of renewable energy generation, which is modeled as a random variable based on real RE generation data, variability of network energy demand, which is considered by dividing the day into periods depending on real traffic traces from an Italian

operator, and variability of Smart Grid request, for which its transition probability are calculated using real data from RTE [106].

The Markovian model provides relevant insights in the system performance investigation by evaluating several performance indicators such as probability of low storage, probability of wasting harvested renewable energy and the total cost of network operation. These indicators are calculate for different size of renewable energy sources and storage capacity, and thus support the decision process of properly sizing the renewable energy source and the storage capacity. Moreover, an optimization algorithm is used to proper configuration settings of the proposed energy management strategy, which allows minimizing the energy operational cost.

Unlike most of the studies that solely focus on the benefits of cellular network (decrease in operational cost usually) while engaging in the Demand Response, this work evaluates the effect of the cellular network on the Smart Grid by calculating the probability of satisfying the requests of the Smart Grid.
A portion of a green mobile access network is considered, consisting of a macro BS and m additional micro BSs for providing further capacity in case of peak demand (see Fig. 9.1). Assuming that the cluster represents a portion of a dense mobile access network in a urban environment, the number of micro BSs, m, has been set equal to 6. The system operation has been modeled based on the stochastic model proposed in Sec. 5.3, that has been used to study the system behavior at the steady state, as Markovian models are effective tools for studying systems at the steady state and they are also adopted for investigating RE powered mobile networks [22, 32, 76]. In particular, it is used to analyze the system performance while the cluster interacts with the SG and evaluate the effectiveness of the RoD strategy, proposed in Sec.3.3.1, in improving the capability of the green access network to contribute in providing ancillary services. Real traffic profiles are adopted, that are those typical of both a residential area and a business area, as described in Sec. 3.2.2. Real location-based data about RE production are derived from traces obtained using the tool PV-Watts [37], based on actual solar irradiation data during the typical meteorological year in the city of Turin. RE production data are provided every half an hour. Only the three months featuring the lowest RE production (January, February, December) have been considered, in order to study the system performance in the worst case conditions. The real data about RE production have been used to derive the probability density functions of the random variable R_p per each period of the day. Each unit of the lead-acid battery set, used for energy harvesting, features a capacity of 200 Ah and voltage 12 V. Considering the impact of the maximum allowed DOD on the battery lifetime, a DOD $\leq 70\%$ is advisable in order to let the battery undergo more than 500-600 cycles before replacement [66]. As earlier mentioned, C_B corresponds to the portion of battery capacity that can actually be exploited, assuming a DOD of 70%. In the real system, the number of battery units is hence dimensioned in order to provide a total nominal capacity equal to $1.43 \cdot C_B$. Charging and discharging losses are not considered in this work.

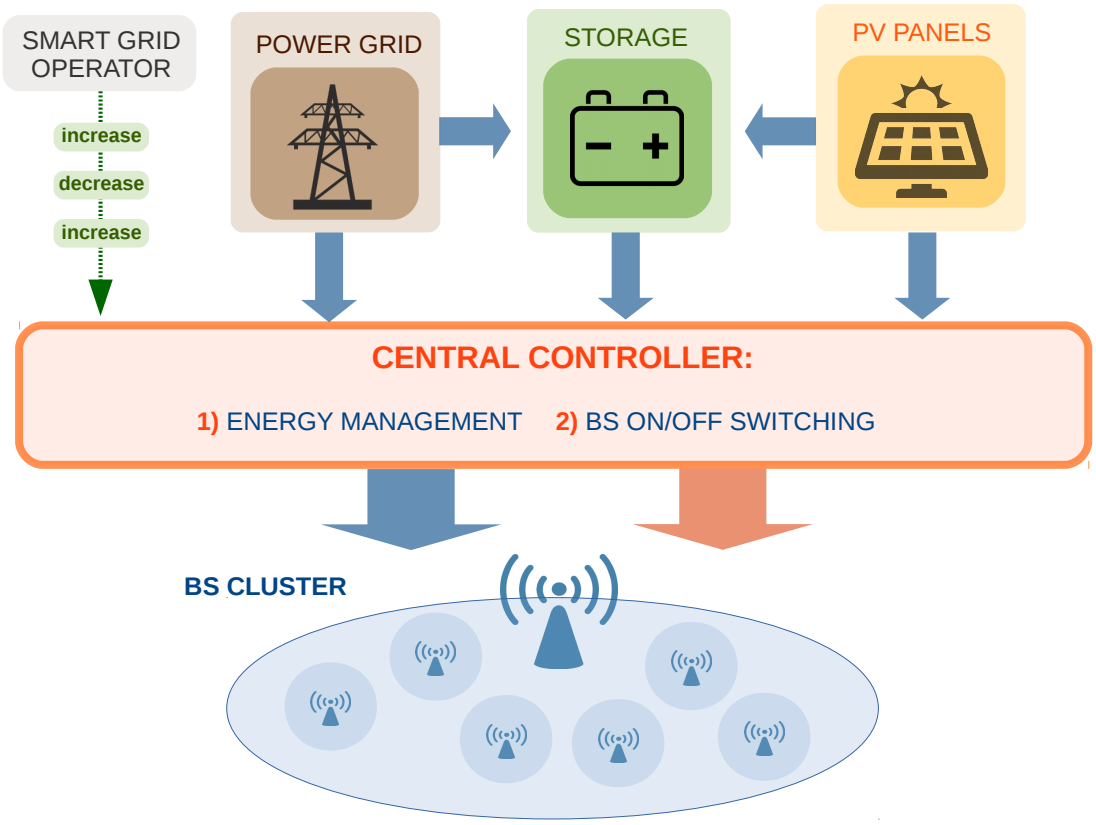

Figure 9.1: The renewable-powered mobile access network interacting with the Smart Grid.

The energy quantization step Q_s is set equal to 50 Wh. Finer quantizations are not advisable, since they would not provide significant gain in accuracy, but would increase the model complexity [32]. The complexity in terms of number of states is proportional to the number of battery levels N and to the number of timeslots in a day: $C = (N \cdot \frac{24[hours]}{\Delta T[hours]})$. N, in turns, depends on the energy quantization step Q_s. In our study the number of states is $200 \cdot 48 = 9600$ in the worst case.

The mobile network consumption per timeslot within each period, E_c, has been obtained by averaging the half-an-hour cluster consumption over each period duration, considering the actual traffic variations and the possible application of the RoD strategy. Real traffic traces have been considered, provided by an Italian mobile operator [15], with the granularity of 30-minutes, for a business area and a residential area (Fig. 3.2). For what concerns changes in the value of the state variable G, we use real data about grid requests provided by a French grid operator [106]. The data report grid requests every half an hour for a one year long period. Pricing data are retrieved from the RÃľseau de Transport d'ElectricitÃł-France (RTE-France) database [106] and the values adopted for energy prices, rewards

and penalty have been computed by averaging over one year the data observed on a 30-minute basis. The value adopted for the average price per unit of energy drawn from the grid, p_E, is 37 €/MWh. The values of the rewards provided in case the mobile network is able to satisfy the SG requests of type UP and DOWN are $r_U = 24$ €/MWh and $r_D = 60$ €/MWh, respectively. The application of the RoD strategy favors the capability of answering DOWN requests, for which the reward received is 2.5 higher than the reward obtained in case of UP. The five periods in which the day is divided have been defined so that they result different in length, but relatively homogeneous in terms of traffic load and energy consumption, as it can be observed from Fig. 9.2, which reports the period boundaries, along with the normalized power consumption for a micro BS during weekday and in the weekend, for the BA and RA traffic profiles. The thresholds on the RE production and the

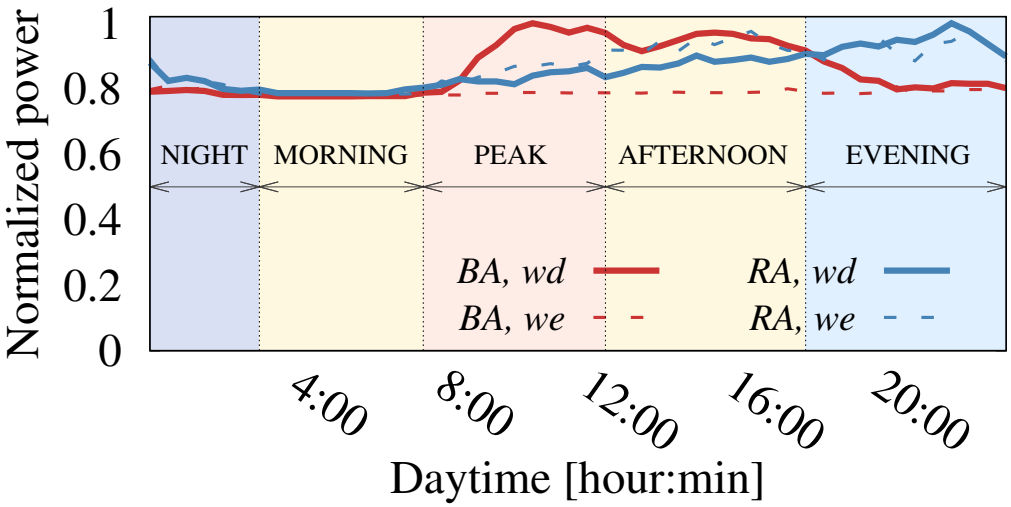

Figure 9.2: Power consumption for a micro BS within a day.

traffic load, based on which the chronological boundaries of the 5 periods have been defined, are reported below, with R_{p_N} denoting the normalized value of R_p:

- *night* (0:30 am - 3:30 am): $R_{p_N} = 0$; $0.05 \leq \rho \leq 0.26$
- *morning* (3:30 am - 8:00 am): $0 \leq R_{p_N} \leq 0.17$; $0.05 \leq \rho \leq 0.13$
- *peak* (8:00 am - 1:00 pm): $0.35 \leq R_{p_N} \leq 1$; $0.17 \leq \rho \leq 0.4$
- *afternoon* (1:00 pm - 6:30 pm): $0.16 \leq R_{p_N} \leq 0.94$; $0.33 \leq \rho \leq 0.6$
- *evening* (6:30 pm - 0:30 am): $R_{p_N} \leq 0.06$; $0.47 \leq \rho \leq 1$

The duration of each timeslot is $\Delta T = 0.5\ h$. This time interval is sufficient to allow a BS to be fully switched off or activated again, since these network configuration operations can be completed in the order of minutes. A finer time quantization is not required, since it would increase the complexity (remind that the number of states is proportional to the number of battery levels N and to the number of timeslots in a day, i.e. $N \cdot 24[hours]/\Delta_T[hours]$) without remarkably improving the accuracy of the performance analysis [32]. Furthermore, the selection of this time scale is consistent also with the fact that the forecast of the amount of renewable energy produced in a period of 30 minutes to few hours, based on the knowledge of short-medium term weather forecast, is sufficiently accurate with negligible error [121, 13, 42, 30, 109]. Two traffic scenarios have been considered, BA and RA, either without and under RoD strategy. The energy management algorithm is always running. Increasing values of PV size (C_{PV} = 1, 3, 5 kWp) and storage capacity (C_B = 6, 8, 10 kWh) have been tested.

9.1.1 Managing the interaction with the SG

The cluster of BSs can be powered either by the locally produced RE or by the energy taken from the grid. The storage is used to harvest the extra amounts of produced RE for future usage or to store the energy taken from the grid when it is convenient. Energy can be drawn from the battery to power the BSs when needed. Denote by E_c the energy needed for the cluster operation in the next timestep, by L_B the current battery level, and by R_p the amount of RE that can be produced in the following timestep. The strategy managing and coordinating the cluster interactions with the SG is detailed in Alg. 2. The energy needed for the cluster operation, E_c, may be derived from RE, from the battery or from the grid, depending on the requests from the grid and on the current battery level. Thresholds on the battery level are used to take decisions, the thresholds are denoted by th_U and th_D for the case of grid request UP and DOWN, respectively. a_U represents a fixed amount of energy that is taken from the grid and stored into the battery when the request from the grid is UP and there is still enough space in the battery. th_U is defined such that $C_B \geq th_U + a_U + RE_M$, where RE_M is the maximum amount of RE that can be produced in the following timestep. The threshold th_D must be larger or equal to E_c. A state denoted as *low storage* can hence be defined, corresponding to any storage level lower than E_c. This means that, according to the proposed algorithm, if the storage level is lower than the energy amount required for the mobile network operation E_c, the system is not able to satisfy a DOWN request from the smart grid, unless some RE is currently being produced. The threshold th_D has been set equal to a fixed value within each period, i.e. the value of E_C in that period, so that in case of NULL request the cluster can completely rely only on the energy stored in the battery, even in case of peak traffic. On the

Algorithm 1 Energy management algorithm

switch *grid request* **do**
  case UP
    draw E_c from the grid;
    if $L_B \leq th_U$ **then**
      draw a_U from the grid and store it into battery;
    end if
  case $DOWN$
    derive $E = \min(E_c, R_p)$ from RE;
    if $L_B \geq th_D$ **then**
      if needed, derive $E_c - E_p$ from the battery;
    else
      if needed, derive $E_c - E_p$ from the grid;
    end if
  case $NULL$
    draw E_c from the grid;
harvest residual RE into battery, waste the extra amount;

contrary, for each configuration setting of [C_{PV},C_B], various combinations from a set of multiple values have been adopted for th_U in the different periods and tested, in order to obtain the best value in this set in terms of cost reduction. Similarly, different values of a_U have been tested, in order to select the best value for this parameter as well. The average value of E_c in the BA is equal to 678 Wh when no RoD strategy is applied, against 487 Wh under RoD. In the RA, the average value of E_c is equal to 701 Wh under no strategy and 635 Wh when the strategy is run.

9.1.2 Performance indicators

The system behavior has been investigated at the steady state, based on numerical solutions, by analyzing the following performance indicators:

S_a - Average storage level

$$S_a = \sum_J \pi(x) \cdot S \tag{9.1}$$

where $\pi(x)$ is the probability of state x at the steady state and J is the whole set of all the possible states in the Markov chain: $J = \Big\{x = (P, S, G)\ s.t.\ S \leq C_B,\ \ \forall P, G\Big\}$.

P_L - Probability of low storage level (i.e. $S < E_c$)

$$P_L = \sum_L \pi(x) \tag{9.2}$$

where L is the subset of states in the Markov chain in which the storage level is too low to satisfy the BS power demand: $L = \Big\{x = (P, S, G)\ s.t.\ S < E_C,\ \ \forall P, G\Big\}$.

P_{U_+}, P_{D_+} - Probability of responding to the grid requests this is the probability providing ancillary services, in case of UP and DOWN request, respectively.

$$P_{U_+} = \frac{\sum_{Ir} \pi(x)}{\sum_{R_U} \pi(x)} \tag{9.3}$$

where Ir (*Increase response*) is the subset of states in the Markov chain in which the SG requires to increase the on-grid energy consumption and the SG request can be satisfied, since there is still enough space in the battery to store the extra amount of energy taken from the grid, that in the policy proposed is a fixed amount: $Ir = \Big\{x = (P, S, G)\ s.t.\ S \leq th_U,\ G = U,\ \forall\ P\Big\}$; R_U is the set of all the states in the Markov chain in which the SG request is of type UP: $R_U = \Big\{x = (P, S, G)\ s.t.\ G = U,\ \forall\ P, S\Big\}$.

$$P_{D_+} = \frac{\sum_{Pr} \pi(x) \cdot p(R_p > 0) + \sum_{Fr} \pi(x)}{\sum_{R_D} \pi(x)} \tag{9.4}$$

where Pr (*Partial response*) is the subset of states in the Markov chain in which the SG requires to decrease the consumption and the storage level is below the threshold th_D: $Pr = \Big\{x = (P, S, G)\ s.t.\ S < th_D,\ G = D,\ \forall\ P\Big\}$. Hence, in this case the SG request cannot be always fulfilled, since the on-grid energy consumption can be reduced only in case RE is generated (i.e. $R_p > 0\ Wh$). Fr (*Full response*) is the subset of states in the Markov chain in which the request from the SG is of type DOWN and the grid request can be always satisfied even if RE is not available, since the storage level is high enough to satisfy the energy demand: $Fr = \Big\{x = (P, S, G)\ s.t.\ th_D \leq S,\ G = D,\ \forall\ P\Big\}$. R_D includes all the possible states in the Markov chain in which the grid request is DOWN:$R_D = \Big\{x = (P, S, G)\ s.t.\ G = D,\ \forall\ P, S\Big\}$.

W_f - Probability of wasting RE it is due to the fact that the RE that is not immediately used by the BS cluster cannot be stored in the battery for lack of residual available capacity.

$$W_f = P_w^U + P_w^D + P_w^N \tag{9.5}$$

where P_w^U, P_w^D and P_w^N are the probabilities of wasting a fraction of the RE produced in the case of requests from the SG of type UP, DOWN and NULL, respectively. These probabilities are derived as reported below:

- $P_w^U = \sum_{R_U} \pi(x) \cdot p(R_p > C_B - S)$, where R_U is the subset of states in the Markov chain in which the SG requires to increase the energy consumption and the battery charge level is higher than th_U: $R_U = \Big\{x = (P, S, G)\ s.t.\ S > th_U,\ G = U,\ \forall\ P\Big\}$. $p(R_p > C_B - S)$ is the probability of generating an amount of RE for which there is not enough space to entirely store it in the battery.
- $P_w^D = \sum_{R_D} \pi(x) \cdot p(R_p > C_B - S + E_c)$ where R_D, as previously defined, is the subset of states in the Markov chain in which the SG request is of type DOWN, whereas $p(R_p > C_B - S + E_c)$ represents the probability of producing an amount of RE such that the RE remaining after having powered the BSs, cannot be entirely stored in the battery, since the storage space is not sufficient.
- $P_w^N = \sum_{R_N} \pi(x) \cdot p(R_p > C_B - S + E_c)$ where R_N is the subset of states in the Markov chain in which the SG request is NULL: $R_N = \Big\{x = (P, S, G)\ s.t.\ G = N,\ \forall\ P, S\Big\}$ Again, $p(R_p > C_B - S + E_c)$ represents the probability of producing an amount of RE such that the RE remaining after having powered the BSs, cannot be entirely stored in the battery, since the storage space is not sufficient.

c - Total cost for the system operation

$$c = p_E \cdot E_G - E_U \cdot r_U - E_D \cdot r_D \tag{9.6}$$

where E_G is the amount of energy bought from the grid, E_U is the amount of additional energy, with respect to the forecast need, drawn from the grid in case of request UP, and E_D is the amount of energy reduction, with respect to forecast need, in the energy required from the grid in case of request DOWN. E_G represents the total amount of energy that is actually drawn from the grid, hence it includes E_U, but not E_D.

The results are derived using, within each period of the day, the optimized values for th_U and a_U, in order to minimize operational costs. The optimization of these parameters has been obtained performing an exhaustive research within a predefined heuristic set of possible values of th_U and a_U. A set of H possible values of th_U and a set of M different values of a_U have been defined to generate the set T, which includes all the possible pairs (th_U,a_U). Within each iteration of the exhaustive search, each period of the day has been assigned a different pair, picked from those in the set T, in such a way that, after all the iterations, all the possible combinations of pairs in the 5 periods of the day would be tested. Therefore, within a single iteration, the value of th_U (or, similarly, of a_U) may differ from one period to another. The total number of iterations performed hence amounts to $(H \cdot M)^5$. In our case, $H = M = 3$, in order to trade off precision versus complexity. The

combination of thresholds allowing to achieve the lowest operational cost c has been adopted to derive all the performance parameters.

9.1.3 RoD strategy and PV panel size role in system performance

Fig. 9.3 shows S_a and P_L for increasing C_{PV} in BA and RA, under no RoD strategy or under RoD, using a battery with C_B= 8 kWh. In the BA S_a tends to increase for growing values of C_{PV}, while P_L tends to decrease for larger of C_{PV} in both cases (no RoD and under RoD), as expected. However, in case of RoD strategy, the level of S_a and P_L results to be respectively higher and lower than under no RoD strategy. The general trend is similar for the RA, but the S_a results to be lower, even under RoD strategy, with a higher probability of low level of storage, resulting in a small difference with respect to the case of no RoD.

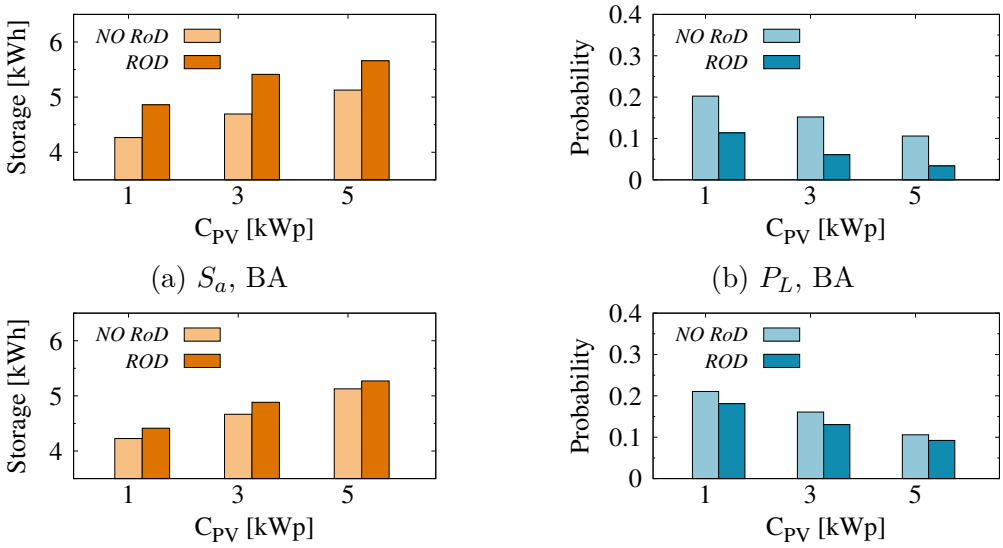

(a) S_a, BA (b) P_L, BA

(c) S_a, RA (d) P_L, RA

Figure 9.3: Average storage level (S_a) and probability of low battery level (P_L), with and without RoD, in BA and RA.

The probabilities of responding to the grid requests, P_{U_+} and P_{D_+}, are reported in Fig. 9.4 for increasing values of C_{PV} and fixed C_B= 8 kWh. From Fig. 9.4a it can be observed that, under no RoD strategy, P_{U_+} gradually decreases for larger values of C_{PV}; when the RoD strategy is applied, P_{U_+} results to be lower and the decrease with growing C_{PV} is slightly steeper. This behavior can be explained by the fact that larger amounts of RE are produced with larger PV panels and, in case of RoD, smaller amounts of energy are consumed by the cluster, leading to higher average levels of the storage, like already shown in Fig. 9.3a. Hence, it is less likely

that the system can draw from the grid additional amounts of energy besides its current need E_C, since the probability of being in a state higher than th_U is higher and in this case there is not enough residual capacity for storing the additional amount of energy a_U from the grid. Conversely, as shown in Fig. 9.4b, P_{D_+} grows larger for rising values of C_{PV} and its values under RoD strategy are always higher while the slope of growth is less steeper than without any RoD policy. Indeed, P_{D_+} under RoD may rise up to almost 1 with large panels and it never results to be lower than 65%. The impact of the PV panel size in increasing P_{D_+} is accounted for by the higher amounts of RE that are produced with larger panels and that can be used instead of the grid energy in case of a DOWN request. Furthermore, the higher level of RE production leads to higher values of S_a, likely higher than th_D, especially under RoD, as it is shown in Fig. 9.3; hence, an additional huge reserve of energy, represented by the storage, is more likely available in case of request DOWN, even when the RE is not currently being produced. In the RA the trend for P_{U_+} and P_{D_+} is very similar to the BA case, but the gap between the values under no RoD strategy and under RoD is much smaller, especially for P_{D_+}, whose maximum values are also lower than in the BA. It is to be noted that,

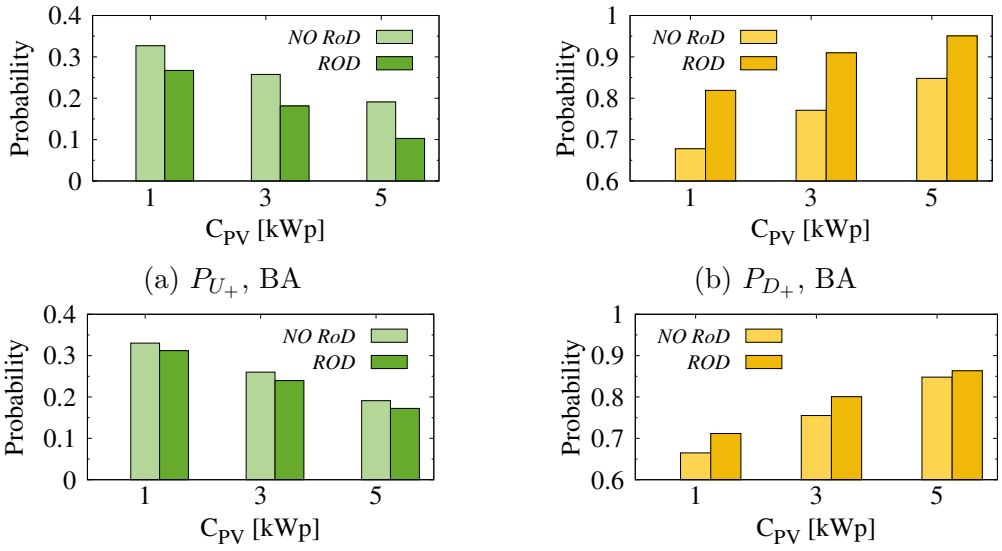

(a) P_{U_+}, BA (b) P_{D_+}, BA

(c) P_{U_+}, RA (d) P_{D_+}, RA

Figure 9.4: Probability of providing ancillary services, P_{U_+} and P_{D_+}, with and without RoD, in BA and RA.

when the RoD strategy is adopted, it is not applied just in case of a request from the SG of decreasing the on-grid consumption. On the contrary, it is continuously running, regardless the type of SG requests. Therefore, the contribution of the RoD strategy in improving the interaction with the SG consists in increasing on average the level of battery charge (Fig. 9.3); on the long term, this leads to higher

probability of providing ancillary services (i.e. satisfying the SG request) in case of request of type DOWN rather than in case of UP (see Fig. 9.4), thus resulting in higher monetary gains, since the reward in case of DOWN is 2.5 higher than in case of UP. The values of W_f are reported in Fig. 9.5 for rising C_{PV}, under the same value of battery storage, for the BA and the RA. In general, for smaller C_{PV} the energy waste is rather limited, around 10%, and no significant difference can be observed under RoD or without any strategy, both in the BA and RA. Nevertheless, for C_{PV} as high as 5 kWp, a sharp increase occurs in W_f under RoD in the BA, rising up to about 30%.

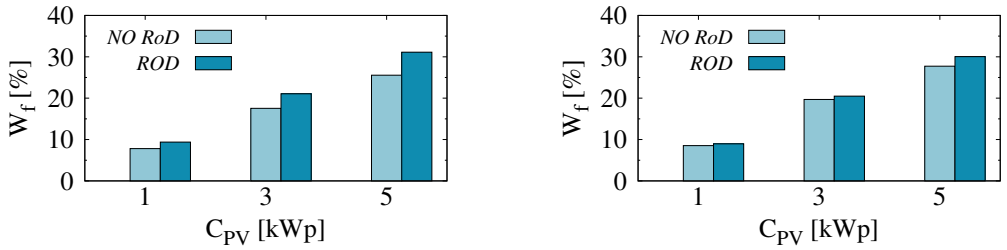

(a) BA (b) RA

Figure 9.5: Average probability of wasting RE (W_f), in BA and RA.

9.1.4 Cost analysis

Fig. 9.6 reports the total cost for the system operation, c, for growing values of C_{PV} and increasing values of C_B, normalized with respect to the cost that should be paid in case all the energy required by the cluster were bought from the grid (without any RoD strategy), denoted as c_g. The results are shown without the application of RoD strategy and under RoD, for the case of BA. For the BA

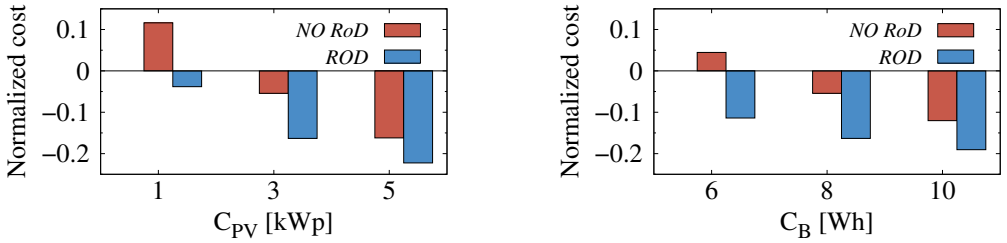

(a) Varying C_{PV}, $C_B = 8\ kWh$ (b) $C_{PV} = 3\ kWp$, varying C_B

Figure 9.6: Cost versus C_{PV} and versus C_B, without RoD strategy and under RoD strategy, in BA.

(Fig. 9.6a), the normalized cost is lowered by almost 90% even with the smallest

C_{PV}, in the case of no RoD policy; a further decrease is observed for increasing values of C_{PV}, with the most relevant reduction observed moving from $C_{PV} = 1\ kWp$ to $C_{PV} = 3\ kWp$, of about 15 percentage points. The introduction of the RoD policy determines a further dramatic drop in the total cost for small panels and the cost is further reduced for larger C_{PV}, although the impact of RoD becomes limited for C_{PV}= 5 kWp. For any C_{PV} the cost becomes negative, meaning a positive gain received from the grid, of up to more than 120% of c_g. The general trend is similar in the RA (data not reported), even though the reduction in the cost is slightly lower. From our results, it can be evinced that the probability of providing ancillary services in case of DOWN requests, P_{D_+}, provides a major contribution in reducing the system operational cost c, with respect to P_{U_+}. Fig. 9.6b shows normalized cost c under RoD and without RoD for increasing values of C_B and fixed C_{PV}= 3 kWp, in the BA. Increasing C_B from 6 kWh to 10 kWh allows to decrease the cost and this effect is more evident when no RoD strategy is applied. The most significant gain is obtained moving from 6 to 8 kWh, whereas further rising the storage capacity only provides a limited advantage.
These results show that the stochastic model proposed in this work could find practical application in system dimensioning. Indeed, it could be useful in supporting the decisional process aiming at properly sizing the PV panels and the storage capacity, based on the target reduction in cost, the feasibility constraints and the possibility of applying RoD strategies.
In order to show that the cost savings are not only due to the overall reduction in energy consumption, simulations have been performed to investigate the same scenario of a RE-powered mobile network, with the same set of macro and micro BSs, the same traffic loads and the same location. A PV panel size of 1 kWp and a storage capacity C_B=8 kWh has been considered. No energy management policies were applied, hence the interaction with the SG in a Demand Response framework was excluded. The average daily cost paid for the energy drawn from the grid has been computed both in the case in which no RoD strategy was applied and in the case in which the RoD was running, as a baseline reference. Finally, the average daily costs obtained from our model under the application of the energy management policy were compared to the baseline costs obtained from simulations, both without radio resource management and under RoD strategy. Under no energy management policy, the application of a RoD strategy allows to achieve significant cost savings of 28.5%. Nevertheless, the contribution of the energy management strategy in reducing costs is much higher, since its application on the top of a RoD strategy allows to further decrease the expenditure by 71.5%, hence erasing the operational cost. Finally, even energy management alone, i.e. without any RoD policy, is very effective in reducing costs, even erasing the operational expenditure.

9.2 WiFi offloading to enhance the interaction with the Smart Grid

We now analyze the case of a mobile access network interacting with the Smart Grid in a Demand-Response framework, in which the mobile operator uses WiFi Offloading in order to respond to the SG requests. Currently, WiFi APs are increasingly deployed by more and more operators and private users, making the WiFi technology become available almost everywhere. Therefore, WO looks a very promising solution to increase the capacity of cellular networks [61]. In our case, WO is exploited to increase the chance of satisfying the requests from the grid of decreasing the consumption, by reducing the traffic load right when the reward for providing ancillary service is higher. This technique can also be combined with RoD to further increase its effectiveness. Indeed, the impact of WiFi offloading in improving the interaction with the SG is evaluated in two different scenarios. In the first scenario, all the BSs are always kept active, even during off-peak periods. In the latter, a RoD strategy is applied in order to adapt over time the network power consumption to the actual traffic demand, hence saving energy and reducing costs for energy bought from the grid. The proposed strategy exploits the possibility of putting the BSs into deep sleep mode, in which negligible consumption can be assumed.

The application of WiFi offloading techniques in mobile access networks can help to better answer to the requests form the SG, in particular in those periods in which the SG asks for a reduction of the consumption. However, their impact may be constrained on the one hand by the minimum capacity to be guaranteed even during off-peak periods for an acceptable Quality of Service and, on the other hand, by the maximum amount of traffic load that can be offloaded to the WiFi APs. Furthermore, this approach does not provide huge margin to satisfy the requests to increase consumption from the grid, since the cluster load cannot be forced to grow. The introduction of photovoltaic panels to power a BS cluster makes it more energy self-sufficient and further increases the probability of satisfying the SG when a reduction of the consumption is required. In addition, the presence of batteries, that are needed to address the typical intermittent and unpredictable nature of renewable energy production, is useful not only for powering the BSs when the requests from the SG is to decrease the consumption, but also for storing some extra energy drawn from the grid when the request is to increase consumption.

A portion of a green mobile access network is hence considered, in order to investigate to what extent the application of a WiFi offloading technique may improve the capability of providing ancillary services and, at the same time, reducing costs for the Mobile Network Operator. The scenario, represented in Fig. 9.7, consists of a cluster composed of one macro and m=6 micro BSs powered by the grid and by PV panels. WiFi offloading can be activated to satisfy the requests from the Smart

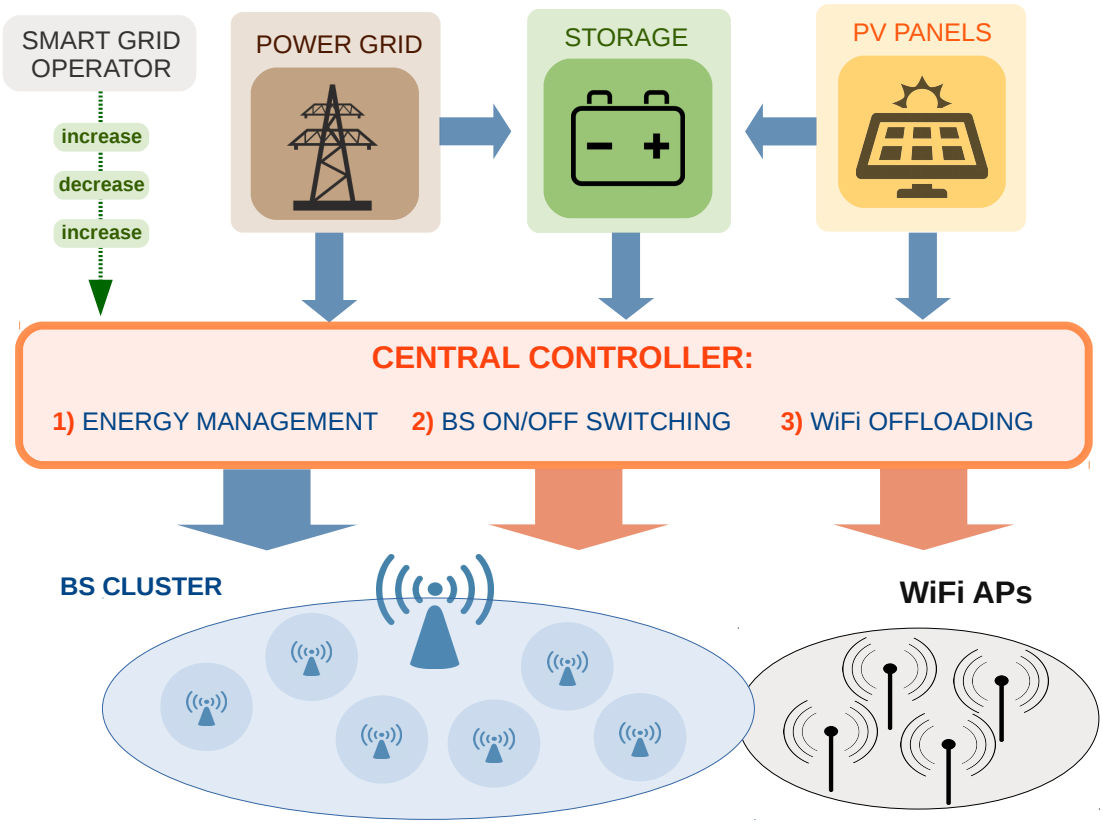

Figure 9.7: The green mobile access network interacting with the Smart Grid.

Grid of decreasing the grid consumption, by moving part of the traffic to neighboring APs. We assume that the neighbor APs available for carrying a fraction of the mobile traffic in case of DOWN requests are owned by some local business holders and/or by private individuals residing in the area that have accepted to periodically handle a portion of the mobile traffic based on some agreement. Furthermore, we assume that the Internet Service Provider (ISP) with which each of the local business holders and the private individuals envolved in the agreement have stipulated a contract for Internet access provisioning to the APs, coincides with the same Mobile Operator owning the cellular access network infrastructure. Hence, these APs form a virtual WiFi network available, under certain conditions, to carry some of the load transferred from the mobile access network. Indeed, some kind of agreement is envisioned between the WiFi network owners and the Mobile Operator, allowing to provide for example additional Internet Services for free or some rate discount to the WiFi network owners in exchange of their consent to make a fraction of the WiFi capacity available to periodically carry some of the mobile traffic. We assume that the mobile traffic can be transferred only when the traffic load of the WiFi network is sufficiently low, in order to be conservative on the

Quality of Service constraints in terms of available bandwidth for both the mobile users and the WiFi network users. In accordance with data from the literature, this corresponds to a maximum capacity available for WiFi offloading of 10% of the peak traffic load handled by the 6 micro BSs, allowing to achieve an average offloading efficiency approximately between 10-20%, depending on the specific case [16, 74, 93].
The RoD scheme operates by switching off one or more micro BSs, depending on the current traffic that has to be handled by each of them, with the purpose of decreasing the overall energy consumption from the grid. If the traffic load decreases below a given threshold, denoted as ρ_{min}, the micro BS can be switched off and its traffic moved to the macro BS, as long as there is still enough capacity on the macro BS to handle the additional load [33]. When the RoD is running, the application of WiFi offloading may allow to increase the number of BSs that can be put into sleep mode in case of request of type DOWN, further reducing the network energy demand.

9.2.1 Energy management policy

The energy management strategy applied to respond to the SG requests is described here. A general description is provided assuming the presence of a RE generator, with a set of PV panels whose capacity is S_{PV} and a set of batteries whose size is B. The same operation holds in case no RE generator is envisioned. In this case, S_{PV} and B are simply equal to 0. C_f denotes the network consumption for each half an hour forecast the day ahead, while C_a is the actual network consumption. Every half an hour, different actions can be taken, based on the type of grid request and the amount of produced RE. The BSs need C_a may be derived from the produced RE, from the storage (always respecting the maximum discharging rate) or from the grid. RE may be used to power BSs, harvested into battery or wasted in some cases. The RE management is based on a *first use - then harvest* principle, meaning that the produced RE can be directly used to power the BSs and only the extra amounts are possibly harvested afterwards. In order to better answer U requests, an additional amount of energy, denoted as E_b, can be drawn from the grid and harvested into battery for future usage. E_b is the maximum amount that can be injected into the battery in half an hour, constrained by the maximum charging rate and the maximum available battery capacity, i.e. B. The RE produced every half an hour is denoted as R_p, while E_g represents the energy drawn from the grid for each half an hour. E_r denotes the residual energy need of the access network after R_p has been used to power the BSs. Every half an hour, energy management decisions are taken according to Alg. 2. Note that, when the WO is active and a D request occurs, part of the traffic load is transferred from some micro BSs to neighboring APs. In case of U request, a reward is obtained if the total energy taken from the grid, E_g, is larger than the predicted consumption

Algorithm 2 Energy management algorithm

1: $E_r = 0$; $E_g = 0$;
2: **switch** *grid request* **do**
3: **case** U:
4: **if** $(R_p < C_a)$ **then**
5: power BSs from the grid;
6: harvest extra energy, E_b, from grid into B;
7: waste R_p;
8: $E_g = C_a + E_b$;
9: **else**
10: use R_p to power BSs;
11: store $(R_p - C_a)$ into B, waste the extra amount;
12: **end if**
13: **if** $(E_g > C_f)$ **then**: a reward is received;
14: **else if** $(E_g < C_f)$ **then**: a penalty is paid;
15: **end if**
16: **case** D:
17: **if** WO is active **then**: offload some traffic;
18: **end if**
19: use R_p to power BSs;
20: compute residual need $E_r = max(0, C_a - R_p)$;
21: **if** $(E_r = 0)$ **then**
22: store $(R_p - C_a)$ into B, waste the extra amount;
23: **else**
24: draw E_r from B and, if needed, from grid;
25: $E_g = max(0, E_r - Battery\ Level)$;
26: **end if**
27: **if** $(E_g > C_f)$ **then**: a penalty is paid;
28: **else if** $(E_g < C_f)$ **then**: a reward is received;
29: **end if**
30: **case** N:
31: code from line 19 to 26;

C_f. The reward is proportional to the extra amount of energy taken from the grid. By converse, in case it is lower, a penalty is paid proportional to the energy gap with respect to the reference level C_f predicted the day ahead. Similarly, in case of D, a reward is obtained if $E_g < C_f$, and vice versa for the penalty.

9.2.2 Performance analysis

The system performance has been investigated in terms of energy yearly taken from the grid, probability of providing ancillary services (ASs), effect of system dimensioning and cost analysis in two scenarios (no RoD and RoD), also considering the application of WO and the introduction of a PV system.

Energy demand from the grid

Fig. 9.8a reports the amount of energy taken from the grid over one year, E_G, in the two baseline scenarios (without and under RoD), comparing the case without WiFi offloading and the case in which WiFi offloading is applied. In the basic scenario, that is when neither RoD nor WO are applied, E_G=12.15 MWh; this value is considered as the reference value, E_G*, with respect to which the energy saving is computed. Under RoD, 10.76 MWh are consumed and drawn from the grid, with a 11.5% saving with respect to E_G*. The application of WO allows to reduce E_G by 6% without RoD and by 13.6% under RoD, again with respect to E_G*. The case with RE production is also shown in Fig. 9.8a, assuming S_{PV}=10 kWp and B=10 kWh. Without RoD running, a remarkable reduction in E_G can be achieved, always higher than 39%. The smallest value of E_G is obtained when both RoD and WO are applied, with 48.2% saving with respect to E_G*.

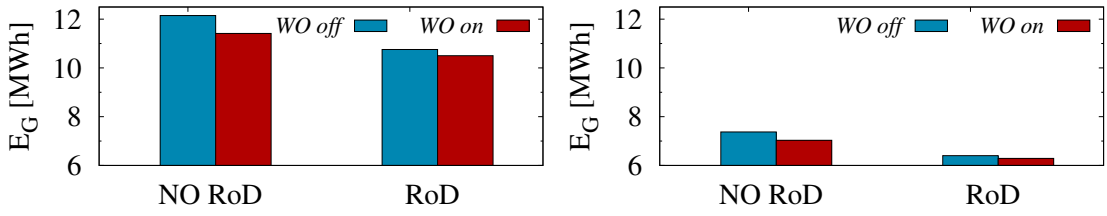

(a) No RE production

(b) With RE production

Figure 9.8: Grid demand, E_G, without and under RE production.

Providing ancillary services

The probabilities of answering both U and D requests from the grid are here reported, for the various considered scenarios. Probabilities are defined as follows:

- P_{U_+}: probability of satisfying a grid request of type U (the SG asks to increase the consumption from the grid and the network is able to do that);
- P_{D_+}: probability of satisfying a grid request of type D (the SG asks to decrease the consumption from the grid and the network is able to do that).

Fig. 9.9 shows the results in case no RE is locally produced. U requests can never been satisfied as it can be seen from P_{U_+}=0 under any scenario (without and under RoD, WO on or off). This is due to two reasons: first, the traffic patterns are assumed to be exactly known in advance so that the forecast traffic load is exact; second, the absence of any energy storage does not allow to draw and harvest extra energy from the grid to answer its U request. D requests can be satisfied only when WO is applied, due to the same assumption of exact predictability of traffic. WO offloading allows to achieve P_{D_+}=78.9% in the baseline scenario and a slightly lower P_{D_+}=54.3% when RoD is applied. Note that the reward for providing ancillary services in case of D is 2.5 times higher than for answering U requests. The probabilities of not answering U or D requests clearly result complementary to P_{U_+} and P_{D_+}. However, no penalties must be paid under any scenario, since no opposition to the SG requests is ever registered, meaning that the SG requests merely result not satisfied.

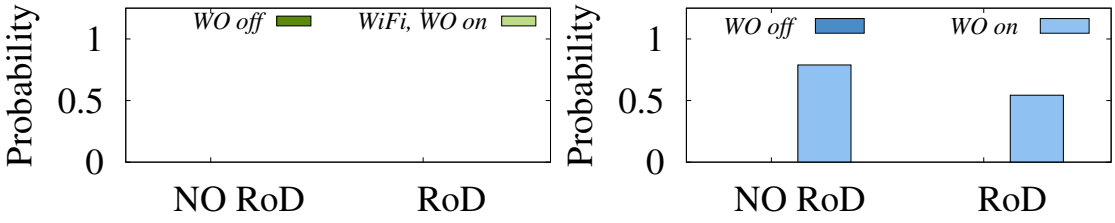

(a) P_{U_+} (b) P_{D_+}

Figure 9.9: Probability of providing ASs, without RE production.

In Fig. 9.10 the probabilities of providing ancillary services are reported for the case in which RE is produced. P_{U_+} is now above 60% under any scenario, with slightly lower values when WO is active, while P_{D_+} is above 96% under any scenario, with WO providing values as high as about 99%. Although the reward for providing ancillary services in case of U is limited and lower than in case of D, a higher average level of battery allows to better answer D requests, hence further increases the gain. The probability of not answering grid requests is highly decreased in case of U requests with respect to the scenario in which no RE is produced and it is almost nullified in case of D requests. Let us denote as E_{U_+} and E_{D_-} the yearly cumulative amount of energy exceeding the forecast consumption in case of U and D request, respectively, while E_{U_-} and E_{D_+} correspond to the absolute values of the yearly cumulative amount of energy representing a negative gap with respect to the predicted consumption in case of U and D requests, respectively. Their values are shown in Fig. 9.11. When a RE generator and a storage are present, despite a lower P_{U_-}, the probability of opposing the U requests is higher than under no RE production, as it can be evinced from Fig. 9.11c. This translates into higher E_{U_-} under any scenario (RoD on/off, WO on/off), for which a penalty is due.

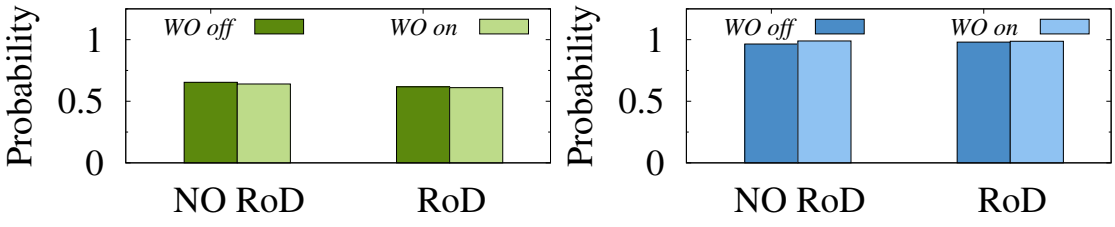

(a) P_{U_+} (b) P_{D_+}

Figure 9.10: Probability of providing ASs, under RE production.

This penalty however is compensated by a null E_{D_-} and by the higher P_{U_+} and P_{D_+}, leading to considerable positive energy gaps with respect to the predicted consumption levels, for which proportional rewards are provided.

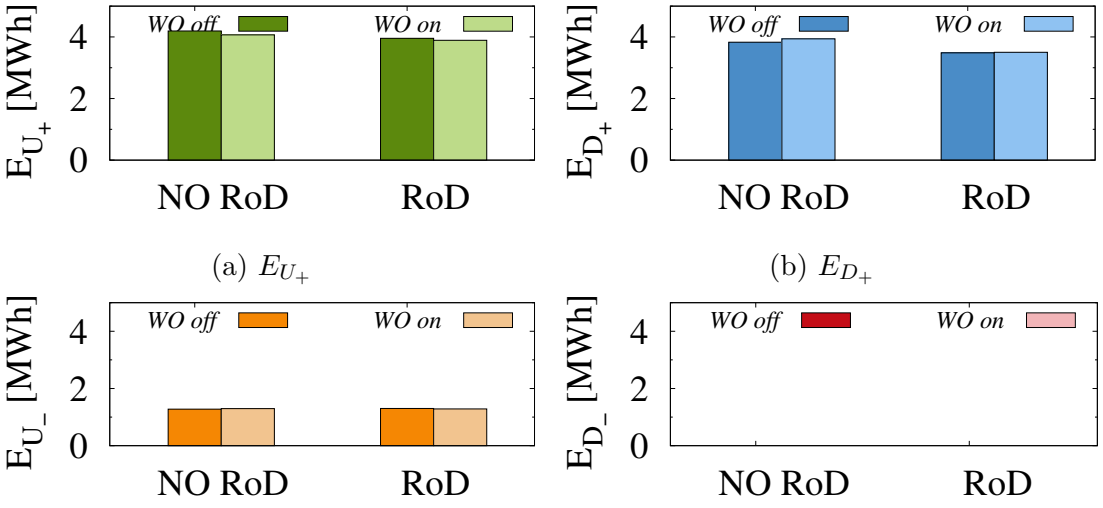

(a) E_{U_+} (b) E_{D_+}

(c) E_{U_-} (d) E_{D_-}

Figure 9.11: Energy for providing ancillary services (E_{U_+}, E_{D_+}) or opposing the SG requests (E_{U_+}, E_{D_+}), under RE production.

Effect of system dimensioning

Fig. 9.12 reports P_{U_+} for the case in which RE is produced and WO is active, both without and under RoD, for increasing S_{PV} and different battery sizes B. P_{U_+} tends to decrease as S_{PV} grows larger, but the reduction rate is smaller for larger panels. Larger B provide lower P_{U_+} for fixed S_{PV}, except for very small S_{PV}, for which a smaller B=5 kWh provides similar (under RoD) or even lower (under no RoD) P_{U_+} with respect to B=10 kWh. Fig. 9.13 shows P_{D_+} for the case in which RE is produced and WO is active, both without and under RoD, for increasing

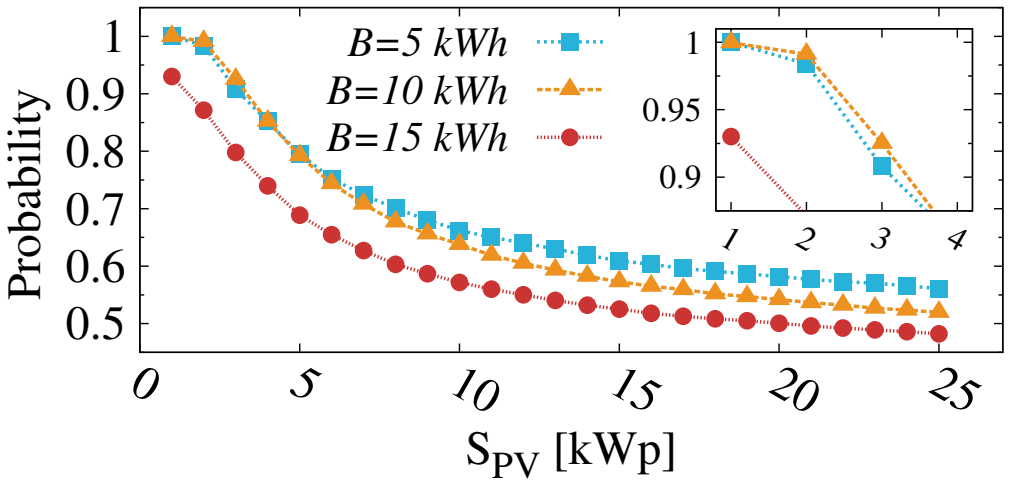

(a) P_{U_+}, RoD off

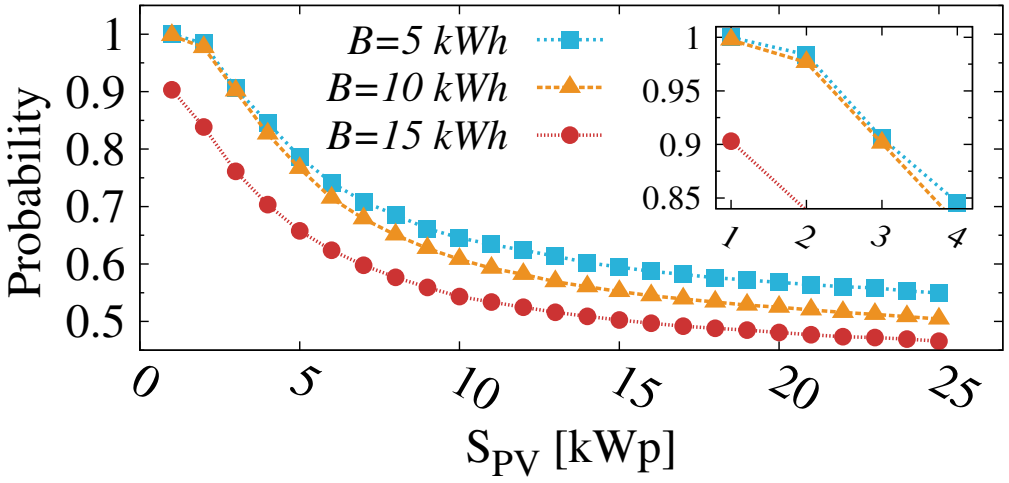

(b) P_{U_+}, RoD on

Figure 9.12: P_{U_+} versus S_{PV}, for different values of B, with WiFi offloading, in the scenarios without and under RoD.

S_{PV} and different battery sizes B. In this case, the impact of S_{PV} is limited, since P_{D_+} only slightly increases as S_{PV} grows larger. Conversely, B=5-10 kWh provide P_{D_+} above 95% under any scenario, while a larger B=15 kWh reduces by up to 17 percentage points the value of P_{D_+}, with lowest value observed when RoD is active.

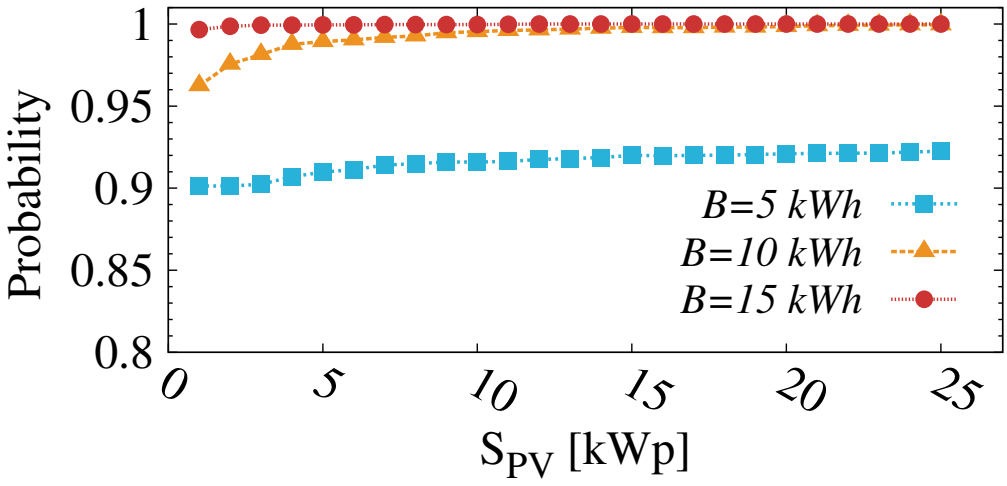

(a) P_{D_+}, RoD off

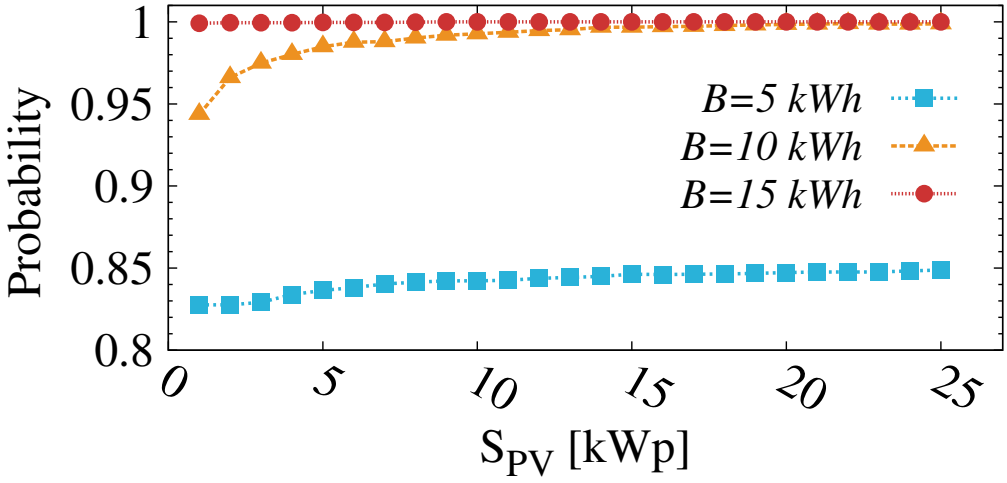

(b) P_{D_+}, RoD on

Figure 9.13: P_{D_+} versus S_{PV}, for different values of B, with WiFi offloading, in the scenarios without and under RoD off.

9.2.3 Remarks about WiFi offloading in a Demand Response framework

In this study we assume that neighbor APs provide capacity for a fraction of the mobile traffic transferred from the cellular access network in case of requests of type DOWN. As better described at the beginning of Sec. 9.2, these APs makes up a sort of virtual WiFi network that is available to accept part of the traffic from the BSs under specific conditions, based on some kind of agreement established in advance with the Mobile Operator, from which the WiFi network owners receive

some kind of reward to compensate their availability to handle additional traffic load coming from the close-by mobile network. This may raise some issues both in terms of global energy balance and Quality of Service.
In relation to the energy balance, this study does not explicitly evaluate the potential increase in energy consumption that may be experienced by the WiFi network due to the additional traffic periodically handled by the APs. Nevertheless, some considerations can be done to this extent. First, it is to be noted that the power consumption of an AP is by far lower than the power needed to operate a BS. Even in the case of a micro BS, an AP consumes an amount of energy that is more than one order of magnitude lower than the BS. Furthermore, the AP consumption is very little traffic proportional. Moreover, it can be observed that the amount of traffic that is transferred is limited to a maximum of only 10% of the traffic carried by the micro BSs, and that the WiFi offloading operation is further limited by the fact that it is active only when requests of type DOWN are issued. Hence, considering that the APs are assumed to be always active regardless the current traffic demand, these constraints lead to an increase in the WiFi network energy consumption, due to the additional traffic transferred from the mobile network, that is actually very limited. We expect that the raise in the WiFi network energy consumption due to the periodic migration of a small fraction of the mobile traffic can likely be neglected with respect to the the energy saving that can be obtained on the mobile side, also in view not only of the rewards that the WiFi network owners receive from the Mobile Operator based on the established agreement, but also in view of the huge cost saving that can be obtained by the Mobile Operator. Finally, the objective of our work in this case is anyways focused on achieving operational cost reduction rather than on decreasing the overall energy consumption. Indeed, according to our results, cost savings higher than 100% can be achieved, against a reduction of just less than 50% of the energy drawn from the grid in specific scenarios. Anyways, further study will be planned as future work to better investigate the actual impact of the energy consumption increase of the neighbor APs, due to the application of WiFi offloading techniques, on the overall energy efficiency balance.
Regarding the Quality of Service in terms of available bandwidth, further investigation is needed to evaluate whether a minimum bandwidth constraint can always be guaranteed for both mobile users, whose traffic is moved from the BSs to neighbor APs, and WiFi network users. However, it should be observed that in our work the application of WiFi offloading is assumed to be only permitted when the traffic handled by the APs is sufficiently low, so that there is capacity available for minimum bandwidth guarantee. This results, according to the data from the literature, in transferring at most 10% of the peak traffic handled by the micro BSs. Finally, since the mobile traffic is transferred in a limited amount and only in case of DOWN, the potential reduction in the minimum available bandwidth, if any, is anyways limited in intensity and in time duration, allowing to be rather

conservative in terms of Quality of Service. However, future study will focus on the evaluation of Quality of Service, in order to investigate more accurately whether the constraint on the minimum bandwidth required to guarantee to mobile users the same quality of experience encountered under the mobile network can be respected even when their traffic is moved to neighbor APs. Furthermore, it might be helpful focusing on the type of traffic that may be transferred to neighbor APs, in order to investigate whether transferring only data traffic that is delay tolerant, and keeping for example the video streaming traffic managed by the BSs, may provide some benefit to this extent, achieving a better trade off between Quality of Service and operational cost reduction.

9.3 Considerations on cost

Clearly, in case of RE production, additional capital expenditures (CAPEX) should be considered besides operational cost, due to the installation of the PV panels and the set of batteries. However, although the initial expenditure might be considerable, based on our results derived for several combinations of S_{PV} and B, it would be possible to select the proper dimensioning allowing to reduce (and possibly minimize) the CAPEX+OPEX, taking into account the PV panel and battery lifetime duration, as shown in Sec. 8.3. Furthermore, according to [85], after 8 years of RE powered mobile network operation the break-even point for CAPEX cost can be achieved. In addition, the introduction of a new energy management strategy could be envisioned, allowing to sell back to the SGO extra amounts of RE that are not immediately used and, in case they cannot be harvested in the storage, are usually wasted. Assuming that the price per each energy unit that is sold back to the grid is half the price due for each energy unit bought by the mobile network operator from the grid, i.e. p_G, cost savings result remarkably high when extra produced RE can be sold back to the grid. To this extent, relevant results (not reported) are available confirming the potential additional revenues obtained from the selling of extra energy to the SG, although they were derived by investigating the same scenario under different settings, i.e. assuming a different location (Sydney, Australia), using real traces of energy prices (provided by the local electricity supplier) to derive the sequence of the SG requests, and adopting a different energy management strategy that envisions, besides the selling of extra amounts of energy to the SG, the application of both RoD and/or WiFi offloading only in case of requests of type DOWN. Under these settings, the overall cost saving results more than twice the energy bill registered in case no RE is present (hence no energy can be sold back to the SG) and no WO or RoD strategies are applied. Indeed, up to 223% cost saving can be achieved by applying WO in conjunction with RoD. However, in relative terms, WO and RoD are equally effective in raising the cost saving, since, when applied alone, they both provide savings that are about

1.8 fold higher those assured with the standard energy management strategy. These revenues may play a relevant role in compensating the higher CAPEX faced for the initial installation of a RE generation system.

Chapter 10

Conclusion

The staggering increase of the mobile traffic is currently leading to huge operational costs for Mobile Network Operators due to power supply. The integration of locally produced renewable energy sources into power supply systems of cellular access networks is needed for cost reduction purposes and for improving the energy self-sufficiency of mobile access networks. The contribution of this thesis consists in investigating various critical issues raised by the introduction of photovoltaic (PV) panels to power the BSs and to enhance the interaction with the Smart Grid, with the main objectives of making the mobile access network more independent from the grid and reducing the energy bill.

When PV panels are employed to power mobile networks, simple and reliable Renewable Energy (RE) production models are needed to facilitate the system design and dimensioning, also in view of the intermittent nature of renewable energy production. A simple stochastic model was proposed where RE production is represented by a shape function multiplied by a random variable, characterized by a mean value and a variance. This random variable characteristics depend on the sun irradiation of the considered location. Our results show that the model is representative of RE production in locations with low intra-day weather variability. Indeed, when considering different distributions of daily production with the same mean and variance, very limited differences can be observed. Simulations revealed also the relevance of RE production variability: for fixed mean production, higher values of the variance imply a reduced BS self-sufficiency and larger PV panels are hence required to move to a sufficient RE production regime.

Moreover, properly designed models are required to accurately represent the complex operation of a mobile access network powered by renewables and equipped with some storage, where electric loads vary with the traffic demand, and some interaction with the Smart Grid can be envisioned. As Markovian models are often adopted to analyze the operation of green mobile networks, in this work various stochastic models based on discrete time Markov chains are designed, featuring different characteristics, which depend on the various aspects of the system operation

they aim to examine. However, the selection of variable discretization settings of the parameters defined in similar models have the potential of highly affecting the evaluation of the system performance when the model is applied to investigate the green mobile network operation. Hence, we also focused on the analysis of the effects of quantization in the analytical models that are used to dimension the power system of solar-powered off-grid base stations. Quantization was investigated for the three main model parameters: time, weather, and energy storage. That is, we discussed the size of the time slot according to which the discrete-time model evolves, the number of levels that are used to describe the weather conditions, and the quantum of energy that is considered when looking at the system batteries. Our study unveiled the critical role of quantization for a correct power system dimensioning. Our main findings can be summarized by saying that a credible and accurate model requires: i) a time granularity that allows capturing the energy production and consumption fluctuations *during* the day, and our experiments indicate that a time slot equal to 1 h can be a reasonable choice; ii) the discretization of the weather conditions according to an equal-probability quantization, using 5 or 7 levels of average daily solar irradiance; iii) a storage energy quantum of the order of 1/5 of the minimum energy consumption per time slot.

In addition, we presented numerical results showing how different traffic profiles impact the amount of consumed/stored energy. Our results showed that differences between the curves for residential and business traffic profiles are marginal for both analyzed cases of Turin and Paris. However, quantitative differences between different PV panel sizes are more pronounced in the case of Paris than for Turin. Moreover, we discussed the impact on the use of renewable energy sources of the technological evolution of base stations, with new product generations that are more parsimonious and more load proportional in energy consumption. Our analysis showed that it is possible to achieve a better performance, with half the solar panel size, with the coming generations of base station technology.

Our work helps understanding how the correct design of solar power systems for off-grid base stations should be approached. In addition, it shows that the solar option is becoming extremely attractive to power new generations of base stations. If the promised improvements in solar cell technologies will materialize soon, bringing efficiency from the current 20% to about 50%, in the coming years the solar option will become the default solution to power base stations in many geographical areas. Clearly, the introduction of RE to power mobile networks entails a proper system dimensioning, in order to balance the solar energy intermittent production, the traffic demand variability and the need for service continuity. In relation to the system dimensioning process in real scenarios, approaches available in the literature typically address the dimensioning issue proposing simulation or optimization methods. However, the dimensioning of a renewable generation system to power BSs by means of simulations or optimization models may be computationally complex and require long computational time. In this study, we proposed a simple

analytical formula for properly sizing a renewable system in a green mobile network, based on the local RE production average profile and variability, in order to guarantee the satisfaction of a given constraint on the maximum allowed storage depletion probability.
Moreover, in a green mobile network scenario, Mobile Operators are encouraged to deploy strategies allowing to further increase the energy efficiency and reduce costs. In the context of RE powered cellular networks, the application of resource management, consisting in BS switching on and off based on demand, shows to be very promising to improve energy efficiency and system feasibility, to reduce costs, both operational and capital expenditure. Overall, this seems a promising way to mobile network self-sustainability. To this extent, we have considered a cluster of BSs powered with a renewable based powering system composed of PV panels and energy storage units. In particular, the results of our simulations show that up to almost 40% of energy can be saved when RoD is applied under proper configuration settings, with a higher impact observed in traffic scenarios in which there is a better match between communication service demand and RE production. While a feasible PV panel and storage dimensioning can be achieved only with high costs and large powering systems, by slightly relaxing the constraint on self-sustainability it is possible to significantly reduce the size of the required PV panels, up to 41.3%, along with a reduction in the corresponding CAPEX and OPEX. The combination of smart resource management of the communication system with new technologies, both for the communication devices and the power supply, is hence opening the way to self-sustainability of mobile access networks, a strategic important goal for the sustainability of future networks.
Finally, the introduction of RE in mobile networks contributes to give Mobile Operators the opportunity of becoming prominent stakeholders in the Smart Grid environment. Indeed, the increasing penetration of the Smart Grid paradigm has deeply changed the energy market, with Demand Response approaches extensively deployed by utility operators to better match the energy demand and the supply. In this context, Mobile Operators may play a relevant role, by making the mobile access network actively interact with the SG and dynamically modulate its energy consumption in accordance with SGO requests. In this study, we investigated a scenario in which a green mobile network is integrated in a Smart Grid. The mobile network implements some Resource on Demand strategy (consisting in properly operating the BSs) to adapt its electric load to smart grid requests. The scenario is investigated through a Markovian model whose parameters are set based on real data about smart grid requests and about the traffic, and realistic simulation of the energy that is generated by solar panels. Our results show that energy management policies adopted in RE-powered mobile access networks to respond to the SG requests are highly effective in reducing the operational cost, that may decrease by up to more than 100% under proper setting of operational parameters. Furthermore, the application of Resource on Demand strategies significantly increases the gain in

terms of operational cost, erasing operational expenditure and even obtaining some revenues, especially where the traffic patterns show longer periods with low traffic loads, during which the radio resources are under-utilized. Moreover, our results show that the stochastic model proposed to represent the system operation could be useful during the decisional process of PV panels and storage dimensioning.
In addition, this work investigated the impact of WiFi Offloading in improving the interaction of a mobile access network with the SG in a Demand Response context, either when WO is applied alone or jointly with a RoD strategy, and considering also the case in which a RE source is locally available to power the BSs. Results suggest that in a Demand Response framework WiFi offloading can be very effective in enhancing the capability of mobile networks to provide ancillary services to the SG operator and reducing the energy bill for the MNO. WO enhances the ancillary service provisioning, even when no RE production is locally available, being capable of raising the probability of accomplishing D requests from the SG, P_{D_+}, up to 74.7% in our scenario. RoD provides only half the benefits obtained under WO, whereas it does not improve P_{D_+} when applied on the top of WO. The introduction of a local RE generation system combined with some storage remarkably improves the probability of providing ancillary services, that results always above 70% both in case of U and D requests even for intermediate system dimensioning in the scenario investigated in our study. Under larger RE systems, the probability to positively react to requests of consumption decrease becomes close to 1, whereas P_{U_+} is decreased and no significant differences are observed between the various combinations of WO and RoD strategies application.
The fact that the migration of a small fraction of the mobile traffic is assumed to occur only when the WiFi network is low loaded, and only when the request of type DOWN are issued, allows to be rather conservative in terms of Quality of Service degradation. Nevertheless, future work is still required to further investigate Quality of Service aspects. Moreover, future research efforts should focus on better quantifying the increase of the energy consumption of the WiFi network due to the traffic migration to neighbor APs. However, since APs consumption results at least one order of magnitude lower with respect to BSs, and it is very little traffic proportional, we expect that the raise in the WiFi network energy consumption due to the periodic migration of a small fraction of the mobile traffic can be negligible with respect not only to the energy saving that can be obtained on the mobile side, but also in terms of the huge cost saving that can be obtained. Indeed, besides being beneficial for providing ancillary services, WO is effective in giving a relevant contribution in cost reduction. When no RE is available, WO alone allows to achieve cost savings that are twofold those obtained under RoD only. The presence of a RE generation system allows to achieve remarkably higher cost saving. Although PV panel and system sizes do not seem to significantly affect the probability of providing ancillary services, they show a huge impact on cost savings. Even with relatively small PV panel and storage dimension, the energy bill can be completely

nullified, whereas under larger RE system size positive revenues can be achieved. The contribution of RE is dominant with respect to WO and RoD, although RoD slightly outperforms WO in reducing the energy bill, especially with intermediate rather than larger system size.
Furthermore, our results show that, in a Demand Response context, the use of RE and a properly designed energy management strategy allows to achieve relevant cost savings even without producing remarkable reduction in the energy drawn from the grid. A reduction of less than 50% in the energy drawn from the grid may correspond to cost saving higher than 100%, resulting in positive revenues, and confirming that a good (in terms of energy bill reduction) energy management strategy does not operate by reducing the total grid consumption, but rather by timely increasing or decreasing the grid consumption exactly when required by the SG. Hence, energy saving strategies like WO and RoD can be effectively applied just for accomplishing D requests from the SG rather than with the purpose of reducing the network energy consumption, still achieving relevant cost reduction. Finally, by envisioning the possibility of selling back to the SG the extra produced RE, cost saving becomes more than twice the energy bill that is paid when no RE is locally available and no WO or RoD strategies are applied. These revenues may contribute to compensate for the CAPEX faced by Mobile Network Operators for the installation of RE generation systems.

Concluding, this work shows that the introduction of RE sources is an effective solution to power mobile networks, and our results prove that a slight relaxation of the constraints on the network self-sustainability allows to deploy feasible RE generation systems at a very reduced cost. Furthermore, the obtained results provide evidence that the application of Resource on Demand techniques in a green mobile network context highly contributes not only to further decrease the operational expenditures, but also to limit the initial investment, by making smaller sized RE generators sufficient for the normal network operation. Finally, this thesis demonstrates that the use of RE to power BSs opens the way to new interesting scenarios, where Mobile Network Operators can profitably interact with the Smart Grid to obtain mutual benefits. Clearly, this interaction definitely requires the integration of suitable energy management strategies into the communication infrastructure management.
The topics of mobile networks powered by renewables and their integration in the Smart Grid as active participants in Demand Response programs will definitely steer further research efforts in the years to come. Indeed, in the next future, the role of renewable energy powering mobile networks is bound to become even more relevant, also considering the imminent deployment and marketing of more efficient PV panels, and especially in view of the shift towards 5G mobile networks, envisioning extremely higher data rates. At the same time, the 5G technology that is widely spreading in mobile networks, entailing the virtualization of the BSs and

leading to Cloud Radio Access Networks (C-RANs), where few centralized processing units manage several distributed physical radio access points, will pose new challenges to this extent. Furthermore, the application of Resource on Demand strategies will have to be adapted to new 5G scenarios, where new constraints will come up. For instance, with the introduction of mobile edge caching and computing in the forthcoming 5G networks, the BSs will provide also caching/computing service, hence it will no longer be possible to apply BS on/off switching strategies only based on the traffic demand. Also, C-RANs will raise load balancing issues and entail the need for dynamic mapping between centralized virtual BBUs and distributed RRH units, therefore these aspects should be considered when designing RoD policies. To this aim, the deployment of machine learning techniques could be useful to predict the mobility and the distribution of mobile users. In relation to the remarkable role that MNOs can play in the SG environment, in the next years the Demand Response paradigm will tend to move towards even more dynamic grid energy markets, where real-time energy pricing policies are implemented. In a similar scenario, new targeted energy management strategies need to be designed for green mobile networks and machine learning techniques will become essential to investigate the complex interaction between multiple factors leading to the energy price variability, in order to deploy effective energy management policies allowing MNOs to optimize their cost saving and revenues. Furthermore, the extensive penetration of cloud computing techniques and the Software Define Networking paradigm in communication networks will enforce the capability of providing online learning techniques that operate in real-time, allowing to increase the accuracy in predicting both the users' demand and the energy prices, and to promptly and timely react by taking efficient decisions in terms of energy management and network configuring.

Appendix A

Notation

Table A.1: Notation of the main variables and performance parameters

m	Number of micro BSs providing additional capacity in an area covered by a macro Base Station
ρ_M, ρ_i	Traffic load of the macro Base Station and of the micro Base Station i, respectively
ρ_{min}	Threshold of minimum traffic load below which a micro Base Station can be turned off
S_{PV}	Nominal capacity of photovoltaic panels [W_p]
B	Nominal storage capacity of the set of lead-acid batteries [Wh]
DOD	Depth of Discharge of the battery [%]
C_B	Actual storage capacity of the set of lead-acid batteries taking into account the constraint on the maximum allowed Depth of Discharge
S_B	Number of elementary units of lead-acid batteries that build up the storage
RE_p	Discrete random variable representing the renewable power production [W] at peak time, for a unitary PV panel (S_{PV}=1 kWp)
M	Peak renewable power production [W] for a photovoltaic panel of capacity S_{PV}
RE_d	Discrete random variable representing the daily total amount of renewable energy production [kWh] for a unitary PV panel (S_{PV}=1 kWp)
RE_D	Total amount of renewable energy that is produced during daytime with a photovoltaic panel of capacity S_{PV}
CV	Coefficient of Variation of the daily renewable energy production RE_d
D_d, D_n	Energy demand during the daytime and during the night, respectively, for a single Base Station
E_c	Energy needed for the BS cluster operation during a time slot
S	Storage level
Q_S	Quantization step adopted to discretize the produced, consumed and harvested energy
N_S	Number of energy quantization steps in which the storage capacity is discretized
N_W	Number of day-types based on the daily weather conditions and on the average level of daily Renewable Energy production
W_i	i^{th} day-type (of N_W day-types) based on the daily weather conditions and on the average level of daily Renewable Energy production
ΔT	Duration of each of the time slots in which the time is discretized
N_T	Number of time slots of duration ΔT in a day
B_O	Average daily battery occupancy
Q_{90}	90^{th} percentile of battery occupancy
P_D	Storage depletion probability
P_L	Probability of low storage level such that the mobile network demand cannot be satisfied in the considered time slot
P_f	Full battery probability
G	Average daily grid energy demand of the mobile access network
E_G	Total energy demand from the Smart Grid over one year of the mobile access network
E_W	Total amount of renewable energy wasted over one year
f_G	Frequency of energy requests from the Smart Grid over one year, measured considering the time granularity of half an hour that is used in the simulator
$F_{G_{max}}$	Constraint representing the target value of maximum allowed f_G
f_W	Frequency of wasting the produced renewable energy that is neither immediately used nor stored in the battery
W_f	Probability of wasting renewable energy in a unitary time slot
$U_{RE_D}(x)$, $U_{RE_d}(x)$	Probability density function of the random variables RE_D and RE_d, respectively, having a uniform distribution
RE_{min}	Minimum possible value of daily renewable energy production per 1 kWp PV panel capacity
RE_{max}	Maximum possible value of daily renewable energy production per 1 kWp PV panel capacity
UP (U)	Smart Grid request of increasing the consumption with respect to forecast demand
DOWN (D)	Smart Grid request of decreasing the consumption with respect to forecast demand
NULL (N)	Smart Grid request with no special action required
P_{U_+}, P_{D_+}	Probability of accomplishing requests from the Smart Grid, i.e. providing ancillary services, in case of UP and DOWN requests, respectively
E_{U_+}, ED_+	Energy amounts traded for providing ancillary services in case of UP and DOWN requests (E_{U_+} and E_{D_+}, respectively), corresponding to the increase or decrease, respectively, of the grid energy consumption with respect to the forecast need
E_{U_-}, E_{D_-}	Energy amounts opposing the SG requests in case of UP and DOWN requests (E_{U_-} and E_{D_-}, respectively), corresponding to the decrease or increase, respectively, of the grid energy consumption with respect to the forecast need
p_E	Average price per unit of energy drawn from the grid [€/MWh]
r_U, r_D	Monetary reward per unit of energy traded to provide ancillary services in case of UP and DOWN request, respectively [€/MWh]

Appendix B

List of acronyms

- AP - Access Point
- AS - Ancillary Service
- BB - BaseBand
- BS - Base Station
- CAPEX - Capital Expenditure
- DOD - Depth of Discharge
- DR - Demand Response
- DTMC - Discrete Time Markov Chain
- ISP - Internet Service Provider
- LTE - Long-Term Evolution
- MNO - Mobile Network Operator
- OPEX - Operational Expenditure
- PA - Power Amplifier
- PV - Photovoltaic
- QoS - Quality of Service
- RE - Renewable Energy
- RoD - Resource on Demand
- RRU - Remote Radio Unit

- SG - Smart Grid
- SGO - Smart Grid Operator
- TMY - Typical Meteorological Year
- WO - WiFi Offloading

Appendix C

List of co-authored publications

Journal publications

- H. A. H. Hassan et al. “A Novel Energy Model for Future Cellular Networks in Smart Grid and Renewable Energy Environment”. In: *IEEE Transactions on Green Communications and Networking* (2018) - *Under review*
- D. Renga and M. Meo. “Dimensioning renewable energy systems to power Mobile Networks”. In: *IEEE Transactions on Green Communications and Networking* (2018) - *Under review*
- D. Renga et al. “Energy management and Base Station on/off switching in green mobile networks for offering Ancillary Services”. In: *IEEE Transactions on Green Communications and Networking* (2018), pp. 1–1
- A. P. Couto da Silva et al. “The Impact of Quantization on the Design of Solar Power Systems for Cellular Base Stations”. In: *IEEE Transactions on Green Communications and Networking* 2.1 (Mar. 2018), pp. 260–274
- M. Deruyck et al. “Accounting for the Varying Supply of Solar Energy When Designing Wireless Access Networks”. In: *IEEE Transactions on Green Communications and Networking* 2.1 (Mar. 2018), pp. 275–290
- M. Dalmasso, M. Meo, and D. Renga. “Radio resource management for improving energy self-sufficiency of green mobile networks”. In: *Performance Evaluation Review*. Vol. 44. 2. Sept. 2016, pp. 82–87
- F. G. Debele et al. “Designing Resource-on-Demand Strategies for Dense WLANs”. In: *IEEE Journal on Selected Areas in Communications* 33.12 (Dec. 2015), pp. 2494–2509

Book chapters

- M. Ali, M. Meo, and D. Renga. "Cost saving and ancillary service provisioning in green Mobile Networks". In: *The Internet of Things for Smart Urban Ecosystems (IoT4SUE)*. ed. by Springer. 2018

Conference publications

- D. Renga and M. Meo. "From self-sustainable Green Mobile Networks to enhanced interaction with the Smart Grid". In: *2018 International Teletraffic Congress (ITC 30)*. 2018 - *Under review*

- M. Meo, D. Renga, and M. T. Sarti. "Household users' cooperation to reduce cost in green mobile networks". In: *2018 International Telecommunications Energy Conference (INTELEC)*. 2018 - *Under review*

- M. Ajmone Marsan et al. "Sharing Renewable Energy in a Network Sharing Context". In: *2018 IEEE Wireless Communication and Networking Conference (WCNC)* PP.99 (Apr. 2018), pp. 1–1

- D. Renga. "Greener and cheaper mobile communication: let the sunshine in". In: *2018 IEEE Wireless Communication and Networking Conference (WCNC)* PP.99 (Apr. 2018), pp. 1–1. Finalist at the *Three Minute Thesis (3MT) Competition*

- D. Renga et al. "Improving the interaction of a green mobile network with the smart grid". In: *2017 IEEE International Conference on Communications (ICC)*. May 2017, pp. 1–7

- M. Ali, M. Meo, and D. Renga. "WiFi offloading for enhanced interaction with the Smart Grid in green mobile networks". In: *2017 IEEE 14th International Conference on Networking, Sensing and Control (ICNSC)*. May 2017, pp. 233–238

- D. Renga and M. Meo. "Modeling renewable energy production for base stations power supply". In: *2016 IEEE International Conference on Smart Grid Communications (SmartGridComm)*. Nov. 2016, pp. 716–722

- M. Deruyck et al. "Reducing the impact of solar energy shortages on the wireless access network powered by a PV panel system and the power grid". In: *2016 IEEE 27th Annual IEEE International Symposium on Personal, Indoor and Mobile Radio Communications - (PIMRC): Mobile and Wireless Networks, Valencia, Spain*. Sept. 2016

Bibliography

[1] M. Ajmone Marsan et al. “Sharing Renewable Energy in a Network Sharing Context”. In: *2018 IEEE Wireless Communication and Networking Conference (WCNC)* PP.99 (Apr. 2018), pp. 1–1.

[2] H. Al Haj Hassan, L. Nuaymi, and A. Pelov. “Renewable energy in cellular networks: a survey”. In: *ONLINEGREENCOMM 2013 : IEEE Online Conference on Green Communications*. 2013, pp. 1–7.

[3] M. Ali, M. Meo, and D. Renga. “Cost saving and ancillary service provisioning in green Mobile Networks”. In: *The Internet of Things for Smart Urban Ecosystems (IoT4SUE)*. Ed. by Springer. 2018.

[4] M. Ali, M. Meo, and D. Renga. “WiFi offloading for enhanced interaction with the Smart Grid in green mobile networks”. In: *2017 IEEE 14th International Conference on Networking, Sensing and Control (ICNSC)*. May 2017, pp. 233–238.

[5] M. Ali, M. Meo, and D. Renga. “WiFi offloading for enhanced interaction with theSmart Grid in green mobile networks”. In: *2017 IEEE International Conference on Networking, Sensing and Control (ICNSC), Calabria, Southern Italy*. May 2017.

[6] Mohammed H. Alsharif, Jeong Kim, and Jin Hong Kim. “Green and Sustainable Cellular Base Stations: An Overview and Future Research Directions”. In: *Energies* 10.5 (2017).

[7] W. N. S. F. W. Ariffin, X. Zhang, and M. R. Nakhai. “Real-time energy trading with grid in green cloud-RAN”. In: *2015 IEEE 26th Annual International Symposium on Personal, Indoor, and Mobile Radio Communications (PIMRC)*. Aug. 2015, pp. 748–752.

[8] Asma Mohamad Aris and Bahman Shabani. “Sustainable Power Supply Solutions for Off-Grid Base Stations”. In: *Energies* 8.10 (2015), pp. 10904–10941.

[9] E. Arriagada et al. “A stochastic economic dispatch model with renewable energies considering demand and generation uncertainties”. In: *PowerTech (POWERTECH), 2013 IEEE Grenoble*. June 2013, pp. 1–6.

[10] Yarhands Dissou Arthur, Kwasi Baah Gyamfi, and SK Appiah. "Probability distributional analysis of hourly solar irradiation in Kumasi-Ghana". In: *International Journal of Business and Social Research* 3.3 (2013), pp. 63–75.

[11] Gunther Auer et al. "How much energy is needed to run a wireless network?" In: *IEEE Wireless Commun.* 18.5 (2011), pp. 40–49.

[12] G. Auer et al. "Energy efficiency analysis of the reference systems, areas of improvements and target breakdown Energy Aware Radio and neTwork tecHnologies (EARTH) project". In: ed. by Muhammad Ali Imran and Efstathios Katranaras (UNIS). 2012 (2010).

[13] R. J. Bessa, A. Trindade, and V. Miranda. "Spatial-Temporal Solar Power Forecasting for Smart Grids". In: *IEEE Transactions on Industrial Informatics* 11.1 (Feb. 2015), pp. 232–241.

[14] Filip Louagie Bjorn Debaillie Claude Desset. "A Flexible and Future-Proof Power Model for Cellular Base Stations". In: *81st IEEE Vehicular Technology Conference*. IEEE, 2015.

[15] Ł. Budzisz et al. "Dynamic Resource Provisioning for Energy Efficiency in Wireless Access Networks: A Survey and an Outlook". In: *IEEE Communications Surveys Tutorials* 16.4 (Fourthquarter 2014), pp. 2259–2285.

[16] Eyuphan Bulut and Boleslaw K. Szymanski. "WiFi Access Point Deployment for Efficient Mobile Data Offloading". In: *Proceedings of the First ACM International Workshop on Practical Issues and Applications in Next Generation Wireless Networks*. PINGEN '12. Istanbul, Turkey: ACM, 2012, pp. 45–50.

[17] S. Buzzi et al. "A Survey of Energy-Efficient Techniques for 5G Networks and Challenges Ahead". In: *IEEE Journal on Selected Areas in Communications* 34.4 (Apr. 2016), pp. 697–709.

[18] V. Chamola and Sikdar B. "Resource provisioning and dimensioning for solar powered cellular base stations". In: *Global Communications Conference (GLOBECOM), 2014 IEEE*. Dec. 2014, pp. 2498–2503.

[19] V. Chamola and B. Sikdar. "A Multistate Markov Model for Dimensioning Solar Powered Cellular Base Stations". In: *IEEE Transactions on Sustainable Energy* 6.4 (Oct. 2015), pp. 1650–1652.

[20] V. Chamola and B. Sikdar. "Dimensioning stand-alone cellular base station using series-of-worst-months meteorological data". In: *Communication Systems (ICCS), 2014 IEEE International Conference on*. Nov. 2014, pp. 339–343.

[21] V. Chamola and B. Sikdar. "Outage estimation for solar powered cellular base stations". In: *Communications (ICC), 2015 IEEE International Conference on*. June 2015, pp. 172–177.

[22] V. Chamola and B. Sikdar. "Outage estimation for solar powered cellular base stations". In: *2015 IEEE International Conference on Communications (ICC)*. June 2015, pp. 172–177.

[23] V. Chamola and B. Sikdar. "Solar powered cellular base stations: current scenario, issues and proposed solutions". In: *IEEE Communications Magazine* 54.5 (May 2016), pp. 108–114.

[24] Vinay Chamola and Biplab Sikdar. "Dimensioning stand-alone cellular base station using series-of-worst-months meteorological data". In: *ICCS*. IEEE, 2014, pp. 339–343.

[25] Vinay Chamola and Biplab Sikdar. "Outage estimation for solar powered cellular base stations". In: *ICC*. IEEE, 2015, pp. 172–177.

[26] Vinay Chamola and Biplab Sikdar. "Resource provisioning and dimensioning for solar powered cellular base stations". In: *GLOBECOM*. IEEE, 2014, pp. 2498–2503.

[27] Vinay Chamola and Biplab Sikdar. "Solar powered cellular base stations: current scenario, issues and proposed solutions". In: *IEEE Communications Magazine* 54.5 (2016), pp. 108–114.

[28] Tian Pau Chang et al. "Investigation on frequency distribution of global radiation using different probability density functions". In: *International Journal of Applied Science and Engineering 8 (2)* (2010), pp. 99–107.

[29] Y. L. Che, L. Duan, and R. Zhang. "Dynamic Base Station Operation in Large-Scale Green Cellular Networks". In: *IEEE Journal on Selected Areas in Communications* 34.12 (Dec. 2016), pp. 3127–3141.

[30] L. Ciabattoni et al. "On line solar irradiation forecasting by minimal resource allocating networks". In: *2012 20th Mediterranean Conference on Control Automation (MED)*. July 2012.

[31] Cisco. In: *Cisco Visual Networking Index: Global Mobile Data Traffic Forecast Update, 2016-2021 White Paper*. Feb. 2017. URL: http://www.cisco.com/c/en/us/solutions/collateral/service-provider/visual-networking-index-vni/mobile-white-paper-c11-520862.html.

[32] A. P. Couto da Silva et al. "The Impact of Quantization on the Design of Solar Power Systems for Cellular Base Stations". In: *IEEE Transactions on Green Communications and Networking* 2.1 (Mar. 2018), pp. 260–274.

[33] M. Dalmasso, M. Meo, and D. Renga. "Radio resource management for improving energy self-sufficiency of green mobile networks". In: *Performance Evaluation Review*. Vol. 44. 2. Sept. 2016, pp. 82–87.

[34] F. G. Debele et al. "Designing Resource-on-Demand Strategies for Dense WLANs". In: *IEEE Journal on Selected Areas in Communications* 33.12 (Dec. 2015), pp. 2494–2509.

[35] M. Deruyck et al. "Accounting for the Varying Supply of Solar Energy When Designing Wireless Access Networks". In: *IEEE Transactions on Green Communications and Networking* 2.1 (Mar. 2018), pp. 275–290.

[36] M. Deruyck et al. "Reducing the impact of solar energy shortages on the wireless access network powered by a PV panel system and the power grid". In: *2016 IEEE 27th Annual IEEE International Symposium on Personal, Indoor and Mobile Radio Communications - (PIMRC): Mobile and Wireless Networks, Valencia, Spain*. Sept. 2016.

[37] A. P. Dobos. *PVWatts Version 5 Manual*. Sept. 2014.

[38] EARTH (Energy Aware Radio and network technologies) project. *Energy efficiency analysis of the reference systems, areas of improvements and target breakdown*. 2012.

[39] F Youcef Ettoumi et al. "Statistical analysis of solar measurements in Algeria using beta distributions". In: *Renewable Energy* 26.1 (2002), pp. 47–67.

[40] M. J. Farooq, H. Ghazzai, and A. Kadri. "A stochastic geometry-based demand response management framework for cellular networks powered by smart grid". In: *2016 IEEE Wireless Communications and Networking Conference*. Apr. 2016, pp. 1–6.

[41] M. J. Farooq et al. "A Hybrid Energy Sharing Framework for Green Cellular Networks". In: *IEEE Transactions on Communications* 65.2 (Feb. 2017), pp. 918–934.

[42] S. A. Fatemi and A. Kuh. "Solar radiation forecasting using zenith angle". In: *2013 IEEE Global Conference on Signal and Information Processing*. Dec. 2013, pp. 523–526.

[43] *Fraunhofer ISE: Photovoltaics Report*. https://www.ise.fraunhofer.de/en/downloads-englisch/pdf-files-englisch/photovoltaics-report-slides.pdf. 2015-11-17.

[44] H. Gharavi and R. Ghafurian. "IEEE Recommended Practice for Sizing Lead-Acid Batteries for Stand-Alone Photovoltaic (PV) Systems IEEE Std 1013-2007". In: *Proceedings IEEE*. Vol. 99. 6. 2011, pp. 917–921.

[45] H. Ghazzai and A. Kadri. "Joint Demand-Side Management in Smart Grid for Green Collaborative Mobile Operators under Dynamic Pricing and Fairness Setup". In: *IEEE Transactions on Green Communications and Networking* PP.99 (2017), pp. 1–1.

[46] H. Ghazzai, E. Yaacoub, and M. S. Alouini. "Multi-Operator Collaboration for Green Cellular Networks under Roaming Price Consideration". In: *2014 IEEE 80th Vehicular Technology Conference (VTC2014-Fall)*. Sept. 2014, pp. 1–5.

[47] H. Ghazzai et al. "Green Networking in Cellular HetNets: A Unified Radio Resource Management Framework with Base Station ON/OFF Switching". In: *IEEE Transactions on Vehicular Technology* PP.99 (2016), pp. 1–1.

[48] H. Ghazzai et al. "Optimized green operation of LTE networks in the presence of multiple electricity providers". In: *2012 IEEE Globecom Workshops*. Dec. 2012, pp. 664–669.

[49] Y. Ghiassi-Farrokhfal et al. "Joint Optimal Design and Operation of Hybrid Energy Storage Systems". In: *IEEE Journal on Selected Areas in Communications* 34.3 (Mar. 2016), pp. 639–650.

[50] Y. Ghiassi-Farrokhfal et al. "Solar Power Shaping: An Analytical Approach". In: *IEEE Transactions on Sustainable Energy* 6.1 (Jan. 2015), pp. 162–170.

[51] L. Gkatzikis, I. Koutsopoulos, and T. Salonidis. "The Role of Aggregators in Smart Grid Demand Response Markets". In: *IEEE Journal on Selected Areas in Communications* 31.7 (July 2013), pp. 1247–1257.

[52] T. Han and N. Ansari. "A Traffic Load Balancing Framework for Software-Defined Radio Access Networks Powered by Hybrid Energy Sources". In: *IEEE/ACM Transactions on Networking* 24.2 (Apr. 2016), pp. 1038–1051.

[53] T. Han and N. Ansari. "Powering mobile networks with green energy". In: *IEEE Wireless Communications* 21.1 (Feb. 2014), pp. 90–96.

[54] H. A. H. Hassan, L. Nuaymi, and A. Pelov. "Classification of renewable energy scenarios and objectives for cellular networks". In: *2013 IEEE 24th Annual International Symposium on Personal, Indoor, and Mobile Radio Communications (PIMRC)*. Sept. 2013, pp. 2967–2972.

[55] H. A. H. Hassan, A. Pelov, and L. Nuaymi. "Cost-efficient radio resource allocation in hybrid energy cellular networks". In: *2014 IEEE Global Communications Conference*. Dec. 2014, pp. 2472–2478.

[56] H. A. H. Hassan et al. "A Novel Energy Model for Future Cellular Networks in Smart Grid and Renewable Energy Environment". In: *IEEE Transactions on Green Communications and Networking* (2018).

[57] H. A. H. Hassan et al. “Renewable Energy Usage in the Context of Energy-Efficient Mobile Network”. In: *Vehicular Technology Conference (VTC Spring), 2015 IEEE 81st*. May 2015, pp. 1–7.

[58] H. A. H. Hassan et al. “The Smart Grid and Future Mobile Networks: Integrating Renewable Energy Sources and Delay Tolerant Users”. In: *Vehicular Technology Conference (VTC Fall), 2015 IEEE 82nd*. Sept. 2015, pp. 1–7.

[59] H. Al Haj Hassan, L. Nuaymi, and A. Pelov. “Renewable energy in cellular networks: A survey”. In: *Online Conference on Green Communications (GreenCom), 2013 IEEE*. Oct. 2013, pp. 1–7.

[60] H. Al Haj Hassan, A. Pelov, and L. Nuaymi. “Integrating Cellular Networks, Smart Grid, and Renewable Energy: Analysis, Architecture, and Challenges”. In: *IEEE Access* 3 (2015), pp. 2755–2770.

[61] Y. He et al. “On WiFi Offloading in Heterogeneous Networks: Various Incentives and Trade-Off Strategies”. In: *IEEE Communications Surveys Tutorials* 18.4 (Fourthquarter 2016), pp. 2345–2385.

[62] N. Horner et al. “Dynamic data center load response to variability in private and public electricity costs”. In: *2016 IEEE International Conference on Smart Grid Communications (SmartGridComm)*. Nov. 2016, pp. 80–85.

[63] Shounan Hua et al. “Application of valve-regulated lead-acid batteries for storage of solar electricity in stand-alone photovoltaic systems in the northwest areas of China”. In: *Journal of Power Sources* 158.2 (2006), pp. 1178–1185.

[64] IEA-ETSAP and IRENA. “Solar photovoltaics: Technology brief”. In: *Energy Technology Systems Analysis Programme and International Renewable Energy Agency, Tech. Rep.* (Jan. 2013).

[65] MA Imran et al. *Energy efficiency analysis of the reference systems, areas of improvements and target breakdown*. Tech. rep. Tech. Rep. ICT-EARTH deliverable, 2011.

[66] M. Jafari et al. “Technical issues of sizing Lead-Acid batteries for application in residential renewable energy systems”. In: *Electric Power and Energy Conversion Systems (EPECS), 2015 4th International Conference on*. Nov. 2015, pp. 1–6.

[67] D. P. Jenkins, J. Fletcher, and D. Kane. “Lifetime prediction and sizing of lead-acid batteries for microgeneration storage applications”. In: *IET Renewable Power Generation* 2.3 (Sept. 2008), pp. 191–200.

[68] L. Jiang and S. Low. “Real-time demand response with uncertain renewable energy in smart grid”. In: *2011 49th Annual Allerton Conference on Communication, Control, and Computing (Allerton)*. Sept. 2011, pp. 1334–1341.

[69] M Jurado, JM Caridad, and V Ruiz. "Statistical distribution of the clearness index with radiation data integrated over five minute intervals". In: *Solar Energy* 55.6 (1995), pp. 469–473.

[70] J. W. Kimball, B. T. Kuhn, and R. S. Balog. "A System Design Approach for Unattended Solar Energy Harvesting Supply". In: *IEEE Transactions on Power Electronics* 24.4 (Apr. 2009), pp. 952–962.

[71] M. L. Ku et al. "Advances in Energy Harvesting Communications: Past, Present, and Future Challenges". In: *IEEE Communications Surveys Tutorials* PP.99 (2015), pp. 1–1. ISSN: 1553-877X.

[72] Kanzumba Kusakana and Herman Jacobus Vermaak. "Hybrid renewable power systems for mobile telephony base stations in developing countries". In: *Renewable Energy* 51.C (2013), pp. 419–425.

[73] "Lead-Acid Battery Guide for Stand-Alone Photovoltaic Systems". In: *IEA Task III, Report IEA-PVPS 3-06:1999*. Dec. 1999.

[74] K. Lee et al. "Mobile Data Offloading: How Much Can WiFi Deliver?" In: *IEEE/ACM Transactions on Networking* 21.2 (Apr. 2013), pp. 536–550.

[75] J. Leithon, T. J. Lim, and S. Sun. "Online energy management strategies for base stations powered by the smart grid". In: *Smart Grid Communications (SmartGridComm), 2013 IEEE International Conference on*. Oct. 2013, pp. 199–204.

[76] G. Leonardi, M. Meo, and M. A. Marsan. "Markovian models of solar power supply for a LTE macro BS". In: *2016 IEEE International Conference on Communications (ICC)*. May 2016, pp. 1–7.

[77] Giuseppe Leonardi, Michela Meo, and Marco Ajmone Marsan. "Markovian models of solar power supply for a LTE macro BS". In: *2016 IEEE International Conference on Communications, ICC 2016, Kuala Lumpur, Malaysia, May 22-27, 2016*. 2016, pp. 1–7.

[78] J. Liu et al. "Increasing wind power penetration level based on hybrid wind and Photovoltaic generation". In: *TENCON 2013 - 2013 IEEE Region 10 Conference (31194)*. Oct. 2013, pp. 1–5.

[79] A. Malik and J. Ravishankar. "A review of demand response techniques in smart grids". In: *2016 IEEE Electrical Power and Energy Conference (EPEC)*. Oct. 2016, pp. 1–6.

[80] M. A. Marsan et al. "Towards zero grid electricity networking: Powering BSs with renewable energy sources". In: *Communications Workshops (ICC), 2013 IEEE International Conference on*. June 2013, pp. 596–601.

[81] Marco Ajmone Marsan et al. “Towards zero grid electricity networking: Powering BSs with renewable energy sources”. In: *IEEE International Conference on Communications, ICC 2013, Budapest, Hungary, June 9-13, 2013, Workshops Proceedings*. 2013, pp. 596–601.

[82] M. Meo, D. Renga, and M. T. Sarti. “Household users’ cooperation to reduce cost in green mobile networks”. In: *2018 International Telecommunications Energy Conference (INTELEC)*. 2018.

[83] Michela Meo et al. “Dimensioning the power supply of a LTE macro BS connected to a PV panel and the power grid”. In: *2015 IEEE International Conference on Communications, ICC 2015, London, United Kingdom, June 8-12, 2015*. 2015, pp. 178–184.

[84] M. Meo et al. “Dimensioning the power supply of a LTE macro BS connected to a PV panel and the power grid”. In: *Communications (ICC), 2015 IEEE International Conference on*. June 2015, pp. 178–184.

[85] M. Meo et al. “Dimensioning the power supply of a LTE macro BS connected to a PV panel and the power grid”. In: *Communications (ICC), 2015 IEEE International Conference on*. June 2015, pp. 178–184.

[86] C. Mi, M. A. Masrur, and D. W. Gao. In: *Hybrid Electric Vehicles: Principles and Applications with Practical Perspectives*. John Wiley and Sons, Ltd, Chichester, UK, 2011.

[87] M. Miozzo et al. “SolarStat: Modeling photovoltaic sources through stochastic Markov processes”. In: *2014 IEEE International Energy Conference (ENERGYCON)*. May 2014, pp. 688–695.

[88] M. Miozzo et al. “Switch-On/Off Policies for Energy Harvesting Small Cells through Distributed Q-Learning”. In: *2017 IEEE Wireless Communications and Networking Conference Workshops (WCNCW)*. Mar. 2017, pp. 1–6.

[89] A. F. Morgera and V. Lughi. “Frontiers of photovoltaic technology: A review”. In: *Clean Electrical Power (ICCEP), 2015 International Conference on*. June 2015, pp. 115–121.

[90] V. Natarajan and A. Closepet. “Statistical Analysis of Cost of Energy Due to Electricity Outages in Developing Countries”. In: *FUTURE COMPUTING 2012 : The Fourth International Conference on Future Computational Technologies and Applications*. July 2012, pp. 39–44.

[91] D. Niyato, X. Lu, and P. Wang. “Adaptive power management for wireless base stations in a smart grid environment”. In: *IEEE Wireless Communications* 19.6 (Dec. 2012), pp. 44–51.

[92] “Off-Grid Power for Mobile Base Stations - Renewable and Alternative Energy Sources for Remote Mobile Telecommunications: Global Market Analysis and Forecasts”. In: *Pike Research* (2013).

[93] E. M. R. Oliveira and A. Carneiro. "Routine-based network deployment". In: *2014 IEEE Conference on Computer Communications Workshops (INFOCOM WKSHPS)*. Apr. 2014, pp. 183–184.

[94] J. Peng, P. Hong, and K. Xue. "Optimal Power Management Under Delay Constraint in Cellular Networks with Hybrid Energy Sources". In: *Comput. Netw.* 78.C (Feb. 2015), pp. 107–118. ISSN: 1389-1286.

[95] N. Ben Rached et al. "Optimized Energy Procurement for Cellular Networks with Uncertain Renewable Energy Generation". In: *2016 IEEE Global Communications Conference (GLOBECOM)*. Dec. 2016, pp. 1–7.

[96] Nadhir Ben Rached et al. "Energy Management Optimization for Cellular Networks Under Renewable Energy Generation Uncertainty". In: *TGCN* 1.2 (2017), pp. 158–166.

[97] R. Rajesh, V. Sharma, and P. Viswanath. "Capacity of Fading Gaussian Channel with an Energy Harvesting Sensor Node". In: *Global Telecommunications Conference (GLOBECOM 2011), 2011 IEEE*. Dec. 2011, pp. 1–6.

[98] I. Razika and I. Nabila. "Modeling of monthly global solar radiation in M'sila region (Algeria)". In: *2016 7th International Renewable Energy Congress (IREC)*. Mar. 2016, pp. 1–6.

[99] F. Rebecchi et al. "Data Offloading Techniques in Cellular Networks: A Survey". In: *IEEE Communications Surveys Tutorials* 17.2 (Secondquarter 2015), pp. 580–603.

[100] D. Renga. "Greener and cheaper mobile communication: let the sunshine in". In: *2018 IEEE Wireless Communication and Networking Conference (WCNC)* PP.99 (Apr. 2018), pp. 1–1.

[101] D. Renga and M. Meo. "Dimensioning renewable energy systems to power Mobile Networks". In: *IEEE Transactions on Green Communications and Networking* (2018).

[102] D. Renga and M. Meo. "From self-sustainable Green Mobile Networks to enhanced interaction with the Smart Grid". In: *2018 International Teletraffic Congress (ITC 30)*. 2018.

[103] D. Renga and M. Meo. "Modeling renewable energy production for base stations power supply". In: *2016 IEEE International Conference on Smart Grid Communications (SmartGridComm)*. Nov. 2016, pp. 716–722.

[104] D. Renga et al. "Energy management and Base Station on/off switching in green mobile networks for offering Ancillary Services". In: *IEEE Transactions on Green Communications and Networking* (2018), pp. 1–1.

[105] D. Renga et al. “Improving the interaction of a green mobile network with the smart grid”. In: *2017 IEEE International Conference on Communications (ICC)*. May 2017, pp. 1–7.

[106] *RTE-France. (Réseau de transport d’electricité)*. 2015. URL: www.rte-france.com.

[107] H. Al-Sheikh and N. Moubayed. “Health status and diagnosis of batteries in renewable energy systems: An overview”. In: *Electrical and Power Engineering (EPE), 2012 International Conference and Exposition on*. Oct. 2012, pp. 922–927.

[108] M. Sheng et al. “Intelligent Energy and Traffic Coordination for Green Cellular Networks With Hybrid Energy Supply”. In: *IEEE Transactions on Vehicular Technology* 66.2 (Feb. 2017), pp. 1631–1646.

[109] J. Shi et al. “Forecasting Power Output of Photovoltaic Systems Based on Weather Classification and Support Vector Machines”. In: *IEEE Transactions on Industry Applications* 48.3 (May 2012), pp. 1064–1069.

[110] H. Smertnik. “Green Power for Mobile Bi-Annual Report, GSM Association”. In: (Aug. 2014).

[111] *SoDa (Solar Radiation Data)*. URL: http://www.soda-pro.com/web-services.

[112] J. Song et al. “Development of a Markov-Chain-Based Energy Storage Model for Power Supply Availability Assessment of Photovoltaic Generation Plants”. In: *IEEE Transactions on Sustainable Energy* 4.2 (Apr. 2013), pp. 491–500.

[113] “Status of solar wind renewable energy in India”. In: *Renewable and Sustainable Energy Reviews* 27 (2013), pp. 1–10.

[114] J. W. Stevens and G. P. Corey. “A study of lead-acid battery efficiency near top-of-charge and the impact on PV system design”. In: *Photovoltaic Specialists Conference, 1996., Conference Record of the Twenty Fifth IEEE*. May 1996, pp. 1485–1488.

[115] S. Sudevalayam and P. Kulkarni. “Energy Harvesting Sensor Nodes: Survey and Implications”. In: *IEEE Communications Surveys Tutorials* 13.3 (Mar. 2011), pp. 443–461.

[116] S. Suman and S. De. “Solar-enabled green base stations: Cost versus utility”. In: *2017 IEEE 18th International Symposium on A World of Wireless, Mobile and Multimedia Networks (WoWMoM)*. June 2017, pp. 1–8.

[117] J Tovar, FJ Olmo, and L Alados-Arboledas. “One-minute global irradiance probability density distributions conditioned to the optical air mass”. In: *Solar energy* 62.6 (1998), pp. 387–393.

[118] D. Valerdi et al. “Intelligent energy managed service for green base stations”. In: *2010 IEEE Globecom Workshops*. Dec. 2010, pp. 1453–1457.

[119] A. Wierman et al. “Opportunities and challenges for data center demand response”. In: *International Green Computing Conference*. Nov. 2014, pp. 1–10.

[120] J. Wu et al. “Energy-Efficient Base-Stations Sleep-Mode Techniques in Green Cellular Networks: A Survey”. In: *IEEE Communications Surveys Tutorials* 17.2 (Secondquarter 2015), pp. 803–826.

[121] H. T. Yang et al. “A Weather-Based Hybrid Method for 1-Day Ahead Hourly Forecasting of PV Power Output”. In: *IEEE Transactions on Sustainable Energy* 5.3 (July 2014), pp. 917–926.

[122] F. Yuan et al. “Optimal Harvest-Use-Store Strategy for Energy Harvesting Wireless Systems”. In: *IEEE Transactions on Wireless Communications* 14.2 (Feb. 2015), pp. 698–710.

[123] Yi Zhang et al. “An overview of energy-efficient base station management techniques”. In: *Digital Communications - Green ICT (TIWDC), 2013 24th Tyrrhenian International Workshop on*. Sept. 2013, pp. 1–6.

[124] Y. Zhang et al. “An Overview of Energy-efficient Base Station Management Techniques”. In: *Proc. of TIWDC’13 (24th Tyrrhenian Int. Workshop on Digital Communications)*. Genoa, Sept. 2013.

[125] S. Zhou, J. Gong, and Z. Niu. “Sleep control for base stations powered by heterogeneous energy sources”. In: *2013 International Conference on ICT Convergence (ICTC)*. Oct. 2013, pp. 666–670.